Naval Research Laboratory

Washington, DC 20375-5320

NRL/MR/7160--17-9701

Bottom Backscattering Strengths Measured in Shallow and Deep Water

Roger C. Gauss
Edward L. Kunz
Joseph M. Fialkowski
Richard Menis

Acoustic Signal Processing and Systems Branch
Acoustics Division

January 18, 2017

REPORT DOCUMENTATION PAGE

Form Approved
OMB No. 0704-0188

1. REPORT DATE *(DD-MM-YYYY)*	**2. REPORT TYPE**	**3. DATES COVERED** *(From - To)*
18-01-2017	Memorandum Report	August 1993 – September 2016

4. TITLE AND SUBTITLE

Bottom Backscattering Strengths Measured in Shallow and Deep Water

5a. CONTRACT NUMBER

5b. GRANT NUMBER

5c. PROGRAM ELEMENT NUMBER
0602747N

6. AUTHOR(S)

Roger C. Gauss,[1] Edward L. Kunz,[1] Joseph M. Fialkowski, and Richard Menis

5d. PROJECT NUMBER

5e. TASK NUMBER

5f. WORK UNIT NUMBER
71-6817-06

7. PERFORMING ORGANIZATION NAME(S) AND ADDRESS(ES)

Naval Research Laboratory, Code 7160
4555 Overlook Avenue, SW
Washington, DC 20375-5320

8. PERFORMING ORGANIZATION REPORT NUMBER

NRL/MR/7160--17-9701

9. SPONSORING / MONITORING AGENCY NAME(S) AND ADDRESS(ES)

Naval Research Laboratory, Code 7160
4555 Overlook Avenue, SW
Washington, DC 20375-5350

10. SPONSOR / MONITOR'S ACRONYM(S)

11. SPONSOR / MONITOR'S REPORT NUMBER(S)

12. DISTRIBUTION / AVAILABILITY STATEMENT

Approved for public release; distribution is unlimited.

13. SUPPLEMENTARY NOTES

[1]Retired from NRL.

14. ABSTRACT

For a low-frequency (LF; < 1 kHz) or mid-frequency (MF; 1 to 10 kHz) active sonar, scattering from the seafloor, coupled with propagation conditions, can severely limit the detectability of returns from features of interest. Acoustic scattering from the seabed can be a complex mix of surface roughness and volume heterogeneity contributions, so that reverberation levels can vary dramatically, depending on the local geology. The Naval Research Laboratory (NRL) performed LF and MF, direct-path bottom backscattering strength (BBS) measurements at 105 sites over 6 experiments in 5 distinct environments from 1993 to 2005. This report presents the BBS results from these experiments, as well as empirical fits to the MF results.

15. SUBJECT TERMS

Bottom scattering
Bottom scattering strength
Reverberation
Underwater acoustics
Active sonar

16. SECURITY CLASSIFICATION OF:			**17. LIMITATION OF ABSTRACT**	**18. NUMBER OF PAGES**	**19a. NAME OF RESPONSIBLE PERSON**
a. REPORT	**b. ABSTRACT**	**c. THIS PAGE**			Joseph M. Fialkowski
Unclassified Unlimited	Unclassified Unlimited	Unclassified Unlimited	Unclassified Unlimited	143	**19b. TELEPHONE NUMBER** *(include area code)* (202) 404-4803

Standard Form 298 (Rev. 8-98)
Prescribed by ANSI Std. Z39.18

TABLE OF CONTENTS

BOTTOM BACKSCATTERING STRENGTHS MEASURED IN SHALLOW AND DEEP WATER

1. INTRODUCTION

For a low-frequency (LF; < 1 kHz) or mid-frequency (MF; 1 to 10 kHz) active sonar, echoes from the seafloor, coupled with propagation conditions, can severely limit the detectability of returns from features of interest. Acoustic scattering from the seabed can be a complex mix of surface roughness and volume heterogeneity contributions, so that reverberation levels can vary dramatically with frequency and grazing angle, and with the local geology. Hence, making accurate predictions of bottom reverberation and active sonar performance will in turn depend on accurately characterizing the acoustic seafloor interactions, in particular providing measures/models of bottom loss (BL) and bottom scattering strength (BSS) as functions of frequency, grazing angle, and bottom properties. This report presents measured LF and MF bottom backscattering strengths that can be of use in developing/validating empirical or physics-based BSS models.

The Naval Research Laboratory (NRL) performed LF and MF direct-path bottom backscattering strength (BBS) measurements at 105 sites in 6 experiments in 5 distinct environments from 1993 to 2005:

- Shallow Water
  - New Jersey Shelf, May 2001 (8 sites)
    - *Boundary Characterization 2001* (B2001); 2.5–5 kHz
  - Malta Plateau,
    - April 2002 (8 sites)
      - *Boundary Characterization 2002* (B2002); 2–4 kHz
    - May 2004 (29 sites)
      - *Boundary Characterization 2004* (B2004); 1.5–4 kHz
  - Stanton Banks, July 2002 (16 sites)
    - *The Technical Cooperation Program (TTCP) Multistatic Active Sonar Technology 2002* (T-MAST 02); 1.5–3.5 kHz
  - Heceta Bank, July 2005 (25 sites: 22 shallow, 1 intermediate, and 2 deep)
    - *Ocean Reverberation Experiment 2005* (OREX-05); 0.6–5 kHz
- Deep Water
  - Scotian Continental Rise, August 1993 (19 sites)
    - *Low-Frequency Active 11* (LFA 11); 190–310 Hz

This report summarizes (in the order above) the bottom backscattering strengths derived from direct-path, near-monostatic, LF and MF measurements in these experiments, as well as empirical power law fits to the MF results (and the relationships between the T-MAST-02 BBS results and local bottom parameters). Selected other NRL BBS measurements are briefly discussed in Sect. 9, and referenced in Sect. 10, of this report.

Manuscript approved December 16, 2016.

2. DATA PROCESSING

This section provides a high-level overview of the standard data processing used to derive the undersea acoustic BBS values. Details particular to a given experiment are discussed in their respective sections.

The sonar geometries were either quasi-monostatic (LFA-11) in towing mode, or near-monostatic (the shallow-water measurements) in drifting/moored mode. The bottom reverberation from transmitted gated continuous wave (CW) and frequency modulated (FM) signals was received on either on a towed horizontal line array (HLA) or a drifting/moored vertical line array (VLA). The MF VLA was used in all shallow-water experiments consisted of 16 elements spaced at 0.1524 m (6 in); the LF VLA (used in OREX-05) consisted of 16 elements spaced at 0.76 m (30 in). The VLA was recently recalibrated (2011) so that some of the previous reported VLA BBS measurement values need adjustment, such as the T-MAST 02 BBS results of Kunz and Gauss (2005) and Gauss *et al*. (2008)—see Sect. 5 for the revised T-MAST 02 BBS results. Spatially-Hanned receiver beams with cosine-spaced main response axes were formed, with the most useful returns coming from the aft-looking beams for the HLA, and from the downward-looking beams closest to broadside for the VLA. A representative example of the shallow-water sonar geometry and reverberation beam-time series are shown in Fig. 2-1.

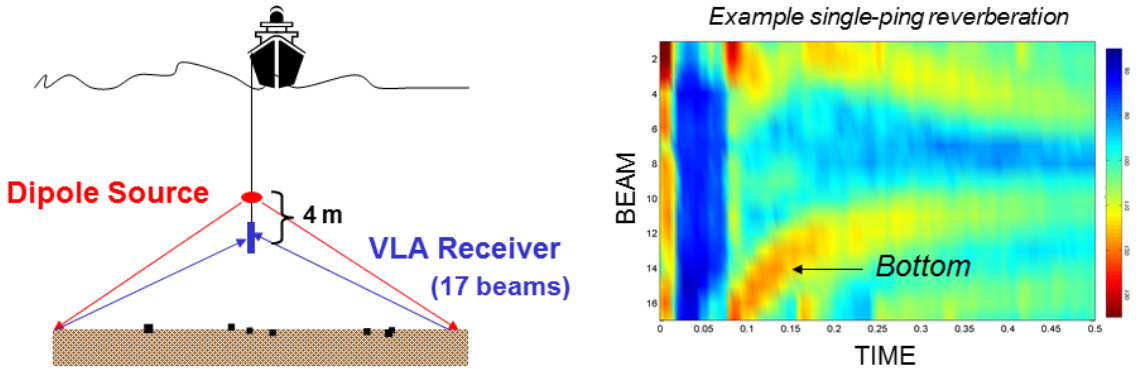

Fig. 2-1 – Typical shallow-water sonar geometry (left) and beam reverberation (right).

After beamforming, reverberation time-series curves were obtained for individual pings using either spectral processing for the CWs or match filtering for the FM sweeps. For the CW ping data, a uniform window matched to the signal duration was slid over the length of each beam time series with either 50% or 90% overlap. The resulting time-series segments were then Fourier transformed to obtain power spectra, with reverberation level computed by integrating the total received signal power over a narrow frequency band centered on the frequency of the transmitted signal. For the FM data, the beam time-series data were matched filtered against the transmitted signal replica. The envelope of the correlator output was computed. In each case, data calibrations were applied to produce an estimate of the received reverberation level in μPa.

For each set of CW and FM data, the individual ping responses were temporally aligned with respect to signal transmit time, and then linearly averaged to produce a single reverberation curve for each beam.

A raytrace program was then used to calculate the geometric effects unique to each measurement (using the *in-situ* sound-speed profile): 1) transmission-loss terms to and from the scattering patch were obtained by separately calculating the geometric spreading loss along each ray path; and 2) scattering-patch areas were obtained using computed beam patterns and raytraces. The plane-wave calculation assumes the source of the seabed scattering is the water-sediment interface; hence, **all the measured BBS values shown in this report represent effective-surface scattering strengths**.

Finally, the average reverberation curves were combined with these geometric parameters and source level to solve the sonar equation for backscattering strength as a function of frequency, beam, and grazing angles:

$$BBS = RL - SL + TL_s + TL_r - 10 \log A$$

where *BBS* is the bottom backscattering strength in dB, *RL* is the measured reverberation level in dB *re* $(1\mu\text{Pa})^2$ at 1 m, *SL* is the source level in dB *re* $(1\mu\text{Pa})^2$ at 1 m, TL_s is the transmission loss from the source to the ensonified patch on the bottom in dB, TL_r is the transmission loss from the ensonified patch on the bottom to the receiver in dB, and *A* is the area of the ensonified patch in m^2. The standard deviations due to ping-to-ping variability within the sets of identical transmissions were typically ± 2 to 3 dB.

Empirical Power Law (EPL) Fits.

EPL fits to the measured shallow-water BBS–vs.–grazing-angle curves were additionally made to ascertain the suitability of commonly-used frequency-independent EPL curves used in reverberation modeling (e.g., Harrison (2003)), namely (for incident and scattered grazing angles):

- Mackenzie curve: $-27 + 10\log_{10}\left(\sin\theta_i \sin\theta_s\right)$
- Lambert's law (rule): $10\log_{10}\left(\mu \sin\theta_i \sin\theta_s\right)$
- Lommel-Seeliger: $10\log_{10}\left(\mu_1 \sin\theta_i \sin\theta_s / \{\sin\theta_i + \sin\theta_s\}\right)$

For our near-monostatic backscattering measurement geometries, the mean grazing angle $\theta = 0.5 \cdot \left(\theta_i + \theta_s\right) \doteq \theta_i$ was used, so, e.g., Lambert's law becomes $10\log_{10}\left(\mu \sin^2\theta\right)$, and the Lommel-Seeliger law becomes $10\log_{10}\left(0.5\mu_1 \sin\theta\right)$.

In this report, the EPL model was of the form $10\log_{10}\left(\mu \sin^{\alpha}\theta\right)$. For the individual site curves, the EPL fits were 'eyeball' fits to the set of curves using integer powers, whereas in the $10\log_{10}(\mu)$–vs.–α plots least-square EPL fits were used.

3. B2001 (SHALLOW WATER – NEW JERSEY SHELF)

NRL performed MF direct-path BBS measurements at 8 sites (Figs. 3-1 and 3-2) in May 2001 on the New Jersey Shelf during the Boundary 2001 experiment. (See Holland *et al*. (2005) for an overview of the B2001 experiment.) This section presents the BBS measurements from these sites.

BOUNDARY 2001 Scattering Sites (NJ Shelf)

Site	Date (JD) Time (Z)	Day or Night	Latitude (deg N)	Longitude (deg W)	Fish From Simrad	*Endeavor* Wind Speed (m/s)	Water Depth (m)	Water Sound Speed at the Interface (m/s)
1	132 0835-0920	N	39.261 39° 15.64′ 39° 15.70′	72.906 72° 54.63′ 72° 54.08′	Lesser # 70-75 m	6.2	76	1494
2	132 1039-1113	SR	39.220 39° 13.18′ 39° 13.28′	73.006 73° 00.42′ 73° 00.27′	Lesser # 70-75 m	5.7	76	1494
3	132 1346-1444	D	39.251 39° 15.06′ 39° 15.05′	72.720 72° 43.07′ 72° 43.31′	No Info	5.2	120	1494
4	133 0319-0354	N	39.116 39° 07.06′ 39° 06.83′	73.066 73° 04.14′ 73° 03.81′	No Info	5.7	75	1473
5	133 0556-0633	N	39.047 39° 03.15′ 39° 02.53′	73.114 73° 07.01′ 73° 06.70′	No Fish	6.7	71	1473
6	133 1430-1626	D	39.071 39° 04.29′	73.075 73° 04.49′	Occas. Fish	6.7	84	1474
7	134 0819-0854	N	39.060 39° 04.04′ 39° 03.13′	72.973 72° 58.36′ 72° 58.46′	Moder # 75-83 m	6.2	85	1492
8	134 1614-1623	D	39.406 39° 24.34′	72.565 72° 33.91′	Occas. Fish	5.7	110	1497

Fig. 3-1 – B2001 BBS measurement and site information (NJ Shelf).

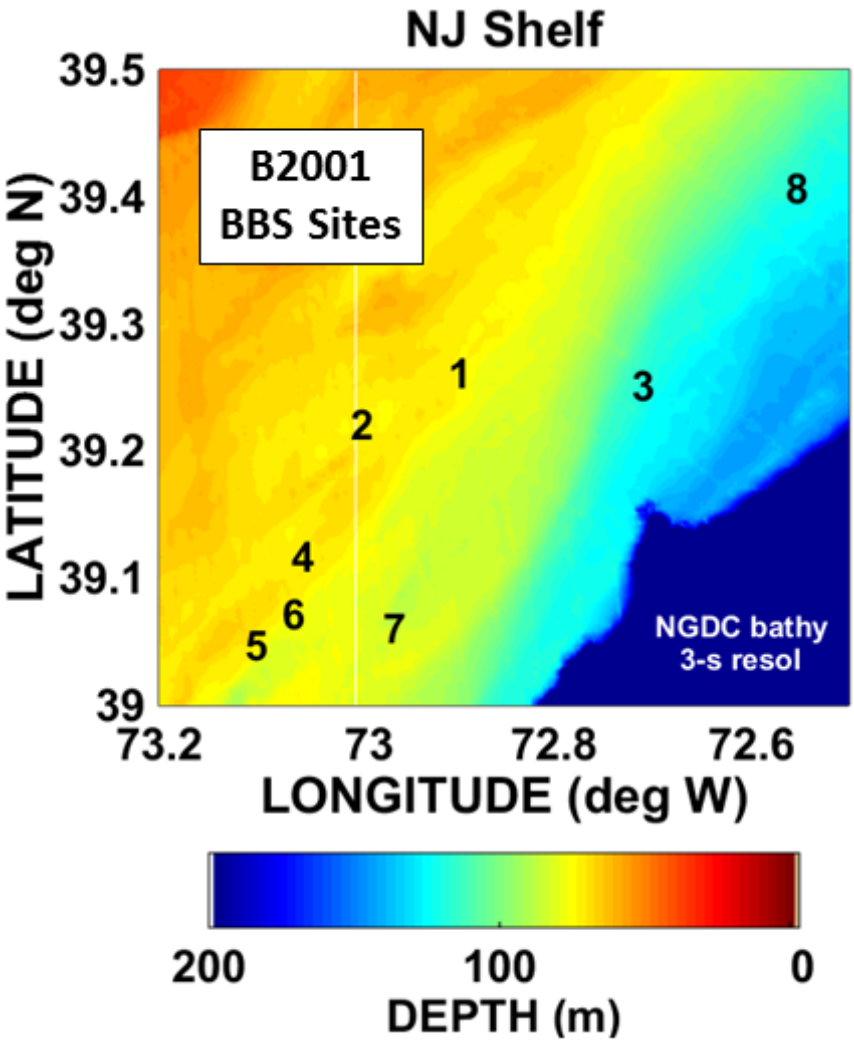

Fig. 3-2 – B2001 geographic locations of BBS sites vs. bathymetry.

A. Test Operations

Direct-path, near-monostatic acoustic BBS measurements were conducted from the R/V *Endeavor* using a 16-element VLA receiver cut for 5000 Hz and a single source. Measurements were made using combinations of 10-ms gated CW signals at 1.5, 2, 2.5, 3, 3.5, 4, 4.5, and 5 kHz, and 100-ms LFMs. (The 1.5- and 2-kHz CW, and the LFM results are not shown here.) Each CW signal was repeated 18 times with a rep rate of 5 s. The source was a transducer (G81; 191.5 dB peak) that was useable over 2.5 to 5 kHz situated 4 m above the center of the VLA. The sonar equation was used at each depth to derive scattering strengths as a function of site, frequency, and grazing angle.

B. Measured Bottom Backscattering Strengths

Figures 3.B-1–3.B-3 show frequency-dependent bottom backscattering strengths measured at the 8 B2001 shallow-water sites vs. mean grazing angle. Figure 3.B-4 shows the best EPL-curve fit values to the B2001 BBS vs. grazing angle curves.

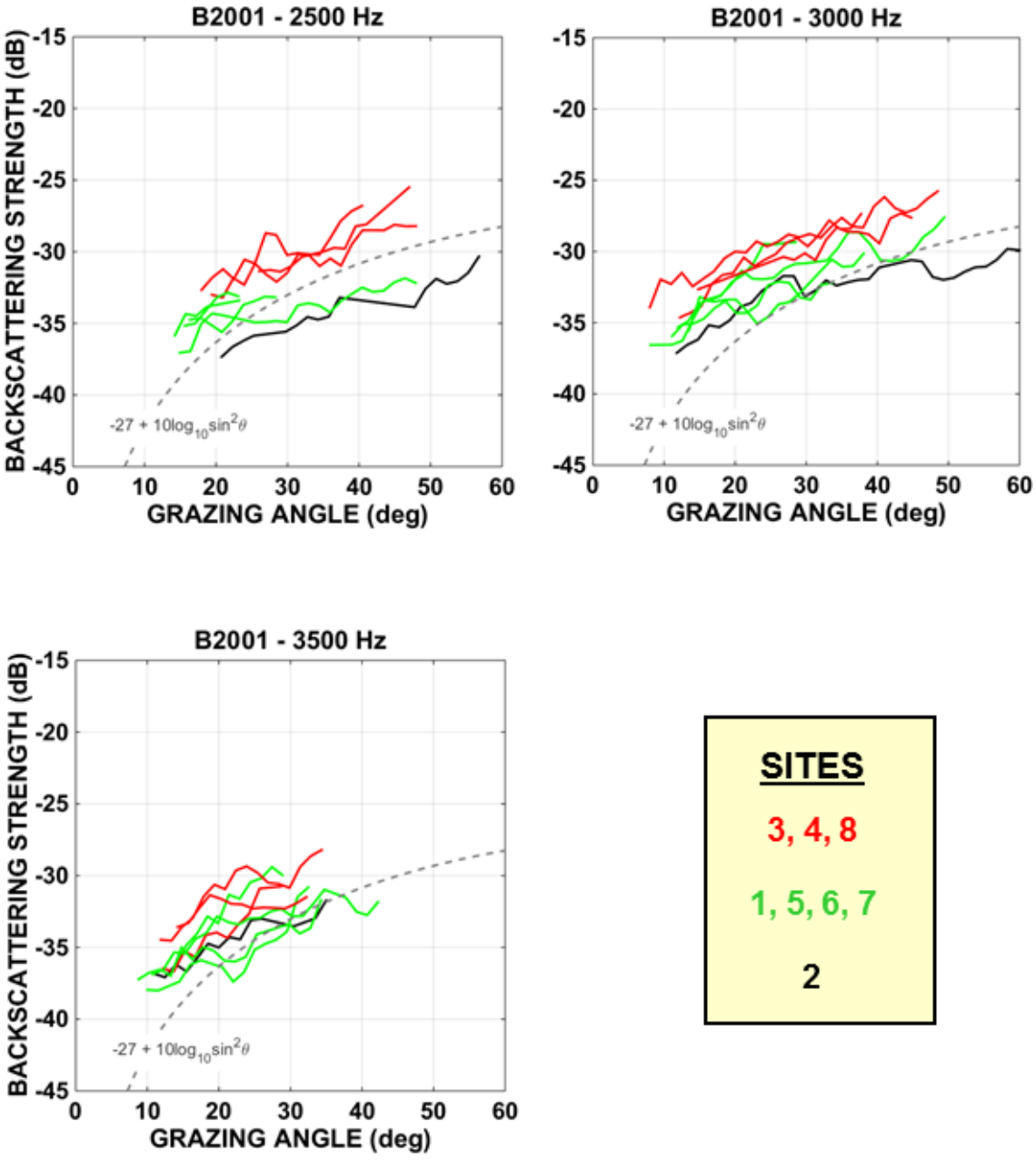

Fig. 3.B-1 – B2001 BBS vs. grazing angle at 3 frequencies for all sites (color-coded just to help visually separate the 8 sites). (Mackenzie curve (dashed) shown as a reference.)

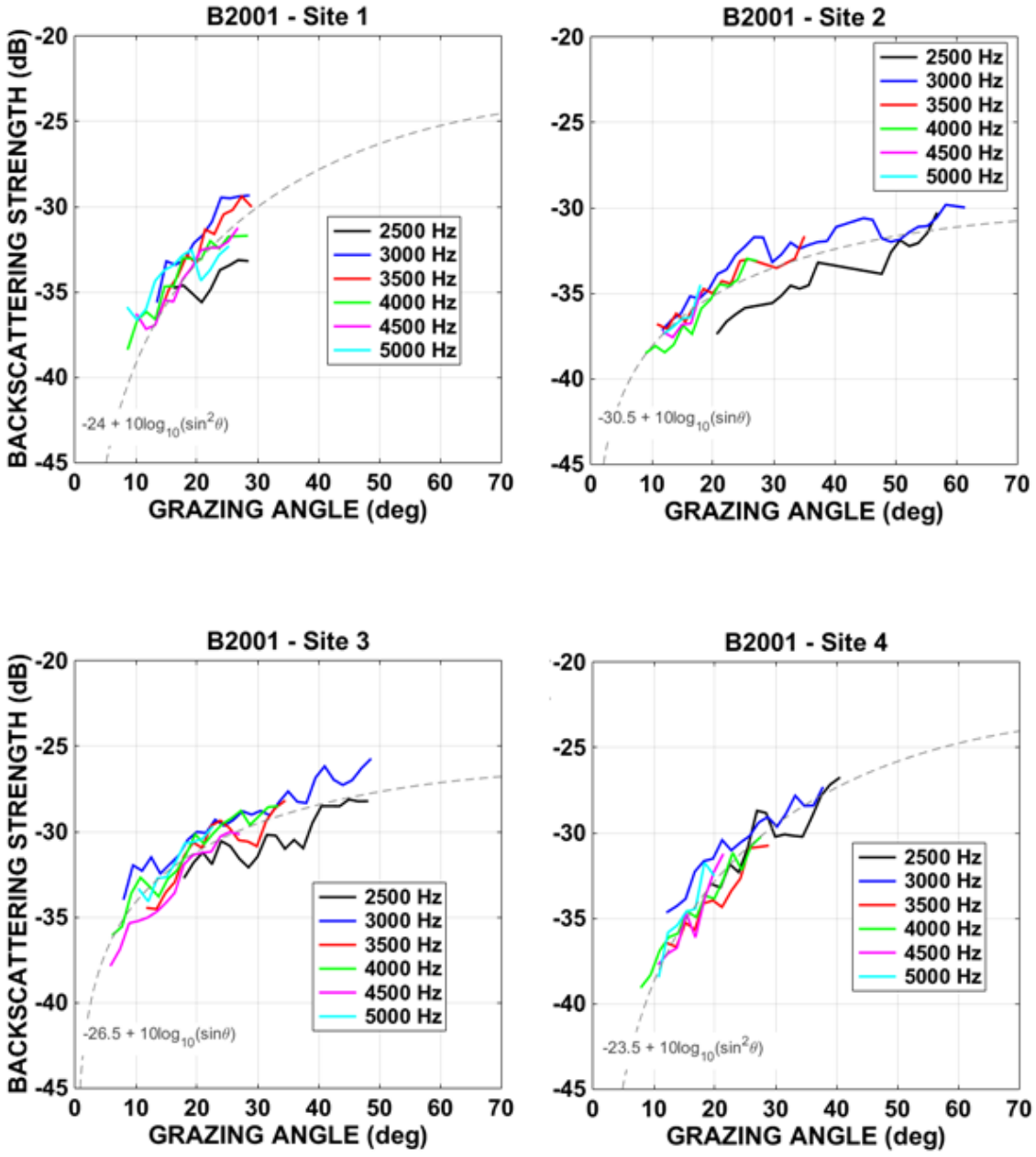

Fig. 3.B-2 – B2001 BBS vs. grazing angle at 6 frequencies for Sites 1, 2, 3, and 4.
(EPL curves matched to the data trend (dashed) are also shown.)

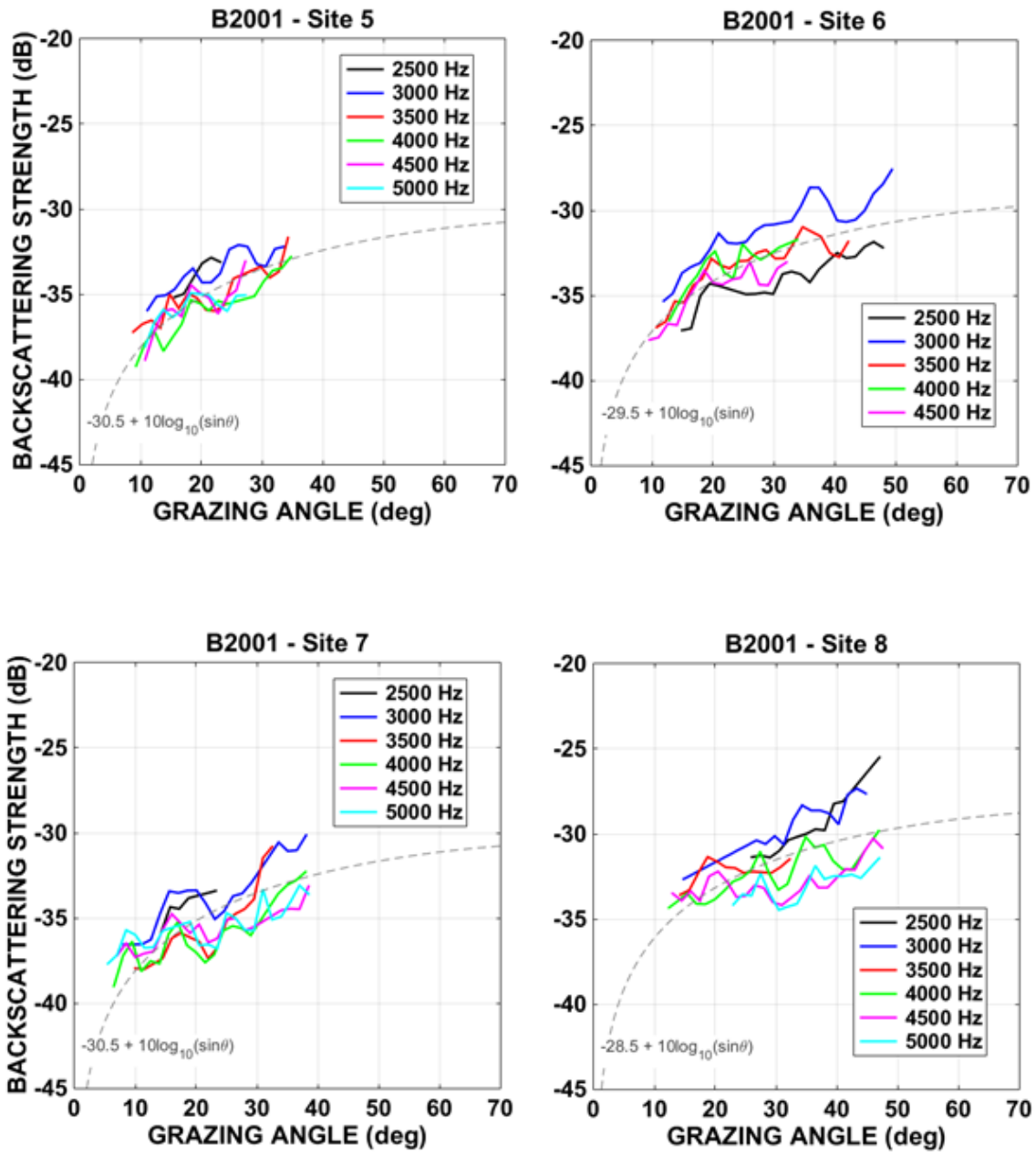

Fig. 3.B-3 – B2001 BBS vs. grazing angle at multiple frequencies for Sites 5, 6, 7, and 8. (EPL curves matched to the data trend (dashed) are also shown.)

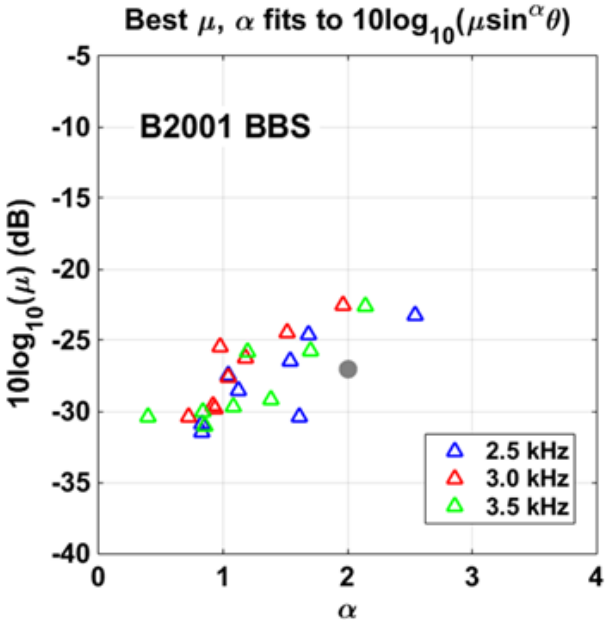

Fig. 3.B-4 – Distribution of best EPL-curve fit values to the B2001 BBS vs. grazing angle curves at 3 frequencies. (Mackenzie curve values (gray dot) shown as a reference.)

C. Comparison to Other Data

Fig. 3.C-1 shows BBS vs. grazing angle measured by 3 different resolution systems in the vicinity of NRL Site 1 (within 2 km of one another). See Holland *et al*. (2005) for details.

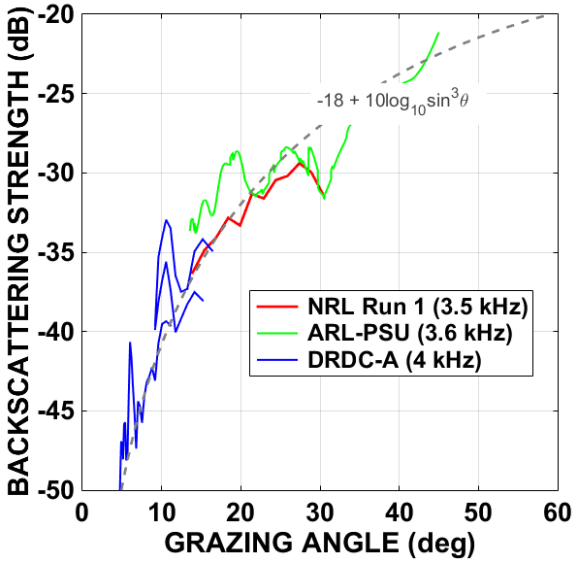

Fig. 3.C-1 – Comparison of NRL B2001 Site 1 BBS at 3.5 kHz with near-by measurements by ARL-PSU at 3.6 kHz, and DRDC-A at 4 kHz (Holland *et al*., 2005), along with an EPL fit to all the data (dashed). (This updates that paper's Fig. 17 via NRL's subsequent receiver recalibration.)

4. B2002 AND B2004 (SHALLOW WATER – MALTA PLATEAU)

NRL performed MF direct-path BBS measurements at 8 sites (Figs. 4-1 and 4-3) in April 2002 on the Malta Plateau (south of Sicily) during the Boundary 2002 experiment, and at 29 sites (Figs. 4-2 and 4-3) in May 2004 on the Malta Plateau during the Boundary 2004 experiment. (See Holland *et al.*, (2005) for an overview of the B2002 and B2004 experiments.) This section presents the 37 BBS measurements from these shallow-water sites.

BOUNDARY 2002 BBS Sites
(Malta Plateau)

Site	Source / Receiver Depths (m)	Date (JD) Time (Z)	Latitude (deg N)	Longitude (deg E)	*Alliance* Wind Speed (m/s)	Water Depth (m)	Water Sound Speed at the Interface (m/s)
2	55 / 58 20 / 23 40 / 43	107 0641-0710 107 1622-1642	36.353 36° 21.18′	14.768 14° 46.08′	7.4 11.7	136	1513
3	50 / 53 25 / 28	110 0923-0952	36.485 36° 29.1′	14.885 14° 53.1′	3.7	94	1512
4	25 / 28 50 / 53	112 0909-0922	36.439 36° 26.34′	14.929 14° 55.74′	2.2	90	1512
5	25 / 28 50 / 53	112 1004-1017	36.395 36° 23.7′	14.923 14° 55.38′	2.5	96	1512
6	25 / 28 50 / 53	112 1318-1331	36.353 36° 21.18′	14.918 14° 55.08′	5.1	96	1513
7	25 / 28 50 / 53	112 1413-1423	36.338 36° 20.28′	14.920 14° 55.2′	4.4	95	1513
8	20 / 23 40 / 43	112 1614-1623	36.640 36° 38.4′	14.638 14° 38.28′	1.0	80	1512
9	20 / 23 40 / 43	112 1703-1712	36.628 36° 37.68′	14.627 14° 37.62′	5.1	82	1512

Fig. 4-1 – B2002 BBS measurement and site information (Malta Plateau).

B2004 Bottom Scattering Sites

Site	Source / Receiver Depths (m)	Date (JD) Time (Z)	Latitude (deg N)	Longitude (deg E)	Wind Speed (kts)	Water Depth (m)	Water Sound Speed at the Interface (m/s)
1	46.5 / 50	137 1306-1310	36.535 36° 32.08'	14.820 14° 49.21'	10	100	1502
2	46.5 / 50	137 1408-1412	36.481 36° 28.86'	14.800 14° 47.98'	9	115	1502
3	56.5 / 60	137 1505-1509	36.442 36° 26.53'	14.782 14° 46.93'	8	125	1503
5	56.5 / 60	137 1636-1640	36.389 36° 23.33'	14.758 14° 45.47'	5	130	1503
6	56.5 / 60	137 1718-1722	36.360 36° 21.62'	14.744 14° 44.65'	5	134	1502
7	56.5 / 60	137 1859-1903	36.325 36° 19.55'	14.729 14° 43.76'	5	134	1502
8	56.5 / 60	137 1937-1941	36.291 36° 17.46'	14.708 14° 42.46'	6	134	1502
9	56.5 / 60	137 2012-2016	36.289 36° 17.34'	14.710 14° 42.60'	5	133	1503
10	46.5 / 50	138 0700-0704	36.276 36° 16.55'	14.877 14° 52.60'	1	103	1503
11	46.5 / 50	138 0834-0838	36.296 36° 17.74'	14.885 14° 53.10'	8	110	1503
12	46.5 / 50	138 1015-1019	36.314 36° 18.85'	14.886 14° 53.18'	15	118	1503
13	46.5 / 50	138 1225-1229	36.314 36° 18.86'	14.924 14° 55.41'	10	110	1503
14	56.5 / 60	138 1310-1314	36.335 36° 20.12'	14.884 14° 53.04'	13	120	1503
15	46.5 / 50	138 1428-1432	36.336 36° 20.16'	14.897 14° 53.82'	6	103	1503
16	46.5 / 50	138 1501-1505	36.355 36° 21.30'	14.903 14° 54.18'	10	111	1503
17	46.5 / 50	138 1649-1653	36.415 36° 24.90'	14.942 14° 56.52'	5	106	1502
18	36.5 / 40	138 1734-1738	36.371 36° 22.26'	14.918 14° 55.08'	6	83	1502
19	46.5 / 50	138 1818-1822	36.374 36° 22.44'	14.907 14° 54.42'	7	105	1502
20	46.5 / 50	138 1849-1853	36.393 36° 23.58'	14.914 14° 54.84'	10	108	1502
21	56.5 / 60	139 0932-0936	36.264 36° 15.84'	14.802 14° 48.12'	5	129	1503
22	51.5 / 55	139 1244-1248	36.278 36° 16.68'	14.876 14° 52.56'	3	103	1502
23	66.5 / 70	139 1720-1724	36.409 36° 24.54'	14.637 14° 38.22'	4	140	1503
24	66.5 / 70	139 1801-1805	36.432 36° 25.92'	14.676 14° 40.56'	3	137	1503
25	36.5 / 40	140 0634-0638	36.599 36° 35.94'	14.849 14° 50.94'	2	74	1502
26	56.5 / 60	140 0800-0804	36.420 36° 25.20'	14.855 14° 51.30'	0	122	1502
27	56.5 / 60	140 0826-0830	36.420 36° 25.20'	14.843 14° 50.58'	0	132	1503
28	56.5 / 60	140 0906-0910	36.378 36° 22.68'	14.831 14° 49.86'	0	128	1502
29	56.5 / 60	140 0940-0944	36.341 36° 20.46'	14.818 14° 49.08'	0	130	1503
30	56.5 / 60	140 1059-1102	36.341 36° 20.46'	14.818 14° 49.08'	4	130	1502

Fig. 4-2 – B2004 BBS measurement and site information (Malta Plateau).

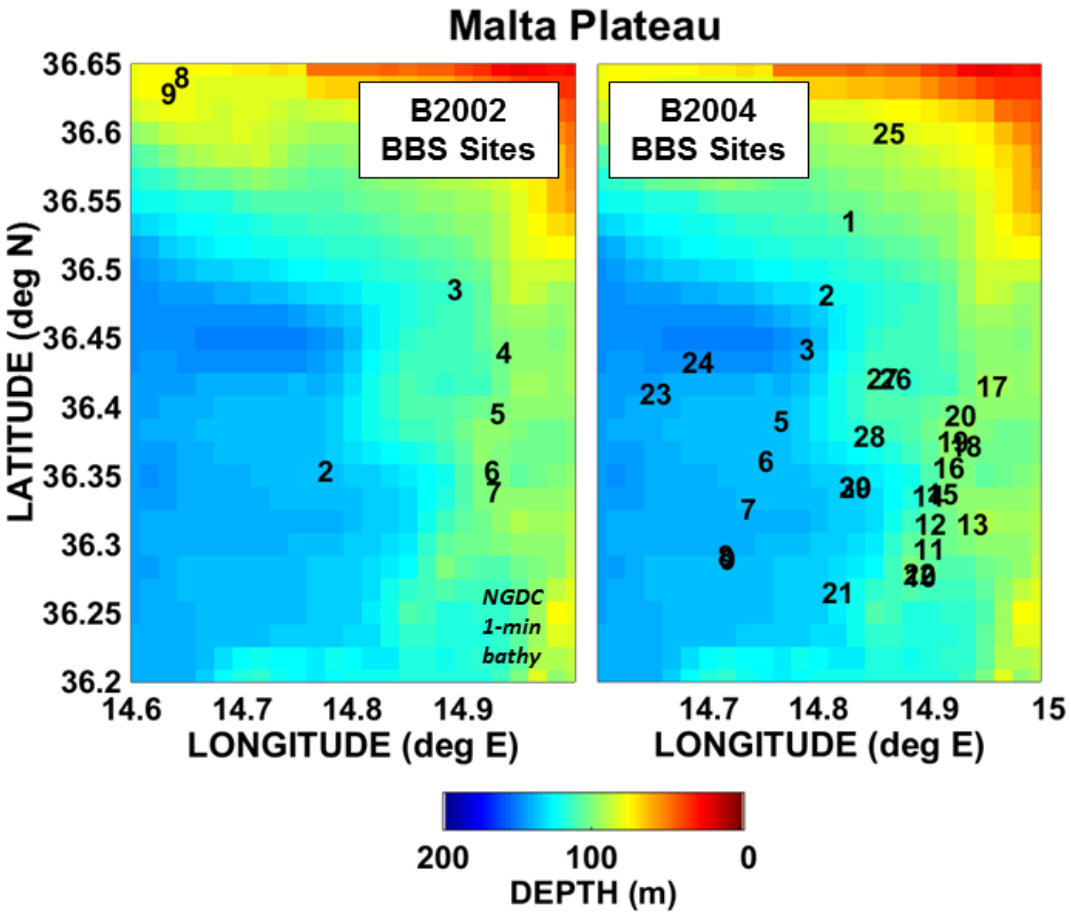

Fig. 4-3 – B2002 and B2004 geographic locations of BBS sites vs. bathymetry.

A. Test Operations

Direct-path, near-monostatic acoustic BBS measurements were conducted from the Italian Navy ships ITS *Vega* (B2002) and from ITS *Tavolara* (B2004) using a 16-element VLA receiver cut for 5000 Hz and a single source. Measurements were made using combinations of 10-ms gated CW signals at 1.5, 2, 2.5, 3, 3.5, 4, 4.5, and 5 kHz, and 100-ms LFMs. (The 4.5- and 5-kHz CW, and the LFM results are not shown here.). Each CW signal was repeated 18 times with a rep rate of 5 s. The source was a transducer (ITC 2010) that was useable over 2 to 4 kHz with source levels ranging from 177 to 187 dB. (In B2004, the source was housed in a metal frame under a v-fin.)

For B2002, the source was usually deployed at two depths at each site. The shallow depth ranged from 20 to 25 m and the deeper depth ranged from 40 to 55 m. For B2004, the receiver was deployed at a single (mid-water) depth, ranging from 40 to 70 m. In B2002, the source was 3 m above the center of the VLA MF aperture, while in B2004, the source was 3.5 m above the VLA aperture center. The sonar equation was used at each depth to derive scattering strengths as a function of site, frequency, and grazing angle.

B. Measured Bottom Backscattering Strengths

B2002 Results

Figures 4.B-1–4.B-3 show frequency-dependent bottom backscattering strengths measured at the 8 B2002 shallow-water sites vs. mean grazing angle.

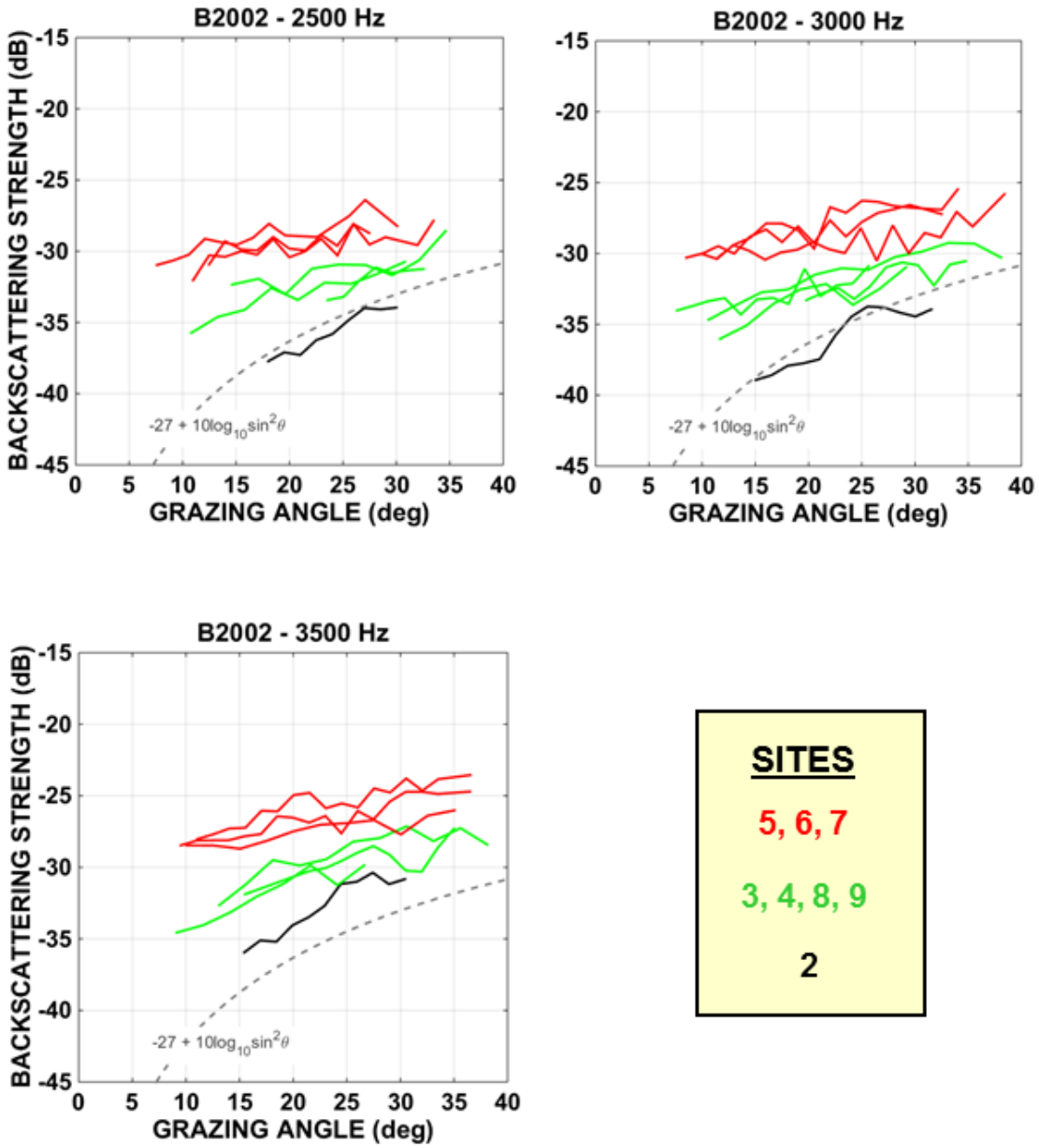

Fig. 4.B-1 – B2002 BBS vs. grazing angle at 3 frequencies for all sites (color-coded just to help visually separate the 8 sites). (Mackenzie curve (dashed) shown as a reference.)

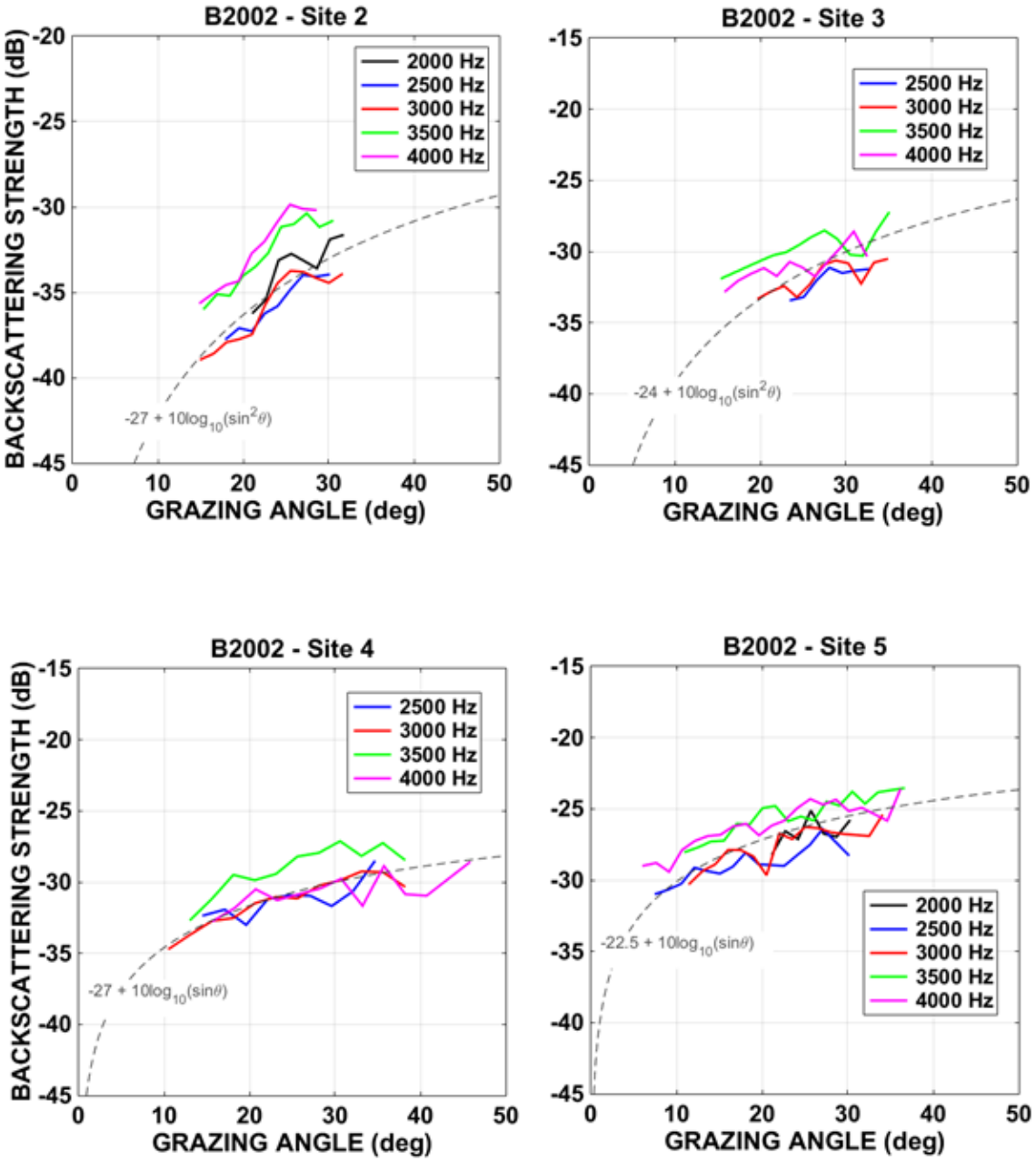

Fig. 4.B-2 – B2002 BBS vs. grazing angle at multiple frequencies for Sites 2, 3, 4, and 5. (EPL curves matched to the data trend (dashed) are also shown.)

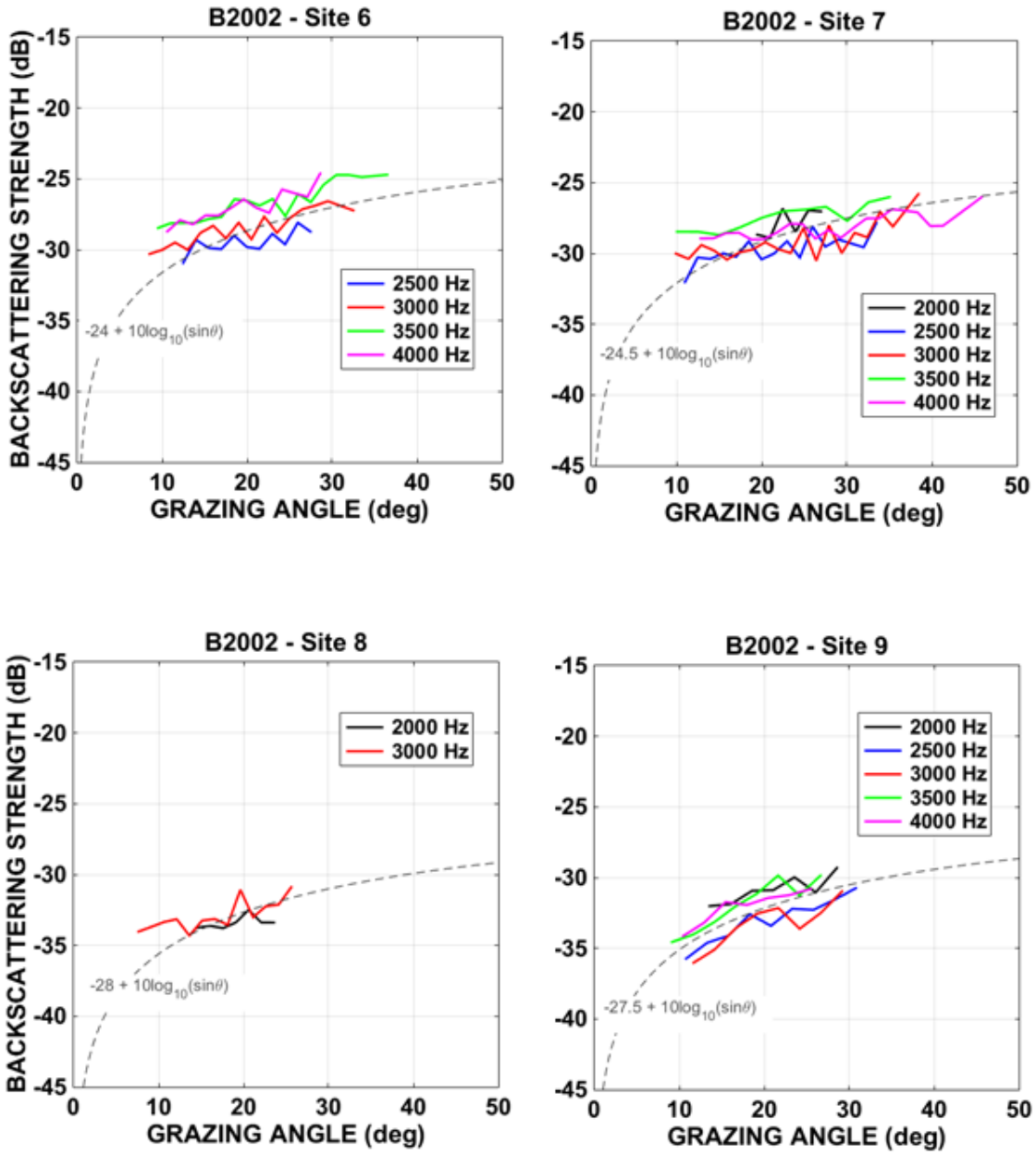

Fig. 4.B-3 – B2002 BBS vs. grazing angle at multiple frequencies for Sites 6, 7, 8, and 9. (EPL curves matched to the data trend (dashed) are also shown.)

B2004 Results

Figures 4.B-4–4.B-11 show frequency-dependent bottom backscattering strengths measured at the 29 B2004 shallow-water sites vs. mean grazing angle.

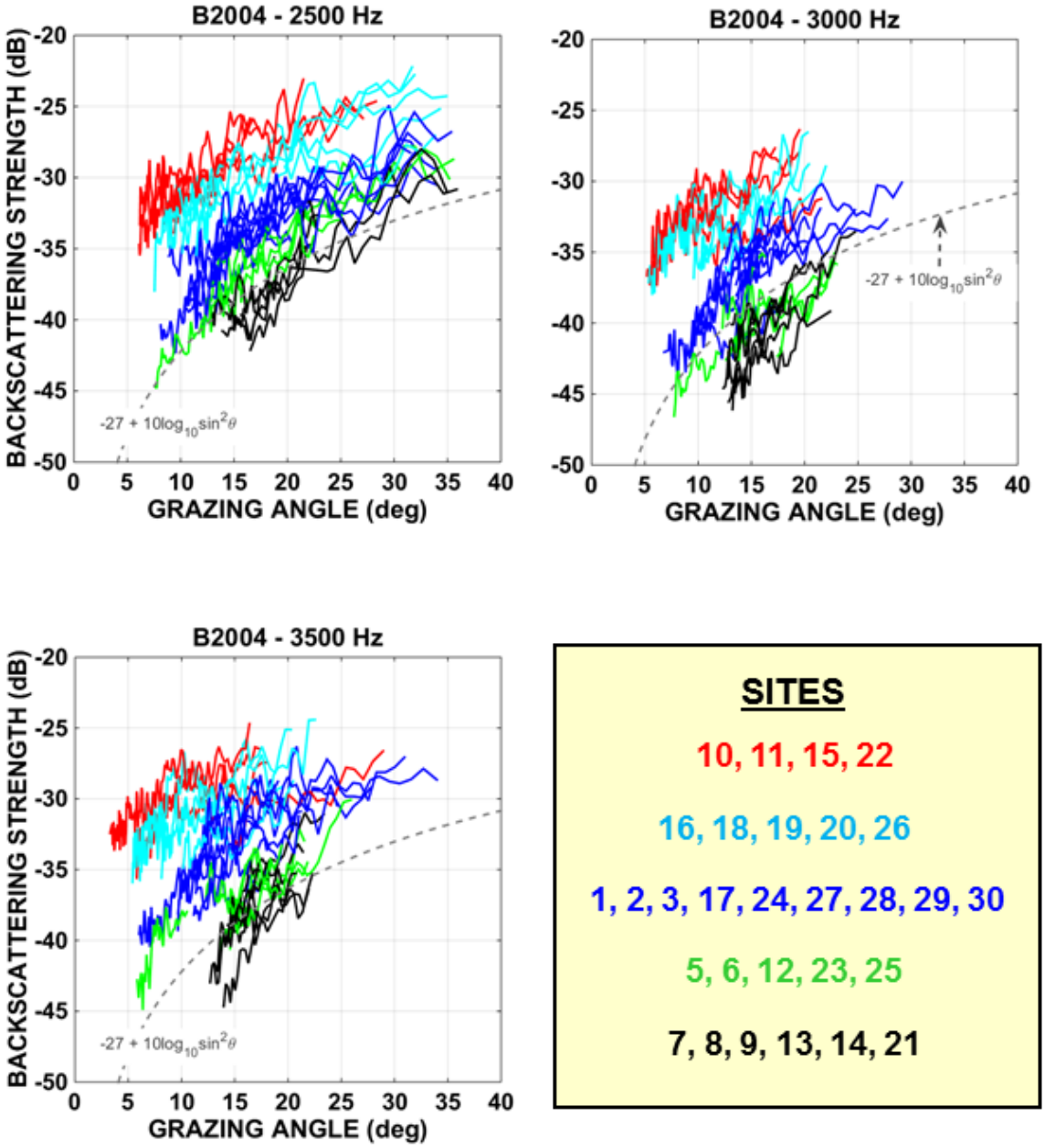

Fig. 4.B-4 – B2004 BBS vs. grazing angle at 3 frequencies for all sites (color-coded just to help visually separate the 29 sites). (Mackenzie curve (dashed) shown as a reference.)

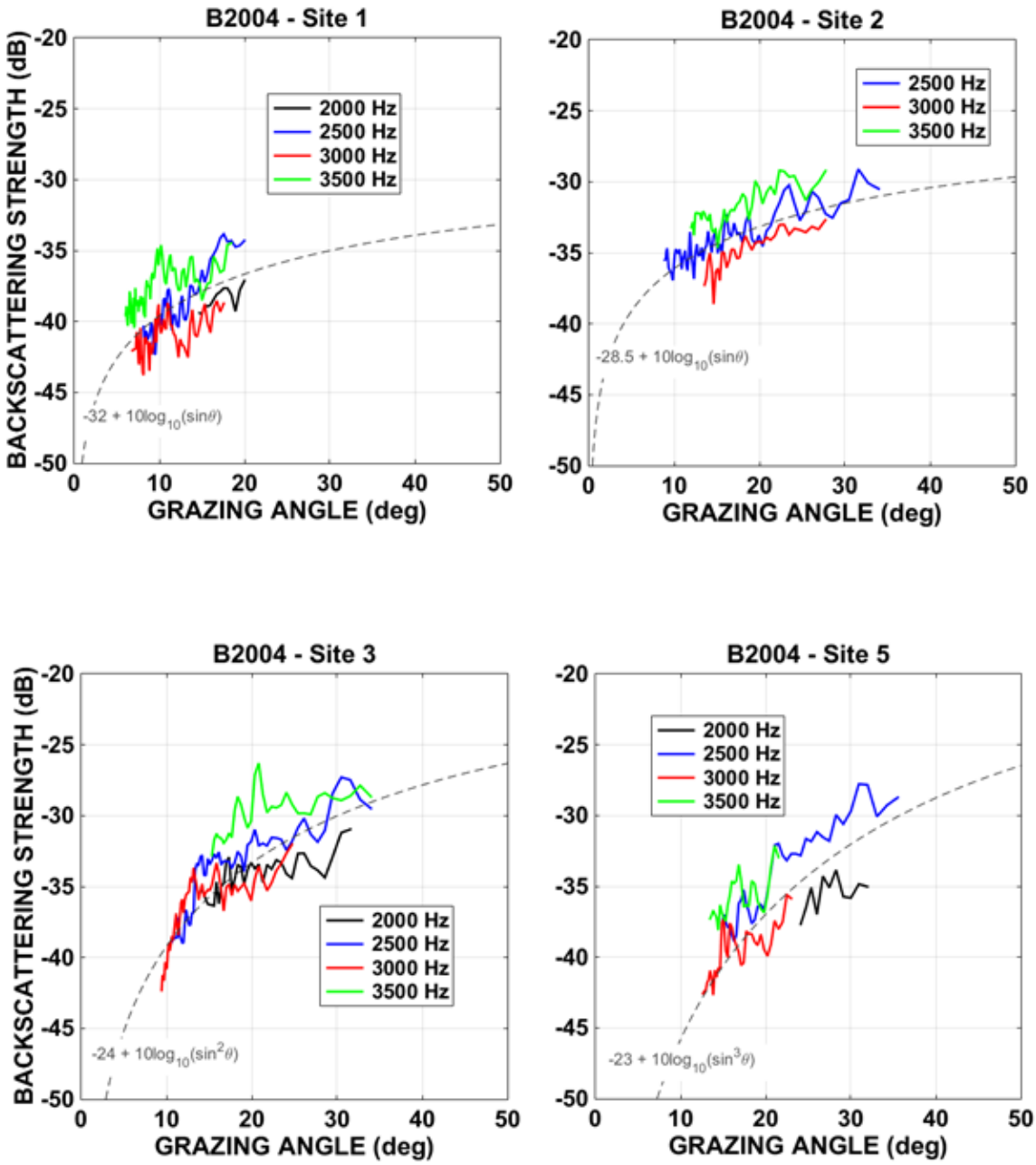

Fig. 4.B-5 – B2004 BBS vs. grazing angle at multiple frequencies for Sites 1, 2, 3, and 5. (EPL curves matched to the data trend (dashed) are also shown.)

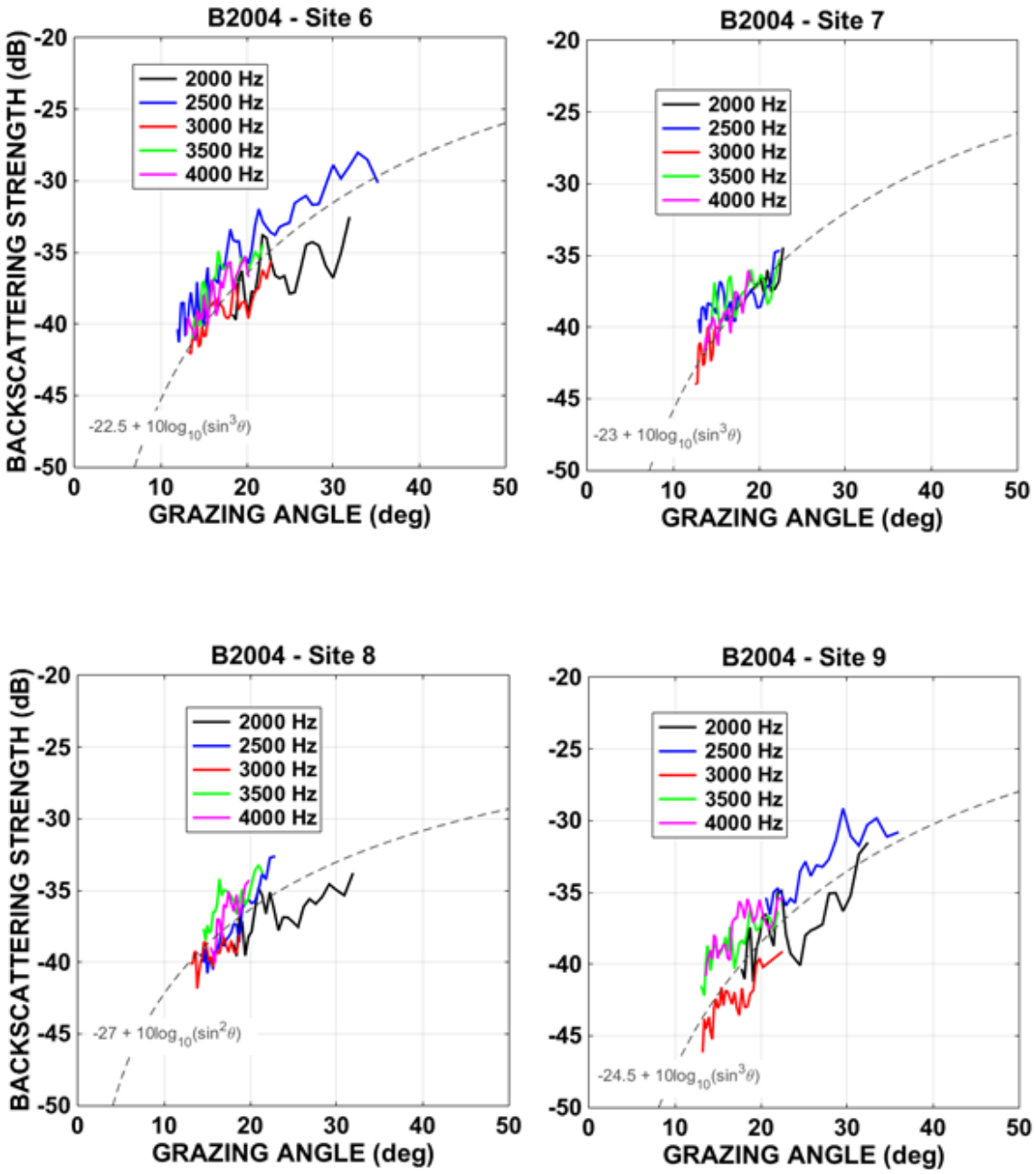

Fig. 4.B-6 – B2004 BBS vs. grazing angle at 5 frequencies for Sites 6, 7, 8, and 9.
(EPL curves matched to the data trend (dashed) are also shown.)

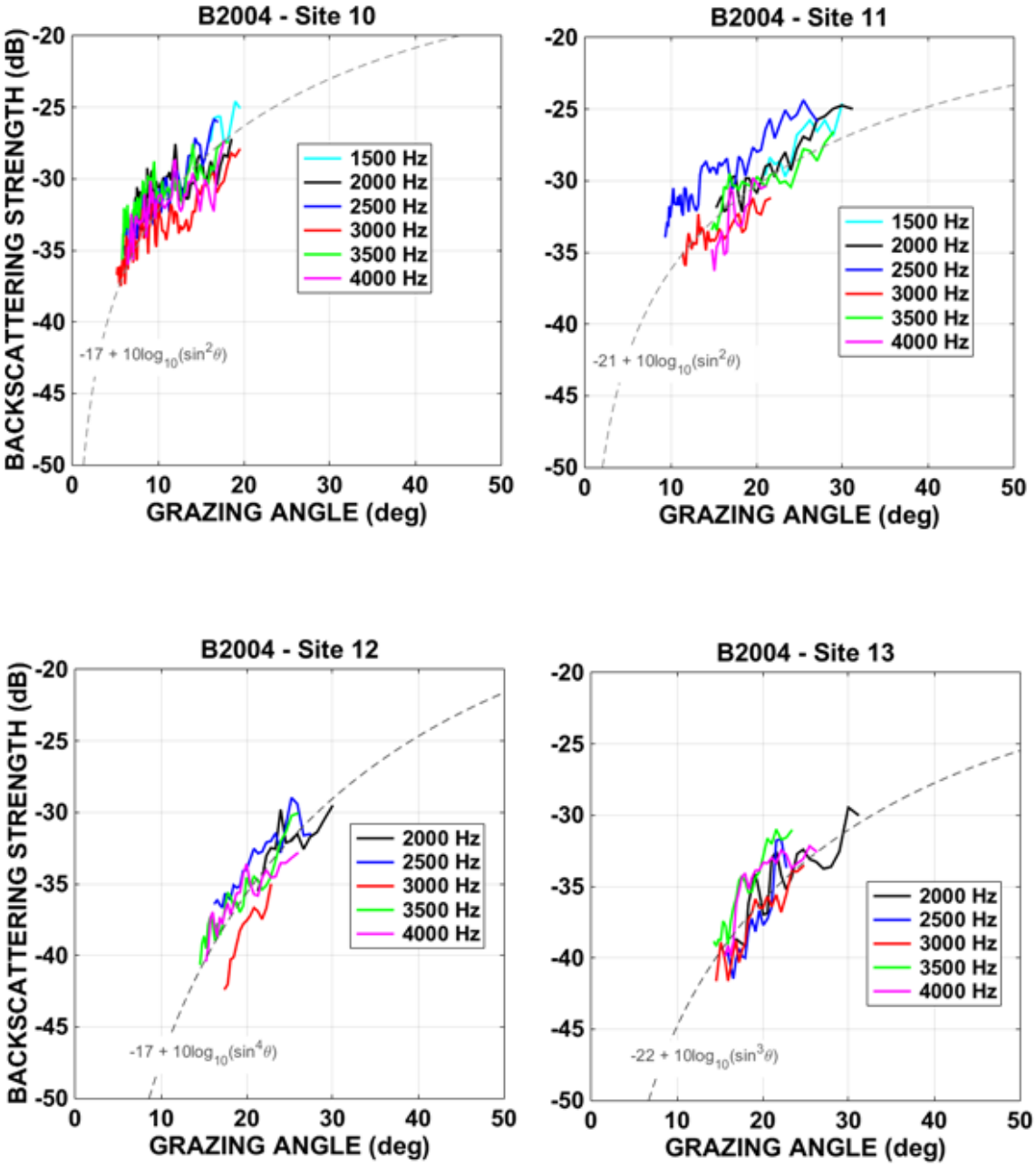

Fig. 4.B-7 – B2004 BBS vs. grazing angle at multiple frequencies for Sites 10, 11, 12, and 13. (EPL curves matched to the data trend (dashed) are also shown.)

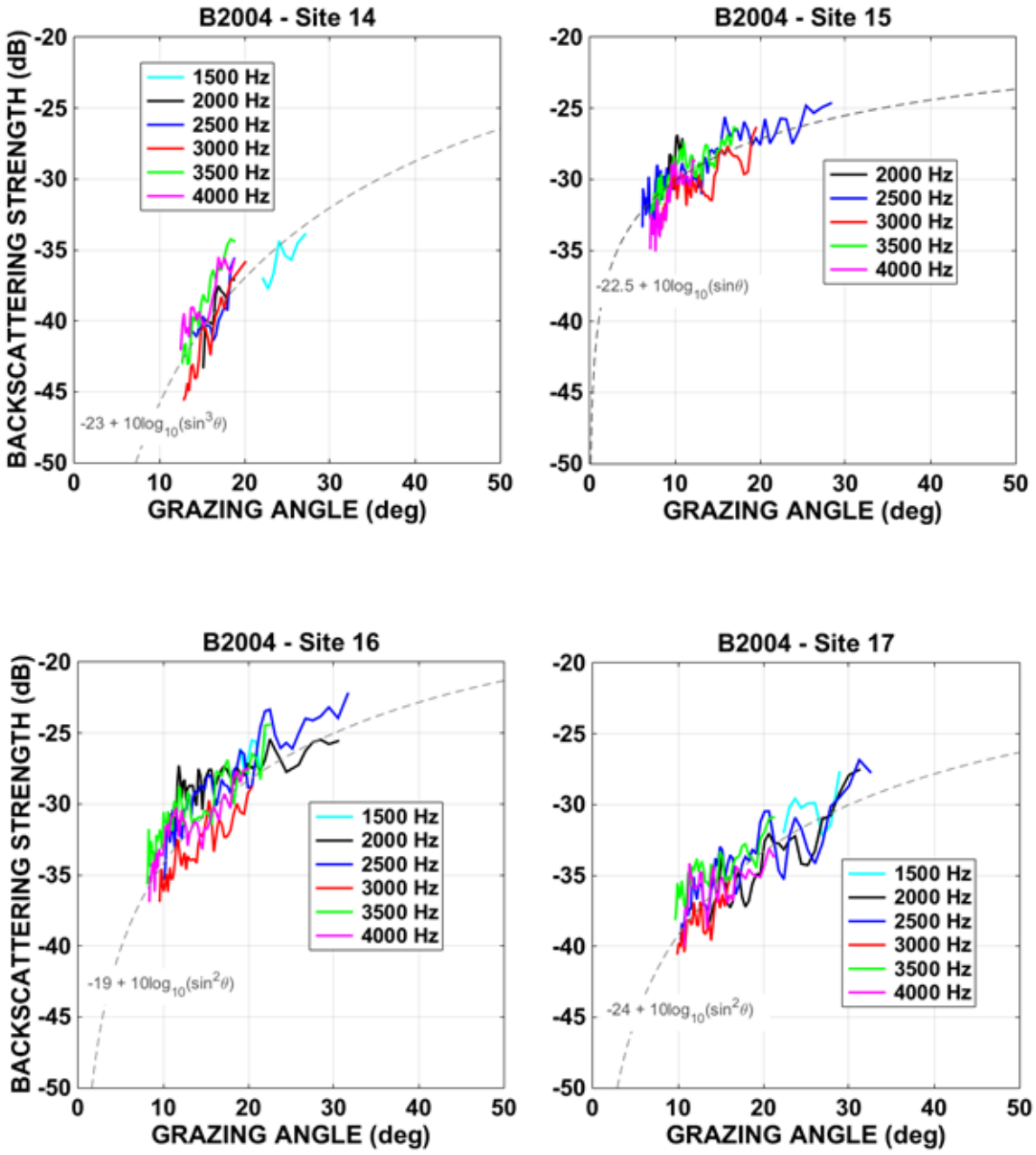

Fig. 4.B-8 – B2004 BBS vs. grazing angle at multiple frequencies for Sites 14, 15, 16, and 17. (EPL curves matched to the data trend (dashed) are also shown.)

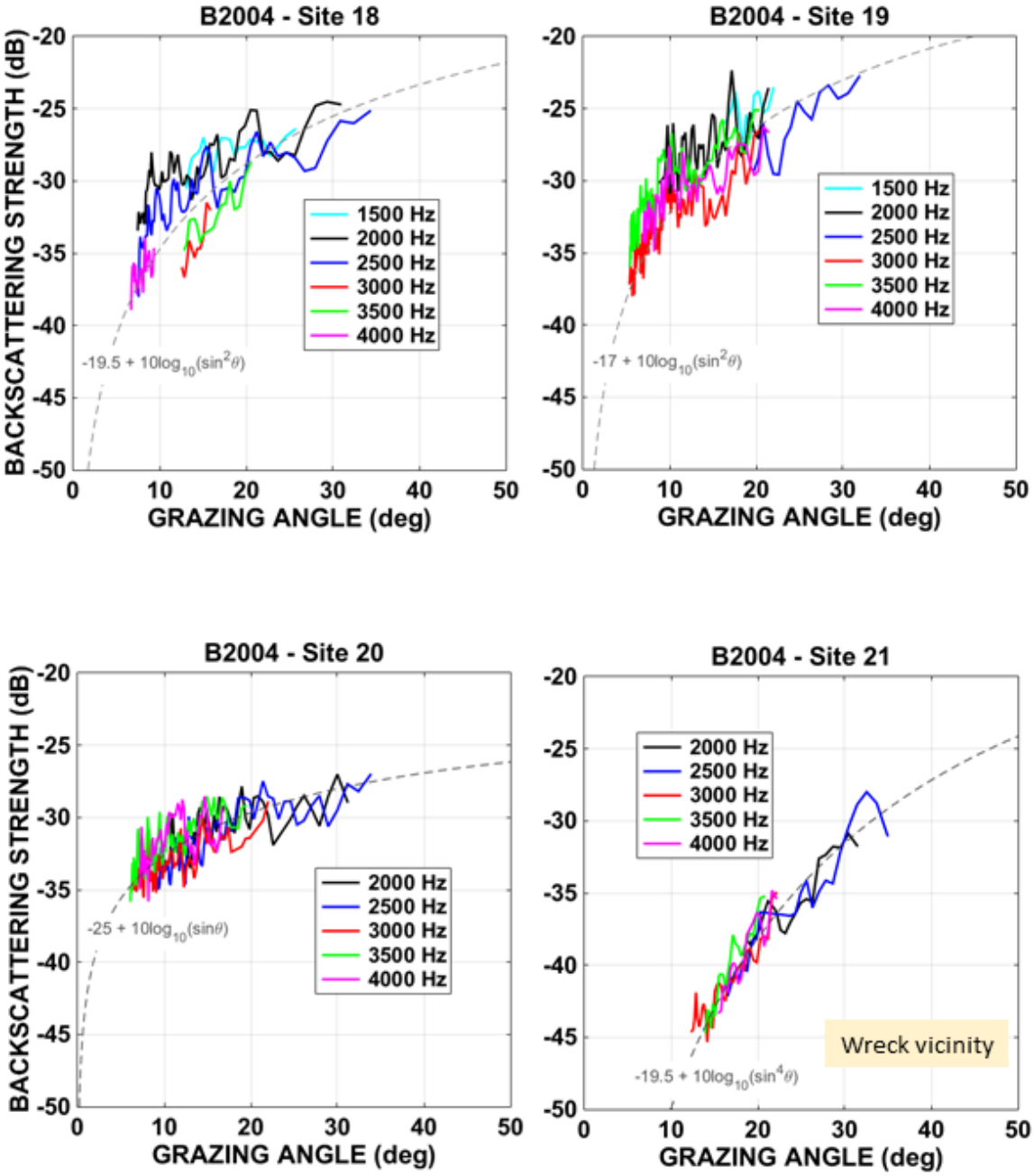

Fig. 4.B-9 – B2004 BBS vs. grazing angle at multiple frequencies for Sites 18, 19, 20, and 21. (EPL curves matched to the data trend (dashed) are also shown.)

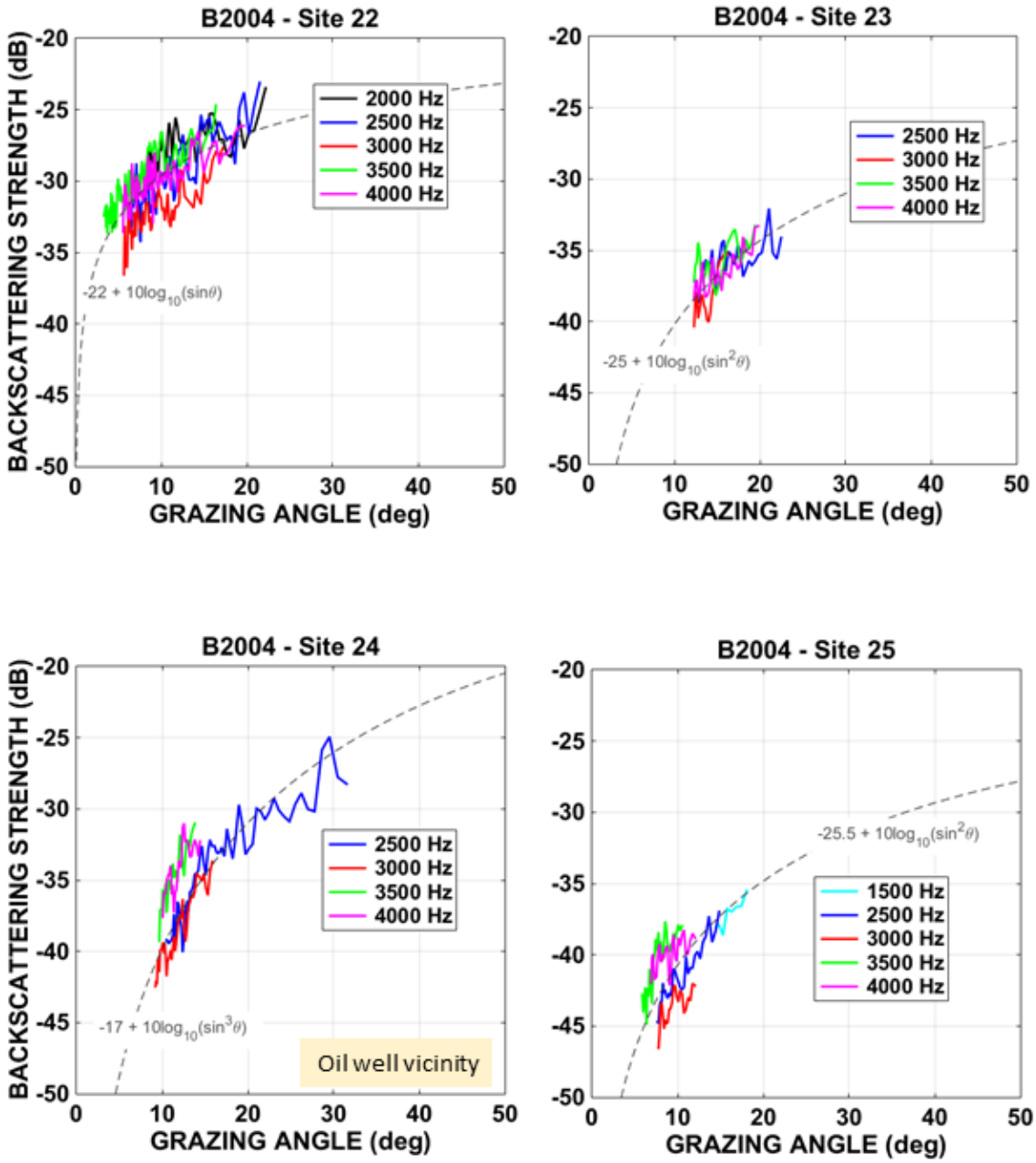

Fig. 4.B-10 – B2004 BBS vs. grazing angle at multiple frequencies for Sites 22, 23, 24, and 25. (EPL curves matched to the data trend (dashed) are also shown.)

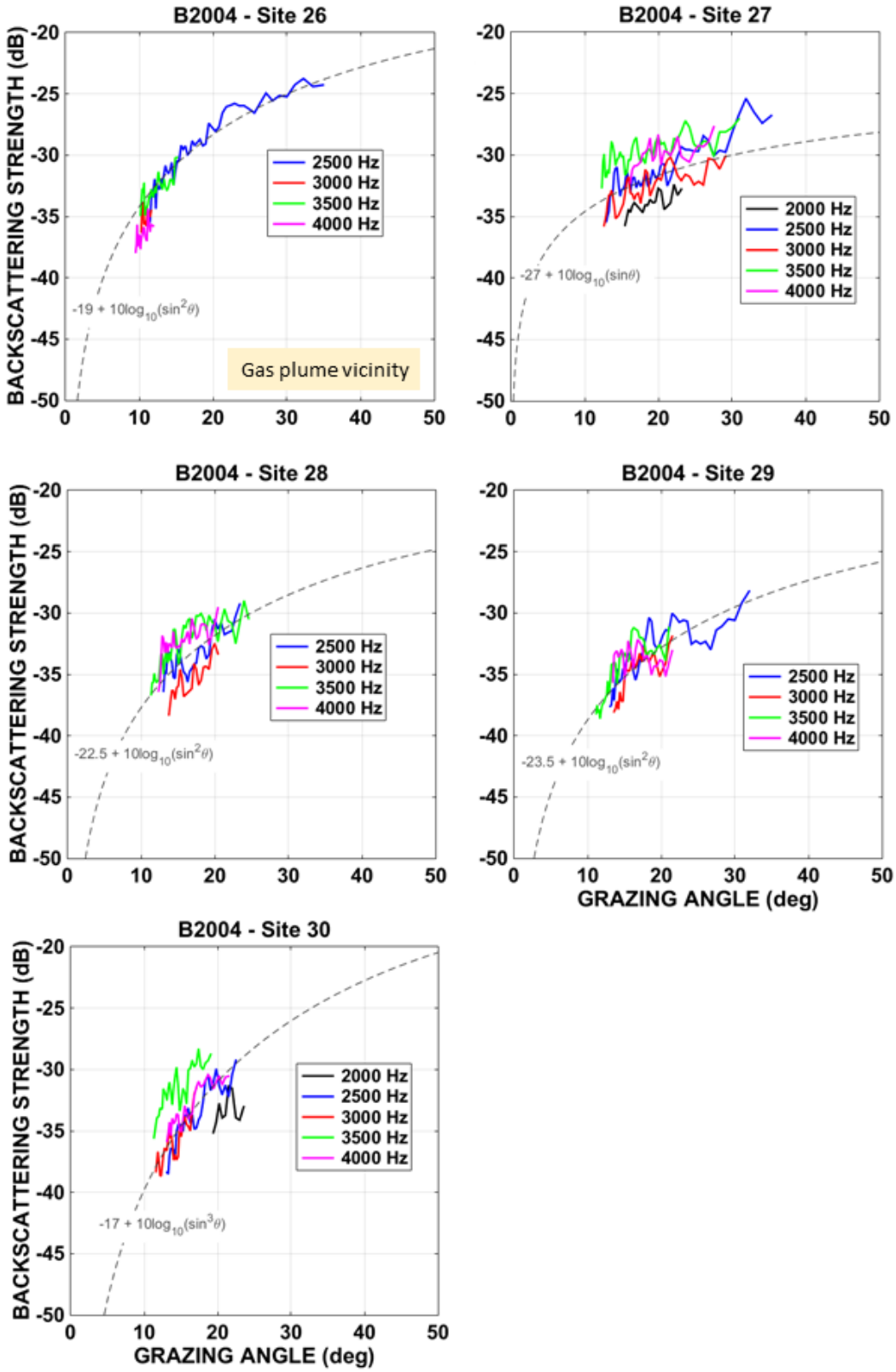

Fig. 4.B-11 – B2004 BBS vs. grazing angle at multiple frequencies for Sites 26, 27, 28, 29, and 30. (EPL curves matched to the data trend (dashed) are also shown.)

Combined B2002 and B2004 Results

Figures 4.B-12 and 4.B-13 show the best EPL-curve fit values to the B2002 and B2004 BBS vs. grazing angle curves.

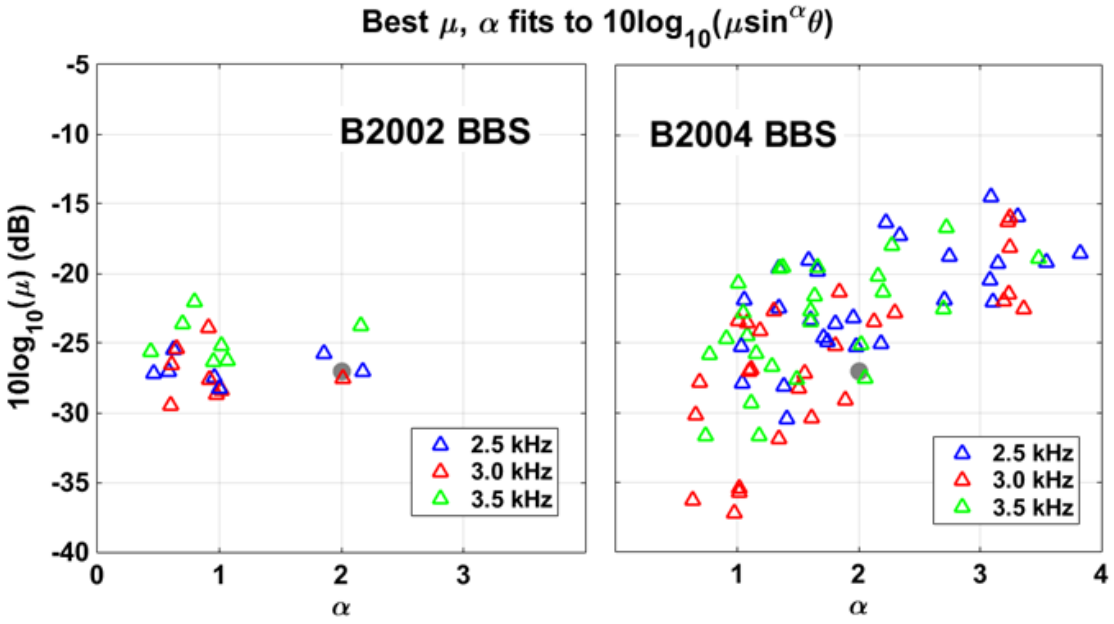

Fig. 4.B-12 – Distribution of best EPL-curve fit values to the B2002 (left) and B2004 (right) BBS vs. grazing angle curves at 3 frequencies.
(Mackenzie curve values (gray dot) shown as a reference.)

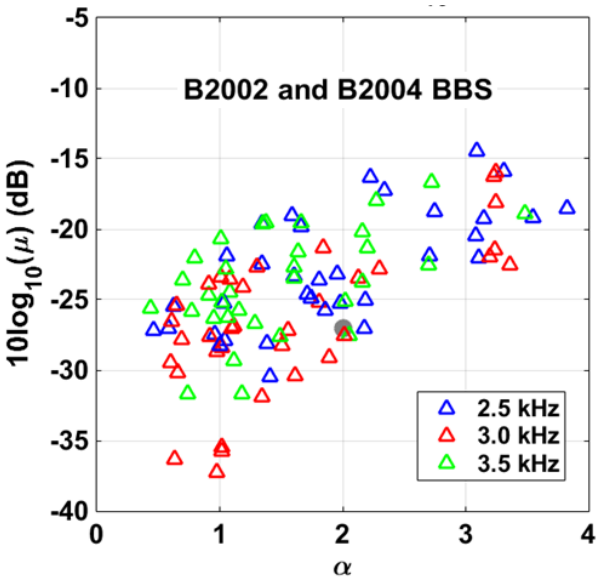

Fig. 4.B-13 – Distribution of best EPL-curve fit values to the combined B2002 and B2004 BBS vs. grazing angle curves at 3 frequencies.
(Mackenzie curve values (gray dot) shown as a reference.)

5. T-MAST 02 (SHALLOW WATER – STANTON BANKS)

NRL performed MF direct-path BBS measurements between 9 and 13 July 2002 at 16 sites (Figs. 5-1 and 5-2) on the Outer Hebrides Platform and the Stanton Banks (north of Ireland; west of Scotland) during the T-MAST 02 experiment. This section presents the BBS measurements from these shallow-water sites.

T-MAST 02 Bottom Scattering Sites

Site	Source / Receiver Depths (m)	Date (JD) Time (Z)	Latitude (deg N)	Longitude (deg E)	Water Depth (m)	Water Sound Speed at the Interface (m/s)
4	60 / 64 30 / 34	193 0454-0458 193 0504-0508	56.155 56° 9.27′	8.277 8° 16.59′	120	1493
5	30 / 34 70 / 74	191 0103-0107 191 0123-0127	56.237 56° 14.19′	8.451 8° 27.05′	150	1494
6	30 / 34 60 / 64	190 2255-2259 190 2310-2314	56.193 56° 11.59′	8.619 8° 37.13′	128	1494
7	30 / 34 70 / 74	192 0801-0805 192 0820-0824	56.280 56° 16.81′	8.402 8° 24.14′	133	1494
8	30 / 34 60 / 64	190 2105-2109 190 2120-2124	56.184 56° 11.03′	8.588 8° 35.30′	126	1493
9	30 / 34 70 / 74	190 1610-1614 190 1630-1634	56.032 56° 1.89′	8.227 8° 13.59′	155	1493
10	70 / 74 30 / 34	192 1511-1515 192 1524-1528	56.280 56° 16.79′	8.128 8° 7.67′	172	1494
11	60 / 64 30 / 34	193 0255-0259 193 0307-0311	56.228 56° 13.68′	8.144 8° 8.66′	164	1494
12	60 / 64 30 / 34	193 0048-0052 193 0104-0108	56.167 56° 10.03′	8.072 8° 4.35′	122	1494
13	70 / 74 30 / 34	193 0906-0910 193 0917-0921	56.027 56° 1.61′	8.458 8° 27.48′	141	1493
14	30 / 34 70 / 74	192 0950-0954 192 1008-1012	56.331 56° 19.85′	8.403 8° 24.15′	158	1494
15	60 / 64 30 / 34	192 2252-2256 192 2305-2309	56.187 56° 11.25′	8.028 8° 1.67′	121	1494
16	70 / 74 30 / 34	192 1713-1717 192 1725-1729	56.330 56° 19.82′	8.035 8° 2.09′	181	1494
17	30 / 34 70 / 74	192 1142-1146 192 1159-1203	56.302 56° 18.13′	8.236 8° 14.18′	130	1494
19	30 / 34 70 / 74	190 1408-1412 190 1427-1431	56.047 56° 2.84′	8.090 8° 5.37′	156	1493
20	60 / 64 30 / 34	192 1856-1900 192 1907-1911	56.219 56° 13.13′	8.002 8° 0.09′	116	1494

Fig. 5-1 – T-MAST02 BBS measurement and site information (Stanton Banks).

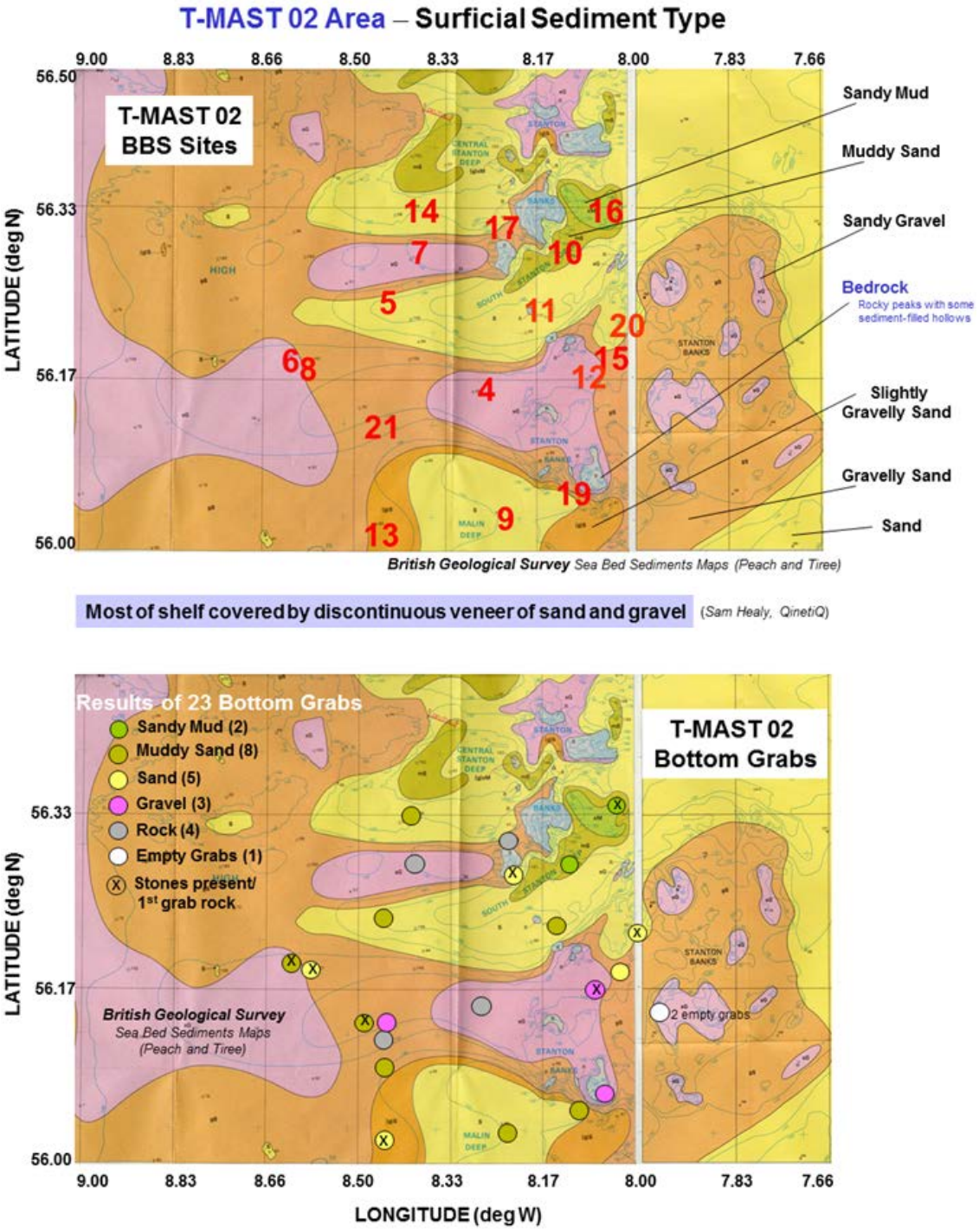

Fig. 5-2 – Geographic locations of T-MAST-02 BBS measurement (top) and bottom-grab (bottom) sites vs. both bathymetry and bottom type.

A. Test Operations

Direct-path, near-monostatic acoustic BBS measurements were conducted from the R/V *Knorr* using a 16-element VLA receiver cut for 5000 Hz and a single source. Measurements were made using combinations of 10-ms CWs at 8 frequencies (1.5, 2, 2.5, … , 5 kHz) and two 100-ms linear frequency modulated (LFM) signals, one sweeping 1.5 to 3 kHz and the other sweeping 3 to 4.5 kHz. (The LFM and 4–5 kHz CW results are not shown here.) Each CW signal was transmitted 18 times at a rep rate of 3 s. The T-MAST 02 source was a transducer (G81; 192 dB peak) usable over 1.5 to 5 kHz situated 4 m above the center of the VLA. Measurements were made at two source depths (30 m and between 50 and 70 m) at each site. The sonar equation was used at each depth to derive bottom backscattering strengths as a function of beam, frequency, and grazing angle.

B. Measured Bottom Backscattering Strengths

Figures 5.B-1–5.B-5 show frequency-dependent bottom backscattering strengths measured at the 16 shallow-water T-MAST-02 sites. Figure 5.B-6 shows the best EPL-curve fit values to the T-MAST-02 BBS vs. grazing angle curves.

In Figs. 5.B-2–5.B-5 British Geological Survey (BGS) bottom type (Fig. 5-2) and bottom-grab information (Sect. 5.C) also shown, (No grab information for Sites 7, 13 and 17 other than they either contained all large rocks or were primarily rocks with little soil.) The BGS and bottom-grab (Fig. 5-2) key used in Figs. 5.B-2–5.B-5 is:

R = rock; SG = sandy gravel; GS = gravelly sand; SGS = slightly GS
S = sand; MS = muddy sand; M = mud

Grab info. Surficial grain size provides a measure of surficial sediment properties and is given in logarithmic units by $-3.32\log_{10}(d/d_0)$ where d is the mean grain size ('diameter'), and d_0 is the reference length of 1 mm. Units are denoted ϕ (phi). See Sect. 5.C for more details. A measure of the width of a sample's grain-size distribution is given by the sorting, which in the T-MAST-02 grain-size analysis was the Inman sorting S.

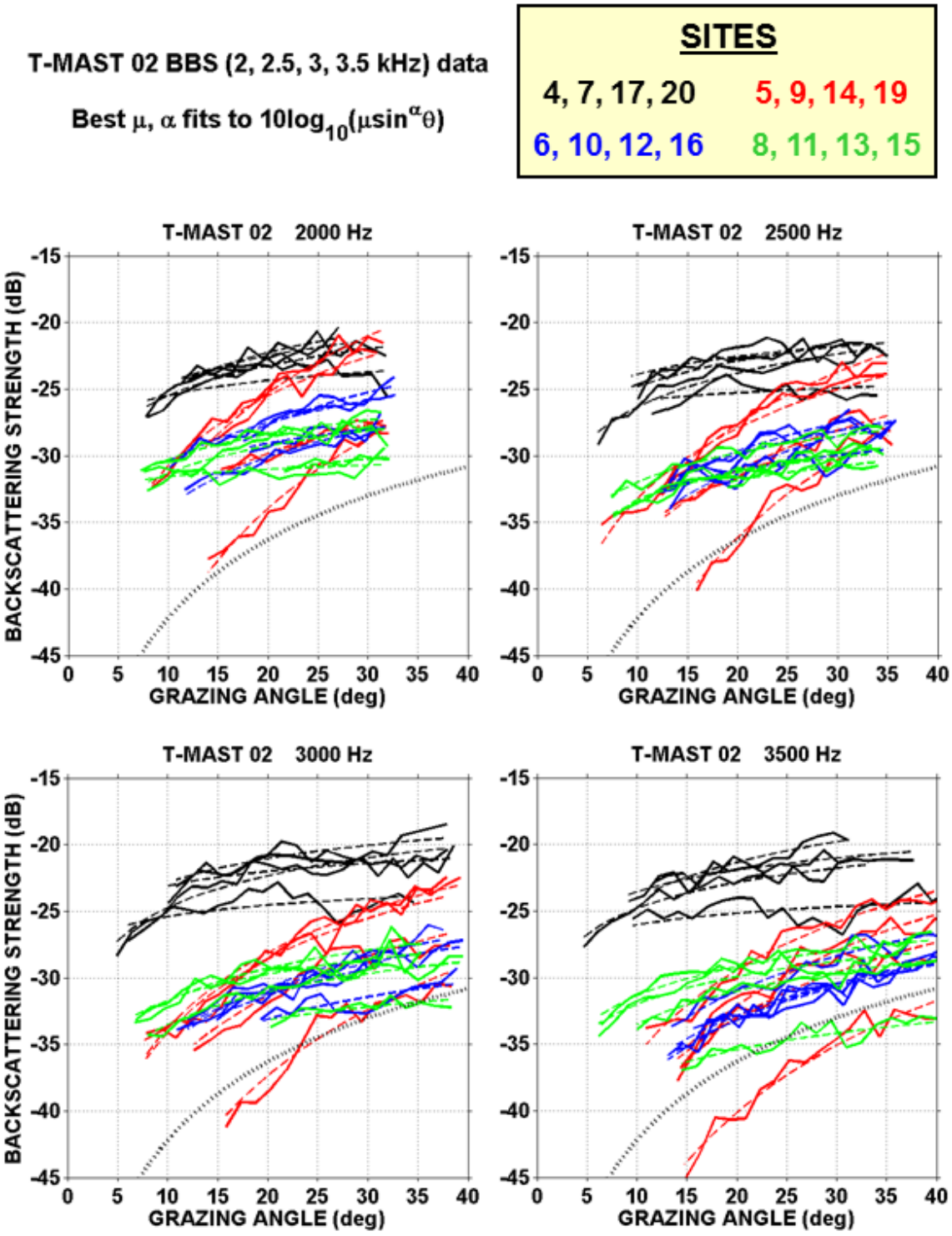

Fig. 5.B-1 – T-MAST-02 BBS vs. grazing angle at 4 frequencies for all sites along with individual EPL fits (color-coded just to help visually separate the 16 sites). (Mackenzie curve (dotted) shown as a reference.)

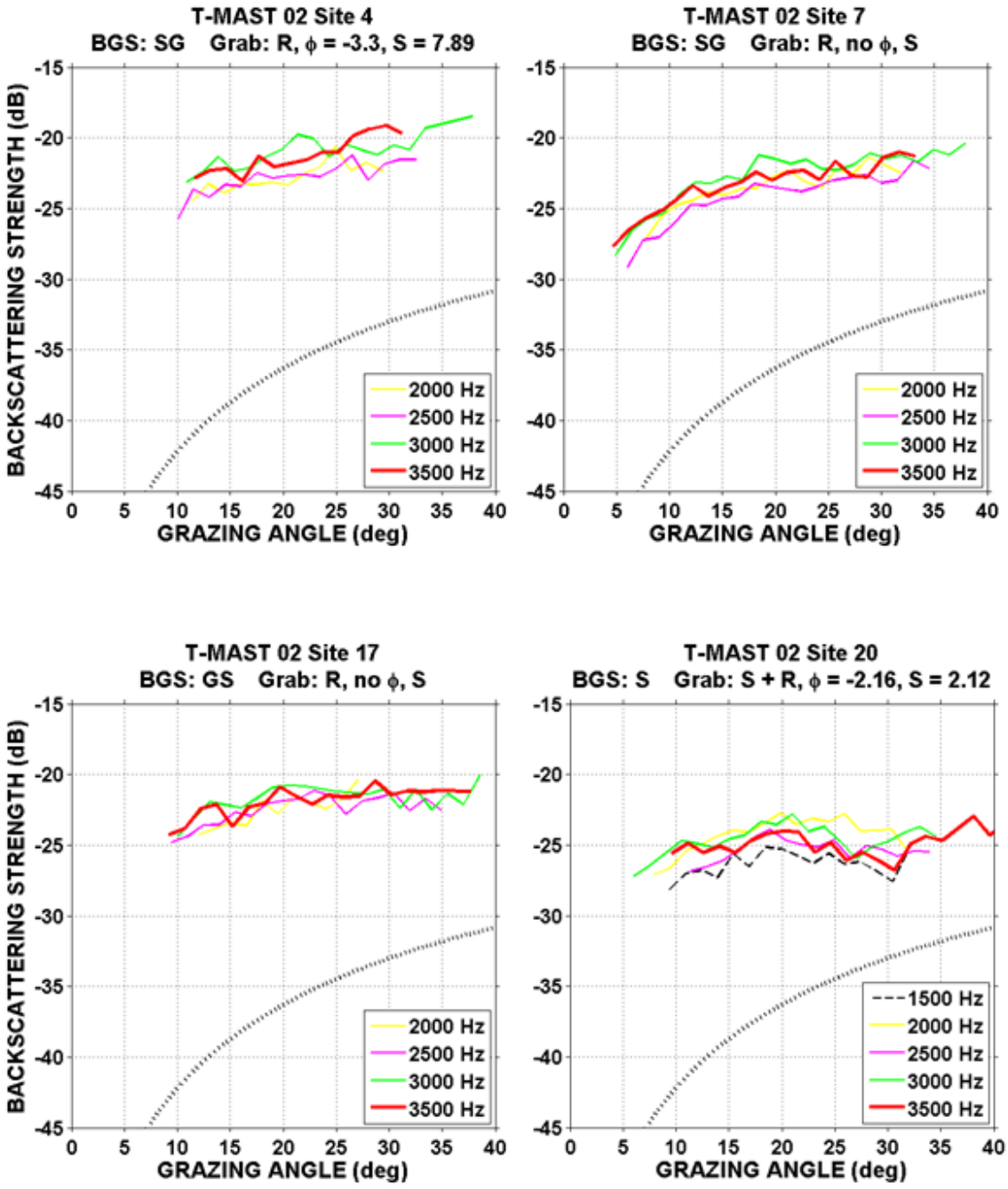

Fig. 5.B-2 – T-MAST-02 BBS vs. grazing angle at multiple frequencies for Sites 4, 7, 17, and 20. Each site's BGS-type and grab info shown atop its plot.
(Mackenzie curve (dotted) shown as a reference.)

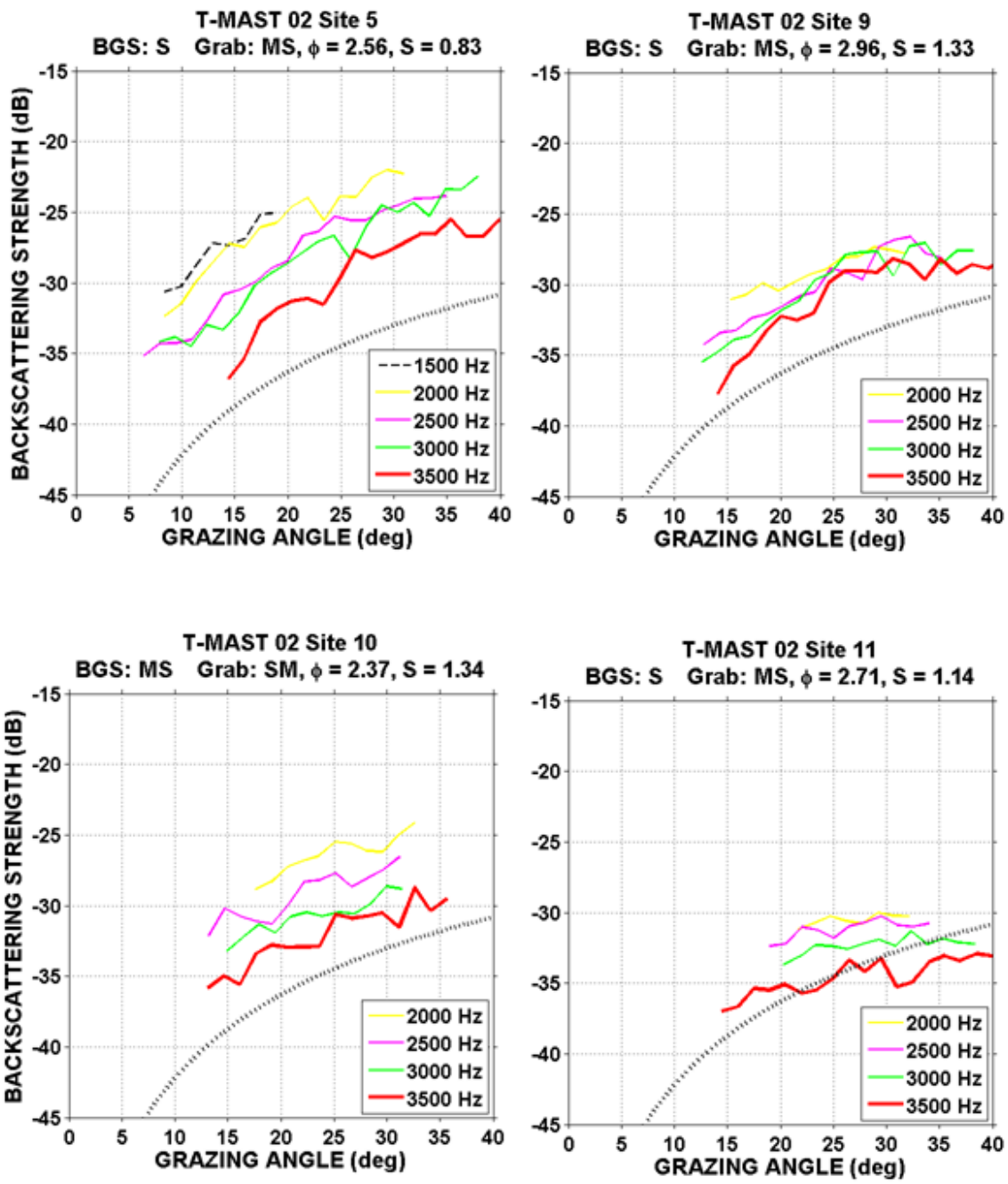

Fig. 5.B-3 – T-MAST-02 BBS vs. grazing angle at multiple frequencies for Sites 5, 9, 10, and 11. Each site's BGS-type and grab info shown atop its plot.
(Mackenzie curve (dotted) shown as a reference.)

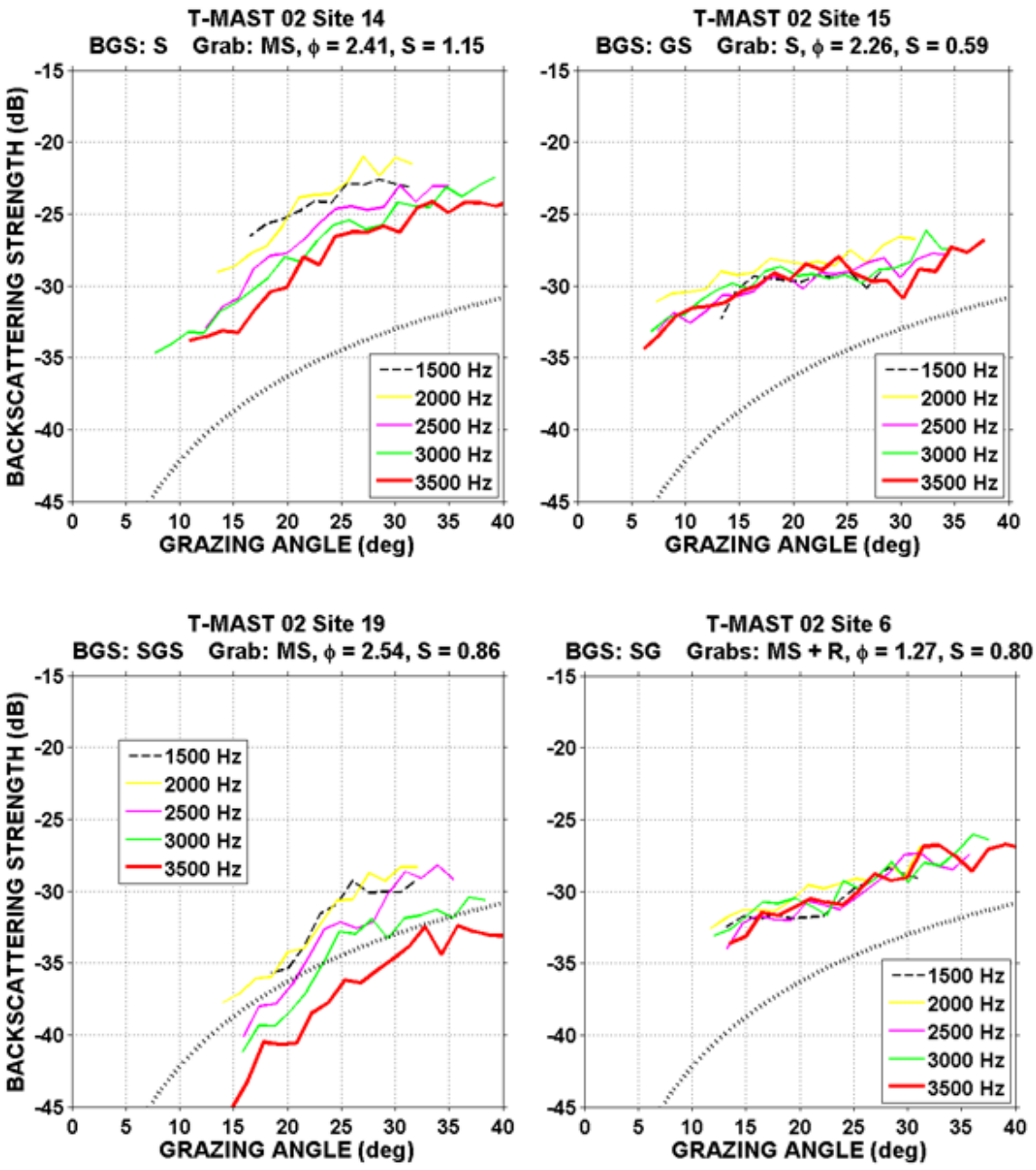

Fig. 5.B-4 – T-MAST-02 BBS vs. grazing angle at 5 frequencies for Sites 14, 15, 19, and 6. Each site's BGS-type and grab info shown atop its plot. (Mackenzie curve (dotted) shown as a reference.)

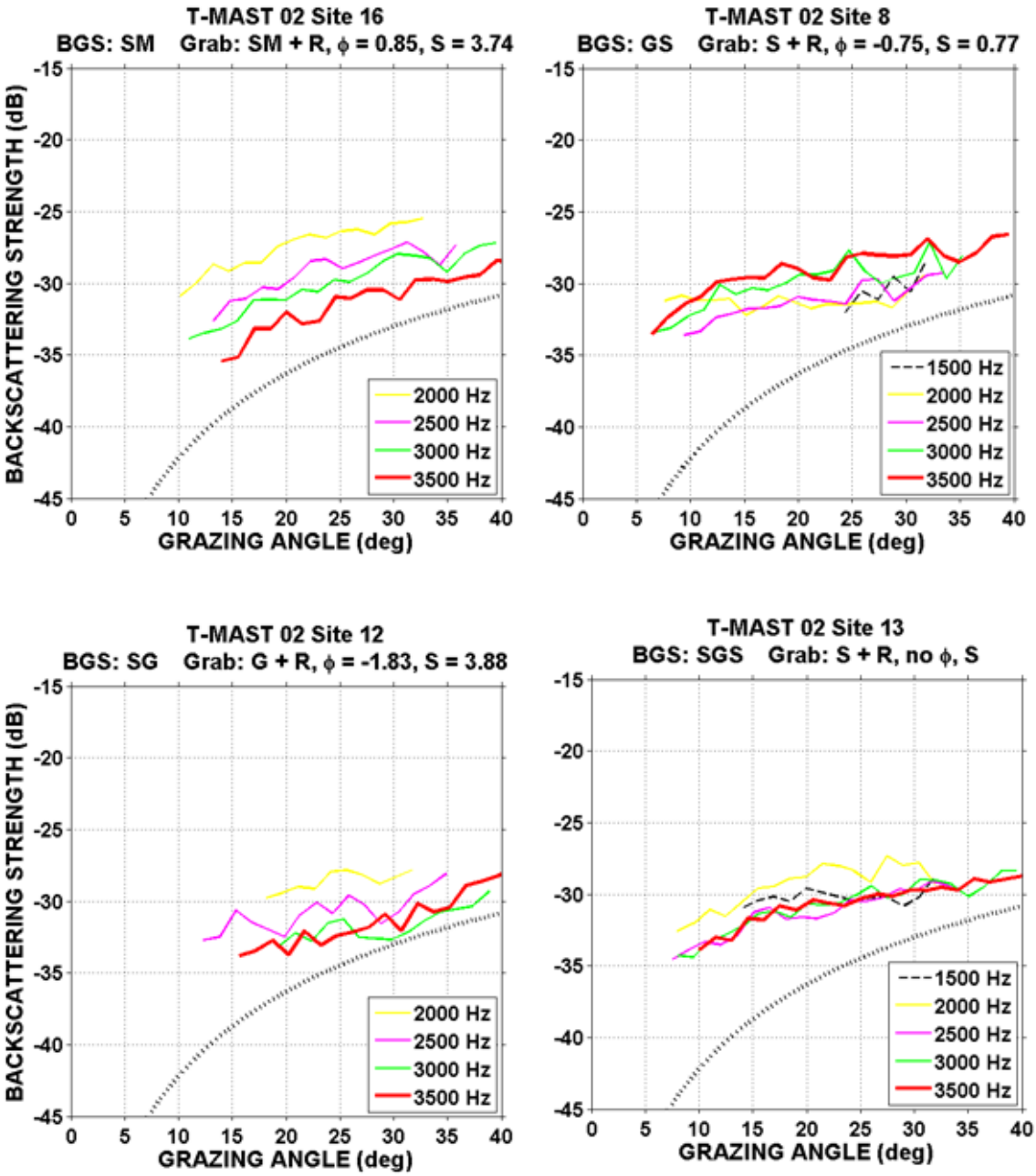

Fig. 5.B-5 – T-MAST-02 BBS vs. grazing angle at multiple frequencies for Sites 16, 8, 12, and 13. Each site's BGS-type and grab info shown atop its plot. (Mackenzie curve (dotted) shown as a reference.)

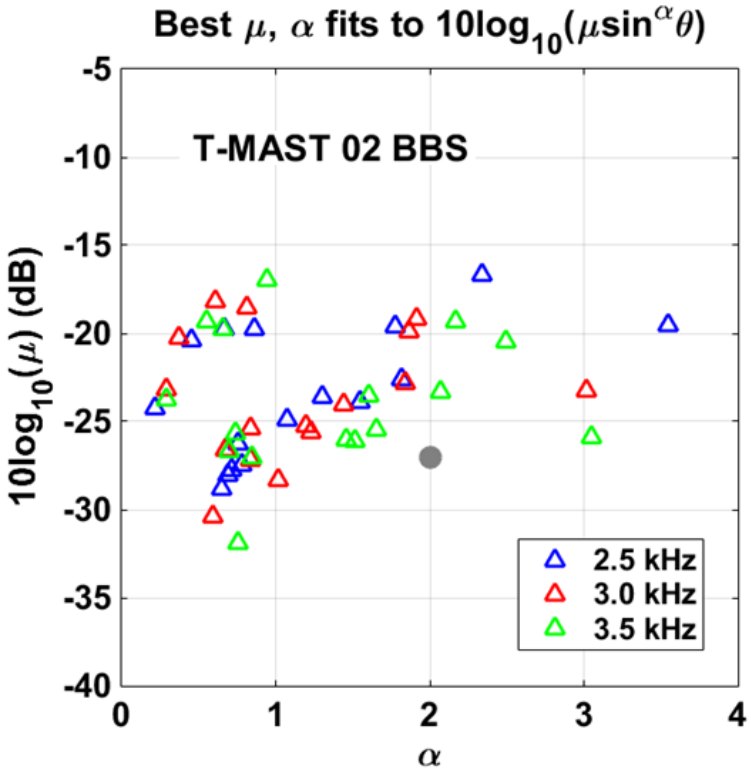

Fig. 5.B-6 – Distribution of best EPL-curve fit values to the T-MAST-02 BBS vs. grazing angle curves at 3 frequencies. (Mackenzie curve values (gray dot) shown as a reference.)

C. *In-Situ* Bottom Grabs

Figures 5.C-1–5.C-13 show bottom grab analysis corresponding to 13 of the 16 BBS sites. Sites 4, 7, and 17 were all large rocks and not analyzed, and Site 20 consisted of primarily rocks with a little soil---these 4 BBS sites did not undergo grain-size analysis; however, a grab was made near Site 4 (Fig. 5.C-1), so that is used as a surrogate for Site 4.

Sediment-sample phi values can range from –12 (hard) to 14 (soft); e.g., cobble ranges from –6 to –8 ϕ, and clay from 8 to 14 ϕ. (See Table 4.1 of Jackson and Richardson, 2007.) At high frequencies (10–100 kHz), surficial grain size has been found to be a useful sediment descriptor. Geoacoustic relationships have been developed between ϕ and the sediment-water density ratio, sediment sound-speed ratio and loss parameters, and sediment spectral parameters. See Jackson and Richardson (2007) for details. However, at T-MAST-02 frequencies (1.5–5 kHz), due to deeper acoustic penetration of transmitted acoustic energy, it is unclear that surficial grain size will necessarily be a useful seafloor descriptor for BBS prediction.

T-MAST 02
Grain-Size Analysis

near Site 4

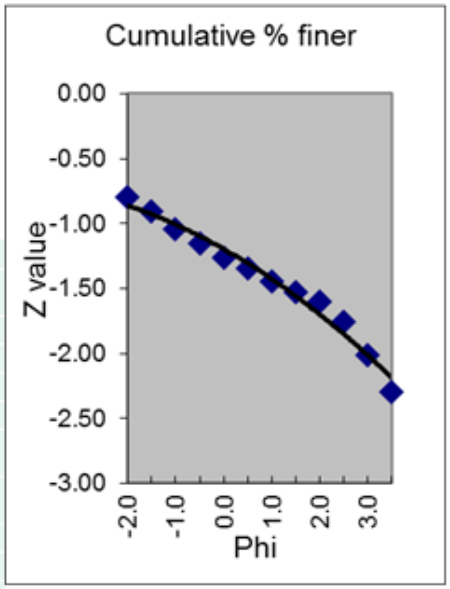

Grain Size Analysis

RV2 Mooring	56.0969 -8.4545		All weights in grams		
14-Nov-2002	Date (dd-month-yyyy)				
Barrios	Analyst				
9.91	mean grain size D50 (mm)		-3.309	D50 (phi)	
-3.31	mean grain size D50 (phi)		-14.74	D84 (phi)	
27375.500	D84 (mm)		1.034	D16 (phi)	
0.488	D16 (mm)				
7.89	sorting (phi84-phi16)/2 (Inman)				

mm	phi	wt (g)	wt (%)	% finer	Z	gross (g)	tare (g)
8.000	-3.0	0.00	0.0	100.0	3.50		
4.000	-2.00	33.60	78.8	21.2	-0.80	89.05	55.45
2.828	-1.50	1.28	3.0	18.2	-0.91	52.13	50.85
2.000	-1.00	1.43	3.4	14.8	-1.04	51.3	49.87
1.414	-0.50	0.98	2.3	12.5	-1.15	47.8	46.82
1.000	0.00	0.90	2.1	10.4	-1.26	46.35	45.45
0.707	0.50	0.63	1.5	8.9	-1.34	44.53	43.9
0.500	1.00	0.66	1.5	7.4	-1.45	41.48	40.82
0.354	1.50	0.43	1.0	6.4	-1.52	39.41	38.98
0.250	2.00	0.39	0.9	5.5	-1.60	36.62	36.23
0.177	2.50	0.63	1.5	4.0	-1.75	36.09	35.46
0.125	3.00	0.75	1.8	2.2	-2.01	35.28	34.53
0.088	3.50	0.49	1.1	1.1	-2.30	34.03	33.54
0.062	4.00	0.46	1.1	0.0	-3.50	6.94	6.48
<0.062	>4.00	0.00	0.0	0.0	-3.50	0	0
		42.63	100.0			561.01	518.38

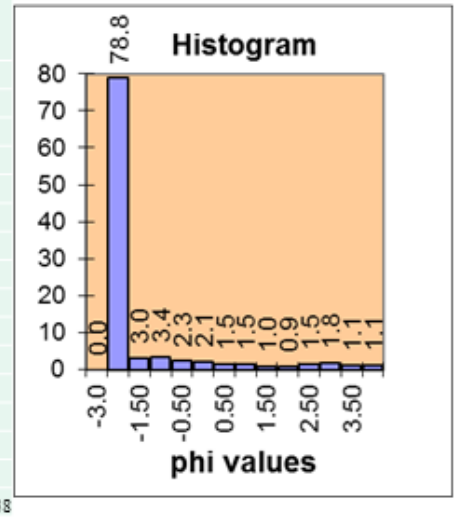

Analysis note: RV2 Mooring consisted of big rocks and mud.
Dried and weighed only the mud.

The grain-size analyses of T-MAST 02 sediment samples were performed (for ONR) by Anna Barrios and Tony Clark, Department of Marine, Earth and Atmospheric Sciences, North Carolina State University

Fig. 5.C-1 – Grain-size analysis for bottom grab sample *near* T-MAST-02 Site 4.

T-MAST 02
Grain-Size Analysis

Site 5

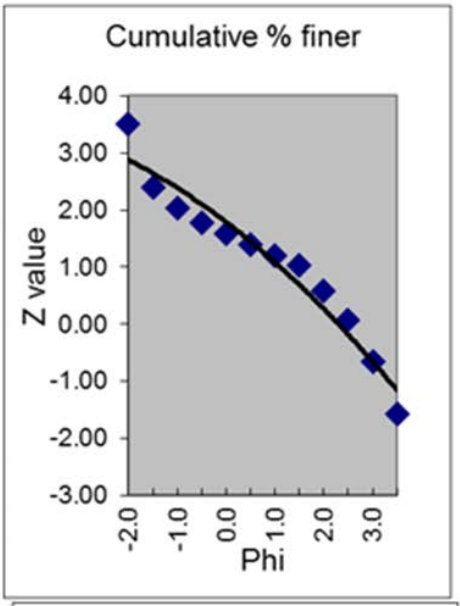

Grain Size Analysis

BSS # 5	56.2364 -8.4572			All weights in grams			
14-Nov-2002	Date (dd-month-yyyy)						
Barrios	Analyst						
0.17	mean grain size D50 (mm)				2.563 D50 (phi)		
2.56	mean grain size D50 (phi)				1.579 D84 (phi)		
0.335	D84 (mm)				3.232 D16 (phi)		
0.106	D16 (mm)						
0.83	sorting (phi84-phi16)/2 (Inman)						
mm	phi	wt (g)	wt (%)	% finer	Z	gross (g)	tare (g)
8.000	-3.0	0.00	0.0	100.0	3.50		
4.000	-2.00	0.00	0.0	100.0	3.50	55.44	55.44
2.828	-1.50	0.17	0.8	99.2	2.40	51.02	50.85
2.000	-1.00	0.27	1.3	97.9	2.03	50.13	49.86
1.414	-0.50	0.35	1.7	96.2	1.77	47.17	46.82
1.000	0.00	0.39	1.9	94.3	1.58	45.85	45.46
0.707	0.50	0.53	2.6	91.7	1.38	44.43	43.9
0.500	1.00	0.66	3.2	88.5	1.20	41.49	40.83
0.354	1.50	0.76	3.7	84.8	1.03	39.76	39
0.250	2.00	2.70	13.1	71.7	0.57	38.94	36.24
0.177	2.50	3.93	19.1	52.6	0.06	39.4	35.47
0.125	3.00	5.59	27.2	25.4	-0.66	40.12	34.53
0.088	3.50	4.03	19.6	5.8	-1.57	37.57	33.54
0.062	4.00	1.19	5.8	0.0	-3.50	7.67	6.48
<0.062	>4.00	0.00	0.0	0.0	-3.50	0	0
		20.57	100.0			538.99	518.42

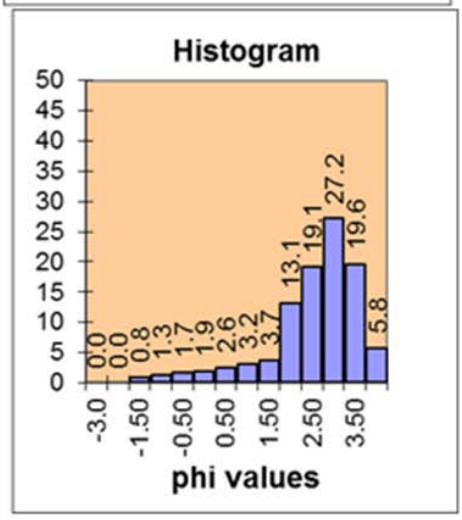

The grain-size analyses of T-MAST 02 sediment samples were performed (for ONR) by Anna Barrios and Tony Clark, Department of Marine, Earth and Atmospheric Sciences, North Carolina State University

Fig. 5.C-2 – Grain-size analysis for bottom grab sample at T-MAST-02 Site 5.

T-MAST 02
Grain-Size Analysis

Site 6

Grain Size Analysis							
BSS # 6	56.1916	-8.6203	All weights in grams				
14-Nov-2002	Date (dd-month-yyyy)						
Barrios	Analyst						
0.42	mean grain size D50 (mm)				1.266	D50 (phi)	
1.27	mean grain size D50 (phi)				0.374	D84 (phi)	
0.772	D84 (mm)				1.975	D16 (phi)	
0.254	D16 (mm)						
0.80	sorting (phi84-phi16)/2 (Inman)						
mm	phi	wt (g)	wt (%)	% finer	Z	gross (g)	tare (g)
8.000	-3.0	0.00	0.0	100.0	3.50		
4.000	-2.00	0.17	0.8	99.2	2.41	55.62	55.45
2.828	-1.50	0.40	1.9	97.4	1.94	51.26	50.86
2.000	-1.00	0.21	1.0	96.4	1.80	50.07	49.86
1.414	-0.50	0.32	1.5	94.9	1.64	47.14	46.82
1.000	0.00	1.13	5.2	89.7	1.26	46.6	45.47
0.707	0.50	1.67	7.7	81.9	0.91	45.56	43.89
0.500	1.00	4.56	21.1	60.8	0.27	45.4	40.84
0.354	1.50	5.14	23.8	37.0	-0.33	44.13	38.99
0.250	2.00	5.09	23.6	13.4	-1.11	41.33	36.24
0.177	2.50	2.22	10.3	3.1	-1.86	37.69	35.47
0.125	3.00	0.60	2.8	0.4	-2.68	35.13	34.53
0.088	3.50	0.07	0.3	0.0	-3.31	33.6	33.53
0.062	4.00	0.01	0.0	0.0	-3.50	6.49	6.48
<0.062	>4.00	0.00	0.0	0.0	-3.50	0	0
		21.59	100.0			540.02	518.43

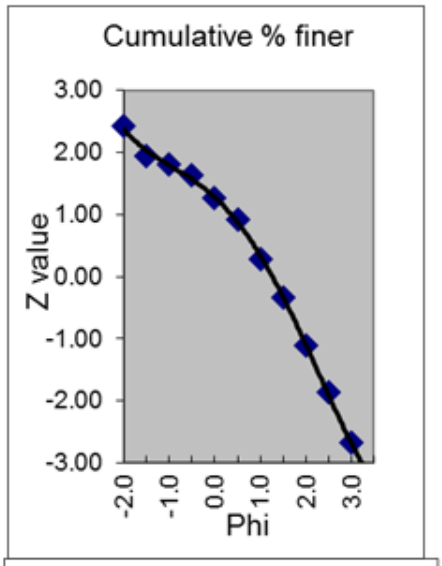

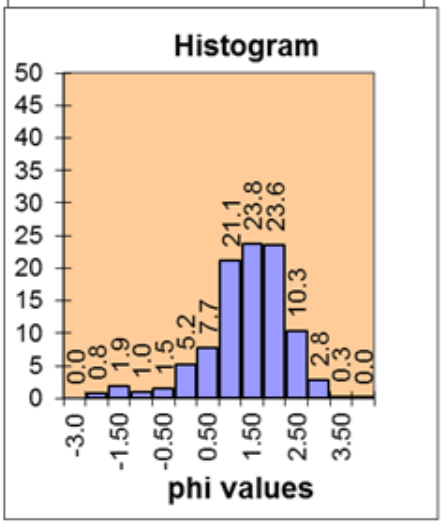

The grain-size analyses of T-MAST 02 sediment samples were performed (for ONR) by Anna Barrios and Tony Clark, Department of Marine, Earth and Atmospheric Sciences, North Carolina State University

Fig. 5.C-3 – Grain-size analysis for bottom grab sample at T-MAST-02 Site 6.

T-MAST 02
Grain-Size Analysis

Site 8

Grain Size Analysis							
BBS # 8	Sample			All weights in grams			
14-Nov-2002	Date (dd-month-yyyy)						
Barrios	Analyst						
1.68	mean grain size D50 (mm)				-0.748	D50 (phi)	
-0.75	mean grain size D50 (phi)				-1.195	D84 (phi)	
2.290	D84 (mm)				0.351	D16 (phi)	
0.784	D16 (mm)						
0.77	sorting (phi84-phi16)/2 (Inman)						
mm	phi	wt (g)	wt (%)	% finer	Z	gross (g)	tare (g)
8.000	-3.0	0.00	0.0	100.0	3.50		
4.000	-2.00	3.55	14.3	85.7	1.07	59.04	55.49
2.828	-1.50	0.20	0.8	84.9	1.03	51.06	50.86
2.000	-1.00	0.51	2.1	82.8	0.95	50.38	49.87
1.414	-0.50	0.90	3.6	79.2	0.81	47.73	46.83
1.000	0.00	3.30	13.3	65.9	0.41	48.77	45.47
0.707	0.50	5.67	22.8	43.1	-0.17	49.58	43.91
0.500	1.00	7.24	29.2	13.9	-1.08	48.08	40.84
0.354	1.50	2.34	9.4	4.5	-1.70	41.33	38.99
0.250	2.00	0.80	3.2	1.2	-2.24	37.03	36.23
0.177	2.50	0.21	0.8	0.4	-2.65	35.68	35.47
0.125	3.00	0.07	0.3	0.1	-3.03	34.6	34.53
0.088	3.50	0.02	0.1	0.0	-3.35	33.55	33.53
0.062	4.00	0.01	0.0	0.0	-3.50	6.49	6.48
<0.062	>4.00	0.00	0.0	0.0	-3.50	0	0
		24.82	100.0			543.32	518.50

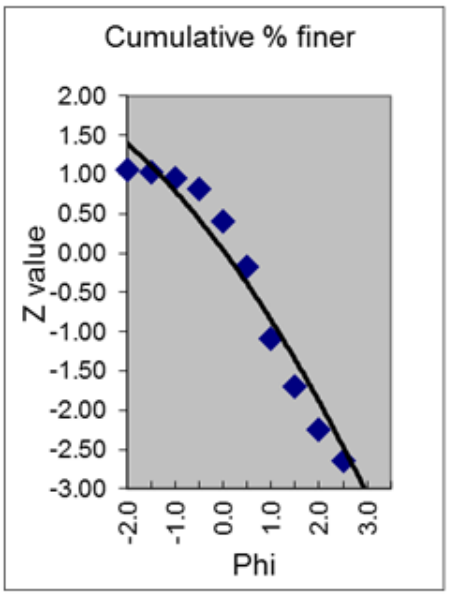

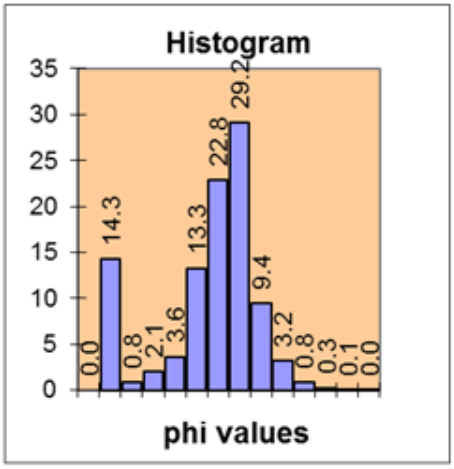

Analysis note: BSS 8 had 3 mid-sized rocks in it with a little soil

The grain-size analyses of T-MAST 02 sediment samples were performed (for ONR) by Anna Barrios and Tony Clark, Department of Marine, Earth and Atmospheric Sciences, North Carolina State University

Fig. 5.C-4 – Grain-size analysis for bottom grab sample at T-MAST-02 Site 8.

T-MAST 02
Grain-Size Analysis

Site 9

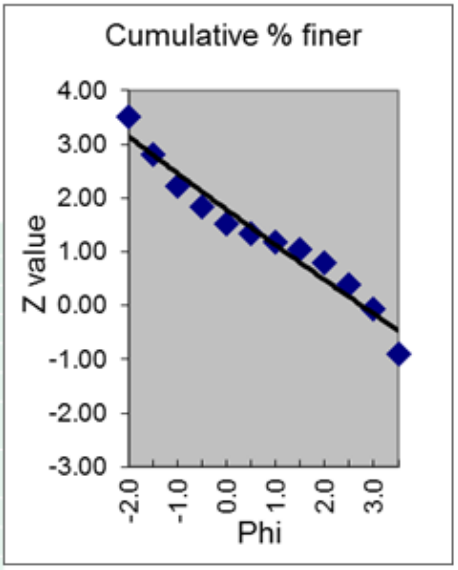

Grain Size Analysis							
BSS # 9	56.0348 -8.2317			All weights in grams			
14-Nov-2002	Date (dd-month-yyyy)						
Barrios	Analyst						
0.13	mean grain size D50 (mm)				2.957	D50 (phi)	
2.96	mean grain size D50 (phi)				0.9	D84 (phi)	
0.536	D84 (mm)				3.56	D16 (phi)	
0.085	D16 (mm)						
1.33	sorting (phi84-phi16)/2 (Inman)						
mm	phi	wt (g)	wt (%)	% finer	Z	gross (g)	tare (g)
8.000	-3.0	0.00	0.0	100.0	3.50		
4.000	-2.00	0.00	0.0	100.0	3.50	55.44	55.44
2.828	-1.50	0.06	0.2	99.8	2.81	50.92	50.86
2.000	-1.00	0.25	1.0	98.7	2.23	50.12	49.87
1.414	-0.50	0.51	2.1	96.6	1.83	47.33	46.82
1.000	0.00	0.70	2.9	93.7	1.53	46.17	45.47
0.707	0.50	0.68	2.8	90.9	1.33	44.58	43.9
0.500	1.00	0.72	3.0	87.9	1.17	41.55	40.83
0.354	1.50	0.64	2.6	85.3	1.05	39.63	38.99
0.250	2.00	1.51	6.2	79.0	0.81	37.75	36.24
0.177	2.50	3.39	14.0	65.0	0.39	38.87	35.48
0.125	3.00	4.16	17.2	47.8	-0.05	38.66	34.5
0.088	3.50	7.10	29.4	18.4	-0.90	40.71	33.61
0.062	4.00	4.46	18.4	0.0	-3.50	10.94	6.48
<0.062	>4.00	0.00	0.0	0.0	-3.50	0	0
		24.18	100.0			542.67	518.49

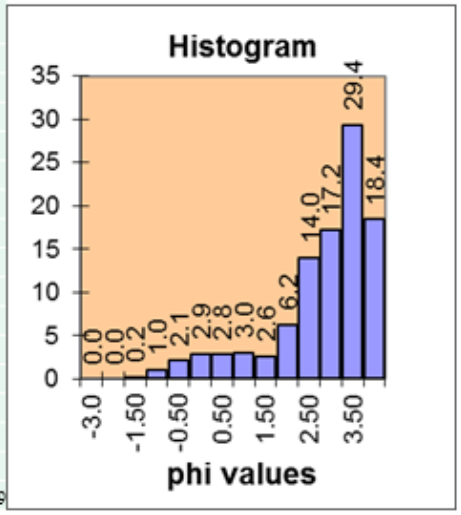

The grain-size analyses of T-MAST 02 sediment samples were performed (for ONR) by Anna Barrios and Tony Clark, Department of Marine, Earth and Atmospheric Sciences, North Carolina State University

Fig. 5.C-5 – Grain-size analysis for bottom grab sample at T-MAST-02 Site 9.

T-MAST 02
Grain-Size Analysis

Site 10

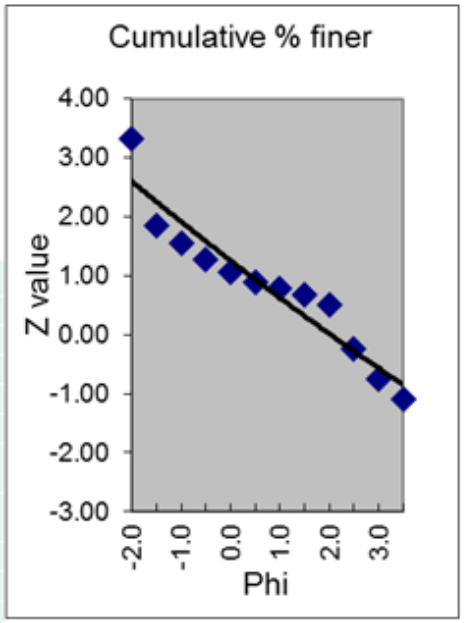

Grain Size Analysis							
BSS # 10	56.2857 -8.1197			All weights in grams			
14-Nov-2002	Date (dd-month-yyyy)						
Barrios	Analyst						
0.19	mean grain size D50 (mm)				2.368	D50 (phi)	
2.37	mean grain size D50 (phi)				0.664	D84 (phi)	
0.631	D84 (mm)				3.345	D16 (phi)	
0.098	D16 (mm)						
1.34	sorting (phi84-phi16)/2 (Inman)						
mm	phi	wt (g)	wt (%)	% finer	Z	gross (g)	tare (g)
8.000	-3.0	0.00	0.0	100.0	3.50		
4.000	-2.00	0.01	0.0	100.0	3.33	55.45	55.44
2.828	-1.50	0.74	3.2	96.8	1.85	51.59	50.85
2.000	-1.00	0.66	2.8	93.9	1.55	50.52	49.86
1.414	-0.50	0.95	4.1	89.8	1.27	47.77	46.82
1.000	0.00	1.04	4.5	85.3	1.05	46.5	45.46
0.707	0.50	0.94	4.1	81.3	0.89	44.85	43.91
0.500	1.00	0.69	3.0	78.3	0.78	41.5	40.81
0.354	1.50	0.69	3.0	75.3	0.69	39.67	38.98
0.250	2.00	1.46	6.3	69.1	0.50	37.69	36.23
0.177	2.50	6.65	28.7	40.4	-0.24	42.14	35.49
0.125	3.00	4.17	18.0	22.4	-0.76	38.71	34.54
0.088	3.50	2.05	8.8	13.6	-1.10	35.59	33.54
0.062	4.00	3.15	13.6	0.0	-3.50	9.63	6.48
<0.062	>4.00	0.00	0.0	0.0	-3.50	0	0
		23.20	100.0			541.61	518.41

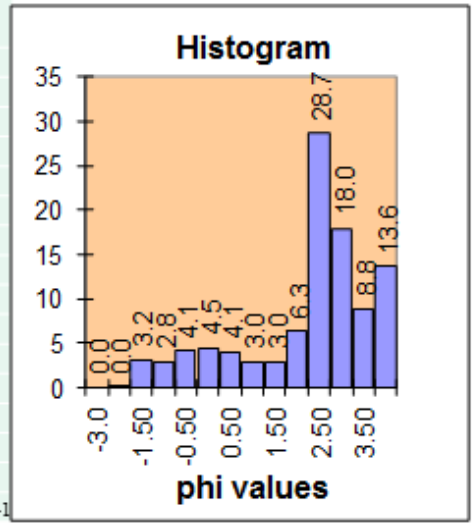

The grain-size analyses of T-MAST 02 sediment samples were performed (for ONR) by Anna Barrios and Tony Clark, Department of Marine, Earth and Atmospheric Sciences, North Carolina State University

Fig. 5.C-6 – Grain-size analysis for bottom grab sample at T-MAST-02 Site 10.

T-MAST 02
Grain-Size Analysis

Site 11

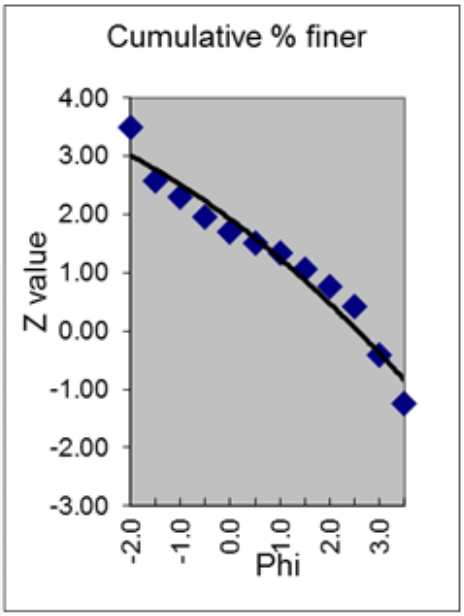

Grain Size Analysis							
BSS # 11	56.2280 -8.1443			All weights in grams			
14-Nov-2002	Date (dd-month-yyyy)						
Barrios	Analyst						
0.15	mean grain size D50 (mm)				2.71	D50 (phi)	
2.71	mean grain size D50 (phi)				1.085	D84 (phi)	
0.471	D84 (mm)				3.356	D16 (phi)	
0.098	D16 (mm)						
1.14	sorting (phi84-phi16)/2 (Inman)						
mm	phi	wt (g)	wt (%)	% finer	Z	gross (g)	tare (g)
8.000	-3.0	0.00	0.0	100.0	3.50		
4.000	-2.00	0.00	0.0	100.0	3.50	55.44	55.44
2.828	-1.50	0.10	0.5	99.5	2.58	50.95	50.85
2.000	-1.00	0.12	0.6	98.9	2.30	49.98	49.86
1.414	-0.50	0.30	1.5	97.4	1.95	47.13	46.83
1.000	0.00	0.37	1.8	95.6	1.71	45.83	45.46
0.707	0.50	0.44	2.2	93.4	1.51	44.35	43.91
0.500	1.00	0.52	2.6	90.9	1.33	41.44	40.92
0.354	1.50	1.08	5.3	85.5	1.06	40.18	39.1
0.250	2.00	1.53	7.6	78.0	0.77	37.77	36.24
0.177	2.50	2.33	11.5	66.5	0.43	37.8	35.47
0.125	3.00	6.56	32.4	34.1	-0.41	41.09	34.53
0.088	3.50	4.73	23.3	10.8	-1.24	38.27	33.54
0.062	4.00	2.18	10.8	0.0	-3.50	8.66	6.48
<0.062	>4.00	0.00	0.0	0.0	-3.50	0	0
		20.26	100.0			538.89	518.63

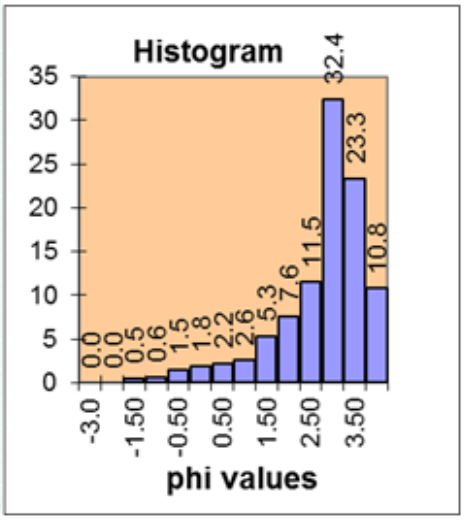

The grain-size analyses of T-MAST 02 sediment samples were performed (for ONR) by Anna Barrios and Tony Clark, Department of Marine, Earth and Atmospheric Sciences, North Carolina State University

Fig. 5.C-7 – Grain-size analysis for bottom grab sample at T-MAST-02 Site 11.

T-MAST 02
Grain-Size Analysis

Site 12

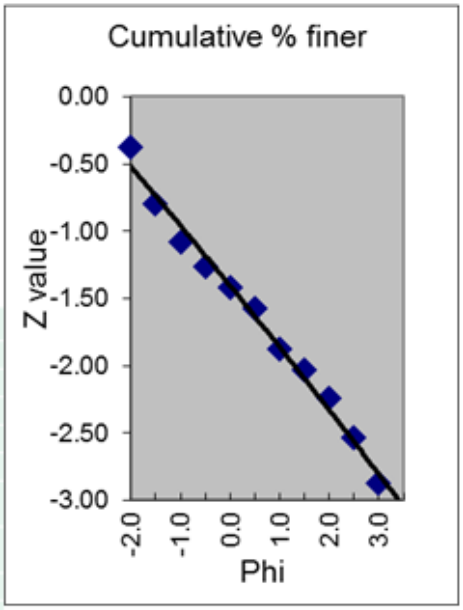

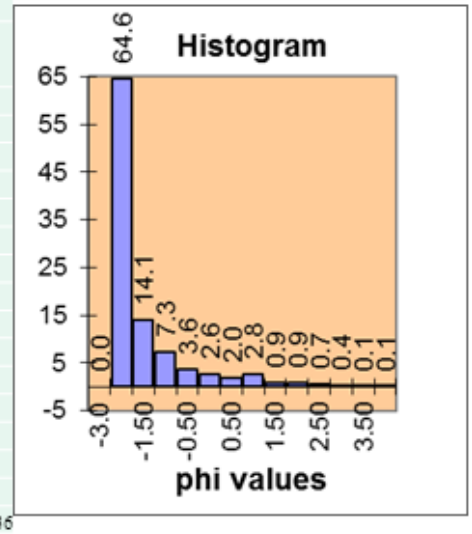

Grain Size Analysis

BSS # 12	56.1672 -8.0725		All weights in grams				
14-Nov-2002	Date (dd-month-yyyy)						
Barrios	Analyst						
3.56	mean grain size D50 (mm)				-1.831	D50 (phi)	
-1.83	mean grain size D50 (phi)				-7.892	D84 (phi)	
237.577	D84 (mm)				-0.125	D16 (phi)	
1.090	D16 (mm)						
3.88	sorting (phi84-phi16)/2 (Inman)						

mm	phi	wt (g)	wt (%)	% finer	Z	gross (g)	tare (g)
8.000	-3.0	0.00	0.0	100.0	3.50		
4.000	-2.00	31.33	64.6	35.4	-0.37	86.78	55.45
2.828	-1.50	6.83	14.1	21.3	-0.80	57.68	50.85
2.000	-1.00	3.53	7.3	14.0	-1.08	53.39	49.86
1.414	-0.50	1.75	3.6	10.4	-1.26	48.57	46.82
1.000	0.00	1.27	2.6	7.8	-1.42	46.72	45.45
0.707	0.50	0.97	2.0	5.8	-1.57	44.87	43.9
0.500	1.00	1.34	2.8	3.0	-1.88	42.17	40.83
0.354	1.50	0.45	0.9	2.1	-2.03	39.43	38.98
0.250	2.00	0.42	0.9	1.2	-2.25	36.65	36.23
0.177	2.50	0.33	0.7	0.6	-2.54	35.79	35.46
0.125	3.00	0.17	0.4	0.2	-2.87	34.69	34.52
0.088	3.50	0.05	0.1	0.1	-3.08	33.58	33.53
0.062	4.00	0.05	0.1	0.0	-3.50	6.53	6.48
<0.062	>4.00	0.00	0.0	0.0	-3.50	0	0
		48.49	100.0			566.85	518.36

The grain-size analyses of T-MAST 02 sediment samples were performed (for ONR) by Anna Barrios and Tony Clark, Department of Marine, Earth and Atmospheric Sciences, North Carolina State University

Fig. 5.C-8 – Grain-size analysis for bottom grab sample at T-MAST-02 Site 12.

T-MAST 02
Grain-Size Analysis

Site 14

Grain Size Analysis							
BSS # 14	56.3345 -8.3993			All weights in grams			
14-Nov-2002	Date (dd-month-yyyy)						
Barrios	Analyst						linear fit
0.19	mean grain size D50 (mm)				2.414	D50 (phi)	-2>phi>+3
2.41	mean grain size D50 (phi)				1.018	D84 (phi)	-2>phi>+2
0.494	D84 (mm)				3.317	D16 (phi)	0>phi>+3.5
0.100	D16 (mm)						
1.15	sorting (phi84-phi16)/2 (Inman)						
mm	phi	wt (g)	wt (%)	% finer	Z	gross (g)	tare (g)
8.000	-3.0	0.00	0.0	100.0	3.50		
4.000	-2.00	0.00	0.0	100.0	3.50	55.45	55.45
2.828	-1.50	0.06	0.3	99.7	2.74	50.92	50.86
2.000	-1.00	0.21	1.1	98.6	2.20	50.07	49.86
1.414	-0.50	0.40	2.0	96.6	1.82	47.22	46.82
1.000	0.00	0.55	2.8	93.8	1.54	46.02	45.47
0.707	0.50	0.47	2.4	91.4	1.36	44.36	43.89
0.500	1.00	0.72	3.7	87.7	1.16	41.53	40.81
0.354	1.50	0.77	3.9	83.8	0.98	39.75	38.98
0.250	2.00	2.23	11.4	72.4	0.59	38.48	36.25
0.177	2.50	4.78	24.4	48.0	-0.05	40.28	35.5
0.125	3.00	3.86	19.7	28.2	-0.58	38.41	34.55
0.088	3.50	3.41	17.4	10.8	-1.24	36.95	33.54
0.062	4.00	2.12	10.8	0.0	-3.50	8.6	6.48
<0.062	>4.00	0.00	0.0	0.0	-3.50	0	0
		19.58	100.0			538.04	518.46

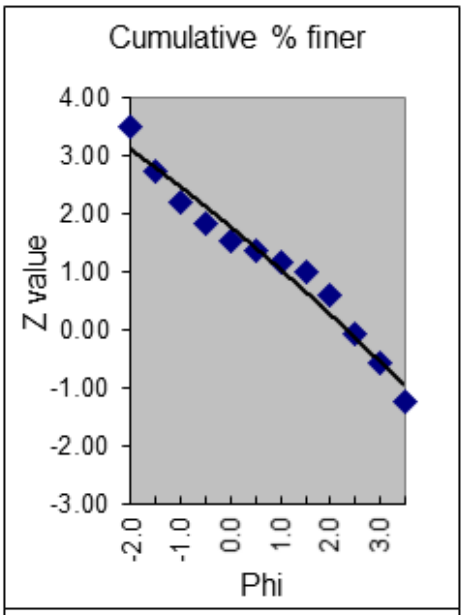

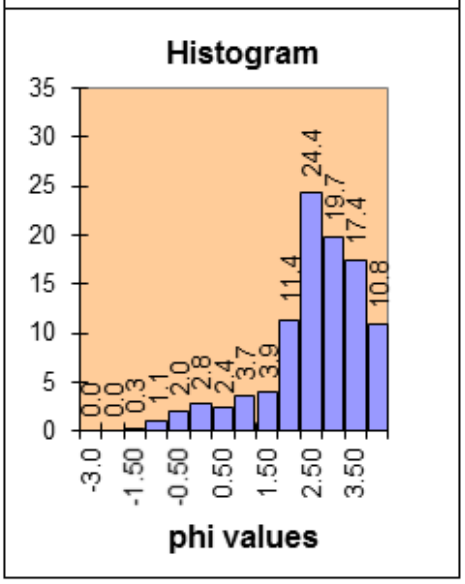

The grain-size analyses of T-MAST 02 sediment samples were performed (for ONR) by Anna Barrios and Tony Clark, Department of Marine, Earth and Atmospheric Sciences, North Carolina State University

Fig. 5.C-9 – Grain-size analysis for bottom grab sample at T-MAST-02 Site 14.

T-MAST 02
Grain-Size Analysis

Site 15

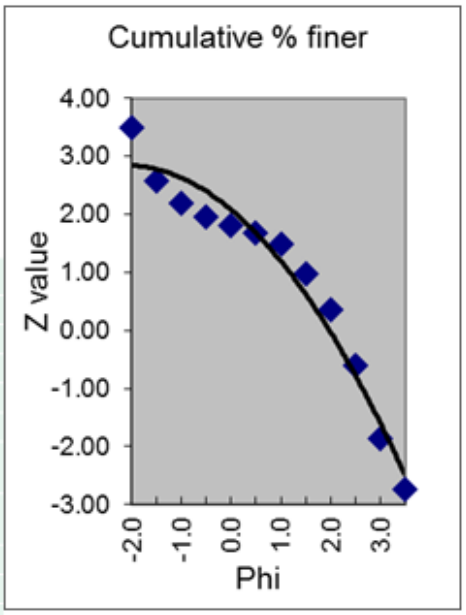

Grain Size Analysis							
BSS # 15	56.1874 -8.0278			All weights in grams			
14-Nov-2002	Date (dd-month-yyyy)						
Barrios	Analyst						
0.21	mean grain size D50 (mm)				2.258 D50 (phi)		
2.26	mean grain size D50 (phi)				1.476 D84 (phi)		
0.360	D84 (mm)				2.656 D16 (phi)		
0.159	D16 (mm)						
0.59	sorting (phi84-phi16)/2 (Inman)						
mm	phi	wt (g)	wt (%)	% finer	Z	gross (g)	tare (g)
8.000	-3.0	0.00	0.0	100.0	3.50		
4.000	-2.00	0.00	0.0	100.0	3.50	55.45	55.45
2.828	-1.50	0.11	0.5	99.5	2.58	50.97	50.86
2.000	-1.00	0.21	0.9	98.6	2.18	50.08	49.87
1.414	-0.50	0.23	1.0	97.5	1.96	47.05	46.82
1.000	0.00	0.22	1.0	96.5	1.81	45.69	45.47
0.707	0.50	0.26	1.2	95.3	1.68	44.15	43.89
0.500	1.00	0.50	2.3	93.1	1.48	41.31	40.81
0.354	1.50	2.15	9.7	83.4	0.97	41.17	39.02
0.250	2.00	4.39	19.8	63.6	0.35	40.63	36.24
0.177	2.50	8.06	36.4	27.2	-0.61	43.56	35.5
0.125	3.00	5.33	24.1	3.1	-1.86	39.89	34.56
0.088	3.50	0.62	2.8	0.3	-2.73	34.15	33.53
0.062	4.00	0.07	0.3	0.0	-3.50	6.55	6.48
<0.062	>4.00	0.00	0.0	0.0	-3.50	0	0
		22.15	100.0			540.65	518.50

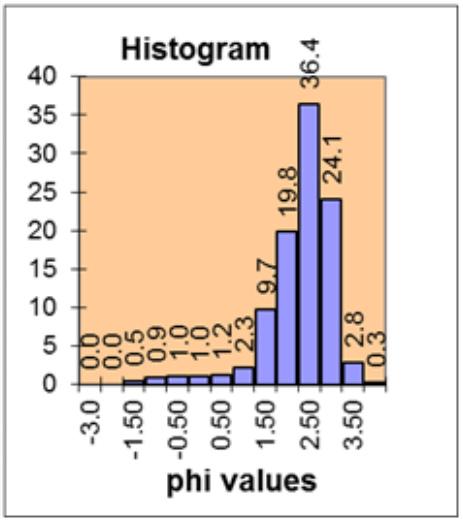

The grain-size analyses of T-MAST 02 sediment samples were performed (for ONR) by Anna Barrios and Tony Clark, Department of Marine, Earth and Atmospheric Sciences, North Carolina State University

Fig. 5.C-10 – Grain-size analysis for bottom grab sample at T-MAST-02 Site 15.

T-MAST 02
Grain-Size Analysis

Site 16

Grain Size Analysis							
BSS # 16	56.3388 -8.0304			All weights in grams			
14-Nov-2002	Date (dd-month-yyyy)						
Barrios	Analyst						
0.55	mean grain size D50 (mm)				0.85	D50 (phi)	
0.85	mean grain size D50 (phi)				-0.521	D84 (phi)	
1.435	D84 (mm)				6.957	D16 (phi)	
0.008	D16 (mm)						
3.74	sorting (phi84-phi16)/2 (Inman)						
mm	phi	wt (g)	wt (%)	% finer	Z	gross (g)	tare (g)
8.000	-3.0	0.00	0.0	100.0	3.50		
4.000	-2.00	0.43	1.2	98.8	2.24	55.88	55.45
2.828	-1.50	0.75	2.2	96.6	1.82	51.61	50.86
2.000	-1.00	1.15	3.3	93.3	1.50	51.03	49.88
1.414	-0.50	1.29	3.7	89.5	1.26	48.11	46.82
1.000	0.00	11.61	33.5	56.0	0.15	47.08	35.47
0.707	0.50	1.35	3.9	52.1	0.05	45.24	43.89
0.500	1.00	0.97	2.8	49.3	-0.02	41.79	40.82
0.354	1.50	0.66	1.9	47.4	-0.07	39.65	38.99
0.250	2.00	0.78	2.3	45.1	-0.12	37.03	36.25
0.177	2.50	0.93	2.7	42.5	-0.19	36.42	35.49
0.125	3.00	1.22	3.5	38.9	-0.28	35.76	34.54
0.088	3.50	2.28	6.6	32.4	-0.46	35.82	33.54
0.062	4.00	11.20	32.4	0.0	-3.50	17.68	6.48
<0.062	>4.00	0.00	0.0	0.0	-3.50	0	0
		34.62	100.0			543.10	508.48

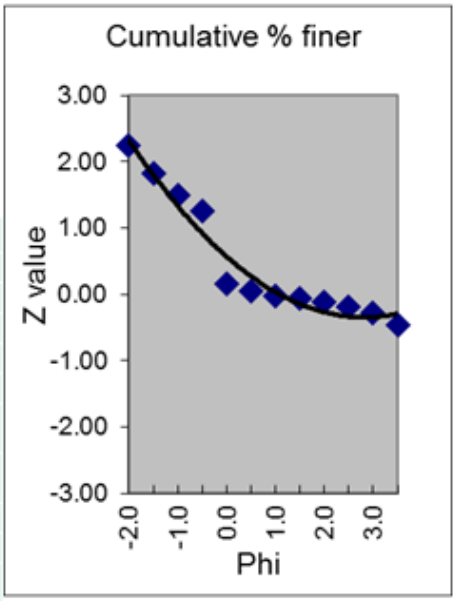

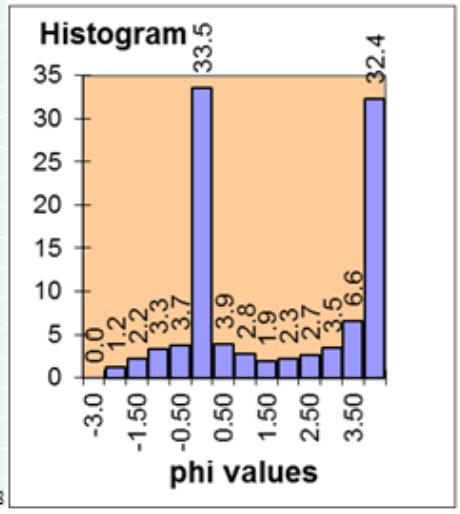

The grain-size analyses of T-MAST 02 sediment samples were performed (for ONR) by Anna Barrios and Tony Clark, Department of Marine, Earth and Atmospheric Sciences, North Carolina State University

Fig. 5.C-11 – Grain-size analysis for bottom grab sample at T-MAST-02 Site 16.

T-MAST 02
Grain-Size Analysis

Site 19

Grain Size Analysis							
BSS # 19	56.0500 -8.0995		All weights in grams				
14-Nov-2002	Date (dd-month-yyyy)						
Barrios	Analyst						
0.17	mean grain size D50 (mm)				2.538	D50 (phi)	
2.54	mean grain size D50 (phi)				1.543	D84 (phi)	
0.343	D84 (mm)				3.263	D16 (phi)	
0.104	D16 (mm)						
0.86	sorting (phi84-phi16)/2 (Inman)						
mm	phi	wt (g)	wt (%)	% finer	Z	gross (g)	tare (g)
8.000	-3.0	0.00	0.0	100.0	3.50		
4.000	-2.00	0.01	0.1	99.9	3.27	55.45	55.44
2.828	-1.50	0.02	0.1	99.8	2.95	50.88	50.86
2.000	-1.00	0.20	1.1	98.8	2.25	50.06	49.86
1.414	-0.50	0.37	2.0	96.8	1.86	47.19	46.82
1.000	0.00	0.38	2.0	94.8	1.63	45.84	45.46
0.707	0.50	0.39	2.1	92.8	1.46	44.28	43.89
0.500	1.00	0.67	3.5	89.2	1.24	41.5	40.83
0.354	1.50	0.81	4.3	84.9	1.03	39.79	38.98
0.250	2.00	2.03	10.7	74.2	0.65	38.26	36.23
0.177	2.50	4.23	22.4	51.8	0.05	39.7	35.47
0.125	3.00	4.86	25.7	26.1	-0.64	39.39	34.53
0.088	3.50	3.41	18.0	8.1	-1.40	36.96	33.55
0.062	4.00	1.53	8.1	0.0	-3.50	8.01	6.48
<0.062	>4.00	0.00	0.0	0.0	-3.50	0	0
		18.91	100.0			537.31	518.40

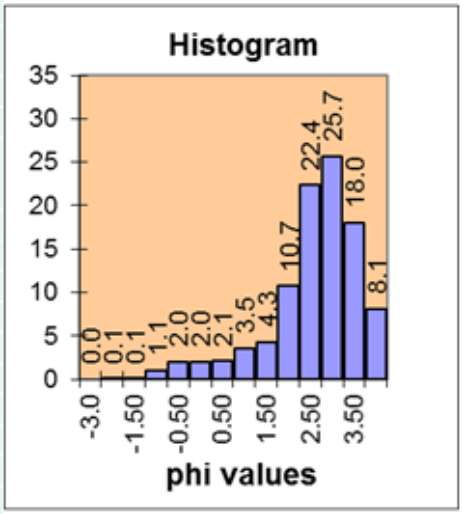

The grain-size analyses of T-MAST 02 sediment samples were performed (for ONR) by Anna Barrios and Tony Clark, Department of Marine, Earth and Atmospheric Sciences, North Carolina State University

Fig. 5.C-12 – Grain-size analysis for bottom grab sample at T-MAST-02 Site 19.

T-MAST 02
Grain-Size Analysis

Site 20

Grain Size Analysis							
BSS # 20	56.2233 -8.0008			All weights in grams			
14-Nov-2002	Date (dd-month-yyyy)						
Barrios	Analyst						
4.46	mean grain size D50 (mm)				-2.157	D50 (phi)	
-2.16	mean grain size D50 (phi)				-2.349	D84 (phi)	
5.094	D84 (mm)				1.885	D16 (phi)	
0.271	D16 (mm)						
2.12	sorting (phi84-phi16)/2 (Inman)						
mm	phi	wt (g)	wt (%)	% finer	Z	gross (g)	tare (g)
8.000	-3.0	0.00	0.0	100.0	3.50		
4.000	-2.00	11.74	63.3	36.7	-0.34	67.18	55.44
2.828	-1.50	0.26	1.4	35.3	-0.38	51.1	50.84
2.000	-1.00	0.30	1.6	33.7	-0.42	50.16	49.86
1.414	-0.50	0.38	2.0	31.6	-0.48	47.2	46.82
1.000	0.00	0.50	2.7	28.9	-0.55	45.95	45.45
0.707	0.50	0.47	2.5	26.4	-0.63	44.37	43.9
0.500	1.00	0.83	4.5	21.9	-0.77	41.65	40.82
0.354	1.50	0.64	3.5	18.5	-0.90	39.62	38.98
0.250	2.00	0.83	4.5	14.0	-1.08	37.06	36.23
0.177	2.50	1.17	6.3	7.7	-1.42	36.63	35.46
0.125	3.00	1.02	5.5	2.2	-2.01	35.55	34.53
0.088	3.50	0.24	1.3	0.9	-2.36	33.77	33.53
0.062	4.00	0.17	0.9	0.0	-3.50	6.65	6.48
<0.062	>4.00	0.00	0.0	0.0	-3.50	0	0
		18.55	100.0			536.89	518.34

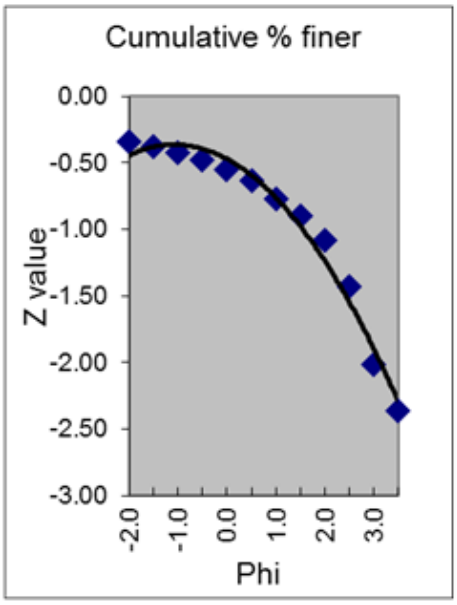

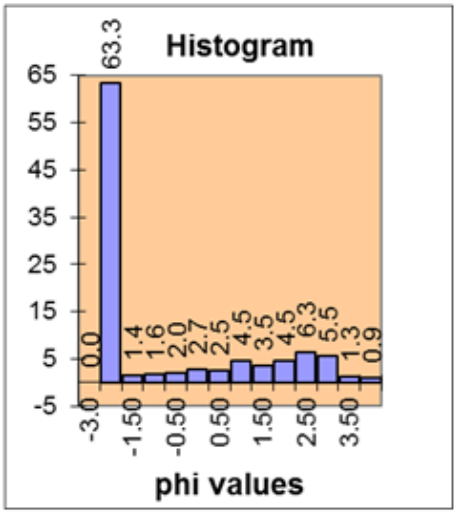

The grain-size analyses of T-MAST 02 sediment samples were performed (for ONR) by Anna Barrios and Tony Clark, Department of Marine, Earth and Atmospheric Sciences, North Carolina State University

Fig. 5.C-13 – Grain-size analysis for bottom grab sample at T-MAST-02 Site 20.

D. BBS vs. Grain Size and Bottom Type

Figure 5.D-1 shows EPL fit values at 4 frequencies vs. BGS bottom type and bottom-grab grain size corresponding to the 16 T-MAST-02 BBS sites.

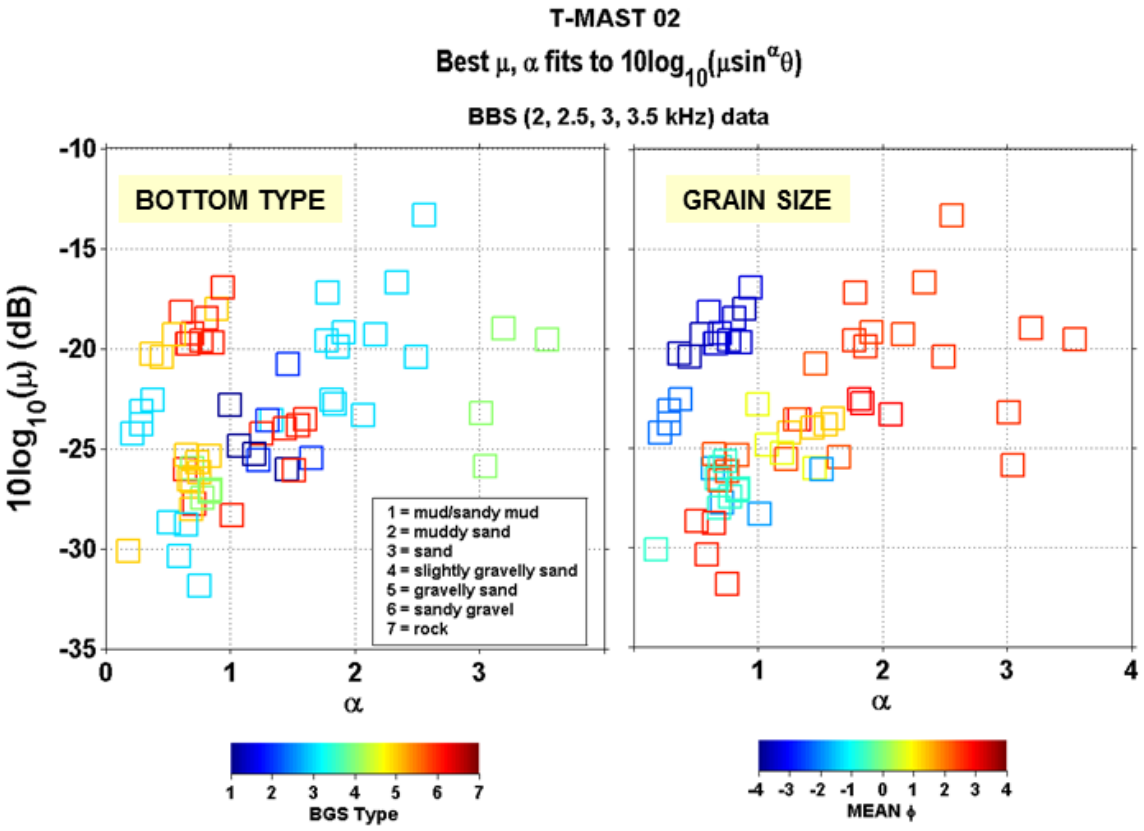

Fig. 5.D-1 – Best EPL-curve fit values vs. BGS bottom type (left) and grain-size (right) for the 16 T-MAST-02 sites over 4 frequencies.

6. OREX-05 (SHALLOW WATER – HECETA BANK)

NRL performed LF and MF direct-path BBS measurements between 16 and 27 July 2005 at 25 sites (Figs. 6-1 and 6-2) during the OREX 05 experiment, 22 on the Heceta Bank (off the Oregon coast), 1 on its western slope, and 2 just off its western slope. This section presents the BBS measurements from these sites.

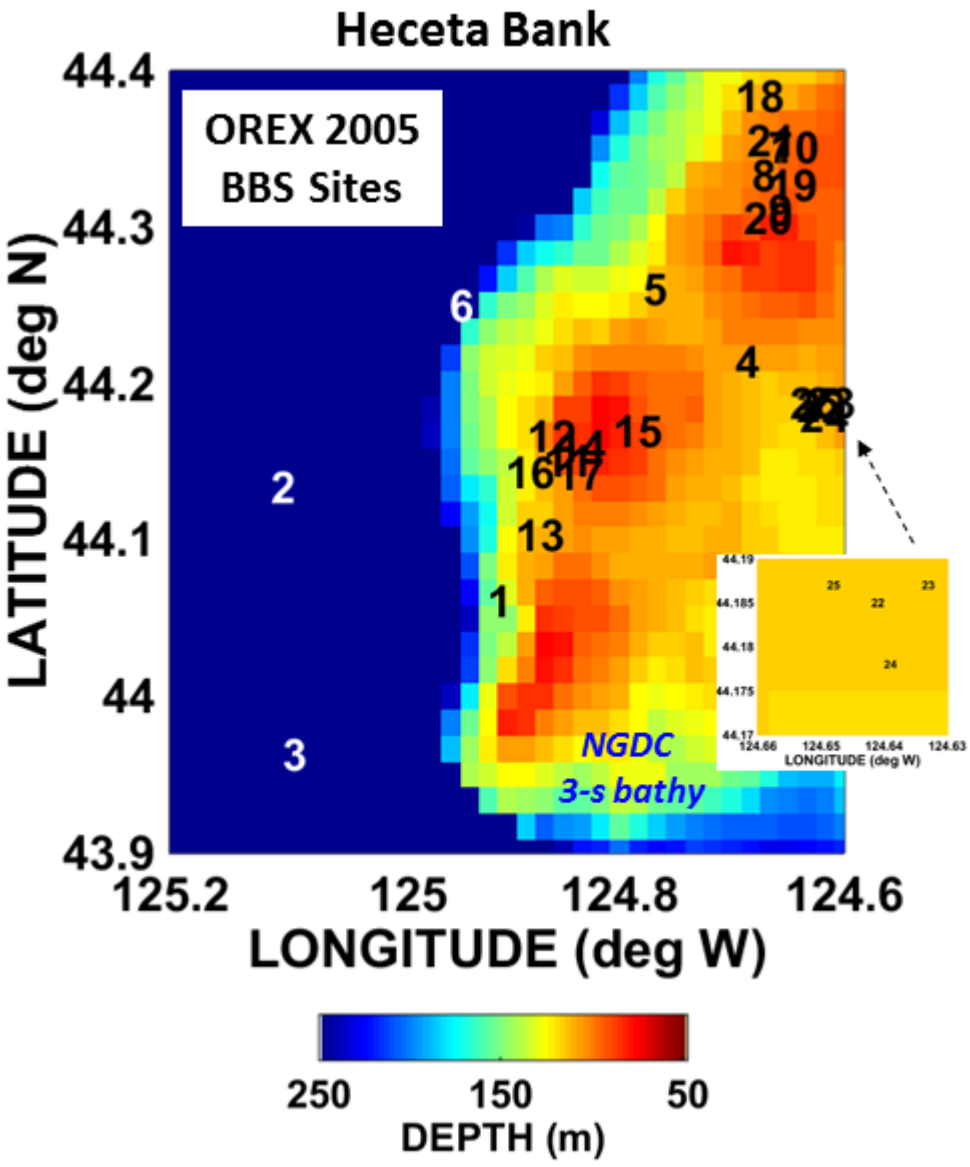

Fig. 6-1 – OREX 2005 geographic location of BBS sites vs. bathymetry.

OREX 2005 Bottom Scattering Sites

Site	XF4 (G81) Source / LF (MF) Receiver Depths (m)	Date (JD) Time (Z)	Latitude (deg N)	Longitude (deg W)	Wind Speed (kts)	Water Depth (m)	Water Sound Speed at the Interface (m/s)
1	47 (48.8) / 57.4 (52.8)	197 0401-0453	44.060 44° 3.58′	124.918 124° 55.05′	17	153	1482
2	80 (81.8) / 90.4 (85.8)	198 0308-0359	44.133 44° 7.98′	125.110 125° 6.60′	31	1460	1485
3	80 (81.8) / 90.4 (85.8)	199 0333-0411	43.962 43° 57.69′	125.100 125° 5.99′	22	1455	1485
4	50 (51.8) / 60.4 (55.8)	199 1652-1658	44.213 44° 12.78′	124.697 124° 41.82′	20	111	1480
5	50 (51.8) / 60.4 (55.8)	200 0230-0311	44.260 44° 15.60′	124.779 124° 46.74′	22	120	1501
6	80 (81.8) / 90.4 (85.8)	200 2109-2205	44.249 44° 14.91′	124.951 124° 57.05′	22	455	1480
7	50 (51.8) / 60.4 (55.8)	202 2333-0002	44.350 44° 21.00′	124.667 124° 40.02′	13	102	1481
8	40 (41.8) / 50.4 (45.8)	203 0109-0223	44.333 44° 19.97′	124.683 124° 40.96′	19	96	1482
9	40 (41.8) / 50.4 (45.8)	203 0315-0343	44.310 44° 18.60′	124.667 124° 40.02′	16	84	1482
10	50 (51.8) / 60.4 (55.8)	203 0435-0458	44.350 44° 20.99′	124.666 124° 39.98′	7	102	1482
11	50 (51.8) / 60.4 (55.8)	205 0343-0406	44.150 44° 9.00′	124.867 124° 52.02′	24	107	1437
12	50 (51.8) / 60.4 (55.8)	205 1416-1439	44.166 44° 9.98′	124.883 124° 53.00′	11	116	1437
13	50 (51.8) / 60.4 (55.8)	205 1559-1638	44.103 44° 6.19′	124.892 124° 53.52′	10	117	1481
14	40 (41.8) / 50.4 (45.8)	205 1726-1751	44.160 44° 9.60′	124.856 124° 51.36′	9	85	1482
15	40 (41.8) / 50.4 (45.8)	205 1830-1852	44.169 44° 10.16′	124.806 124° 48.36′	10	78	1482
16	60 (61.8) / 70.4 (65.8)	205 2000-2024	44.143 44° 8.56′	124.901 124° 54.05′	9	141	1438
17	50 (51.8) / 60.4 (55.8)	205 2102-2227	44.142 44° 8.52′	124.858 124° 51.48′	10	105	1482
18	50 (51.8) / 60.4 (55.8)	206 0018-0040	44.383 44° 22.95′	124.697 124° 41.85′	15	125	1437
19	50 (51.8) / 60.4 (55.8)	206 0128-0150	44.326 44° 19.55′	124.668 124° 40.06′	16	99	1481
20	40 (41.8) / 50.4 (45.8)	206 0252-0314	44.305 44° 18.31′	124.690 124° 41.37′	16	93	1481
21	50 (51.8) / 60.4 (55.8)	206 0403-0424	44.355 44° 21.29′	124.687 124° 41.24′	15	110	1481
22	40 (41.8) / 50.4 (45.8)	208 1626-1649	44.185 44° 11.10′	124.642 124° 38.52′	20	119	1481
23	40 (41.8) / 50.4 (45.8)	208 1727-1753	44.187 44° 11.23′	124.634 124° 38.06′	18	117	1481
24	40 (41.8) / 50.4 (45.8)	208 1830-1852	44.178 44° 10.69′	124.640 124° 38.40′	19	120	1437
25	50 (51.8) / 60.4 (55.8)	208 1949-2011	44.187 44° 11.23′	124.649 124° 38.96′	21	117	1437

Fig. 6-2 – OREX 2005 BBS measurement and site information (Heceta Bank).

A. Test Operations

Direct-path, near-monostatic acoustic BBS measurements were conducted from the R/V *Wecoma* using a vertical line array (VLA) receiver cut for 1000 Hz and 5000 Hz and two sources. There were two VLA apertures: a MF aperture of 16 phones with a 6-inch spacing and a LF aperture of 16 phones with a 30-inch spacing. Measurements were made using combinations of 10-ms CWs at 16 frequencies (0.6, 0.8, 1, 1.2, 1.4, 1.5, 1.6, 1.8, 2, 2.2, 2.5, 3, 3.5, 4, 4.5 and 5 kHz). Each CW signal was transmitted 18 times at a rep rate of 3 s. The OREX-05 sources were a MF transducer (G81; 194 dB peak) usable over 1.5 to 5 kHz situated 4 m above the center of the VLA and a LF transducer (XF-4; 194 dB peak) usable over 0.6 kHz to 2.2 kHz located 10.4 m above the center of the VLA. Measurements were made at source depths ranging from 40 m to 80 m at each site. The sonar equation was used at each depth to derive scattering strengths as a function of beam, frequency, and grazing angle.

B. Measured Bottom Backscattering Strengths

Figure 6.B-1 shows BBS vs. mean grazing angle at 3 frequencies for 19 OREX-05 shallow-water sites. Figures 6.B-2–6.B-14 show bottom backscattering strengths measured at the 25 OREX-05 sites for up to 16 of the transmitted frequencies: .6, .8, 1, 1.2, 1.4, 1.5, 1.6, 1.8, 2, 2.2, 2.5, 3, 3.5, 4, 4.5 and 5 kHz; for each sites, the images on the left are the MF data results using the G81 source, and those on the right are the data results using the XF-4 source. Figure 6.B-15 shows the best EPL-curve fit values to the OREX-05 BBS vs. grazing angle curves for the 19 sites shown in Fig. 6.B-1. (See also Kunz and Gauss (2000) for LWAD 99-3 Heceta Bank BBS measurement and modeling results.)

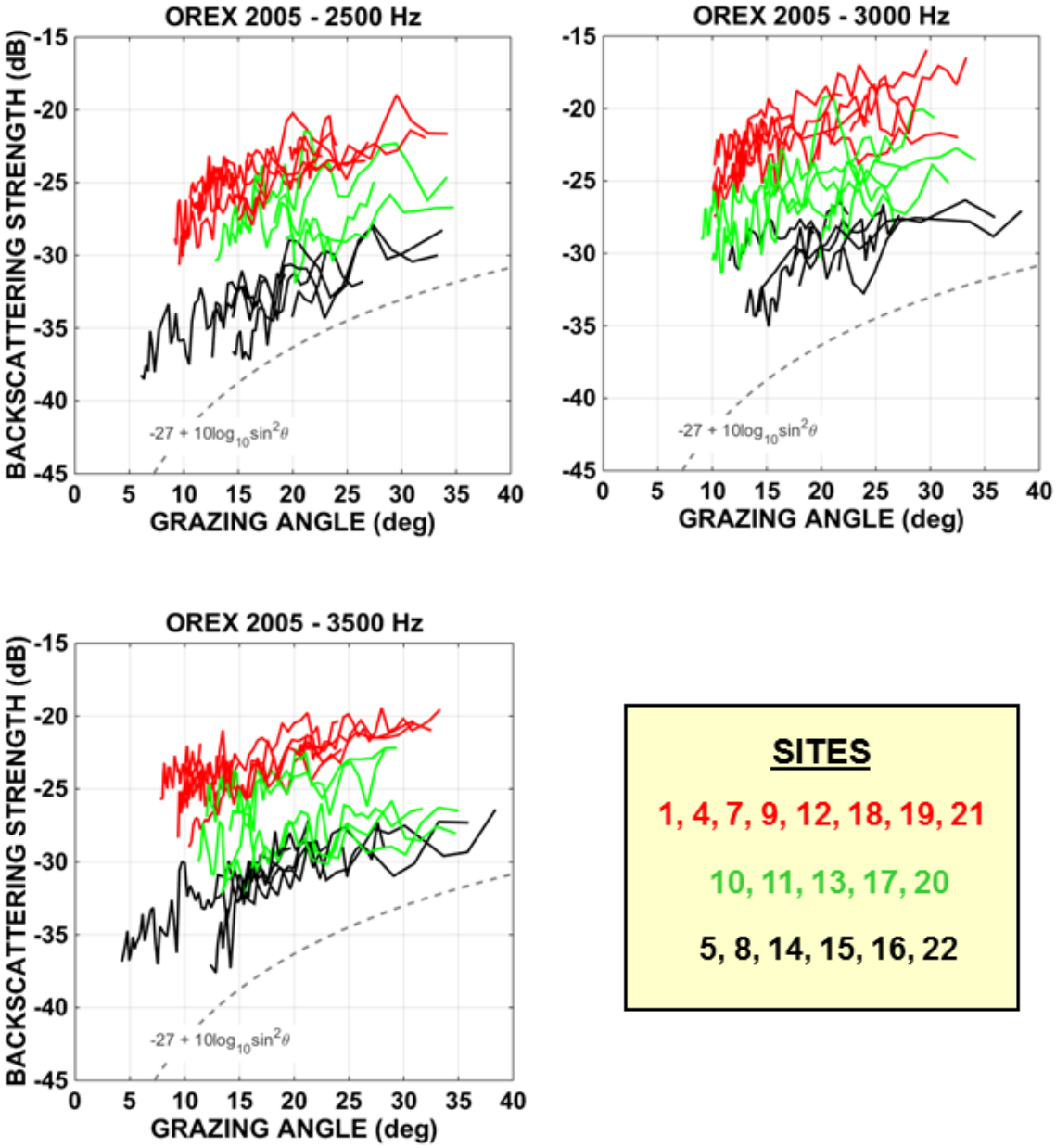

Fig. 6.B-1 – OREX-05 BBS vs. grazing angle at 3 frequencies for 19 shallow-water sites (color-coded just to help visually separate the sites).
(Mackenzie curve (dashed) shown as a reference.)

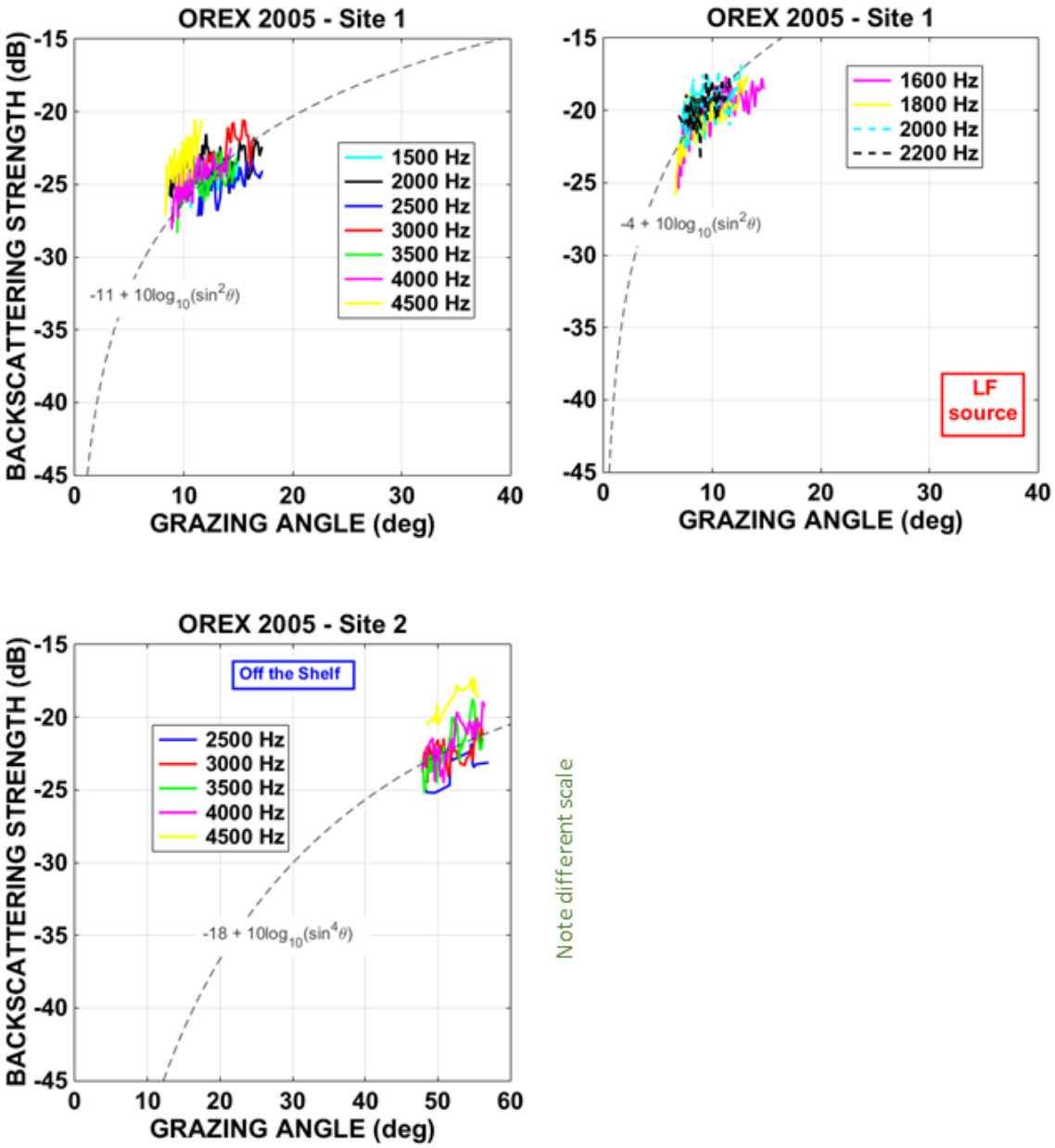

Fig. 6.B-2 – OREX-05 MF (left) and LF (right) BBS vs. grazing angle at multiple frequencies for Sites 1 and 2. (EPL curves matched to the data trend (dashed) are also shown.)

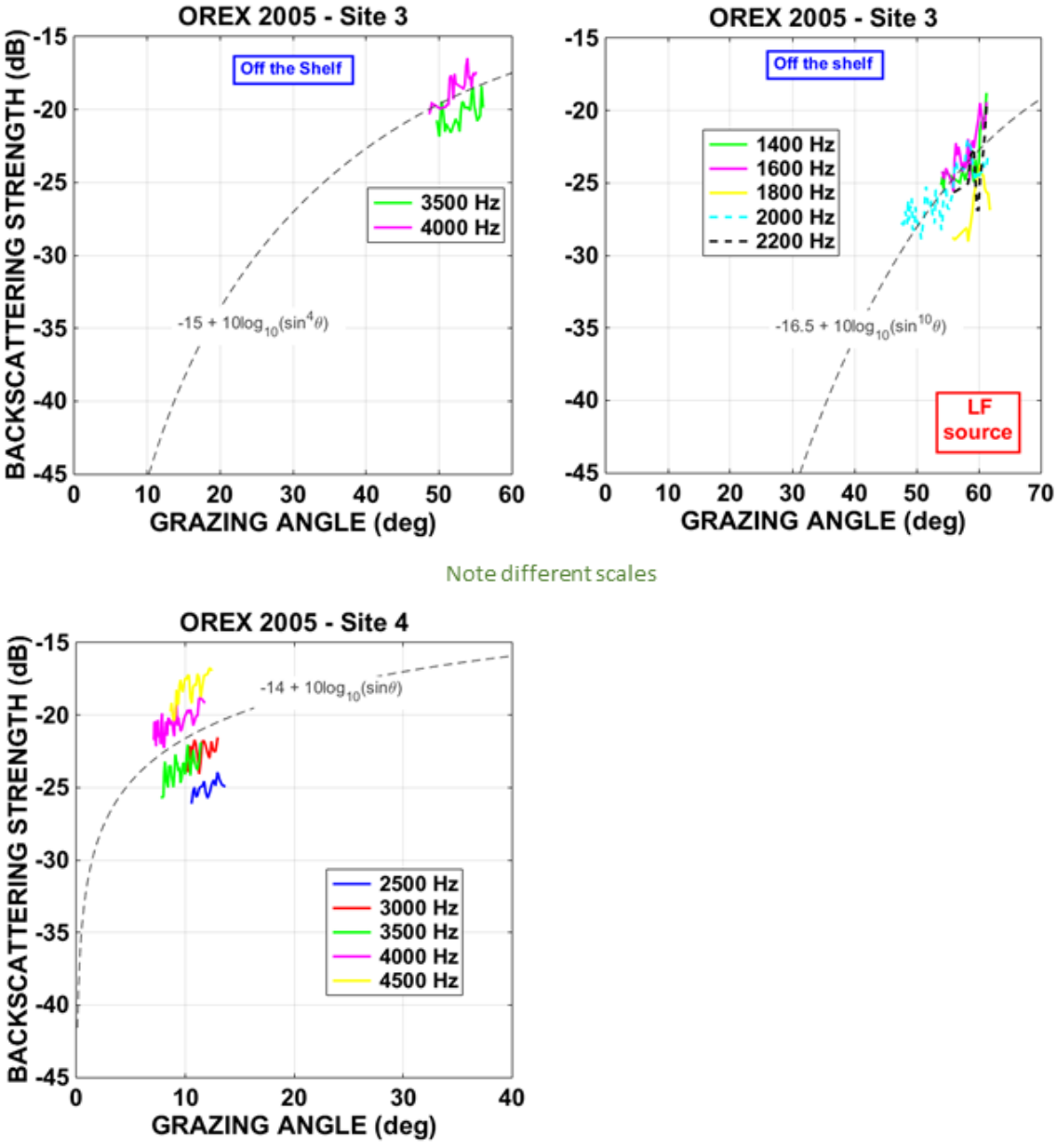

Fig. 6.B-3 – OREX-05 MF (left) and LF (right) BBS vs. grazing angle at multiple frequencies for Sites 3 and 4. (EPL curves matched to the data trend (dashed) are also shown.)

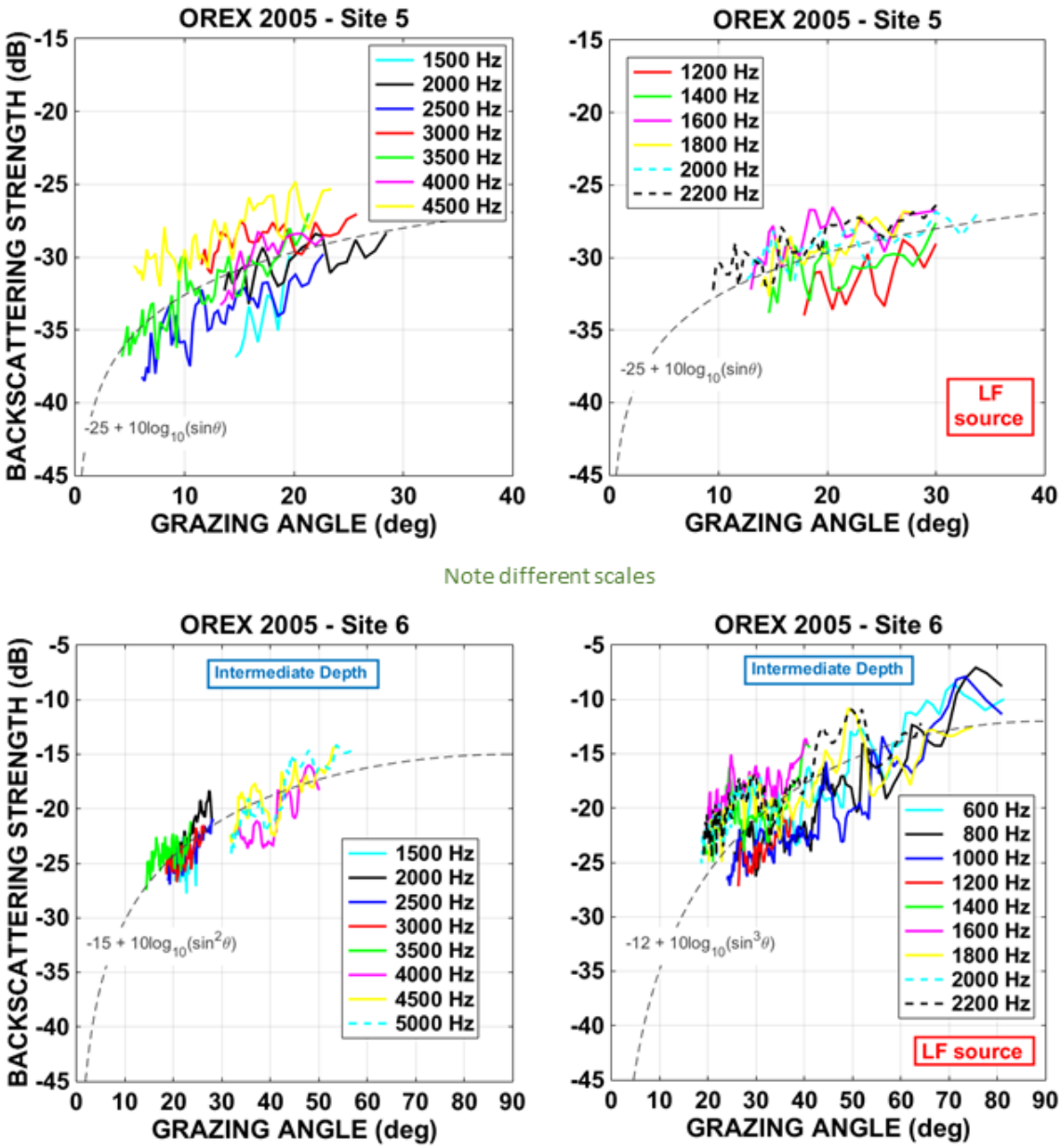

Fig. 6.B-4 – OREX-05 MF (left) and LF (right) BBS vs. grazing angle at multiple frequencies for Sites 5 and 6. (EPL curves matched to the data trend (dashed) are also shown.)

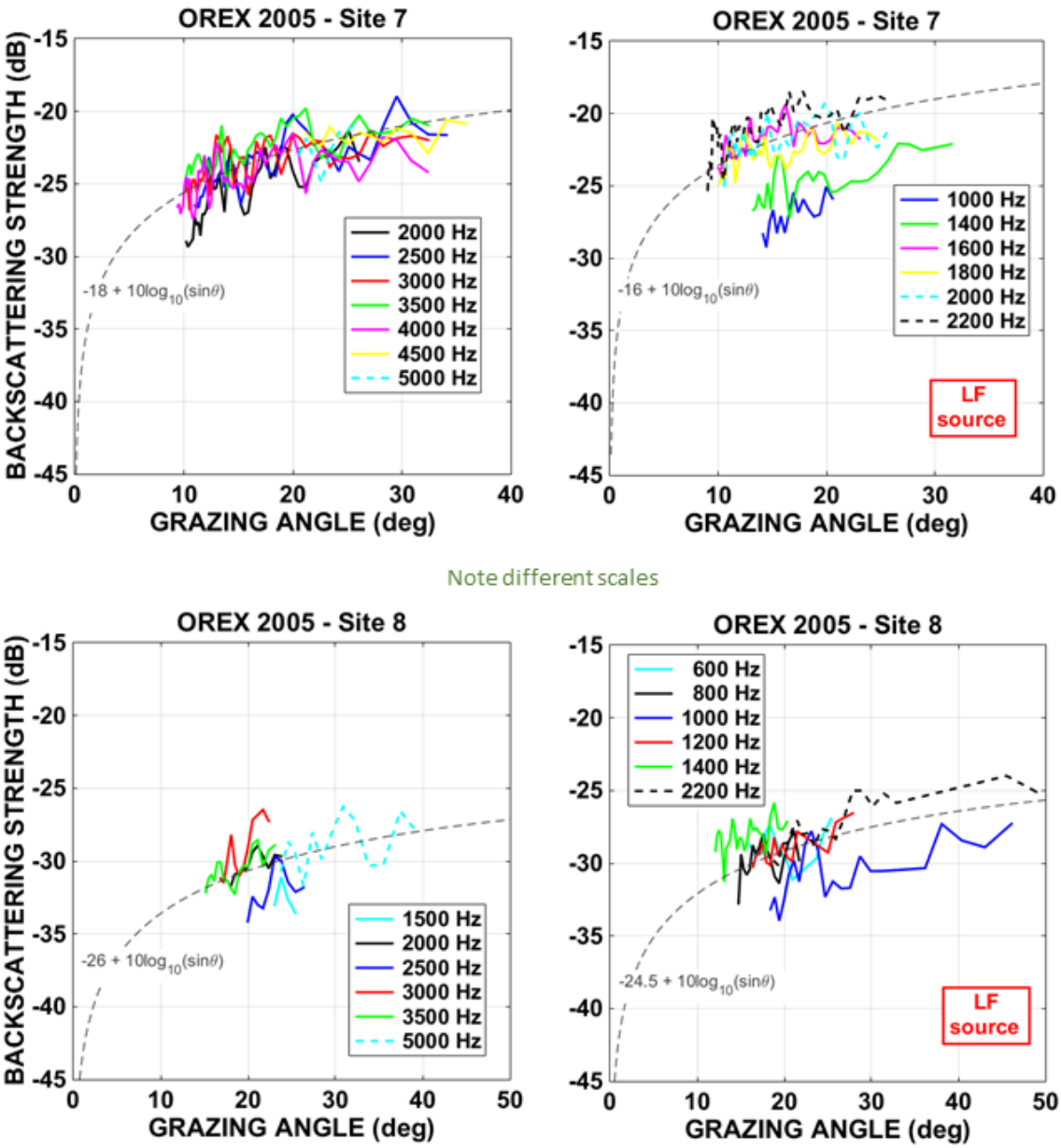

Fig. 6.B-5 – OREX-05 MF (left) and LF (right) BBS vs. grazing angle at multiple frequencies for Sites 7 and 8. (EPL curves matched to the data trend (dashed) are also shown.)

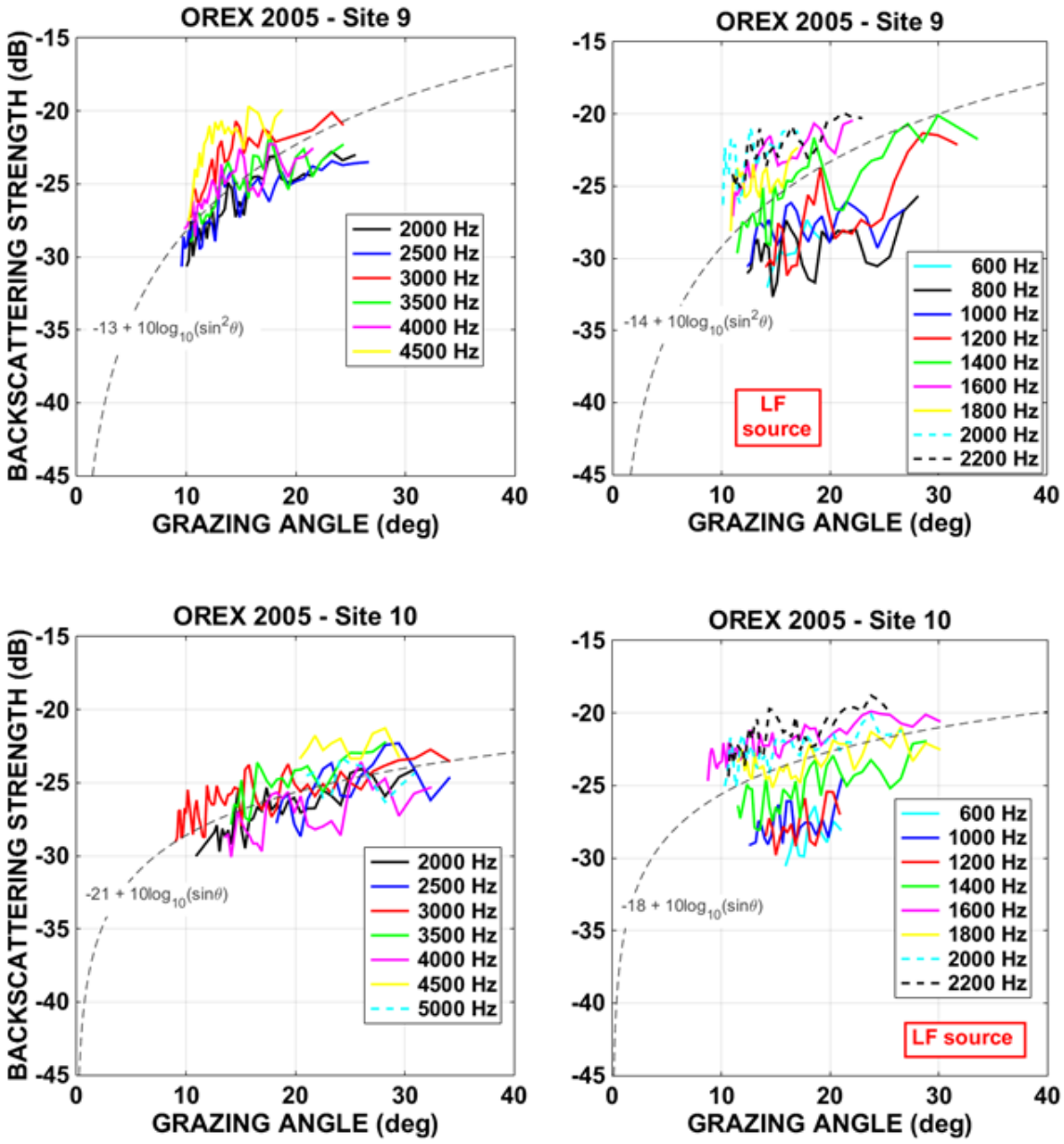

Fig. 6.B-6 – OREX-05 MF (left) and LF (right) BBS vs. grazing angle at multiple frequencies for Sites 9 and 10. (EPL curves matched to the data trend (dashed) are also shown.)

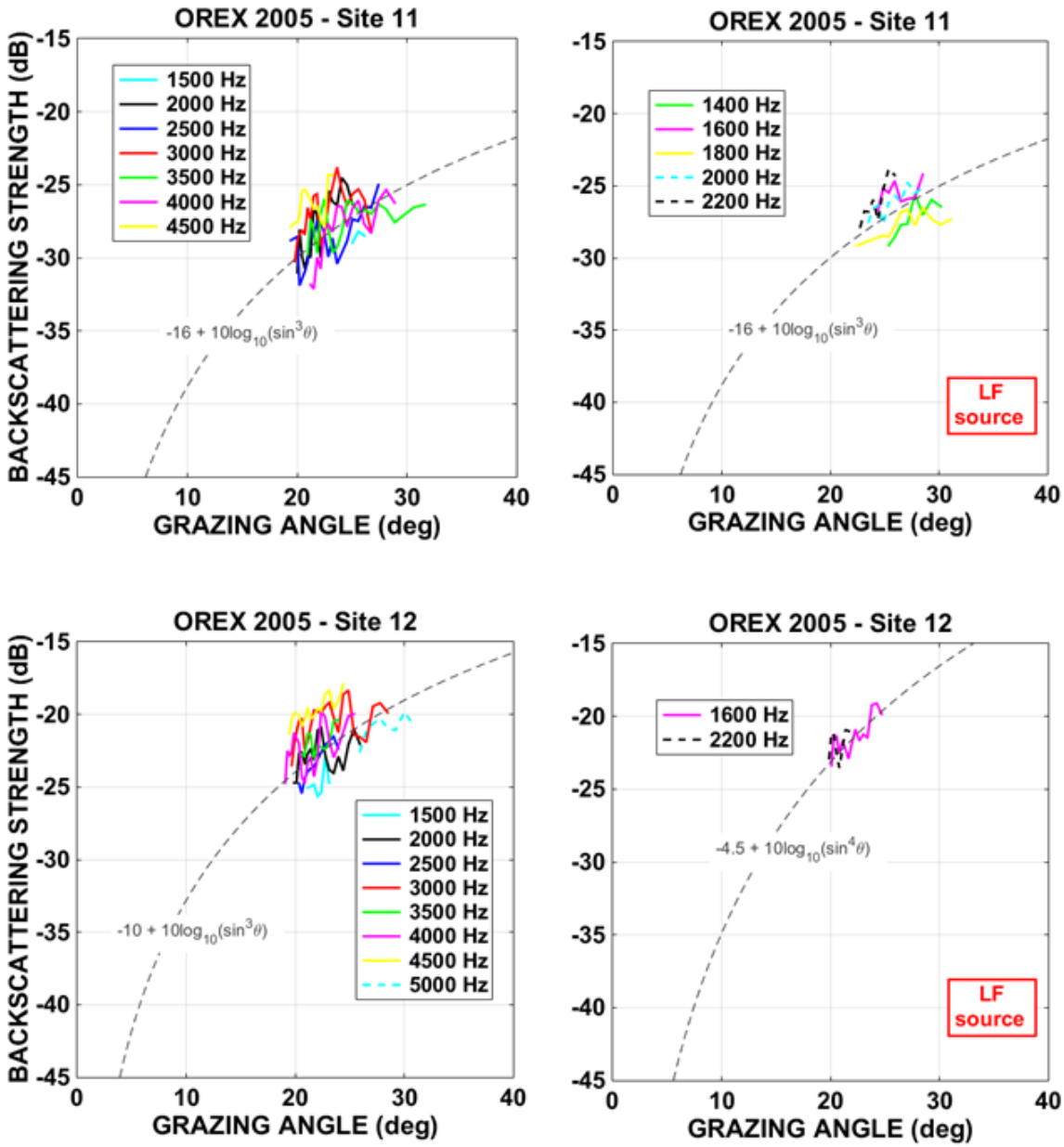

Fig. 6.B-7 – OREX-05 MF (left) and LF (right) BBS vs. grazing angle at multiple frequencies for Sites 11 and 12. (EPL curves matched to the data trend (dashed) are also shown.)

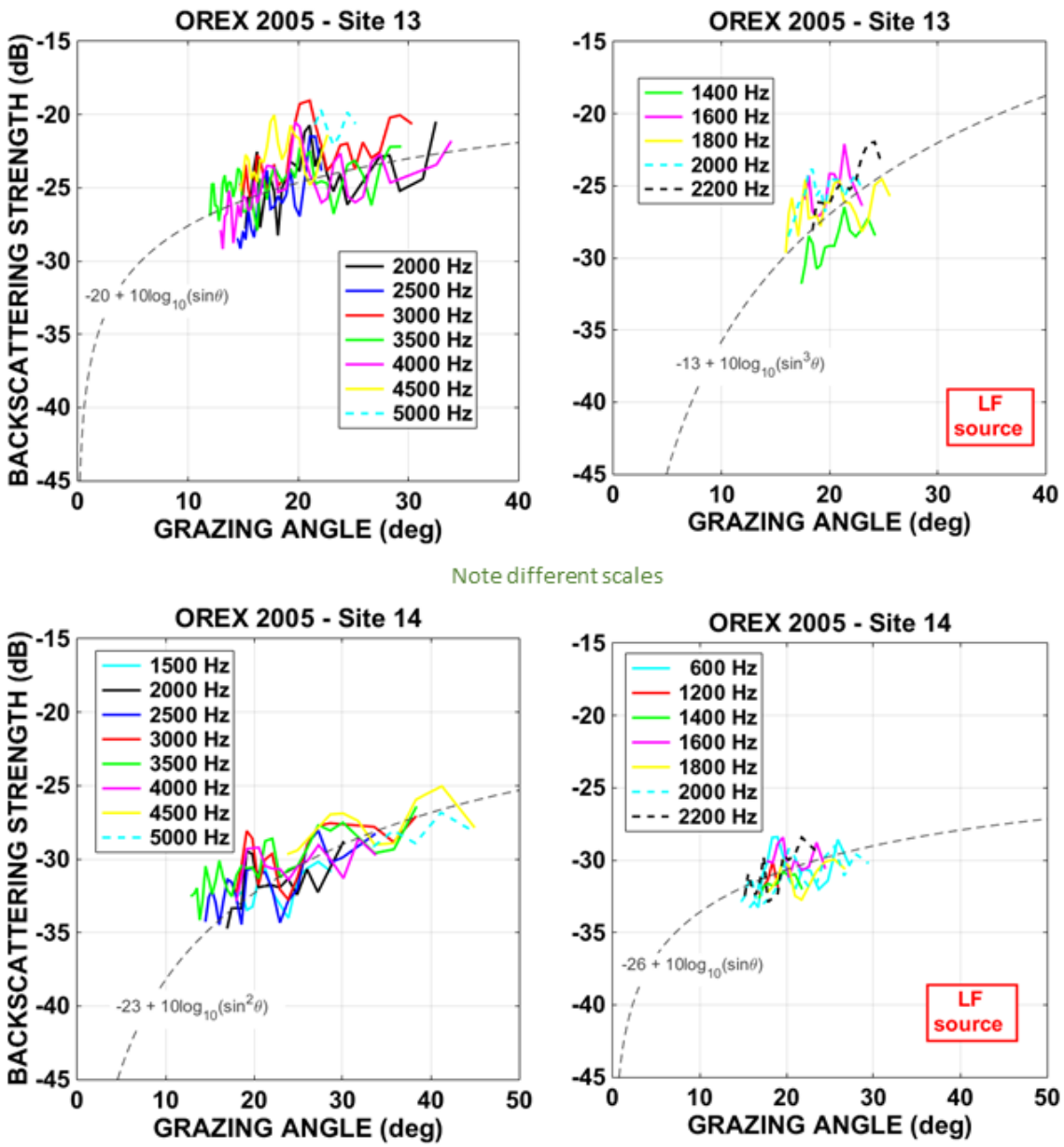

Fig. 6.B-8 – OREX-05 MF (left) and LF (right) BBS vs. grazing angle at multiple frequencies for Sites 13 and 14. (EPL curves matched to the data trend (dashed) are also shown.)

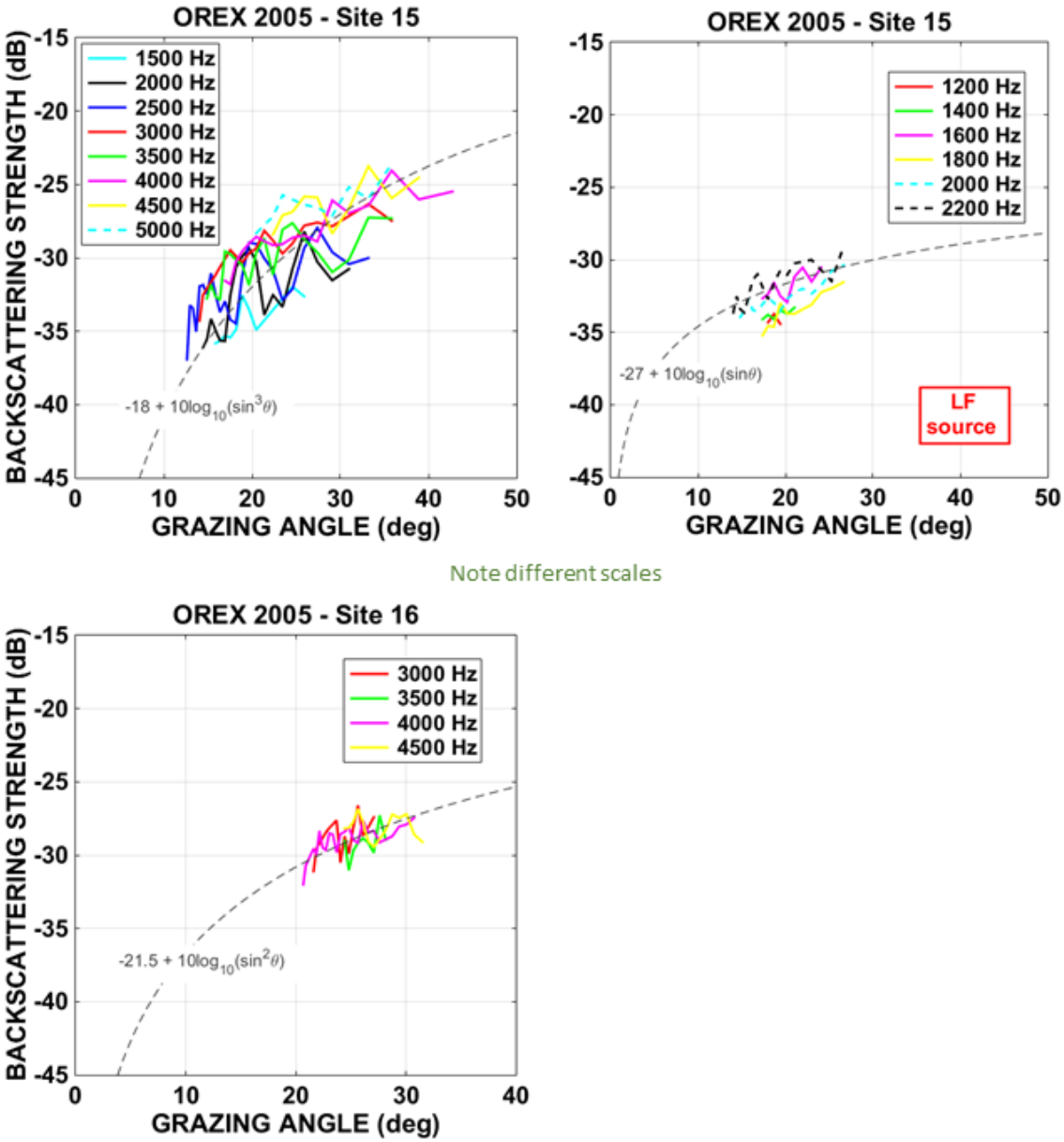

Fig. 6.B-9 – OREX-05 MF (left) and LF (right) BBS vs. grazing angle at multiple frequencies for Sites 15 and 16. (EPL curves matched to the data trend (dashed) are also shown.)

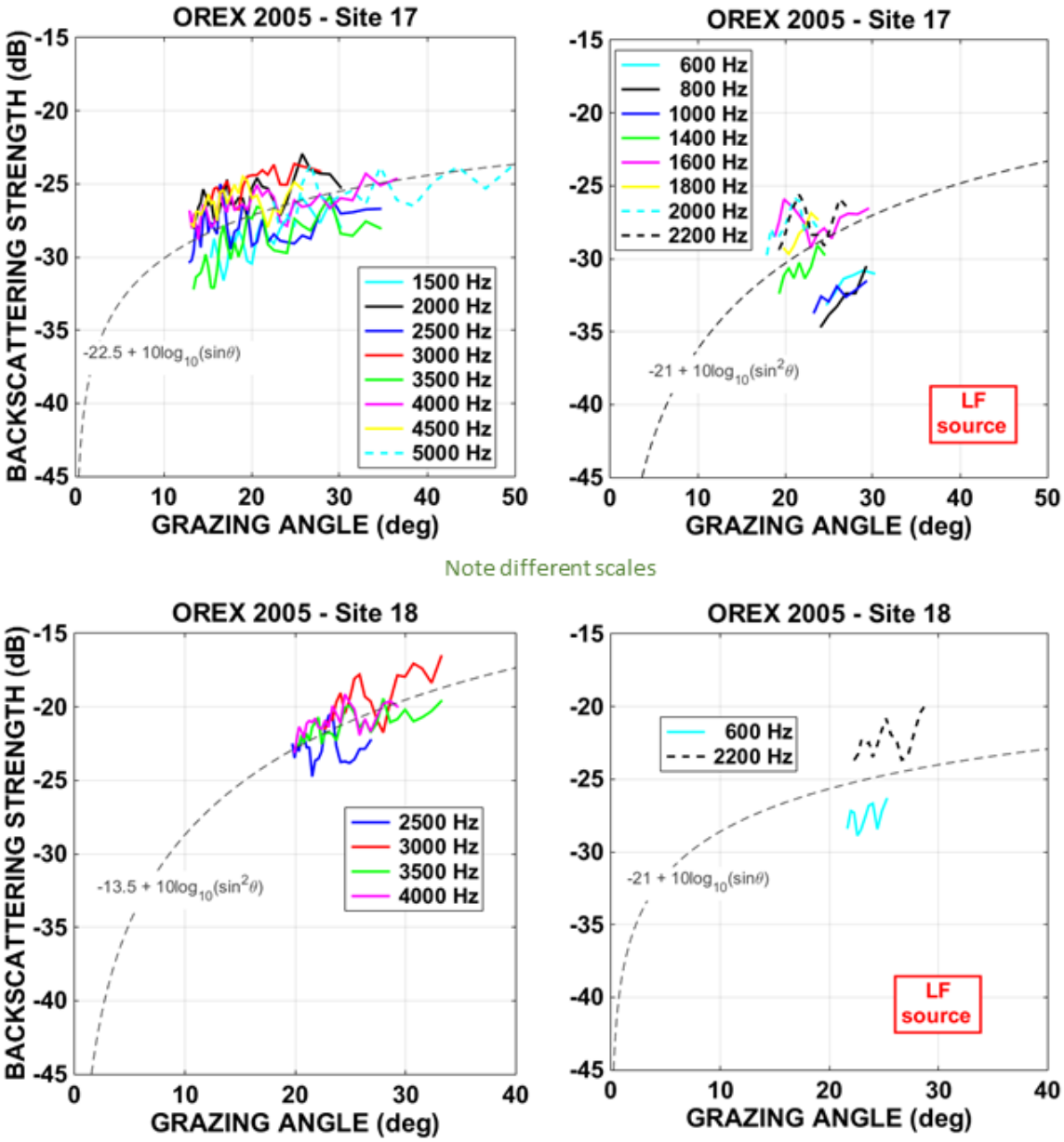

Fig. 6.B-10 – OREX-05 MF (left) and LF (right) BBS vs. grazing angle at multiple frequencies for Sites 17 and 18. (EPL curves matched to the data trend (dashed) are also shown.)

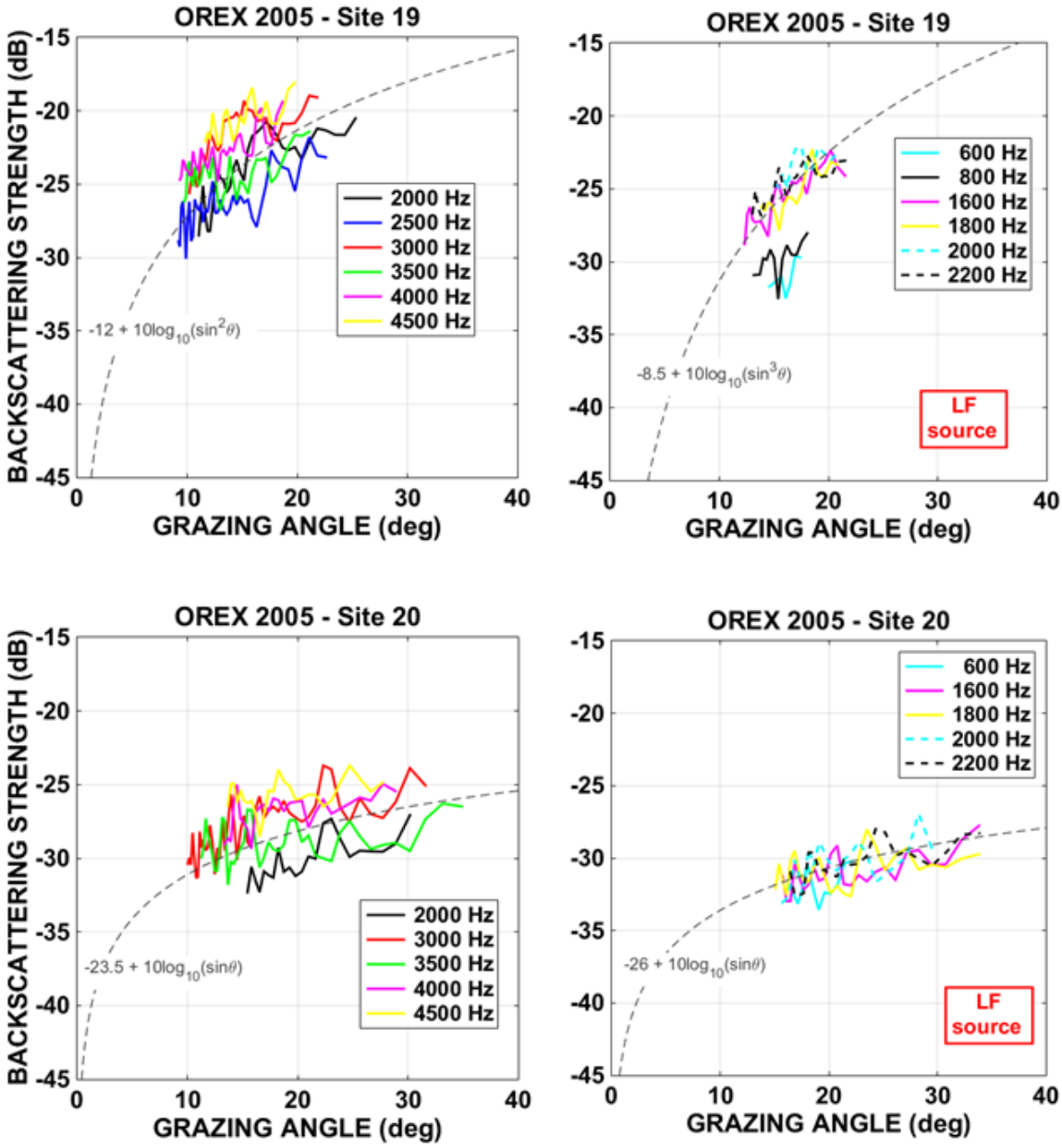

Fig. 6.B-11 – OREX-05 MF (left) and LF (right) BBS vs. grazing angle at multiple frequencies for Sites 19 and 20. (EPL curves matched to the data trend (dashed) are also shown.)

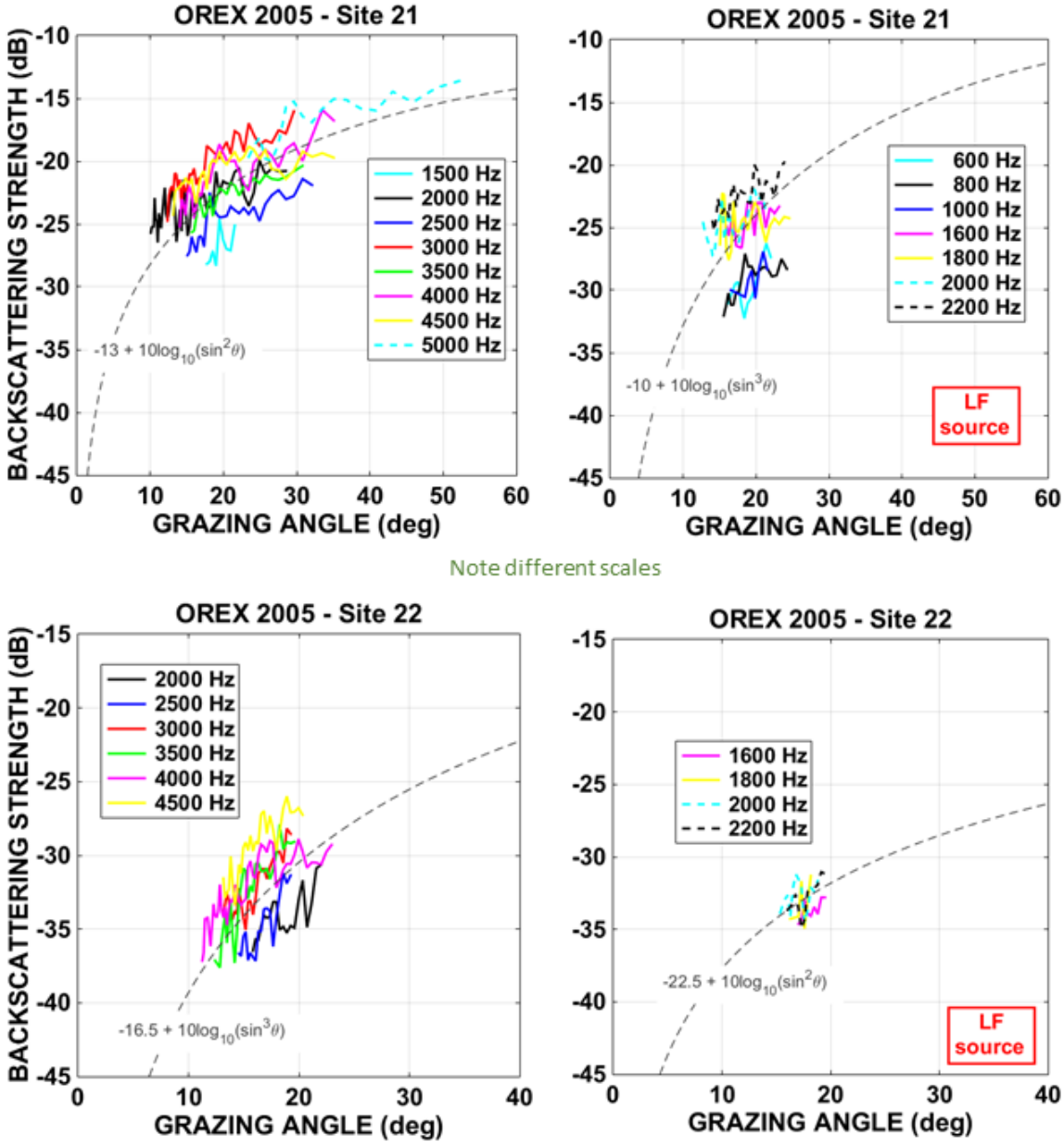

Fig. 6.B-12 – OREX-05 MF (left) and LF (right) BBS vs. grazing angle at multiple frequencies for Sites 21 and 22. (EPL curves matched to the data trend (dashed) are also shown.)

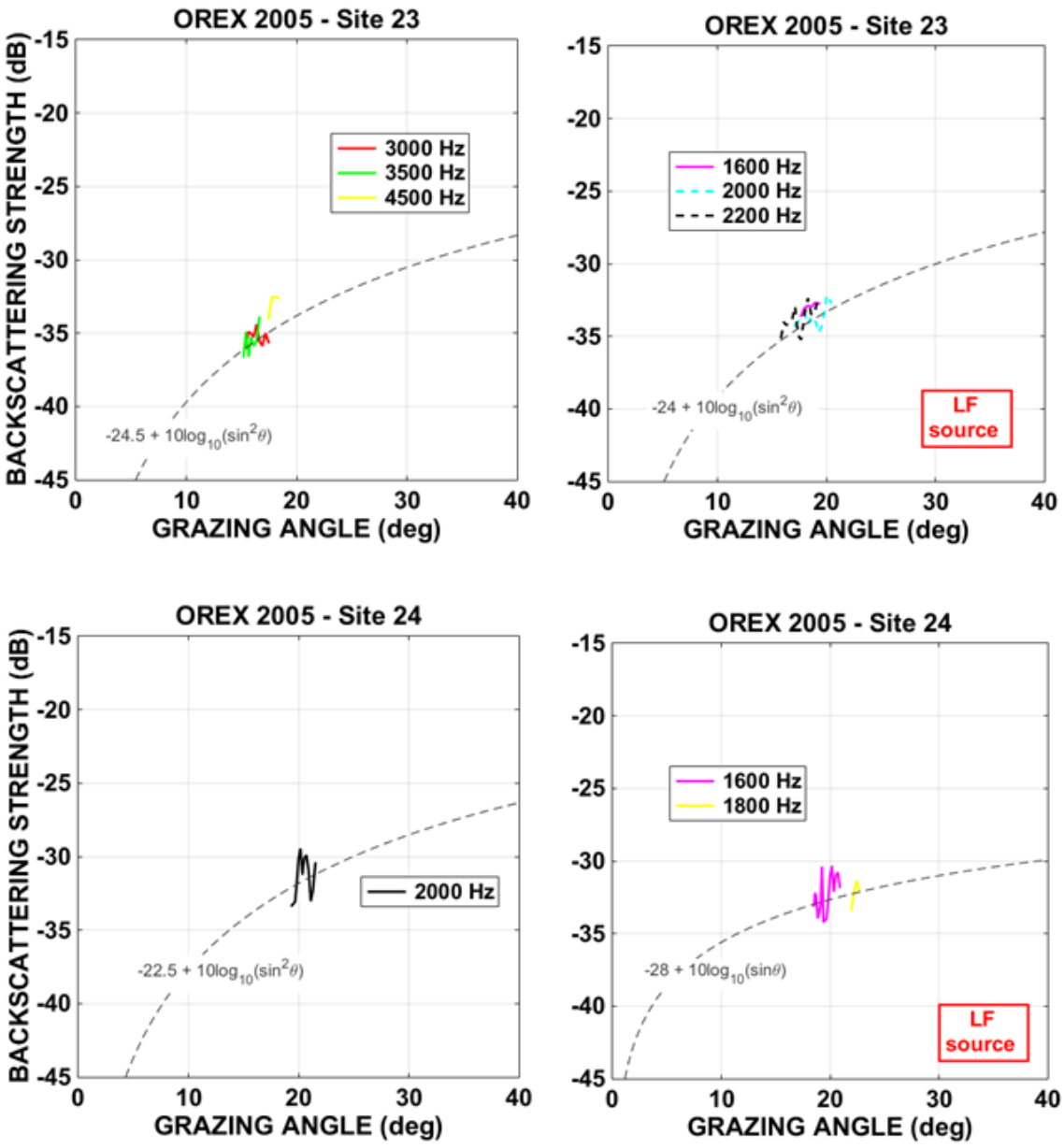

Fig. 6.B-13 – OREX-05 MF (left) and LF (right) BBS vs. grazing angle at multiple frequencies for Sites 23 and 24. (EPL curves matched to the data trend (dashed) are also shown.)

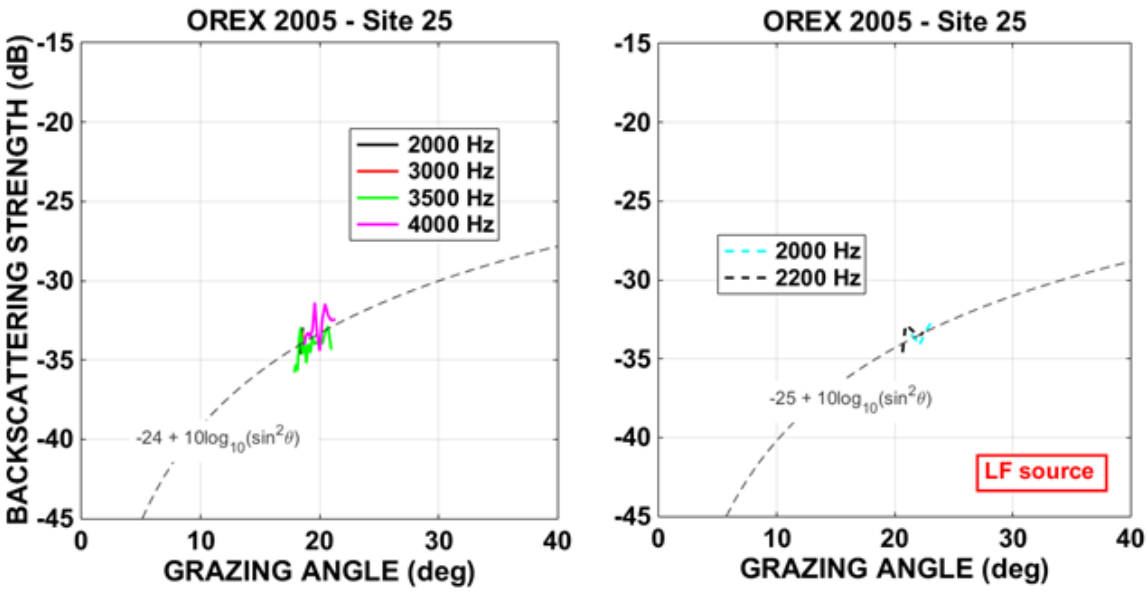

Fig. 6.B-14 – OREX-05 MF (left) and LF (right) BBS vs. grazing angle at multiple frequencies for Site 25. (EPL curves matched to the data trend (dashed) are also shown.)

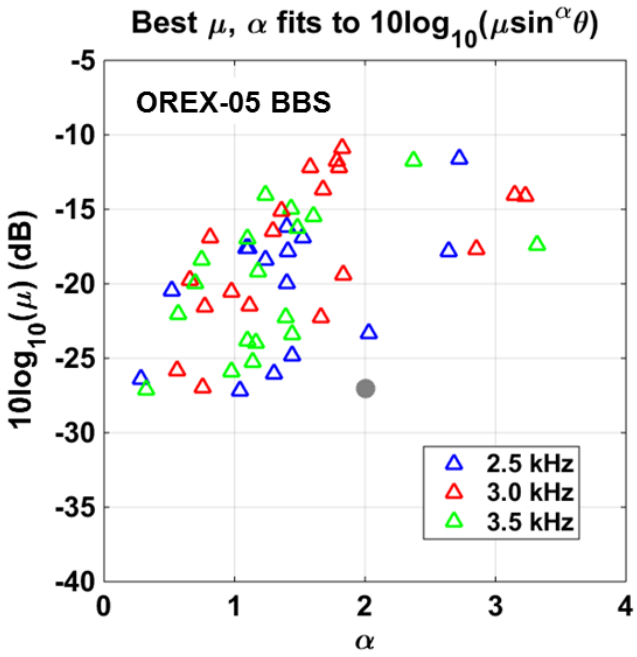

Fig. 6.B-15 – Distribution of best EPL-curve fit values to OREX-05 BBS vs. grazing angle curves at 3 frequencies for the 19 shallow-water sites shown in Fig. 6.B-1. (Mackenzie curve values (gray dot) shown as a reference.)

7. CROSS-EXERIMENT EPL-FIT VALUES (SHALLOW WATER)

Figure 7-1 shows the best EPL BBS fit values at 3 frequencies across all the shallow-water experiments, showing that the standard Mackenzie curve and Lambert's law do not match the BBS data grazing-angle curves well over moderate grazing angles (~10–40 deg) at MF in shallow water.

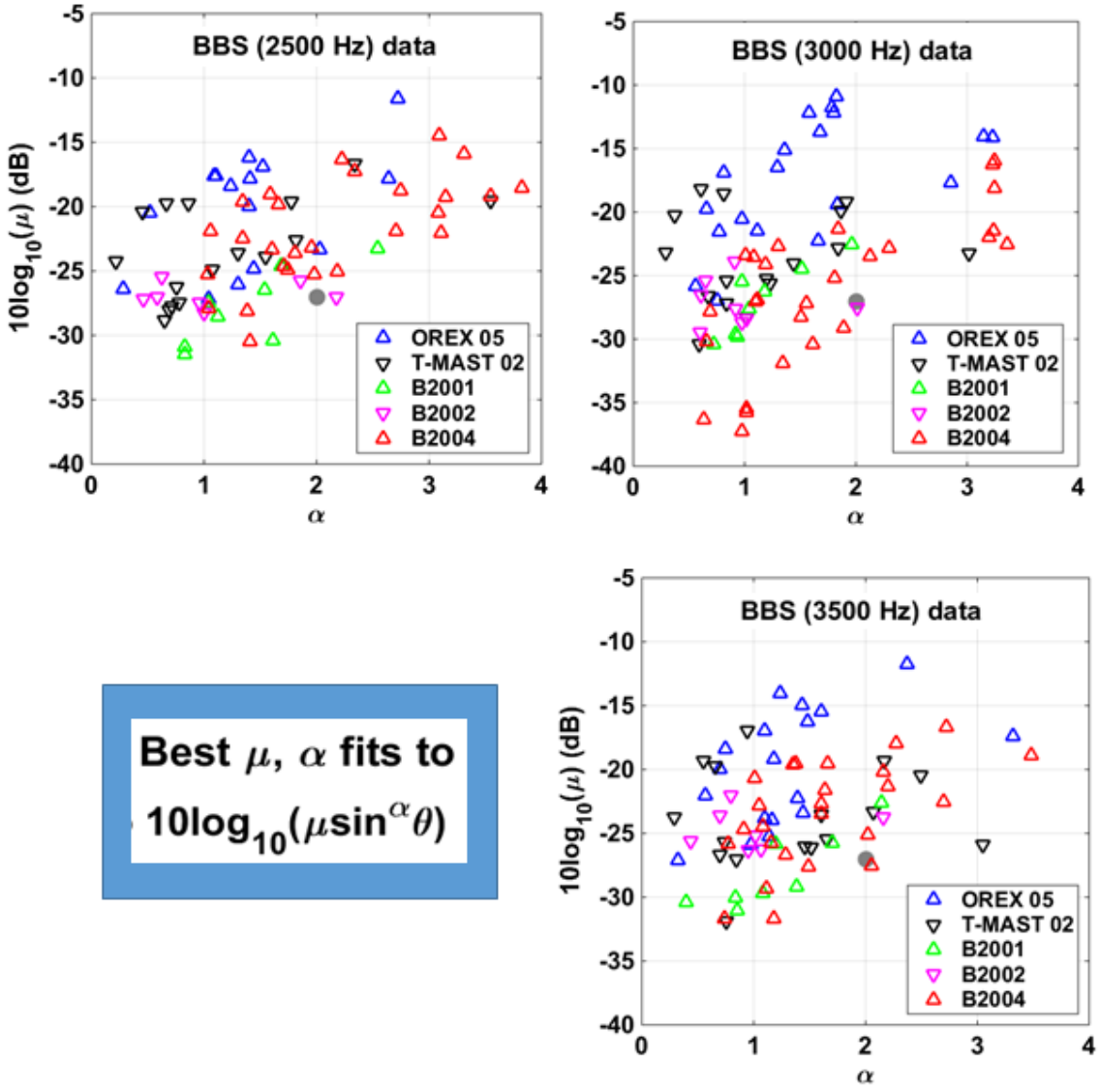

Fig. 7-1 – Distribution of best EPL-curve fit values to BBS vs. grazing angle curves at 3 frequencies for all the shallow-water sites (B2001, B2002, B2004, T-MAST-02, and OREX-05). (Mackenzie curve values (gray dot) shown as a reference.)

8. LFA-11 (DEEP WATER – SCOTIAN CONTINENTAL RISE)

NRL performed LF direct-path BBS measurements between 26 and 31 August 1993 at 19 sites (Figs. 8-1 and 8-2) on the deeply-sedimented (mostly mud) Scotian Continental Rise during the LFA-11 experiment. This section presents the BBS measurements from these sites (runs).

Set ID	Start Time (Z)	Wavetrain	# of Reps	Source Steer Angle	Latitude (deg N)	Longitude (deg W)	Water Depth (m)	Damuth Prov. Type	Receive Depth (m)	Source Depth (m)	Source Tilt (aft)	XBT Cast #
AUG 26, 1993												
20	238 0646	WTBS001	7	−24	42° 40.6′	60° 11.8′	3500		80?	119	2.5°	106
	0653	WTBS002	5	−24	42° 39.9′	60° 12.0′		TD				
	0700	WTBS001	7	−13	42° 39.6′	60° 12.2′						
	0707	WTBS002	7	−13	42° 39.4′	60° 12.4′						107
21	238 0846:39	WTBS001	3	−13	42° 35.5′	60° 14.8′	3600	TD/IA	80?	119	2.7°	107
Starting NEW WTBS001 with Set No. 22 (see logs)												
22	238 1734	WTBS001	7	−20	42° 13.6′	60° 28.8′	3950		80	119	3.4°	109
	1741	WTBS002	4	−20	42° 13.3′	60° 28.9′		IA				
	1748	WTBS001	3–4	−30	42° 13.1′	60° 29.1′						110
Rep rate for WTBS002 in Set No. 22 was 2 min (asked for 1 min)												
23	238 2025	WTBS001	8	−20	42° 06.4′	60° 33.3′	4150	IA	85	119	3.4°	111
Note new wavetrain order starting with Set No. 24 (except Set No. 31)												
24	239 0000	WTBS001	7	−30	41° 56.5′	60° 39.1′	4230		94	119	4.2°	112
	0007	WTBS001	7	−20	41° 56.1′	60° 39.3′		IA				
	0014	WTBS002	7	−20	41° 55.9′	60° 39.8′						
26	239 0619:04	WTBS001	8	−20	41° 38.6′	60° 50.7′	4420		93	119	4.2°	114
	0627:04	WTBS001	8	−30	41° 38.2′	60° 50.9′		IIB/V				
	0635:04	WTBS002	6	−20	41° 37.8′	60° 51.0′						
	0642:04	WTBS002	7	−30	41° 37.5′	60° 51.3′						
27	239 1723	WTBS001	7	−30	41° 10.5′	60° 51.9′	4630		85	118	4.2°	118
	1730	WTBS001	7	−20	41° 09.9′	60° 52.0′		V				
	1737	WTBS002	7	−20	41° 09.6′	60° 52.0′						119
28	239 2327	WTBS001	7	−30	41° 05.2′	60° 50.7′	4670		97	118	4.2°	121
	2334	WTBS001	7	−20	41° 05.5′	60° 50.7′		V				break
	2341	WTBS002	7	−20	41° 05.8′	60° 50.6′						
29	240 0533	WTBS001	8	−20	41° 15.8′	60° 51.8′	4590		85	118	6.0°	123
	0541	WTBS001	8	−30	41° 15.1′	60° 51.7′		IIA				
	0549	WTBS002	7	−20	41° 14.5′	60° 51.7′		(V)				
	0556	WTBS002	7	−30	41° 14.2′	60° 51.7′						
30	240 1154	WTBS001	7	−20	40° 53.3′	60° 50.9′	4750		87	119	3.2°	125
	1201	WTBS001	7	−30	40° 52.9′	60° 50.8′		V				
	1208	WTBS001	2–3	−20	40° 52.7′	60° 50.8′						
31	240 1723	WTBS001	7	−20	40° 33.6′	60° 50.5′	4870		125	119	2.2°	127
	1730	WTBS002	7	−20	40° 33.3′	60° 50.5′		IIA/V				
	1737	WTBS001	7	−30	40° 32.9′	60° 50.5′						
	1744	WTBS002	7	−30	40° 32.5′	60° 50.5′						
32	241 0000	WTBS001	8	−20	40° 14.8′	60° 52.8′	4970		85	118	6°	130
	0008	WTBS001	8	−30	40° 15.0′	60° 53.1′		V/IIA	75			
	0016	WTBS002	7	−20	40° 15.3′	60° 53.4′			75			
	0023	WTBS002	7	−30	40° 15.5′	60° 53.6′			75			
33	241 1221	WTBS001	7	−30	40° 22.7′	60° 53.9′	4910		117	118		134
	1228	WTBS001	7	−20	40° 22.3′	60° 53.9′		IIA				
	1235	WTBS002	5	−20	40° 21.8′	60° 53.9′		(V)				
34	241 1824	WTBS001	7	−30	40° 04.8′	60° 54.0′	5030		68	118	5.5°	136
	1831	WTBS001	7	−20	40° 05.0′	60° 53.9′		IIA				
	1838	WTBS002	6	−20	40° 05.1′	60° 53.9′		(V)				
35	241 2351	WTBS001	7	−30	39° 54.0′	60° 57.4′	5090		102	118	1°	138
	2358	WTBS001	7	−20	39° 53.7′	60° 57.4′		IIA				
	242 0005	WTBS002	6	−20	39° 53.3′	60° 57.5′						
36	242 0646	WTBS001	3	−30	39° 42.5′	61° 08.5′	5150	IIA	63	118	7°	140
	0650:44	WTBS001	4	−30	39° 42.5′	61° 08.8′						
37	242 1215	WTBS001	8	−20	39° 42.0′	61° 31.3′	5130		63	118	7°	142
	1223	WTBS001	8	−30	39° 41.7′	61° 31.6′		IIA				
	1231	WTBS002	5	−20	39° 41.5′	61° 32.1′						
38	242 2348	WTBS001	8	−20	40° 03.3′	62° 00.2′	4970		85	118	3.5°	146
	2356	WTBS001	8	−30	40° 03.7′	61° 59.9′						
	243 0004	WTBS002	6	−20	40° 04.1′	61° 59.3′						
	0011	WTBS002	7	−30	40° 04.4′	61° 59.0′		IIB/IIA				
	0018:30	WTBS001	7	−20	40° 04.7′	61° 58.7′			83			
	0025:30	WTBS001	7	−30	40° 05.0′	61° 58.2′						
	0032:30	WTBS002	2	−20	40° 05.3′	61° 57.7′						
AUG 31, 1993												
39	243 0512:26	WTBS001	8	−20	40° 01.5′	61° 36.7′	4990		69	119	5.5°	148
	0520:26	WTBS001	8	−30	40° 01.2′	61° 35.9′		IIA				
	0528:26	WTBS002	1	−20	40° 00.9′	61° 35.4′						

Damuth Province Key (Echo Type)

IA - Distinct echoes (sharp echoes with several parallel subbottoms)
IIA - Indistinct echoes (semi-prolonged echoes with intermittent or discontinuous subbottoms)
IIB - Indistinct echoes (very prolonged echoes with no subbottoms)
V - Miscellaneous echoes (distinct echoes with conformable to non-conformable subbottoms)
TD - Generalized echoes (Turbidite deposition. Echo types IA, IIA and IIB)

Fig. 8-1 – LFA-11 BBS site/run ('Set ID') information.

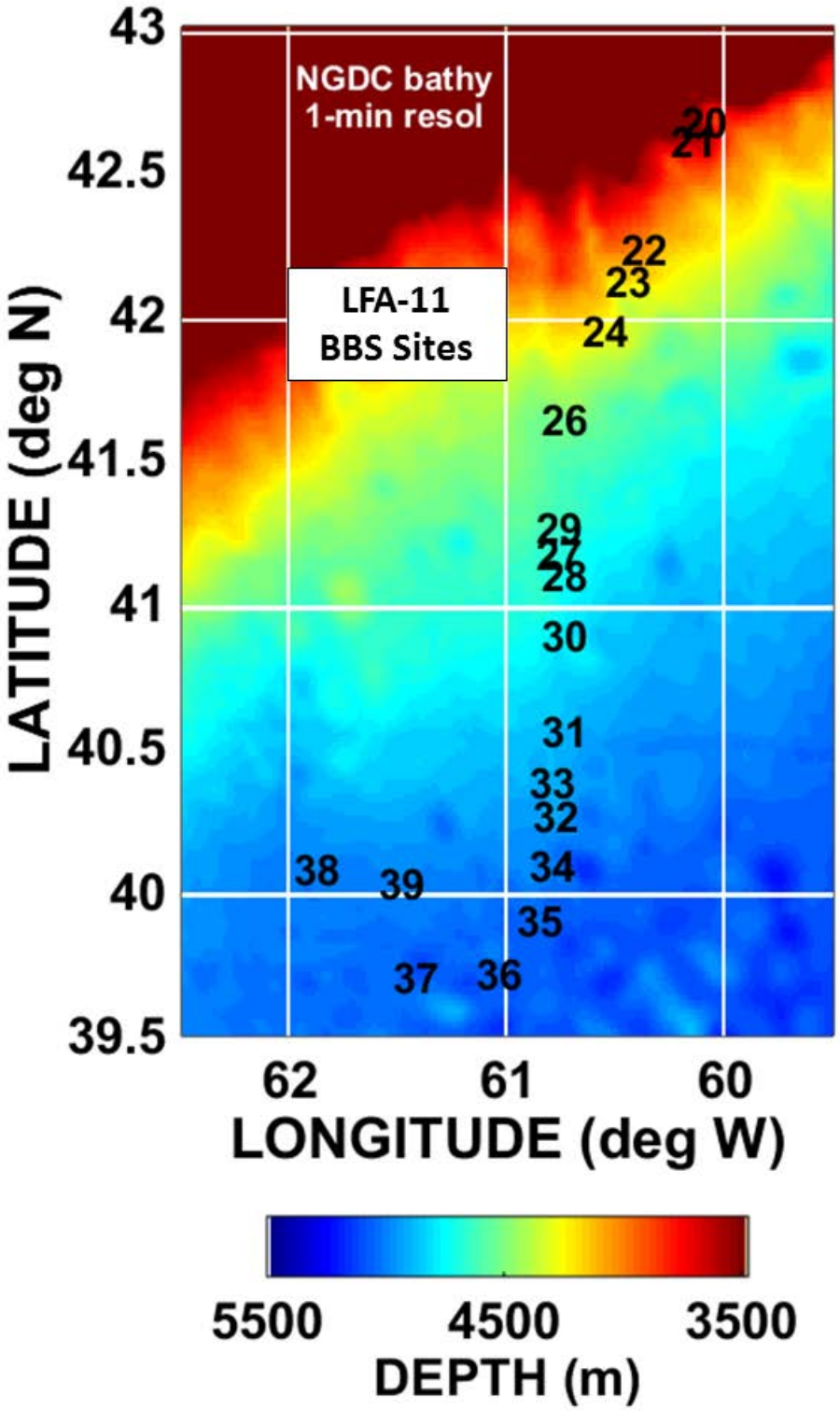

Fig. 8-2 – LFA-11 BBS sites (runs) geographically vs. bathymetry.

A. Test Operations

Direct-path, quasi-monostatic acoustic BBS LF measurements were conducted under the auspices of SPAWAR (PMW 182) from the M/V *Cory Chouest* using a high-resolution HLA and a source with vertical directivity, jointly towed at ~1.5 m/s. Measurements were made primarily using combinations of 0.1- and 1-s CWs at 190 and 270 Hz, and 1- and 4-s HFM sweeps spanning 210-230 and 290-310 Hz. Each signal was typically transmitted 7 times at a rep rate of 60 s. Subsets of these signals were repeated at two source steering angles to enhance the grazing-angle coverage. The relatively shallow receiver and source center depths are listed in Fig. 8.1. The receiver-look directions used in deriving the BSS values were ~130–160°R. The sonar equation was used at each depth to derive scattering strengths as a function of beam, frequency, and grazing angle.

B. Measured Bottom Backscattering Strengths

Figures 8.B-1–8.B-64 show bottom backscattering strengths measured at the 19 LFA-11 'Segment 3' sites/runs (Figs. 8-1 and 8-2) for the above signal combinations. The header at the top of each image gives the signal duration and frequency, along with the source-steering angle. (Generally, the axes limits are the same, but occasionally the x-axis upper limit varies, e.g., Site/Run 24.)

The low-frequency BBS oscillations are hypothesized to be a propagation effect due to a standing wave being generated between the water-sediment interface and a caustic in the very thick sediment (Gauss *et al*., 1996). The change of depth of the caustic with range is responsible for the oscillations with grazing angle; the sediment sound-speed profile drives the amplitude. See Holland and Neumann (1998) for a theoretical model of the phenomenon with application to CST-5 data at 225 and 930 Hz. See Vogt and Tucholke (1986) for details on the geology of the Scotian Continental Rise.

Run 20

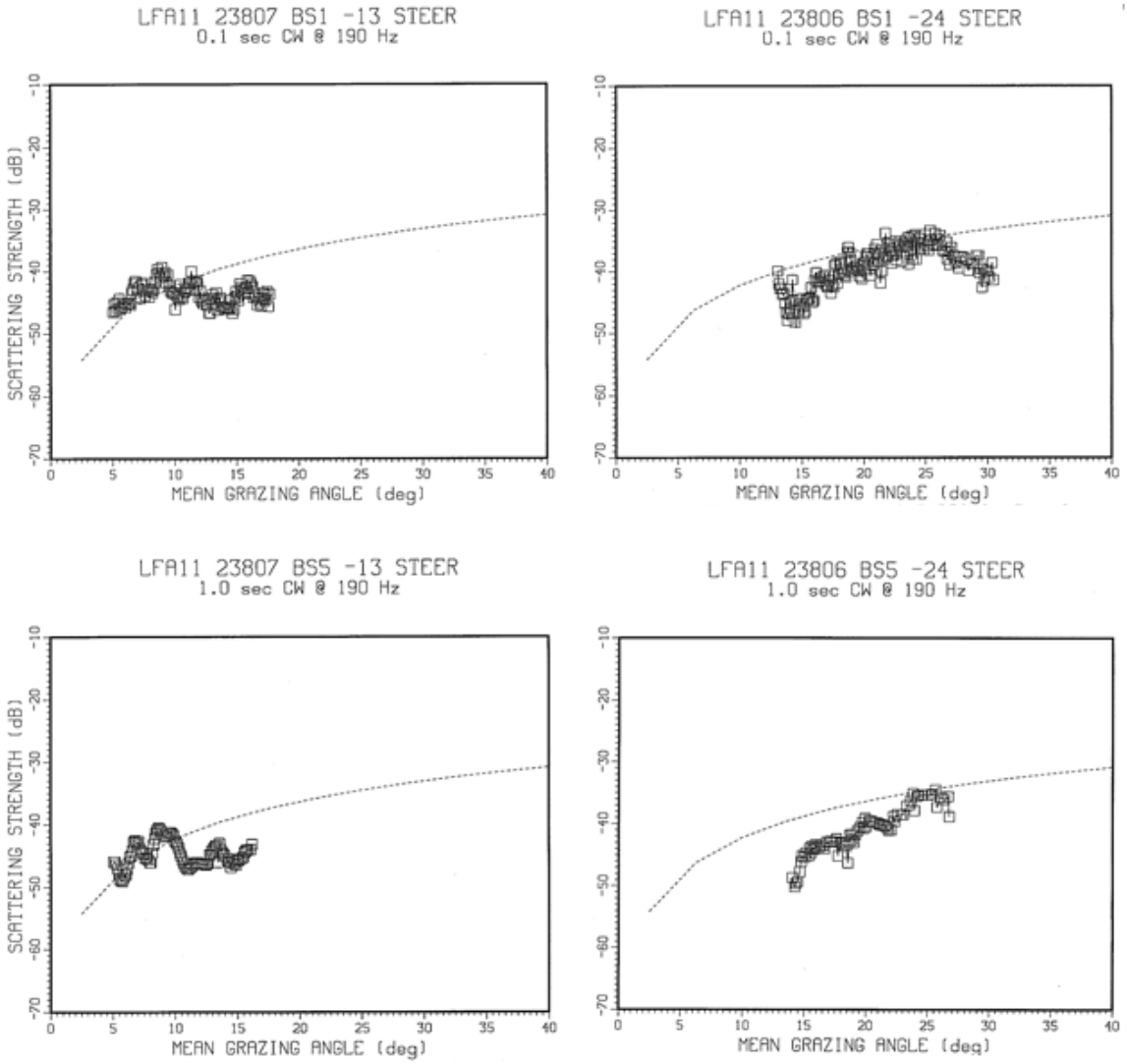

Fig. 8.B-1 – Site 20 LFA-11 BBS vs. grazing angle for 0.1-s (top) and 1-s (bottom) CW signals at 190 Hz and source-steering angles of down 13 (left) and down 24 (right) deg. (Mackenzie curve (dotted) shown as a reference.)

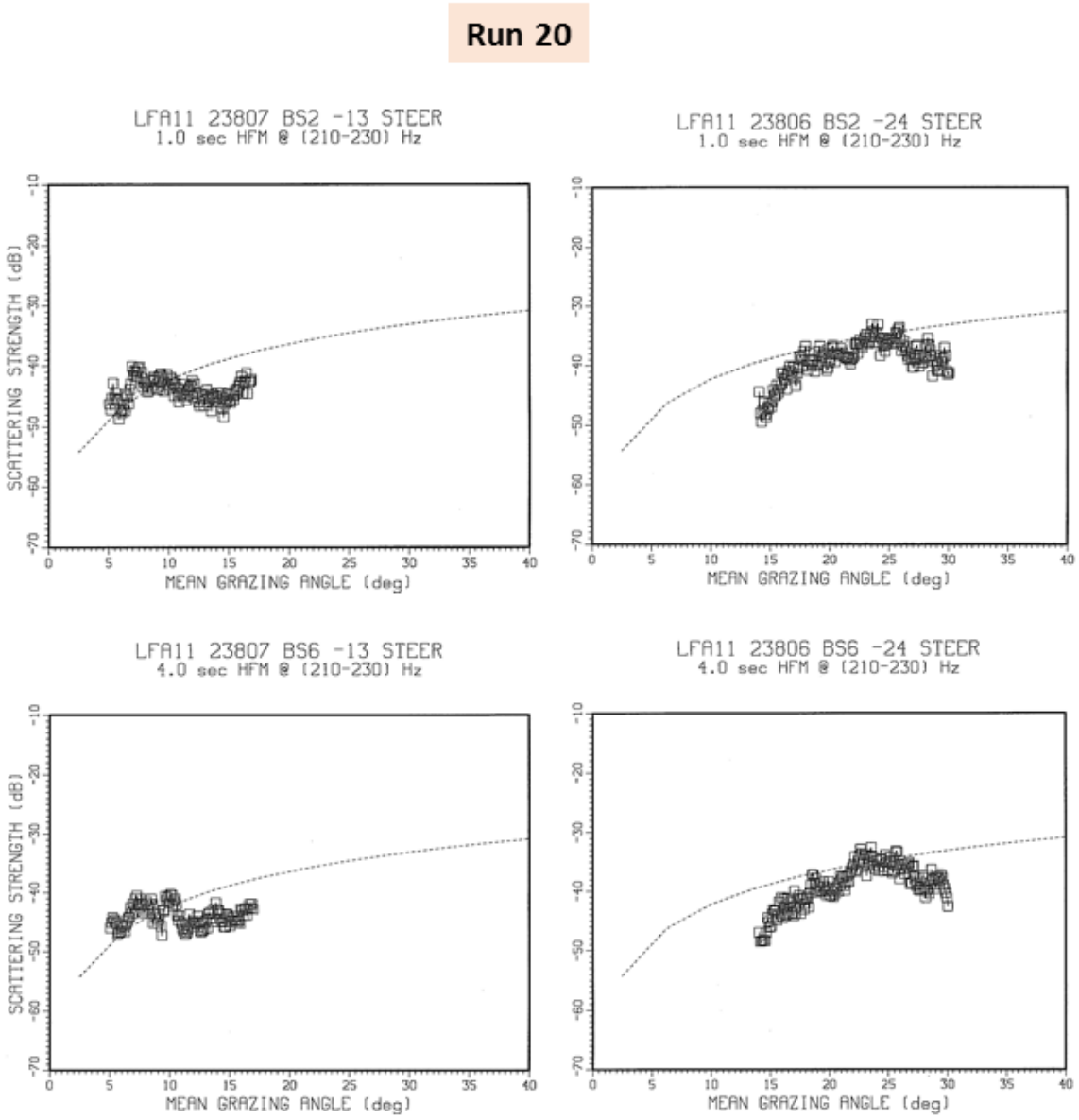

Fig. 8.B-2 – Site 20 LFA-11 BBS vs. grazing angle for 1-s (top) and 4-s (bottom) HFM signals sweeping 210–230 Hz and source-steering angles of down 13 (left) and down 24 (right) deg. (Mackenzie curve (dotted) shown as a reference.)

Run 20

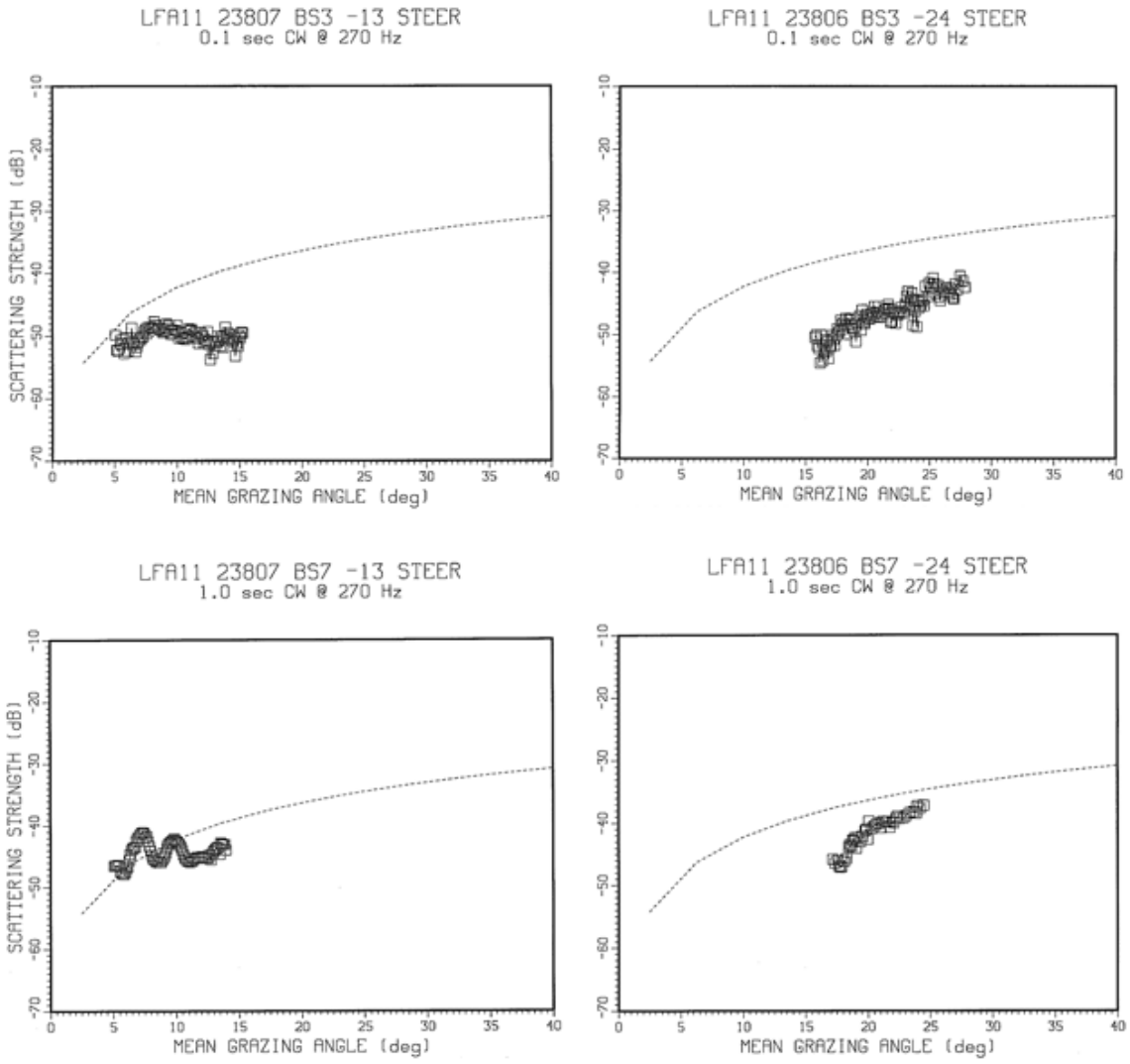

Fig. 8.B-3 – Site 20 LFA-11 BBS vs. grazing angle for 0.1-s (top) and 1-s (bottom) CW signals at 270 Hz and source-steering angles of down 13 (left) and down 24 (right) deg. (Mackenzie curve (dotted) shown as a reference.)

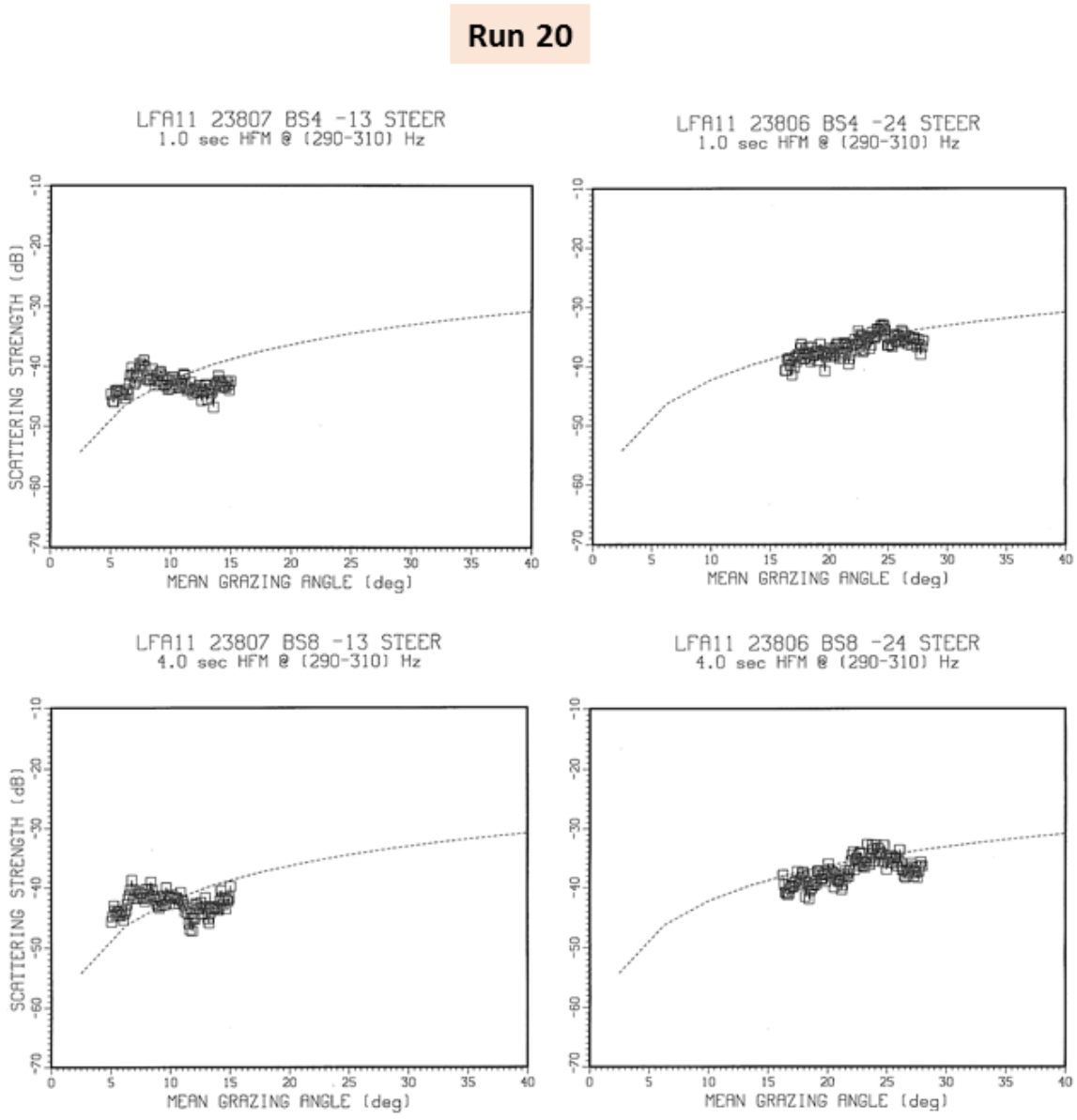

Fig. 8.B-4 – Site 20 LFA-11 BBS vs. grazing angle for 1-s (top) and 4-s (bottom) HFM signals sweeping 290–310 Hz and source-steering angles of down 13 (left) and down 24 (right) deg. (Mackenzie curve (dotted) shown as a reference.)

Run 21

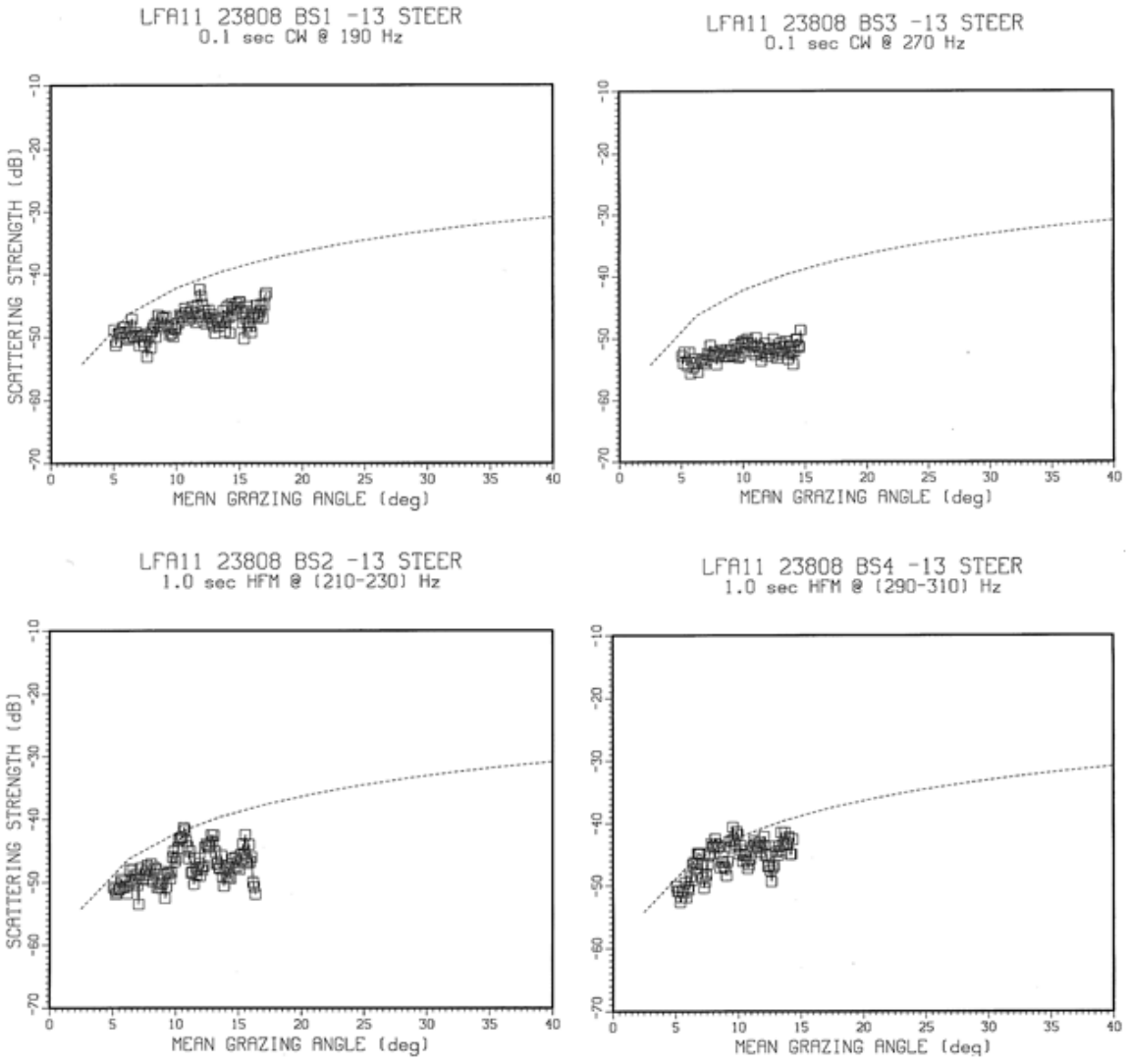

Fig. 8.B-5 – Site 21 LFA-11 BBS vs. grazing angle for 4 signals: 0.1-s CWs (top) at 190 (left) and 270 (right) Hz; and 1-s HFMs (bottom) sweeping 210–230 (left) and 290–310 (right) Hz. The source-steering angle was down 13 deg.
(Mackenzie curve (dotted) shown as a reference.)

Run 22

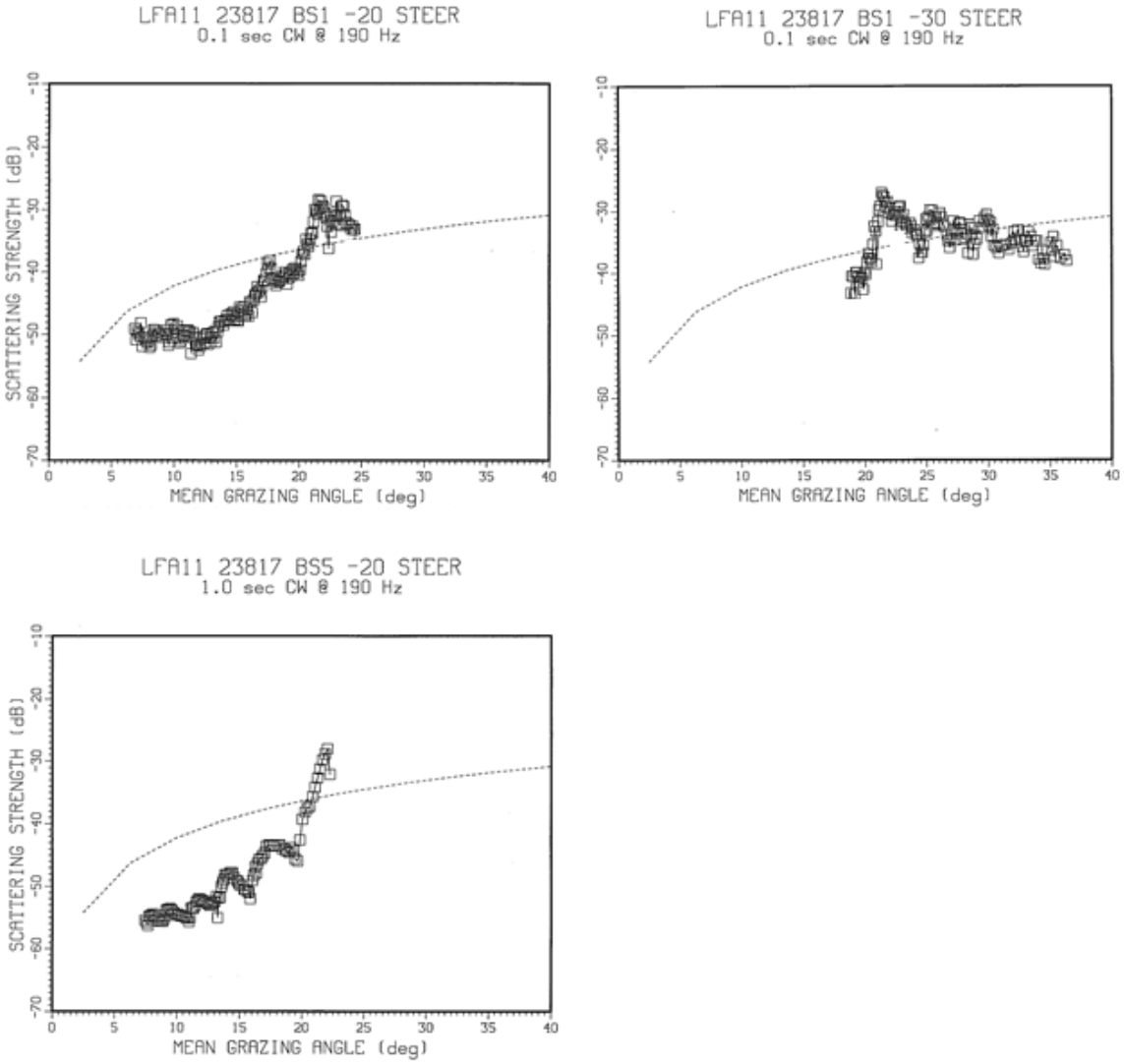

Fig. 8.B-6 – Site 22 LFA-11 BBS vs. grazing angle for 0.1-s (top) and 1-s (bottom) CW signals at 190 Hz and source-steering angles of down 20 (left) and down 30 (right) deg. (Mackenzie curve (dotted) shown as a reference.)

Run 22

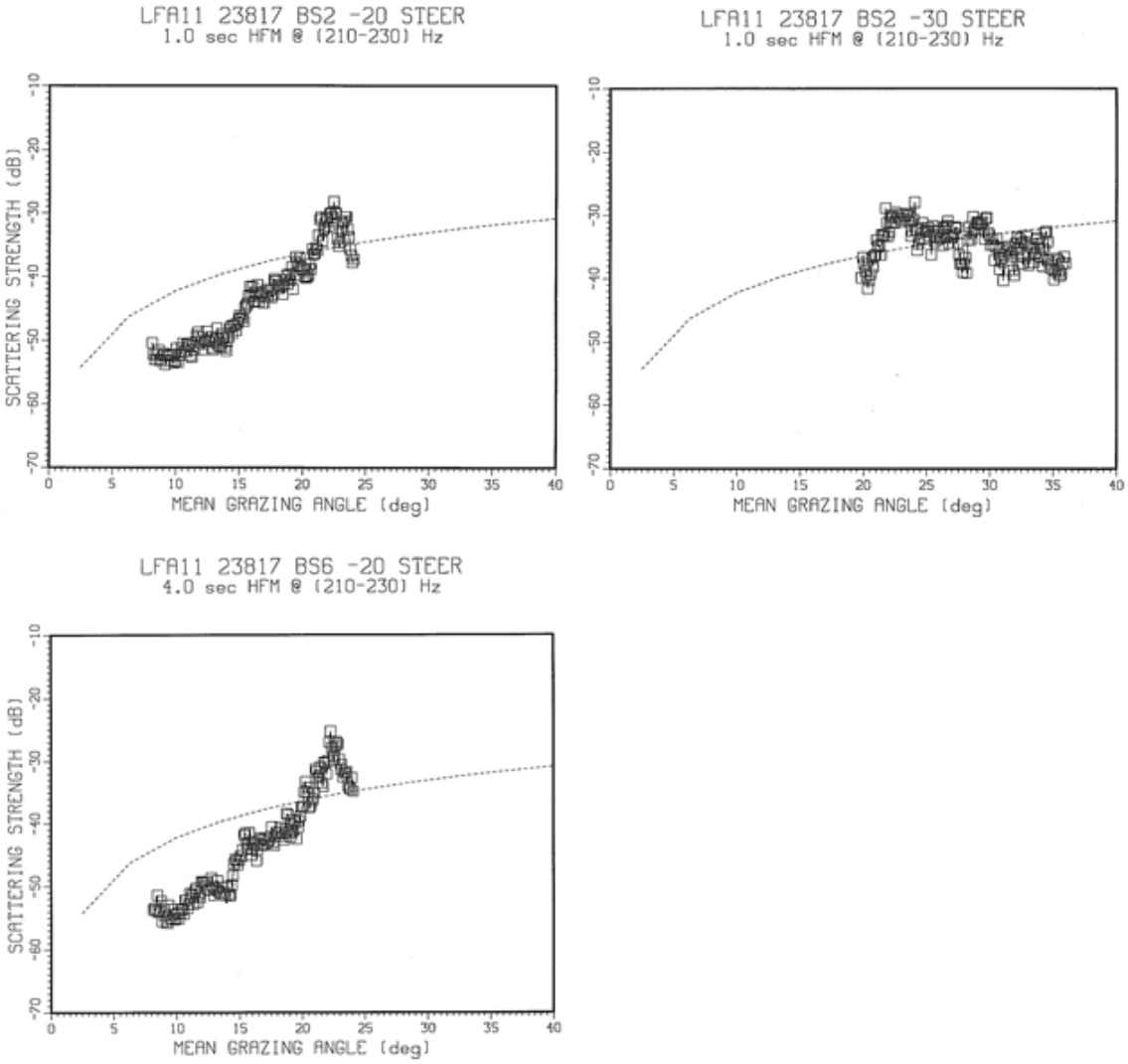

Fig. 8.B-7 – Site 22 LFA-11 BBS vs. grazing angle for 1-s (top) and 4-s (bottom) HFM signals sweeping 210–230 Hz and source-steering angles of down 20 (left) and down 30 (right) deg. (Mackenzie curve (dotted) shown as a reference.)

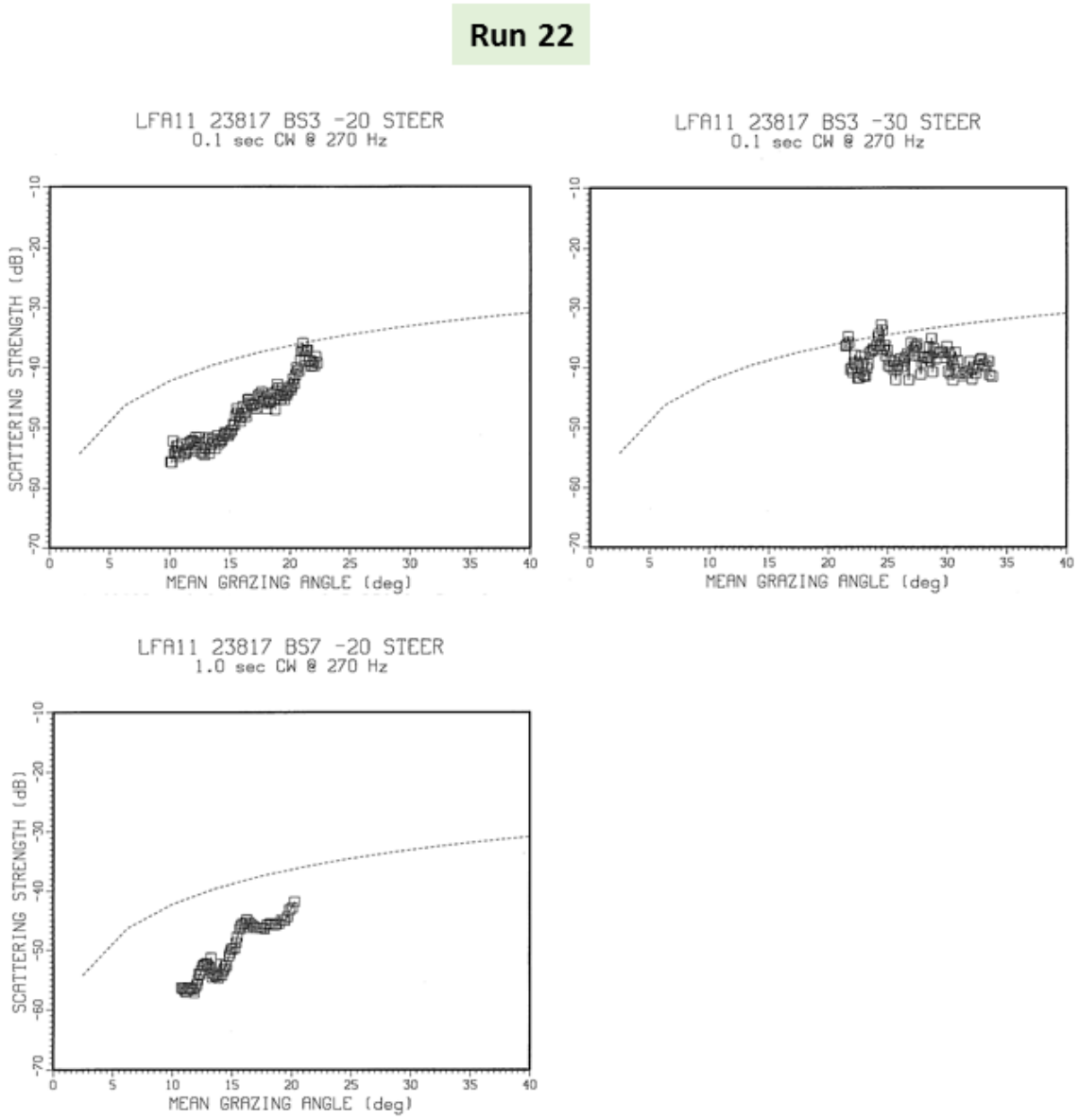

Fig. 8.B-8 – Site 22 LFA-11 BBS vs. grazing angle for 0.1-s (top) and 1-s (bottom) CW signals at 270 Hz and source-steering angles of down 20 (left) and down 30 (right) deg. (Mackenzie curve (dotted) shown as a reference.)

Run 22

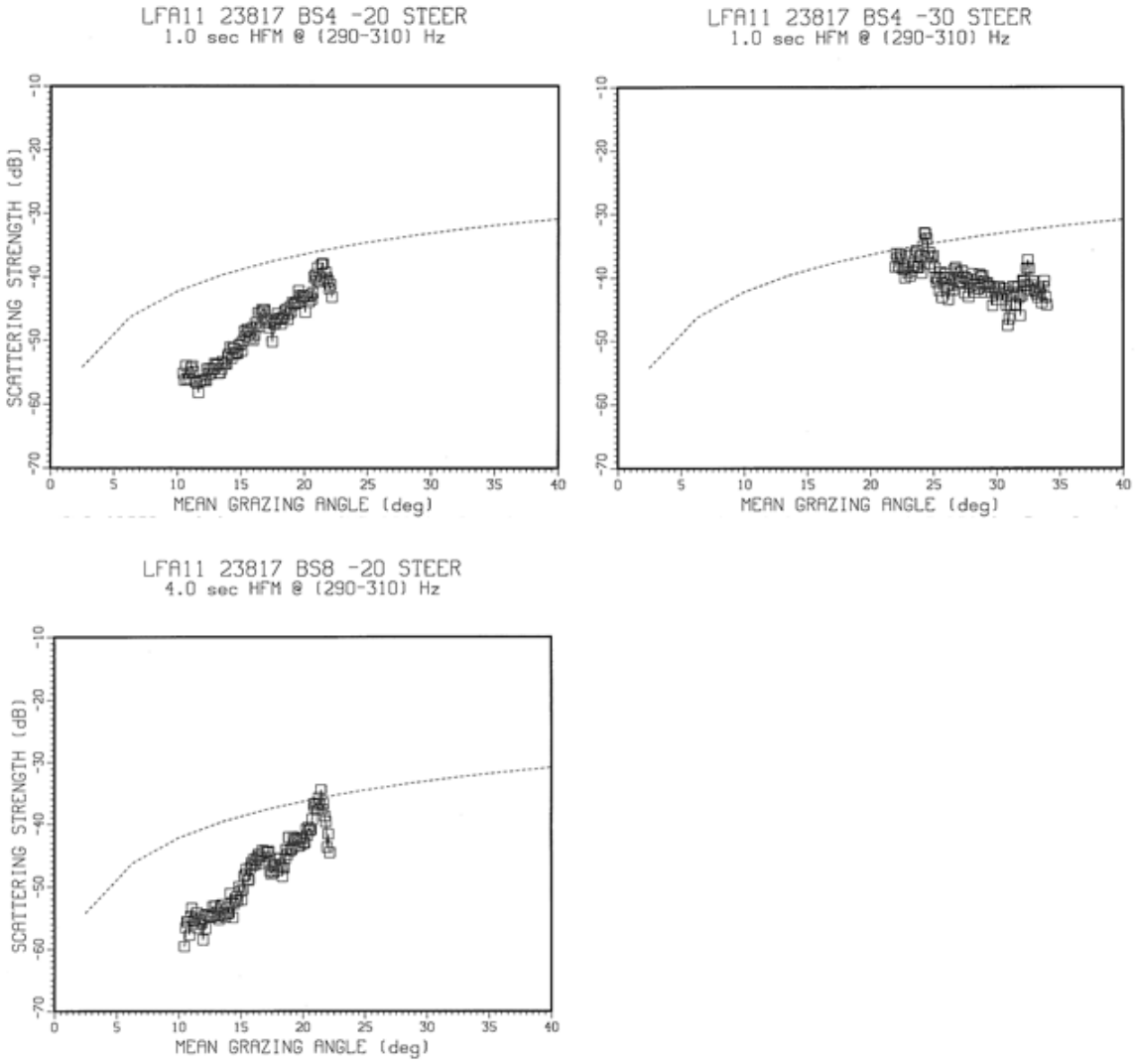

Fig. 8.B-9 – Site 22 LFA-11 BBS vs. grazing angle for 1-s (top) and 4-s (bottom) HFM signals sweeping 290–310 Hz and source-steering angles of down 20 (left) and down 30 (right) deg. (Mackenzie curve (dotted) shown as a reference.)

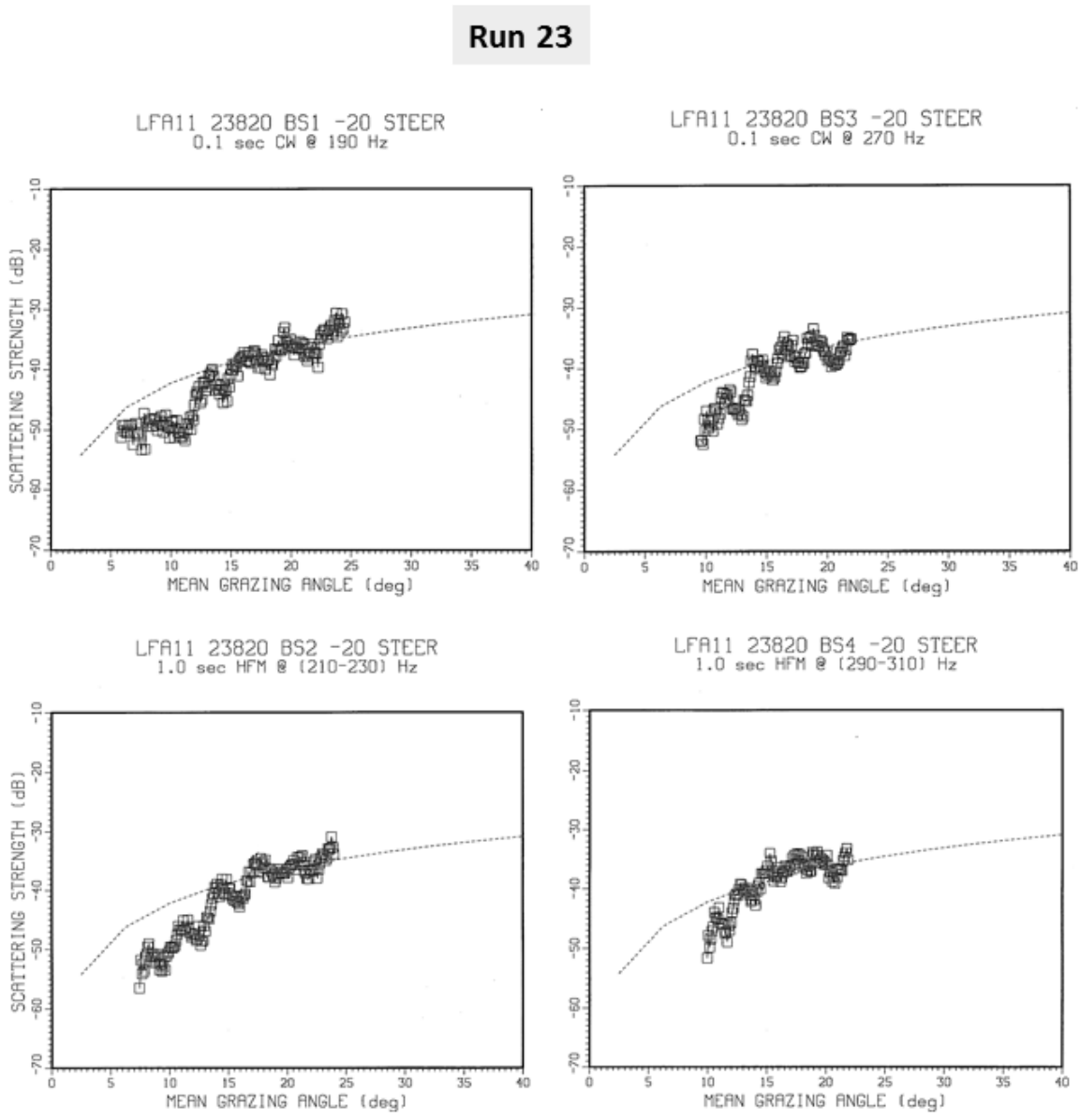

Fig. 8.B-10 – Site 23 LFA-11 BBS vs. grazing angle for 4 signals: 0.1-s CWs (top) at 190 (left) and 270 (right) Hz; and 1-s HFMs (bottom) sweeping 210–230 (left) and 290–310 (right) Hz. The source-steering angle was down 20 deg.
(Mackenzie curve (dotted) shown as a reference.)

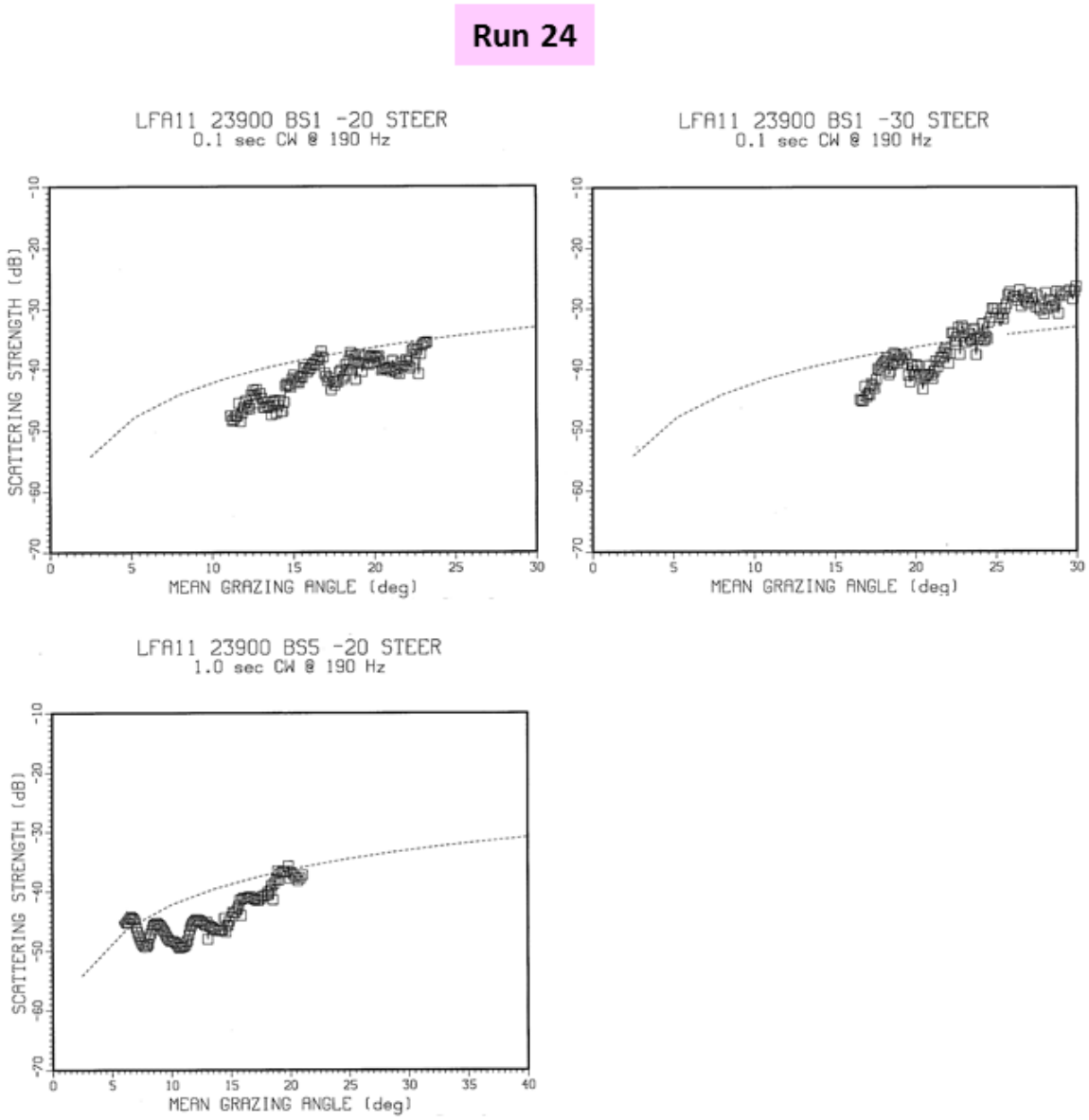

Fig. 8.B-11 – Site 24 LFA-11 BBS vs. grazing angle for 0.1-s (top) and 1-s (bottom) CW signals at 190 Hz and source-steering angles of down 20 (left) and down 30 (right) deg. (Mackenzie curve (dotted) shown as a reference.)

Run 24

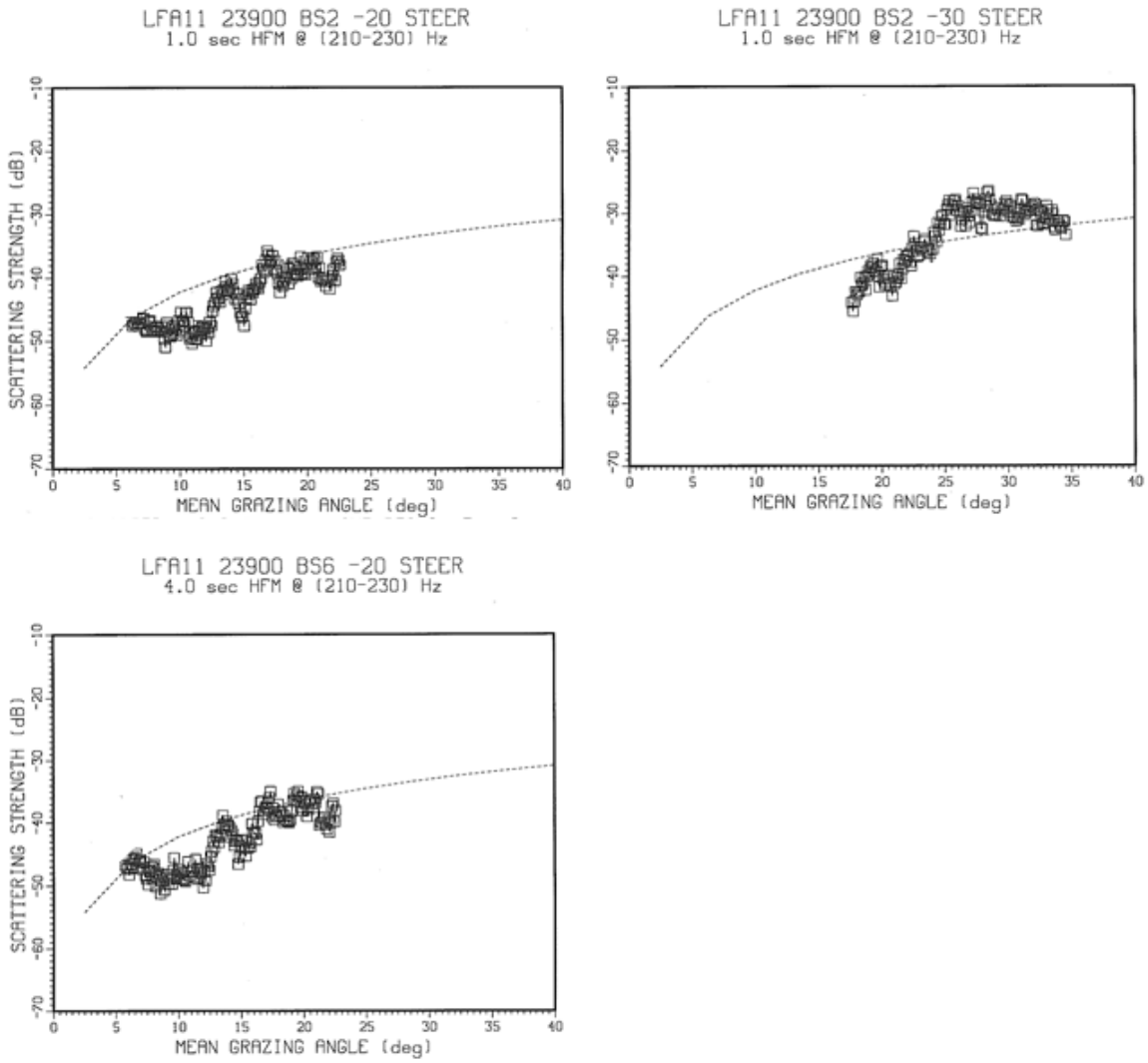

Fig. 8.B-12 – Site 24 LFA-11 BBS vs. grazing angle for 1-s (top) and 4-s (bottom) HFM signals sweeping 210–230 Hz and source-steering angles of down 20 (left) and down 30 (right) deg. (Mackenzie curve (dotted) shown as a reference.)

Run 24

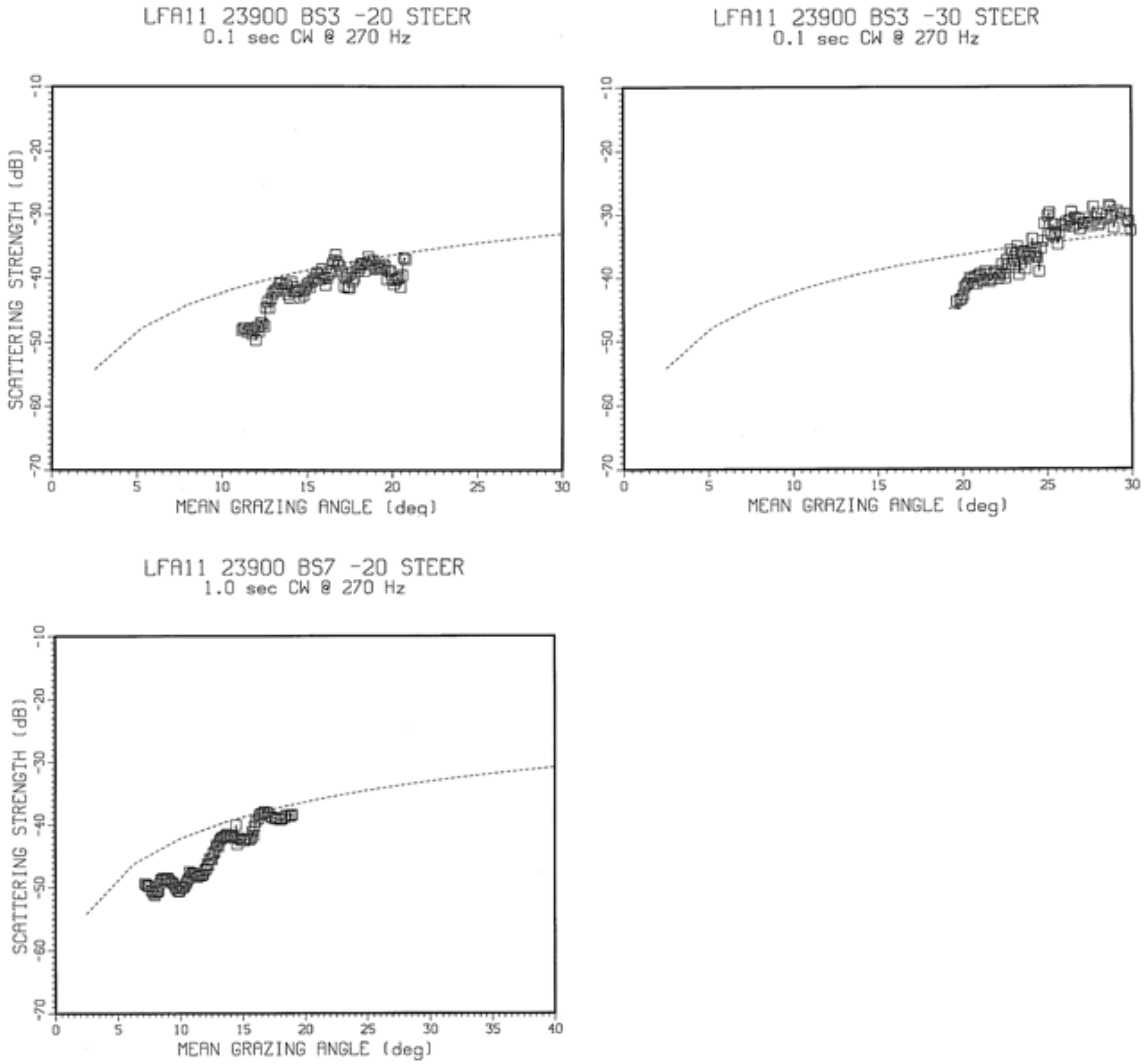

Fig. 8.B-13 – Site 24 LFA-11 BBS vs. grazing angle for 0.1-s (top) and 1-s (bottom) CW signals at 270 Hz and source-steering angles of down 20 (left) and down 30 (right) deg. (Mackenzie curve (dotted) shown as a reference.)

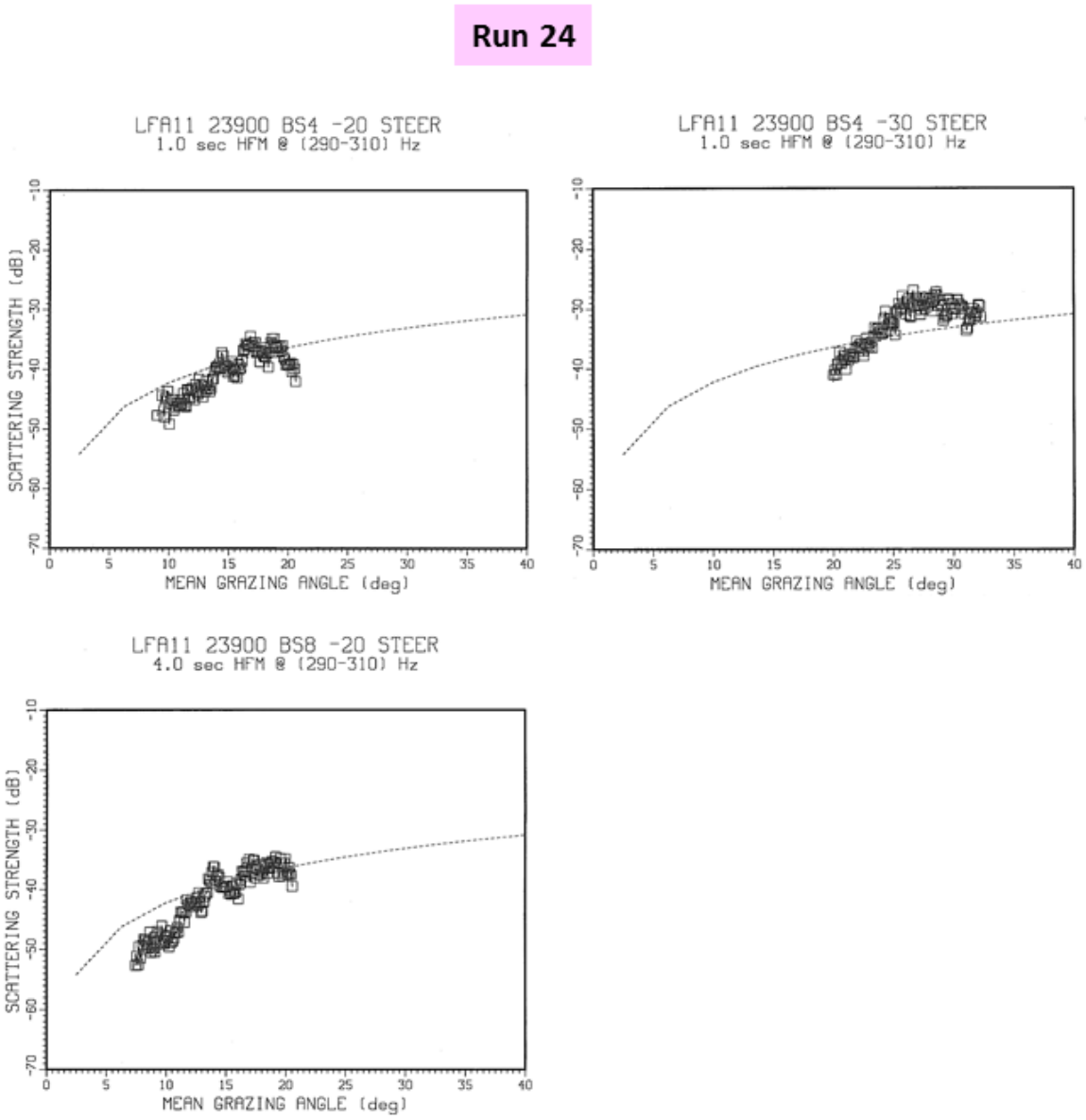

Fig. 8.B-14 – Site 24 LFA-11 BBS vs. grazing angle for 1-s (top) and 4-s (bottom) HFM signals sweeping 290–310 Hz and source-steering angles of down 20 (left) and down 30 (right) deg. (Mackenzie curve (dotted) shown as a reference.)

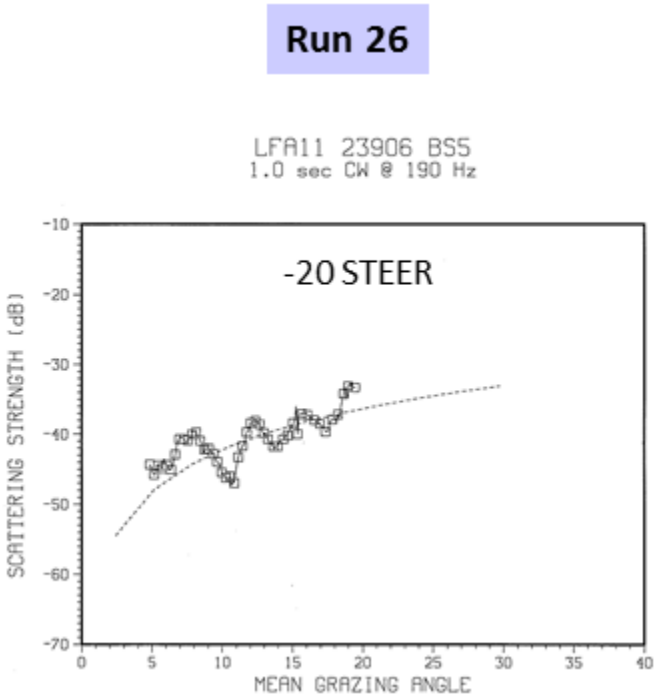

Fig. 8.B-15 – Site 26 LFA-11 BBS vs. grazing angle for 1-s CW signals at 190 Hz and a source-steering angle of down 20 deg. (Mackenzie curve (dotted) shown as a reference.)

Run 27

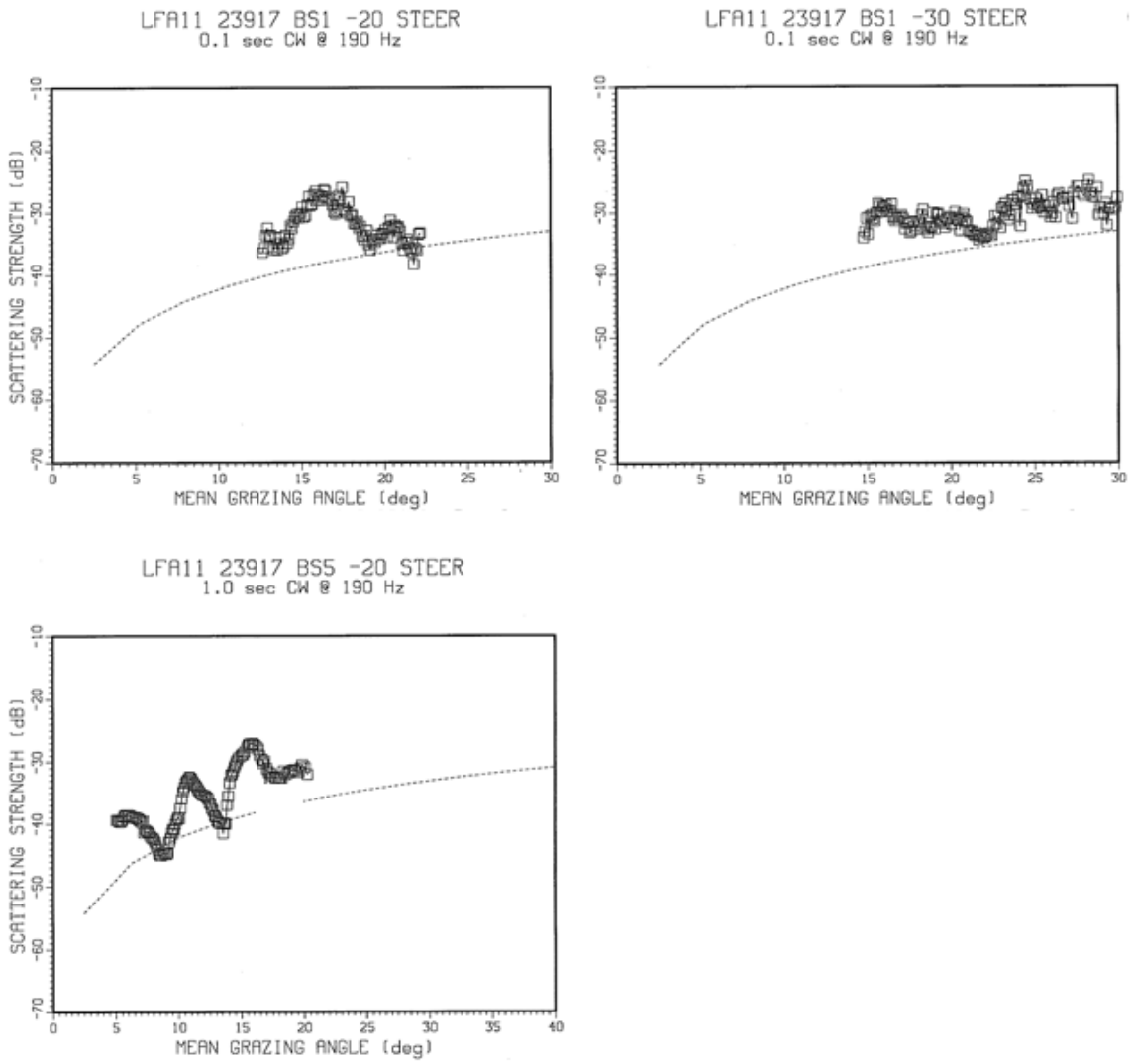

Fig. 8.B-16 – Site 27 LFA-11 BBS vs. grazing angle for 0.1-s (top) and 1-s (bottom) CW signals at 190 Hz and source-steering angles of down 20 (left) and down 30 (right) deg. (Mackenzie curve (dotted) shown as a reference.)

Run 27

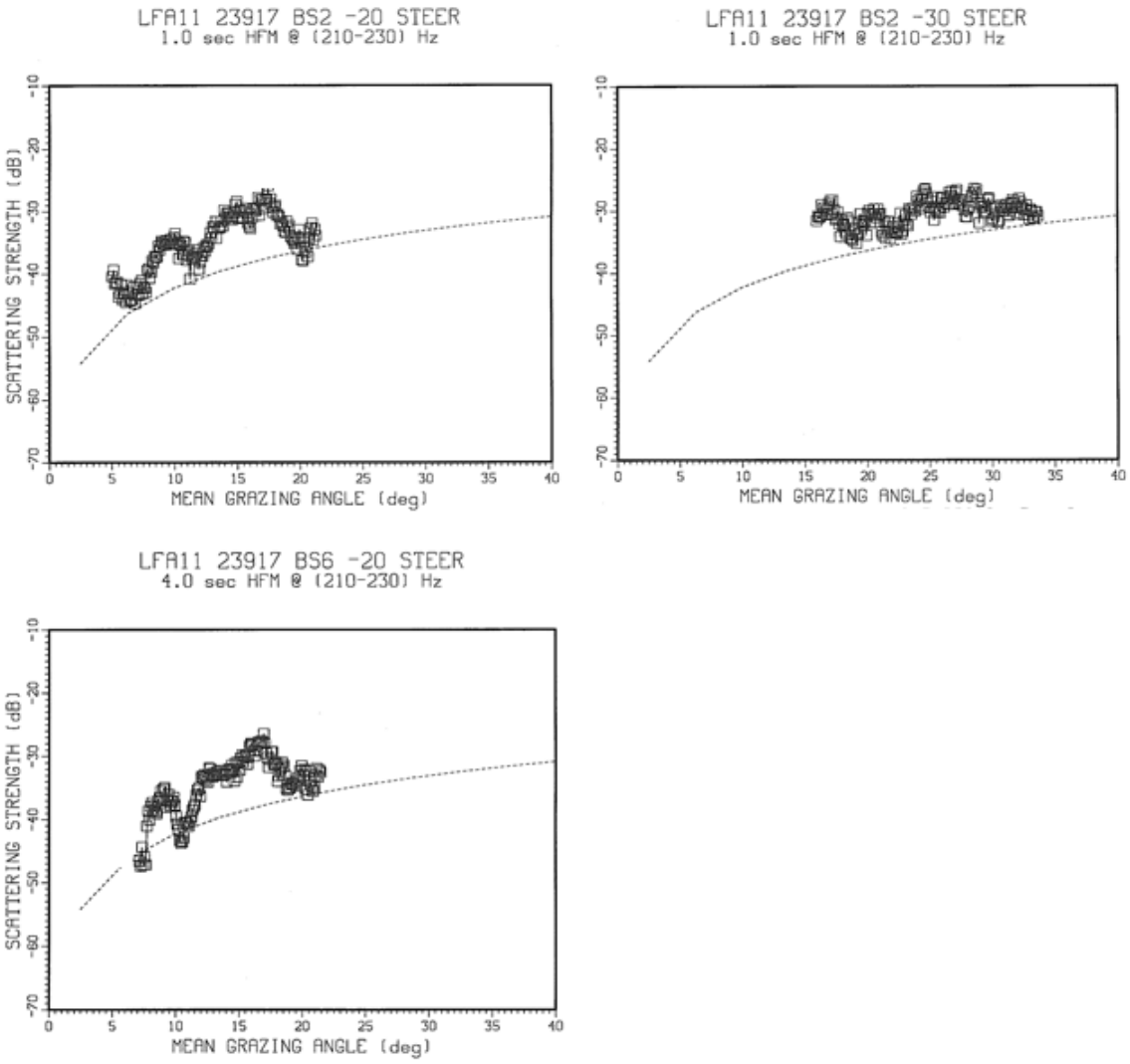

Fig. 8.B-17 – Site 27 LFA-11 BBS vs. grazing angle for 1-s (top) and 4-s (bottom) HFM signals sweeping 210–230 Hz and source-steering angles of down 20 (left) and down 30 (right) deg. (Mackenzie curve (dotted) shown as a reference.)

Run 27

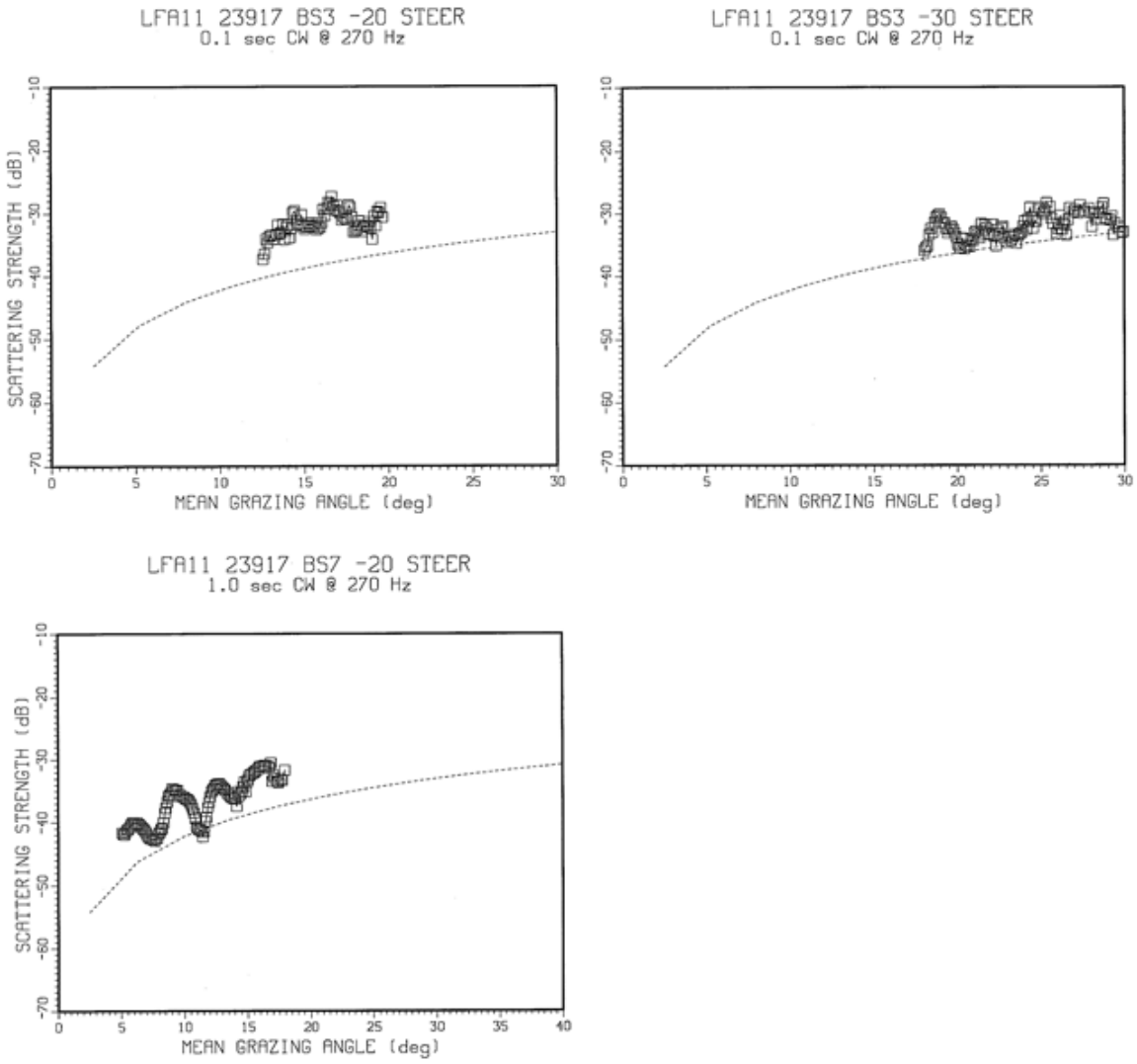

Fig. 8.B-18 – Site 27 LFA-11 BBS vs. grazing angle for 0.1-s (top) and 1-s (bottom) CW signals at 270 Hz and source-steering angles of down 20 (left) and down 30 (right) deg. (Mackenzie curve (dotted) shown as a reference.)

Run 27

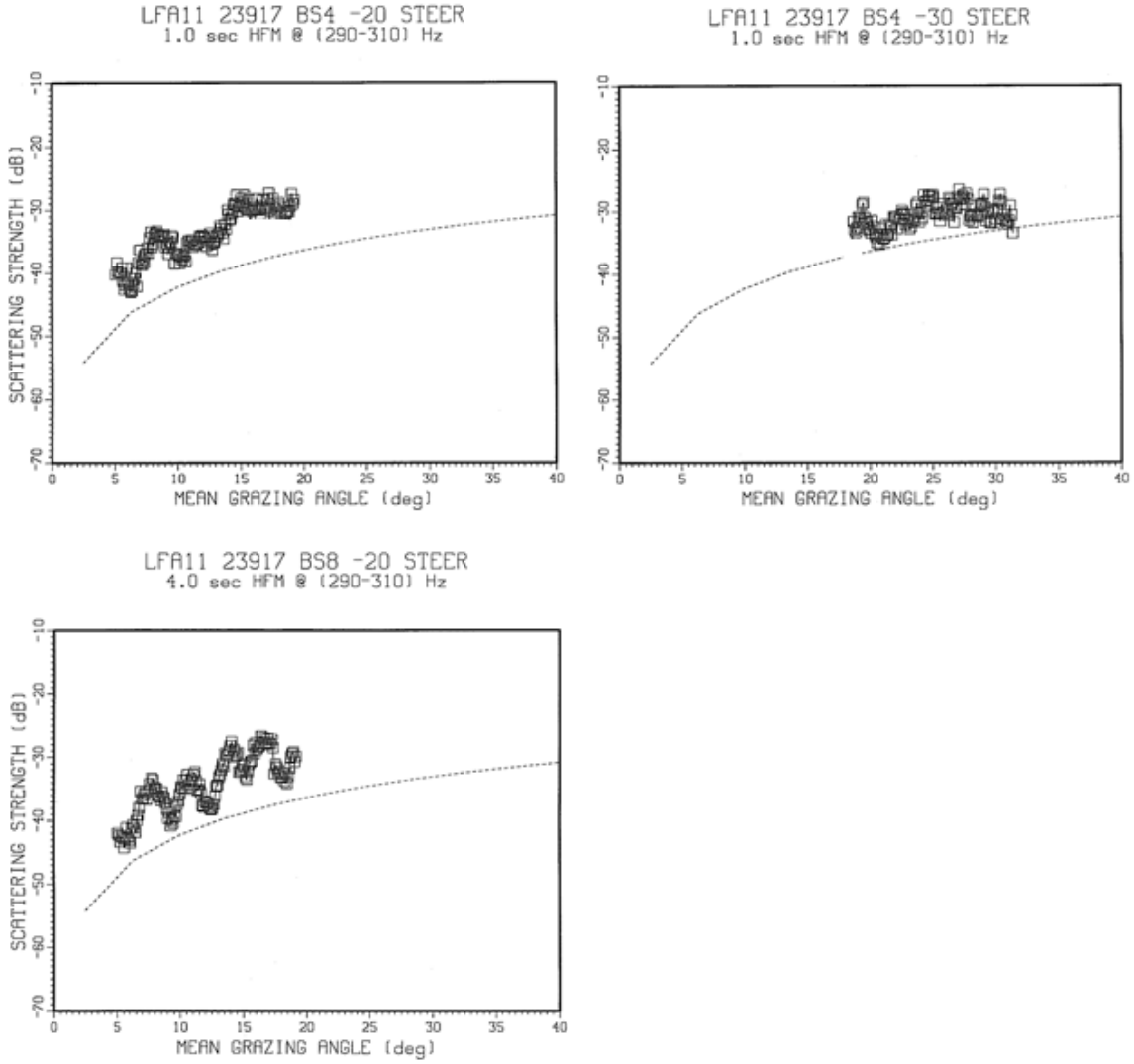

Fig. 8.B-19 – Site 27 LFA-11 BBS vs. grazing angle for 1-s (top) and 4-s (bottom) HFM signals sweeping 290–310 Hz and source-steering angles of down 20 (left) and down 30 (right) deg. (Mackenzie curve (dotted) shown as a reference.)

Run 28

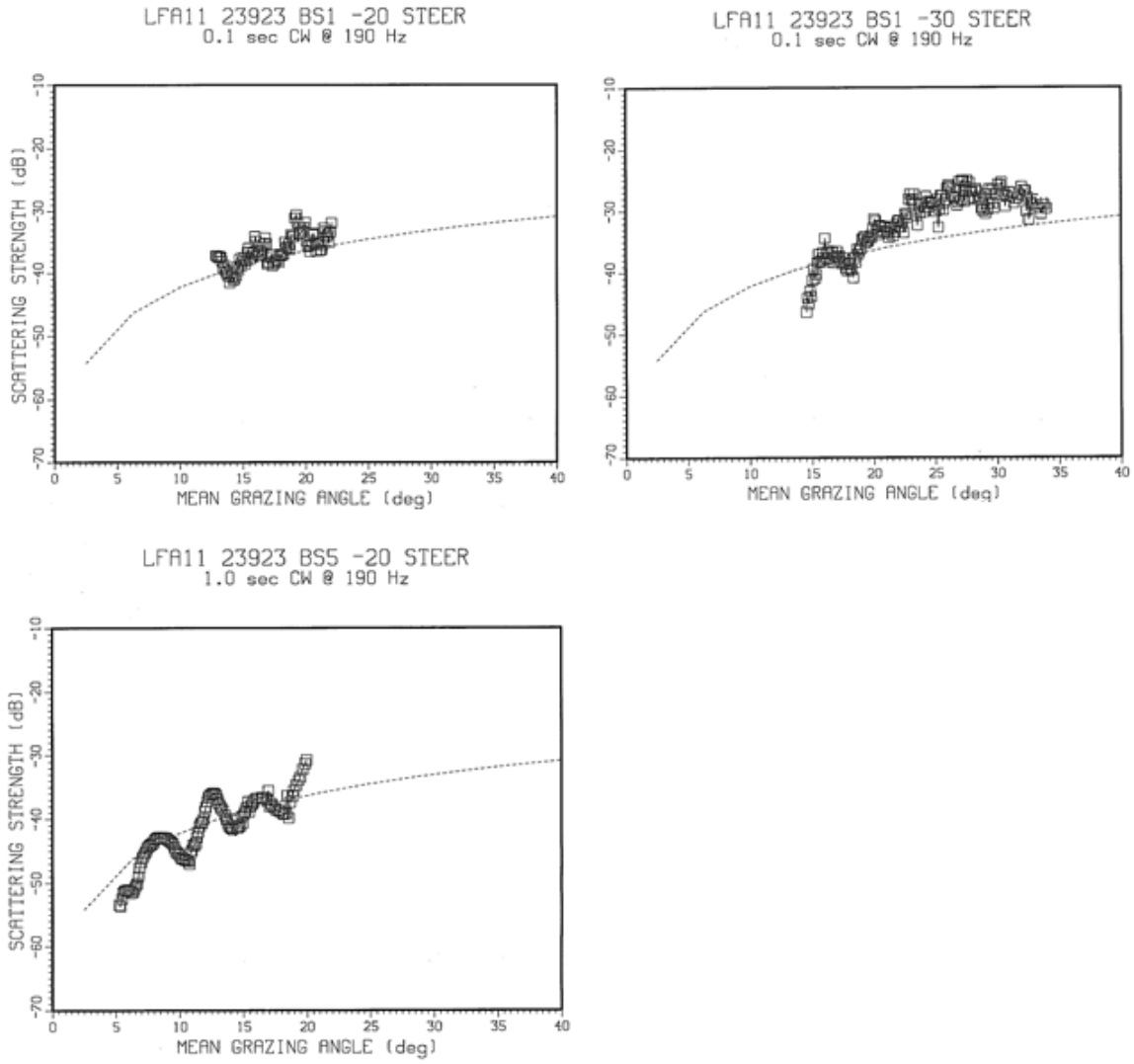

Fig. 8.B-20 – Site 28 LFA-11 BBS vs. grazing angle for 0.1-s (top) and 1-s (bottom) CW signals at 190 Hz and source-steering angles of down 20 (left) and down 30 (right) deg. (Mackenzie curve (dotted) shown as a reference.)

Run 28

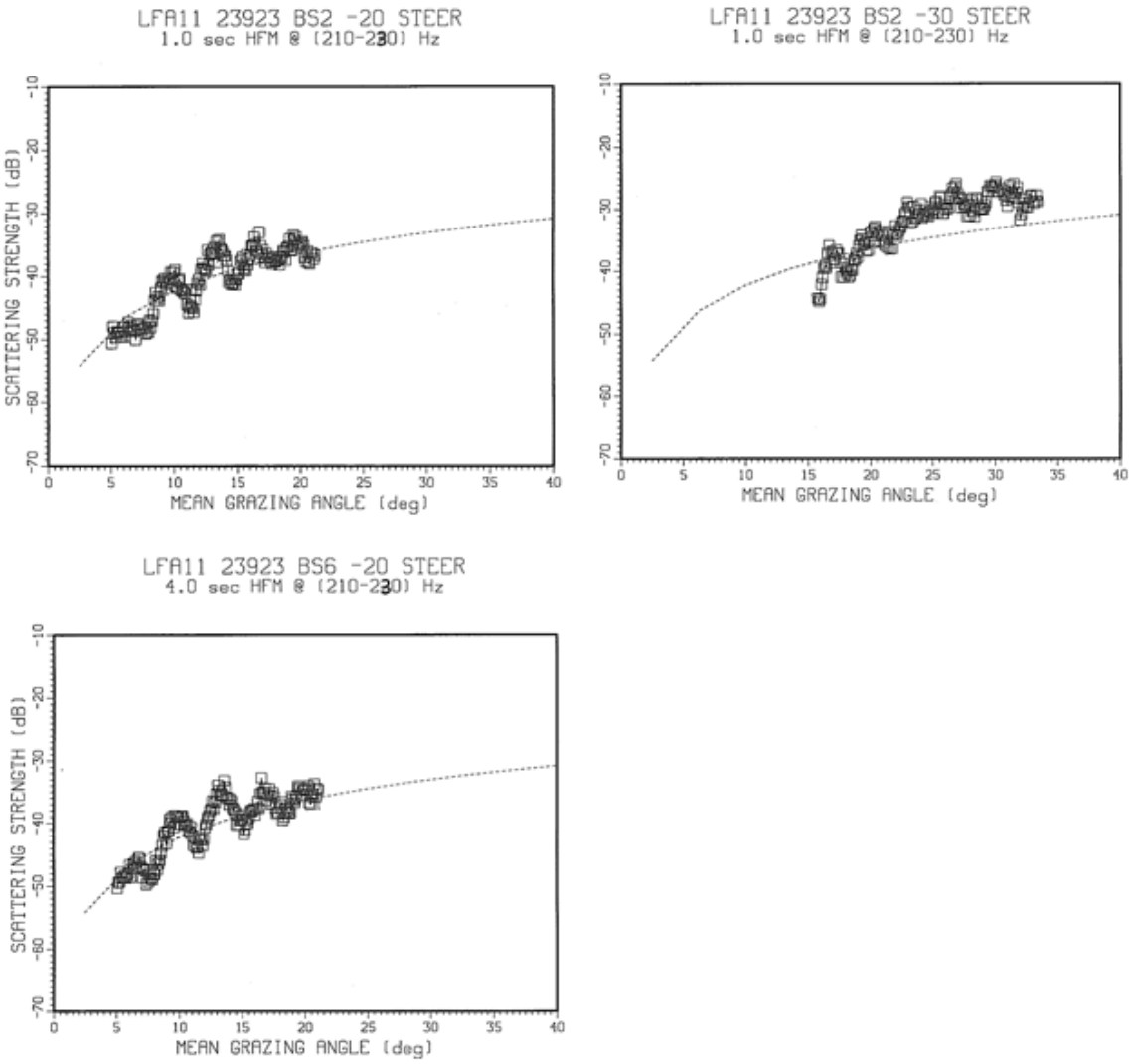

Fig. 8.B-21 – Site 28 LFA-11 BBS vs. grazing angle for 1-s (top) and 4-s (bottom) HFM signals sweeping 210–230 Hz and source-steering angles of down 20 (left) and down 30 (right) deg. (Mackenzie curve (dotted) shown as a reference.)

Run 28

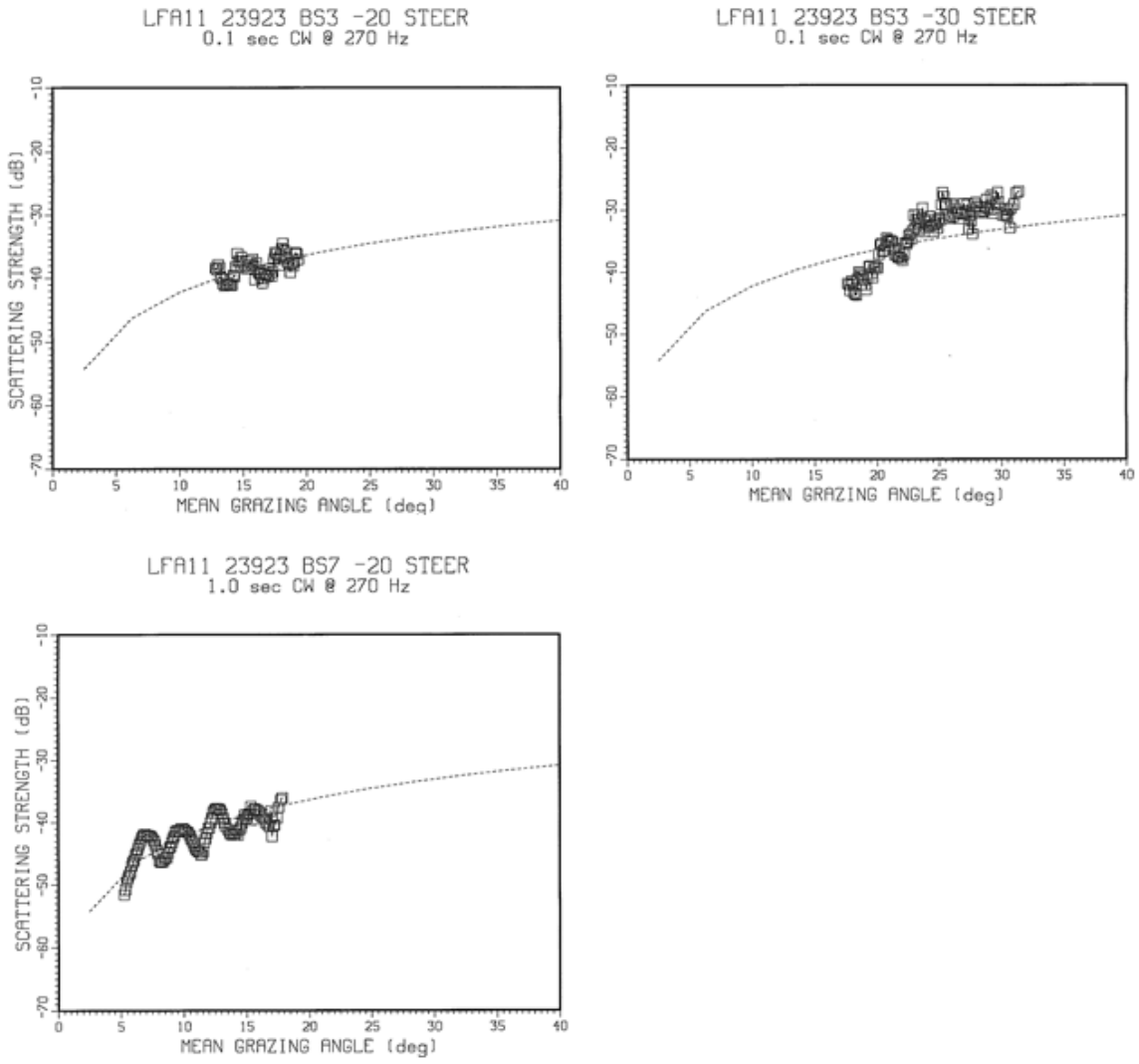

Fig. 8.B-22 – Site 28 LFA-11 BBS vs. grazing angle for 0.1-s (top) and 1-s (bottom) CW signals at 270 Hz and source-steering angles of down 20 (left) and down 30 (right) deg. (Mackenzie curve (dotted) shown as a reference.)

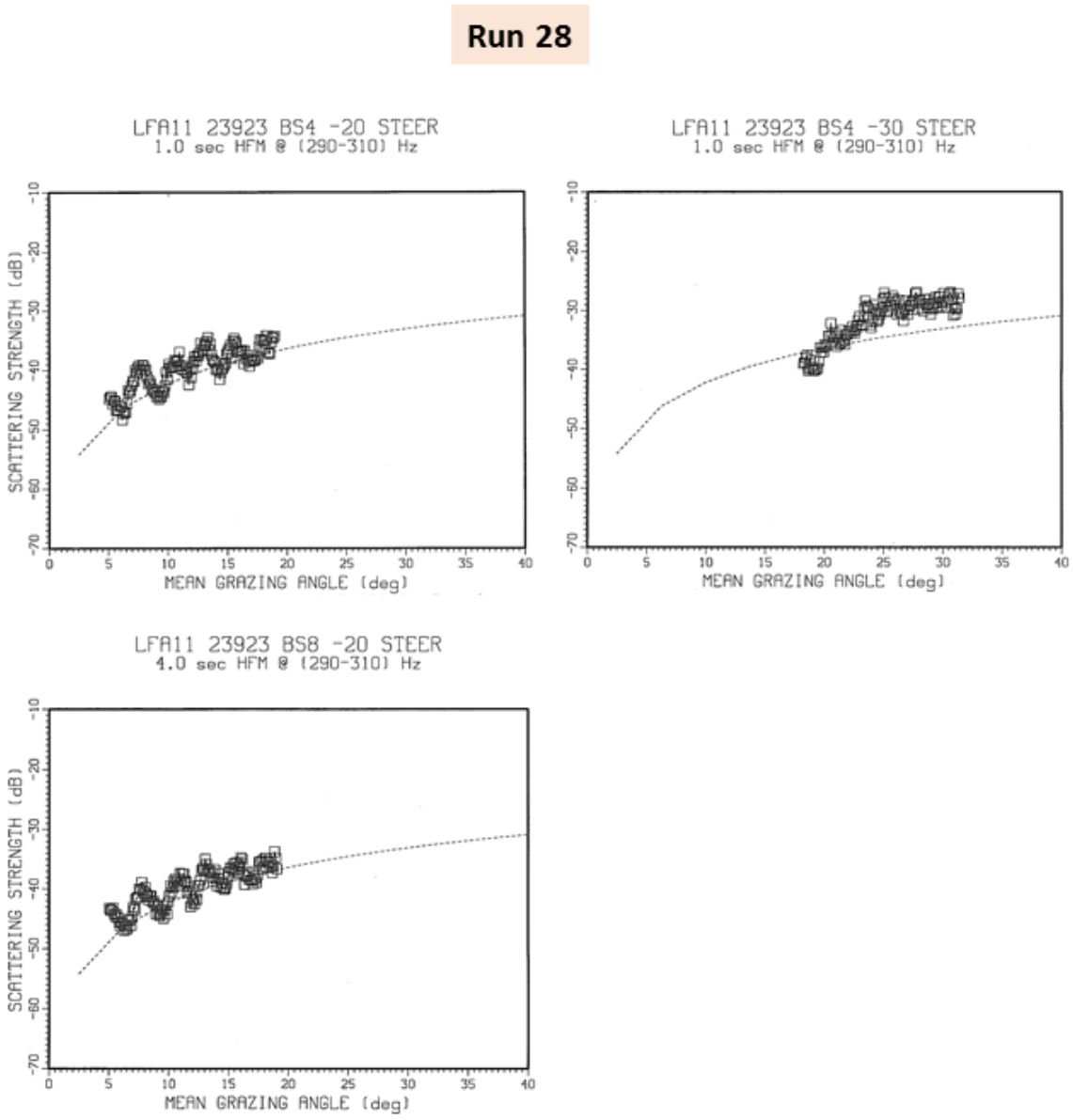

Fig. 8.B-23 – Site 28 LFA-11 BBS vs. grazing angle for 1-s (top) and 4-s (bottom) HFM signals sweeping 290–310 Hz and source-steering angles of down 20 (left) and down 30 (right) deg. (Mackenzie curve (dotted) shown as a reference.)

Run 29

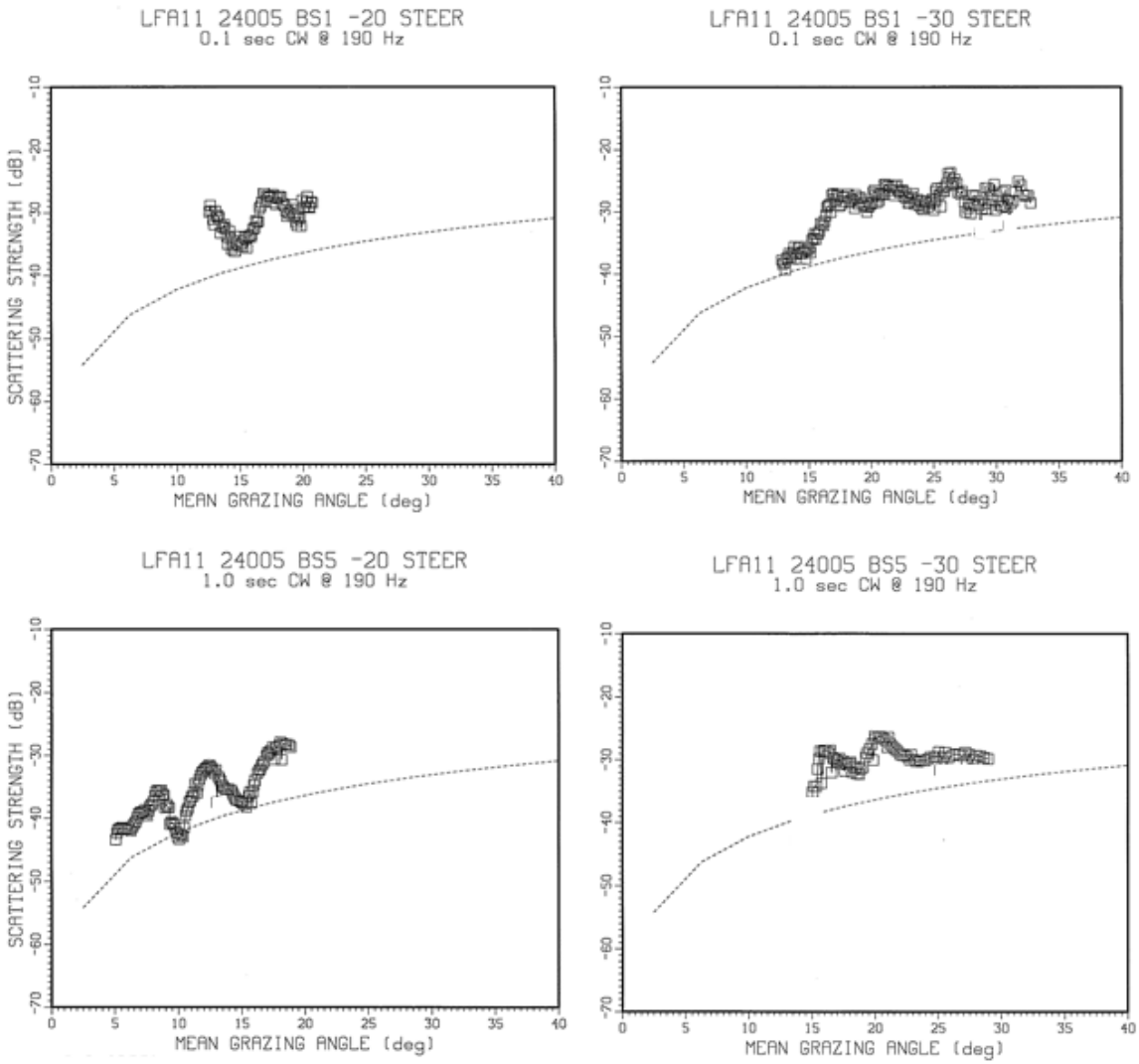

Fig. 8.B-24 – Site 29 LFA-11 BBS vs. grazing angle for 0.1-s (top) and 1-s (bottom) CW signals at 190 Hz and source-steering angles of down 20 (left) and down 30 (right) deg. (Mackenzie curve (dotted) shown as a reference.)

Run 29

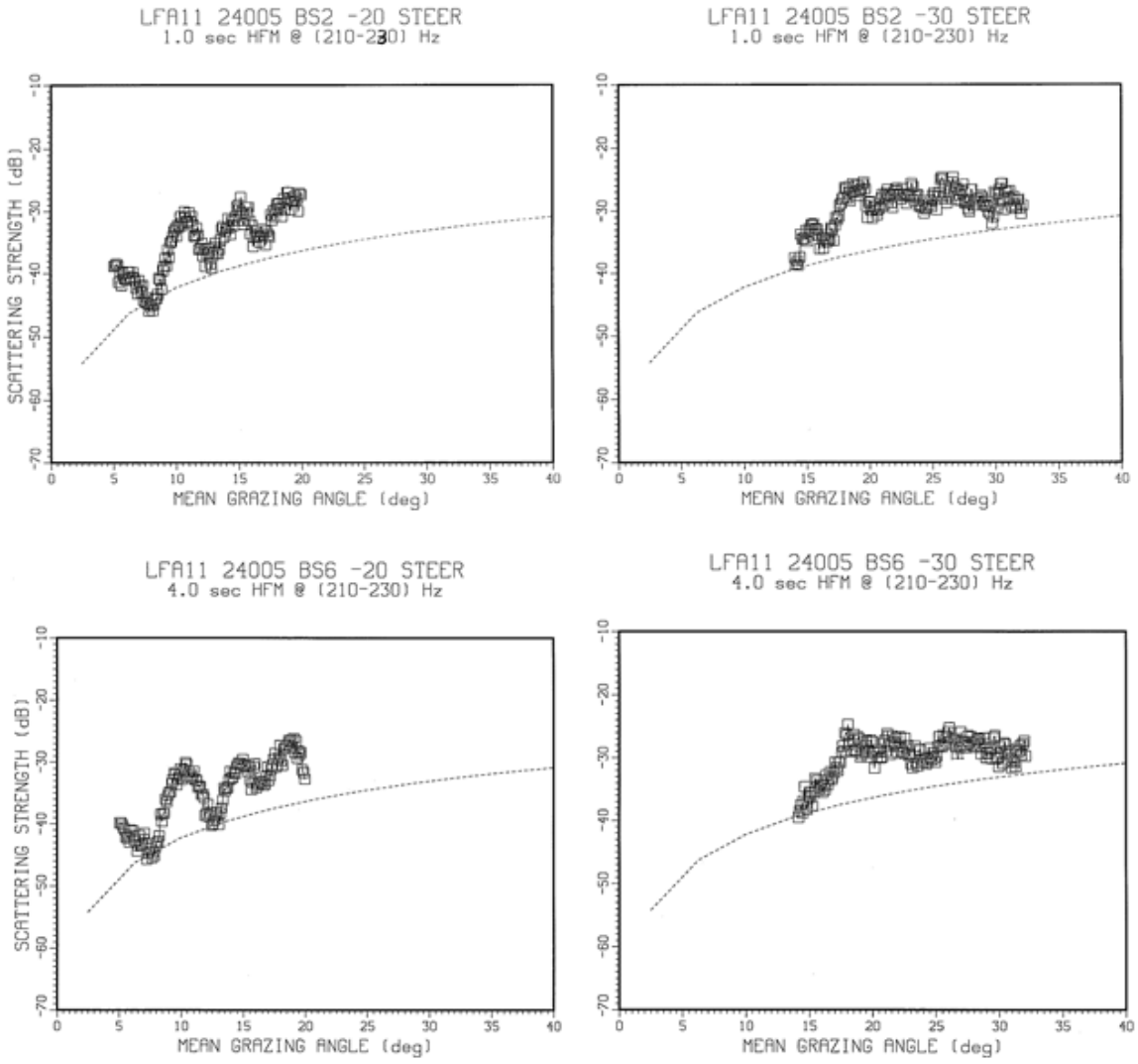

Fig. 8.B-25 – Site 29 LFA-11 BBS vs. grazing angle for 1-s (top) and 4-s (bottom) HFM signals sweeping 210–230 Hz and source-steering angles of down 20 (left) and down 30 (right) deg. (Mackenzie curve (dotted) shown as a reference.)

Run 29

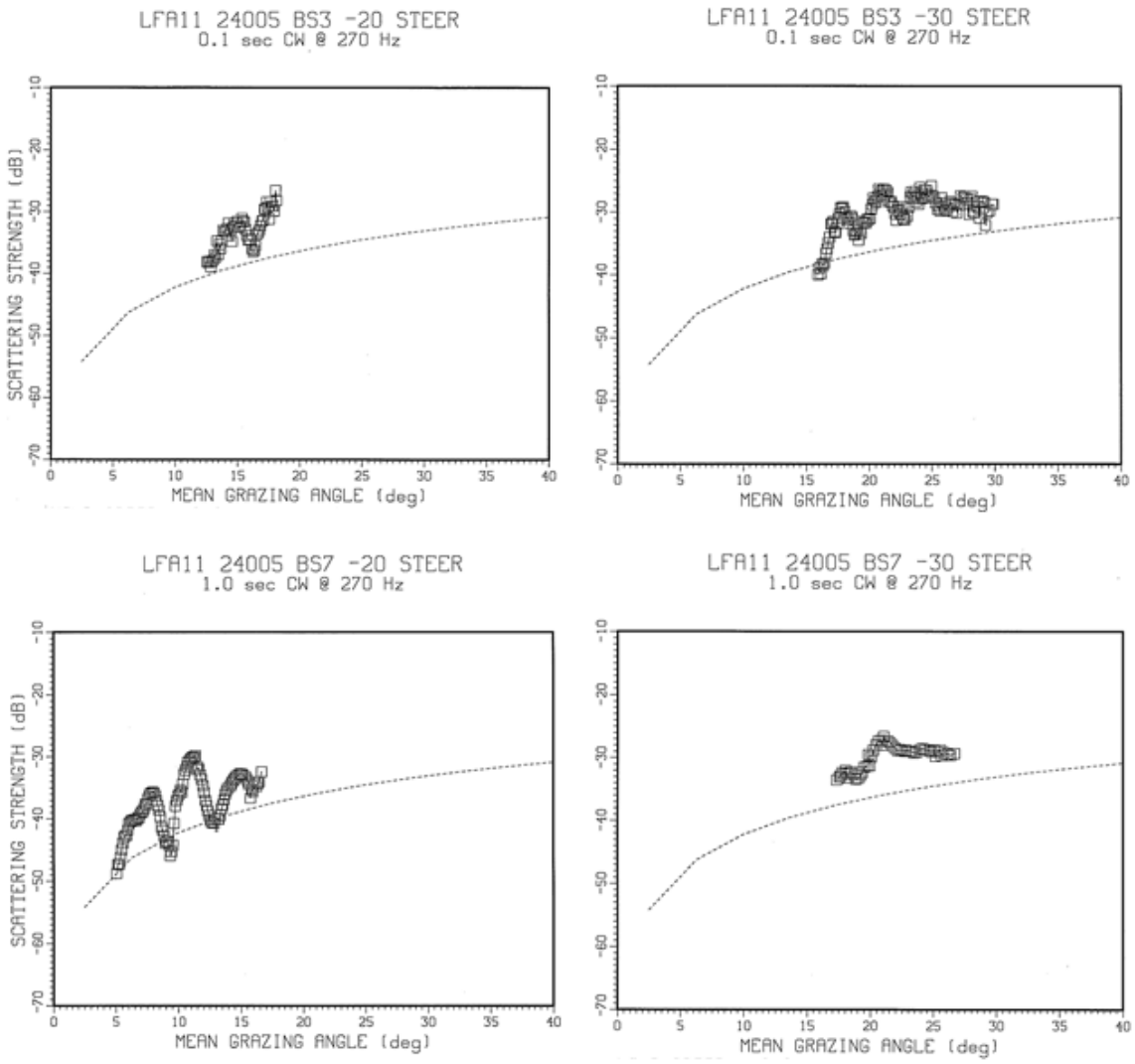

Fig. 8.B-26 – Site 29 LFA-11 BBS vs. grazing angle for 0.1-s (top) and 1-s (bottom) CW signals at 270 Hz and source-steering angles of down 20 (left) and down 30 (right) deg. (Mackenzie curve (dotted) shown as a reference.)

Run 29

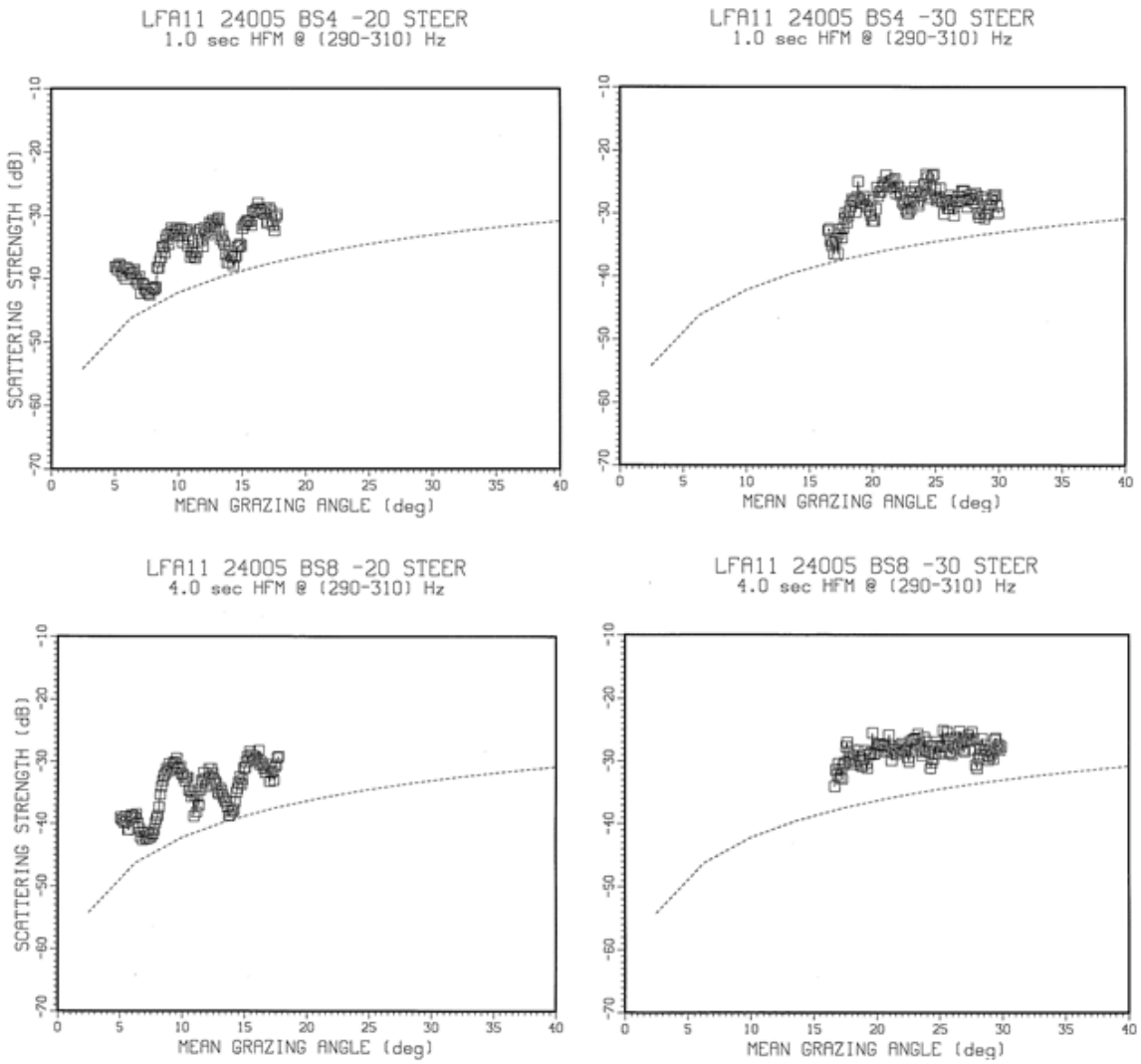

Fig. 8.B-27 – Site 29 LFA-11 BBS vs. grazing angle for 1-s (top) and 4-s (bottom) HFM signals sweeping 290–310 Hz and source-steering angles of down 20 (left) and down 30 (right) deg. (Mackenzie curve (dotted) shown as a reference.)

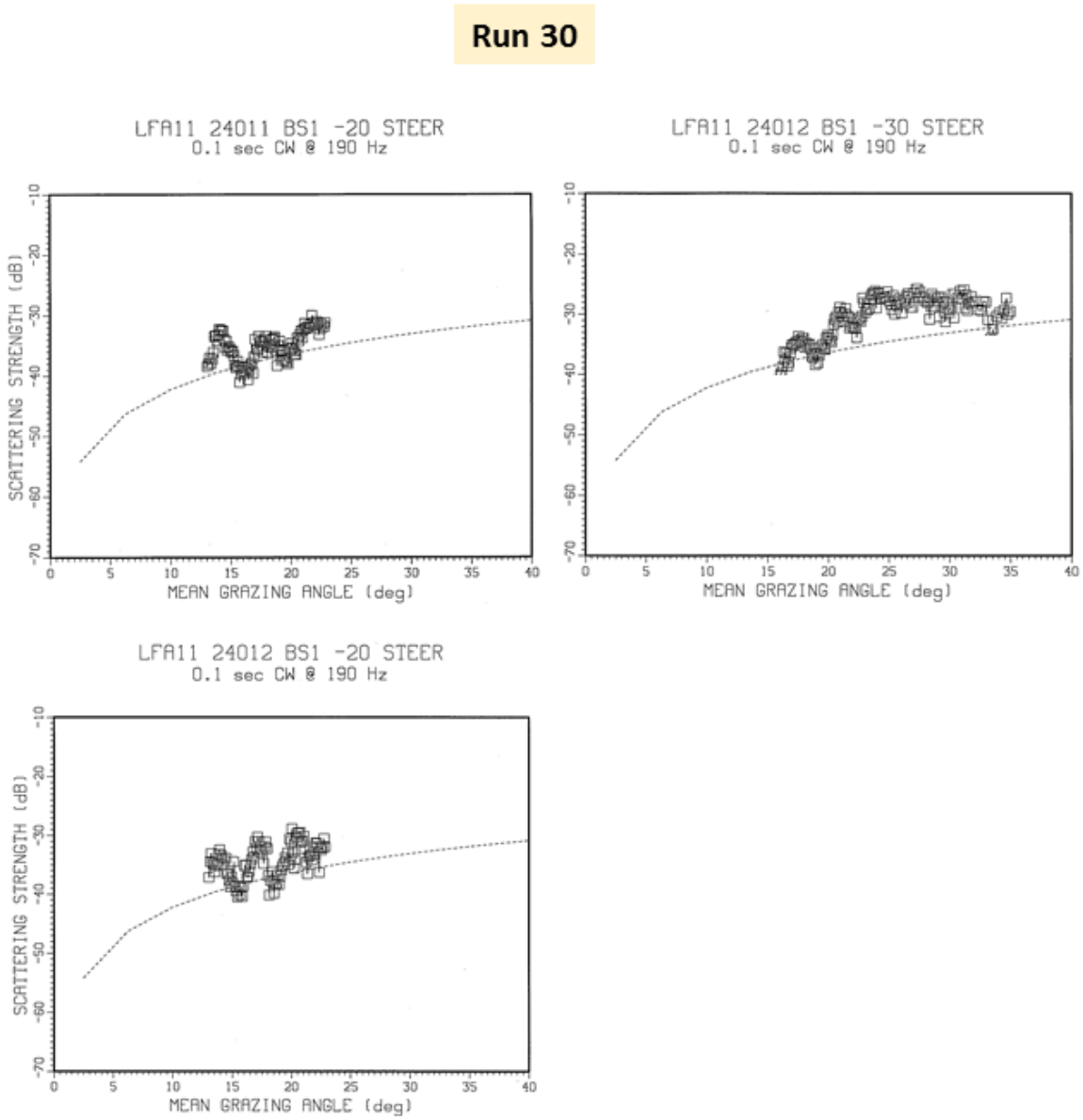

Fig. 8.B-28 – Site 30 LFA-11 BBS vs. grazing angle for 0.1-s 190-Hz CW signals and source-steering angles of down 20 (left) and down 30 (right) deg. (Mackenzie curve (dotted) shown as a reference.)

Run 30

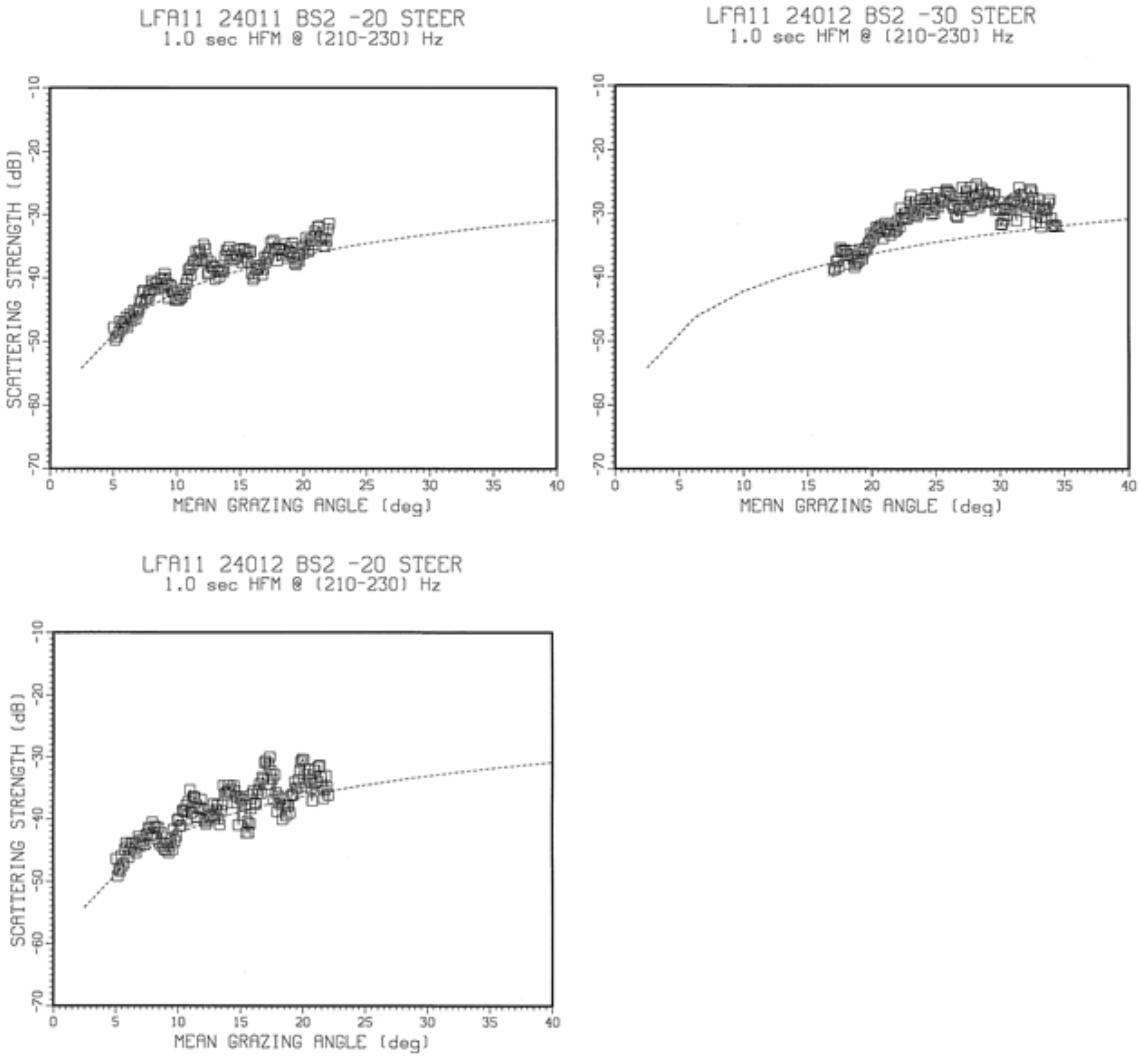

Fig. 8.B-29 – Site 30 LFA-11 BBS vs. grazing angle for 1-s HFM signals sweeping 210–230 Hz and source-steering angles of down 20 (left) and down 30 (right) deg.
(Mackenzie curve (dotted) shown as a reference.)

Run 30

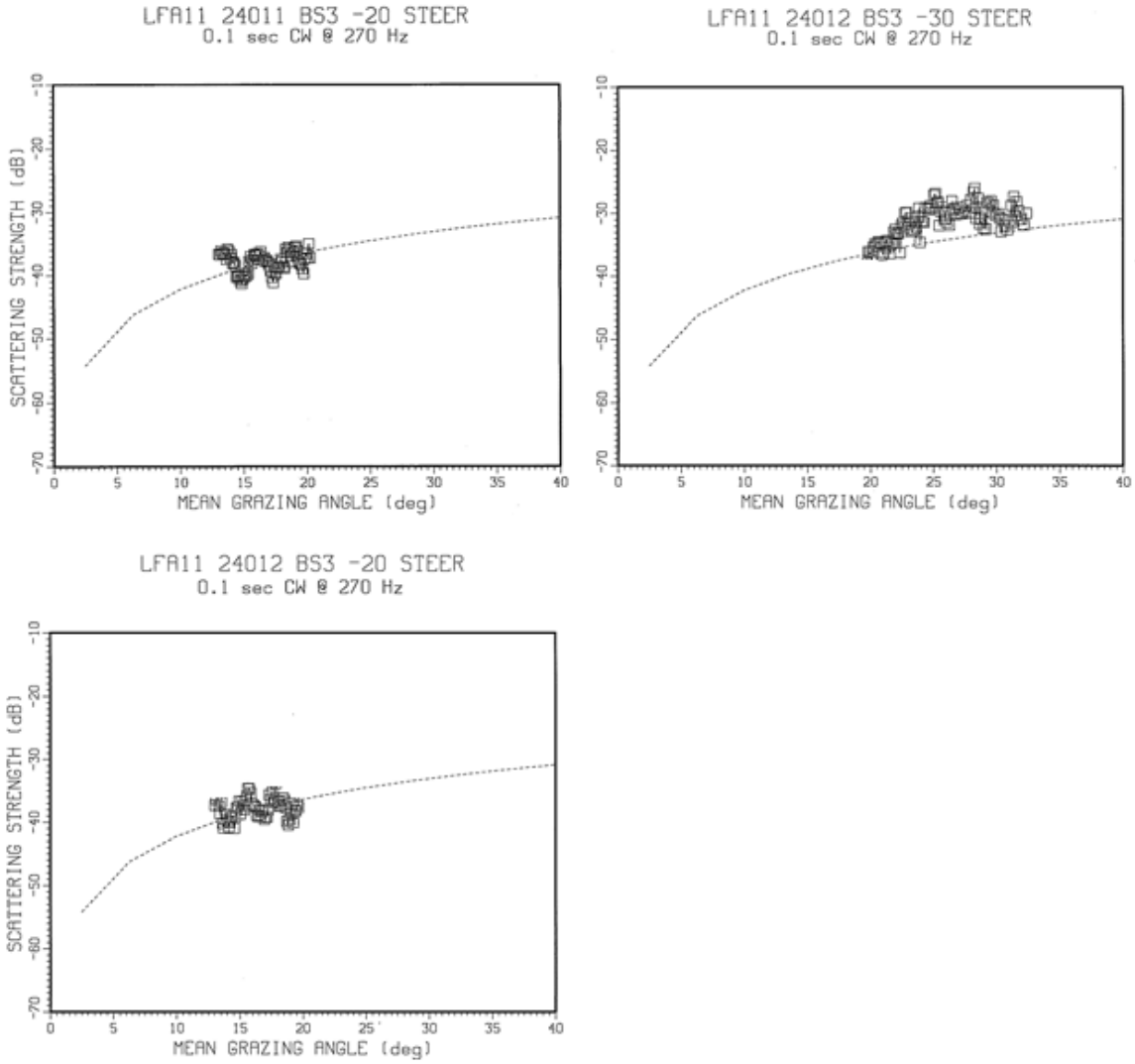

Fig. 8.B-30 – Site 30 LFA-11 BBS vs. grazing angle for 0.1-s 270-Hz CW signals and source-steering angles of down 20 (left) and down 30 (right) deg. (Mackenzie curve (dotted) shown as a reference.)

Run 30

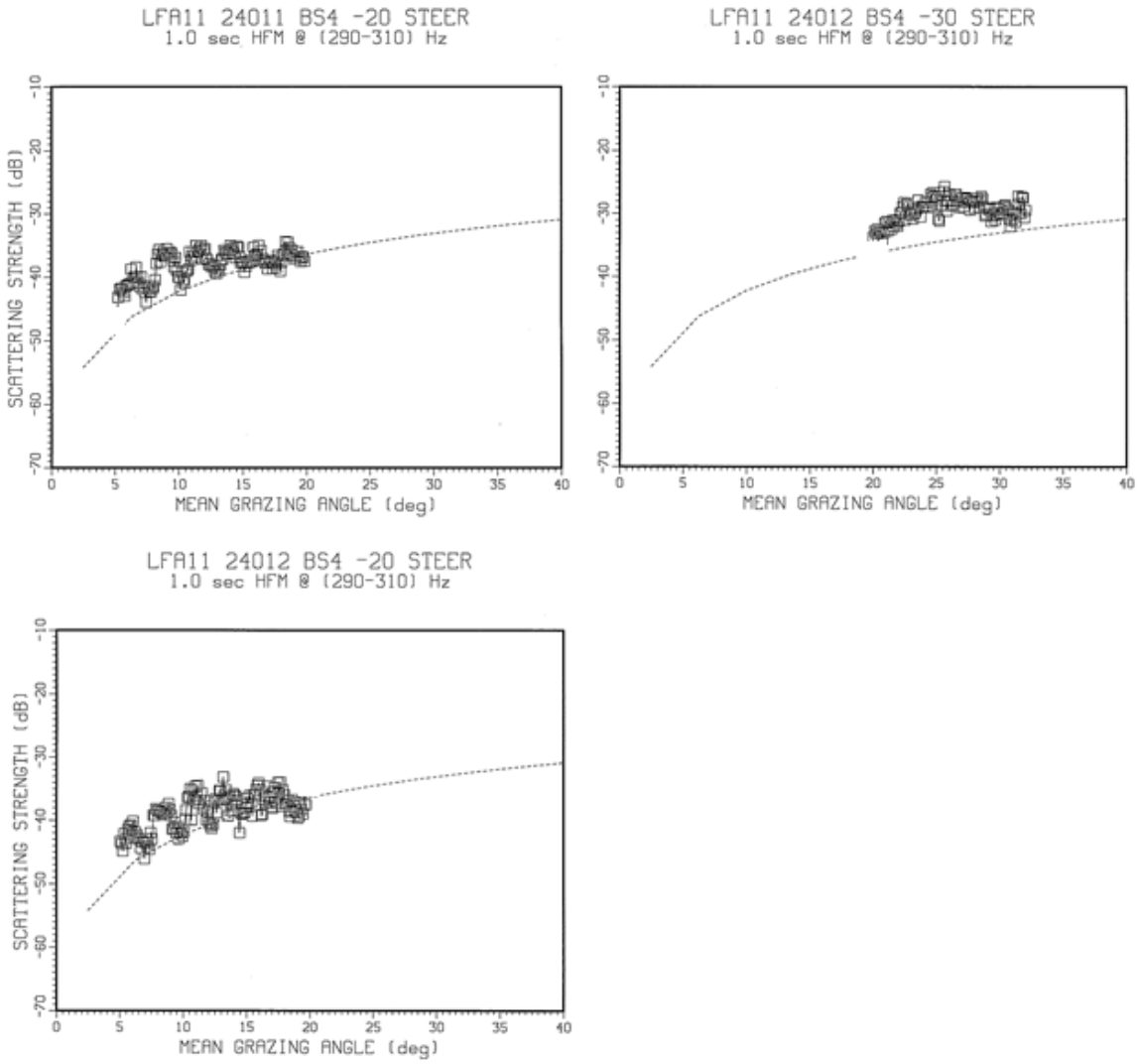

Fig. 8.B-31 – Site 30 LFA-11 BBS vs. grazing angle for 1-s HFM signals sweeping 290–310 Hz and source-steering angles of down 20 (left) and down 30 (right) deg.
(Mackenzie curve (dotted) shown as a reference.)

Run 31

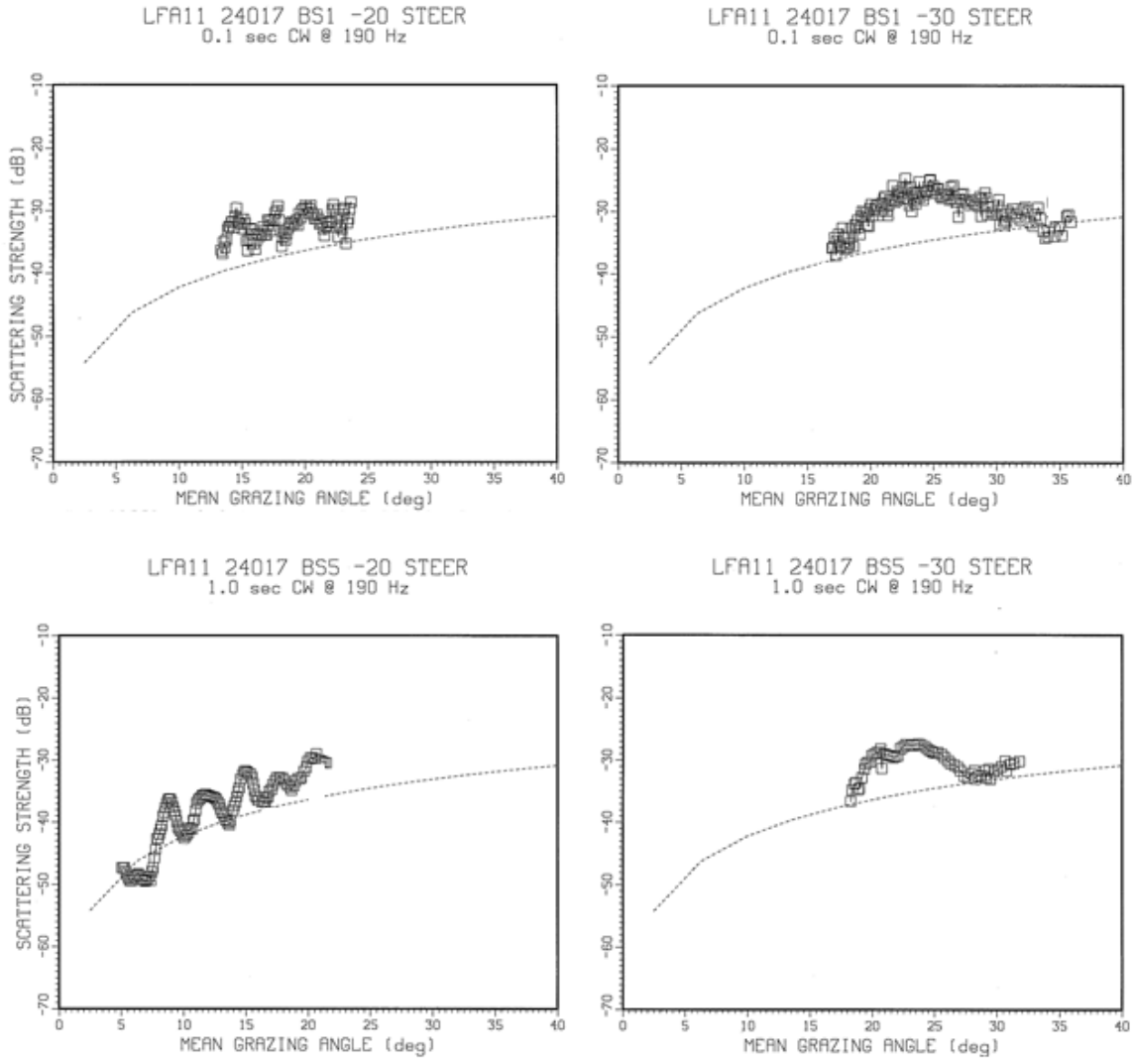

Fig. 8.B-32 – Site 31 LFA-11 BBS vs. grazing angle for 0.1-s (top) and 1-s (bottom) CW signals at 190 Hz and source-steering angles of down 20 (left) and down 30 (right) deg. (Mackenzie curve (dotted) shown as a reference.)

Run 31

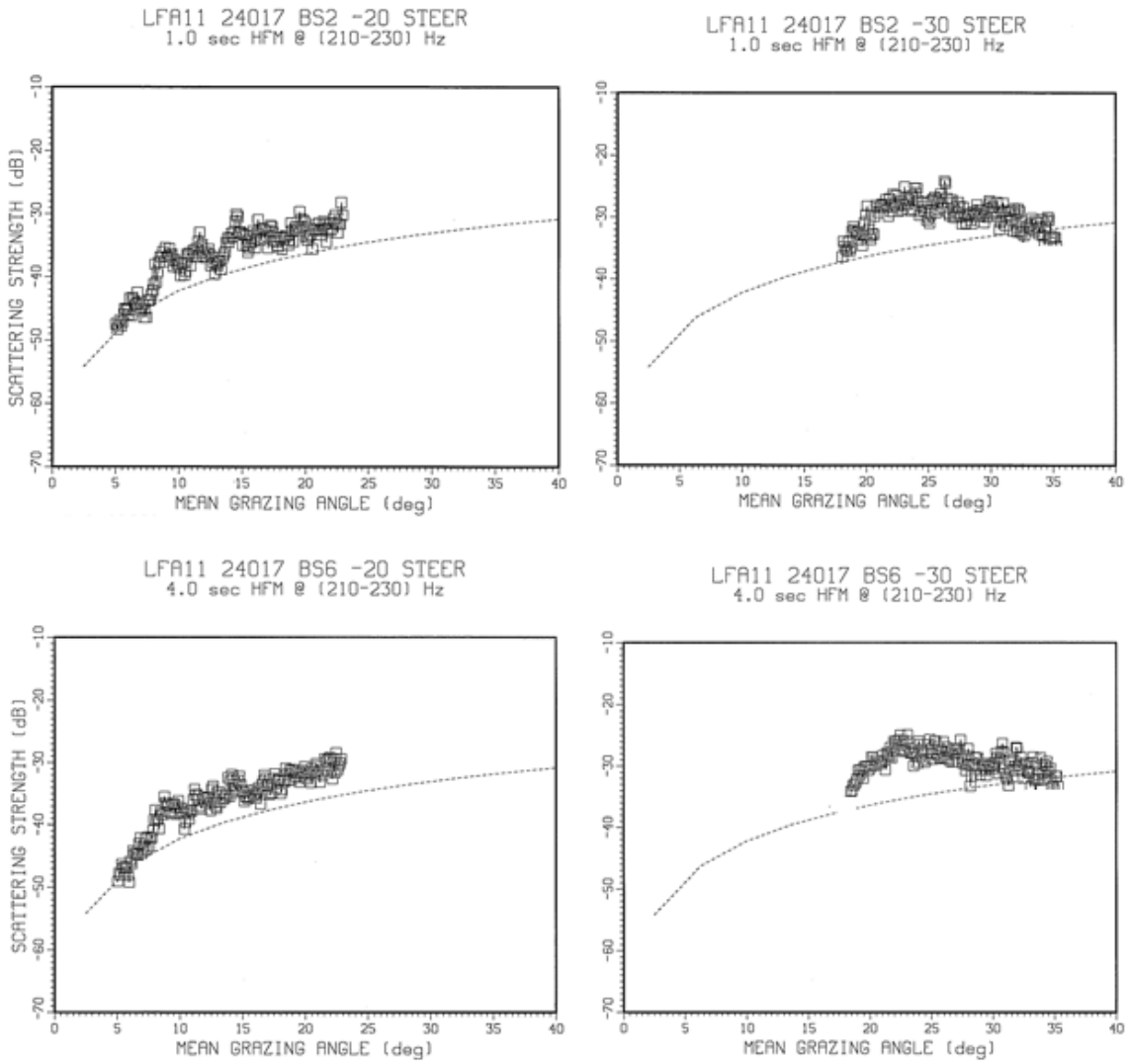

Fig. 8.B-33 – Site 31 LFA-11 BBS vs. grazing angle for 1-s (top) and 4-s (bottom) HFM signals sweeping 210–230 Hz and source-steering angles of down 20 (left) and down 30 (right) deg. (Mackenzie curve (dotted) shown as a reference.)

Run 31

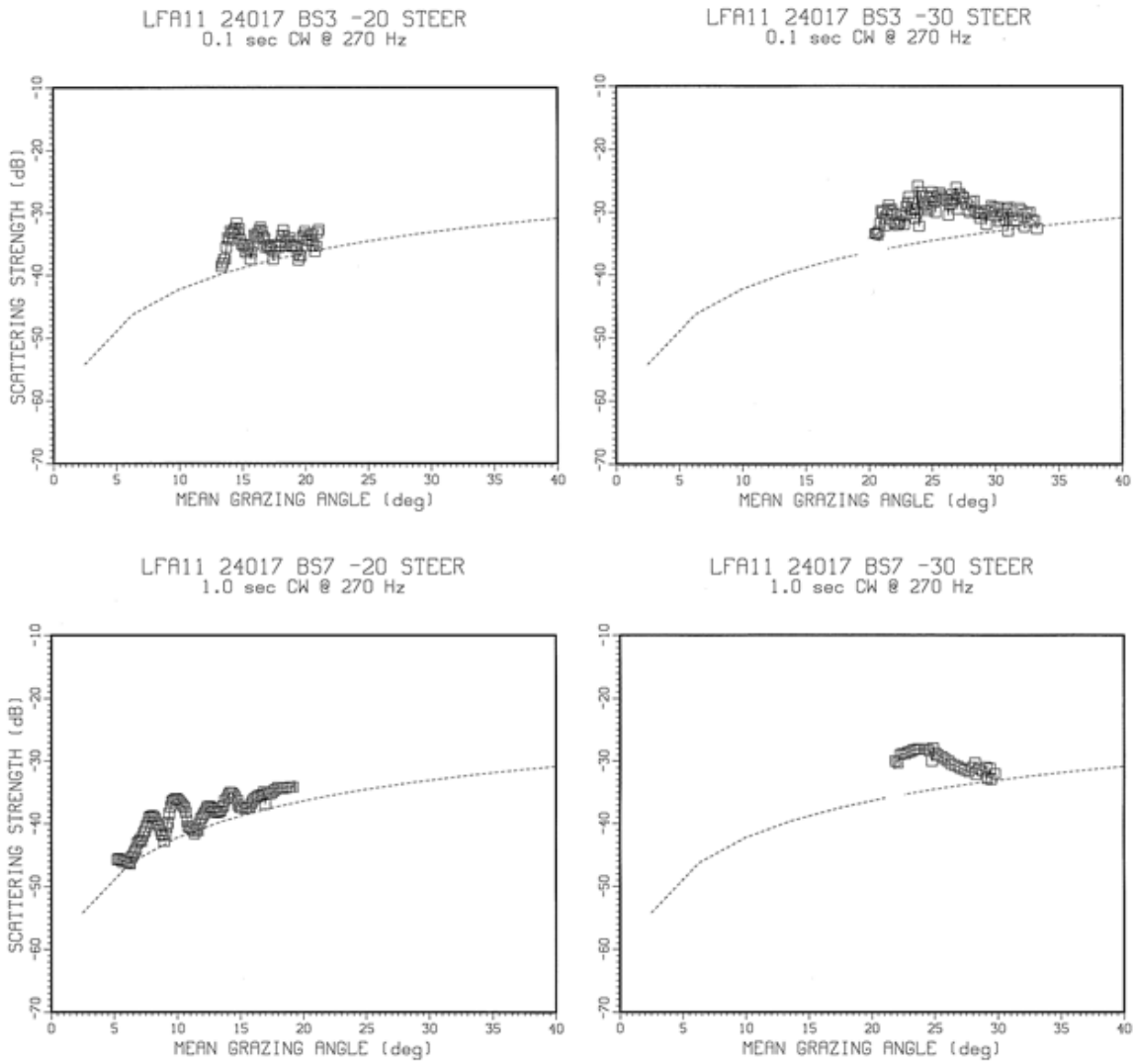

Fig. 8.B-34 – Site 31 LFA-11 BBS vs. grazing angle for 0.1-s (top) and 1-s (bottom) CW signals at 270 Hz and source-steering angles of down 20 (left) and down 30 (right) deg. (Mackenzie curve (dotted) shown as a reference.)

Run 31

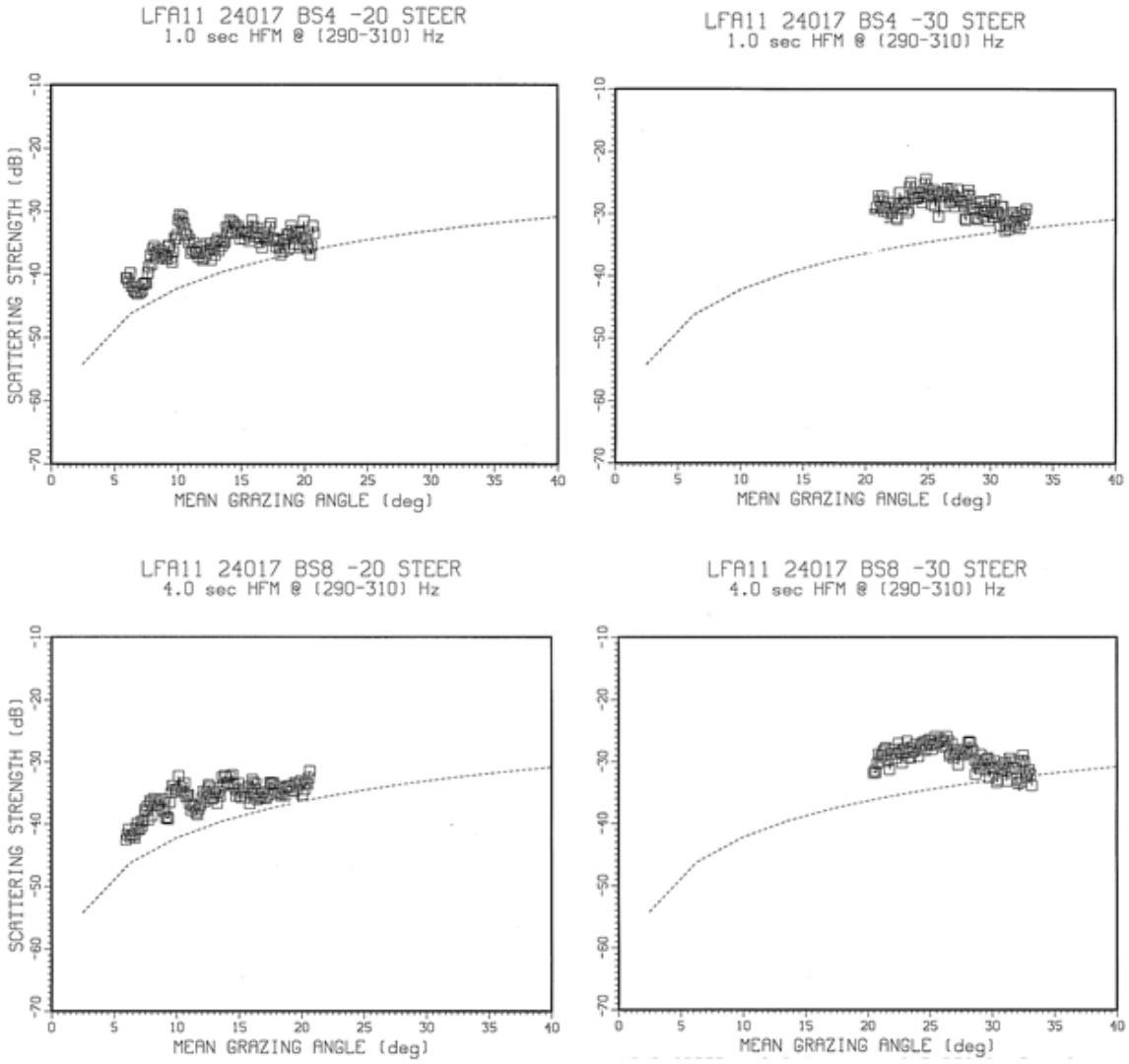

Fig. 8.B-35 – Site 31 LFA-11 BBS vs. grazing angle for 1-s (top) and 4-s (bottom) HFM signals sweeping 290–310 Hz and source-steering angles of down 20 (left) and down 30 (right) deg. (Mackenzie curve (dotted) shown as a reference.)

Run 32

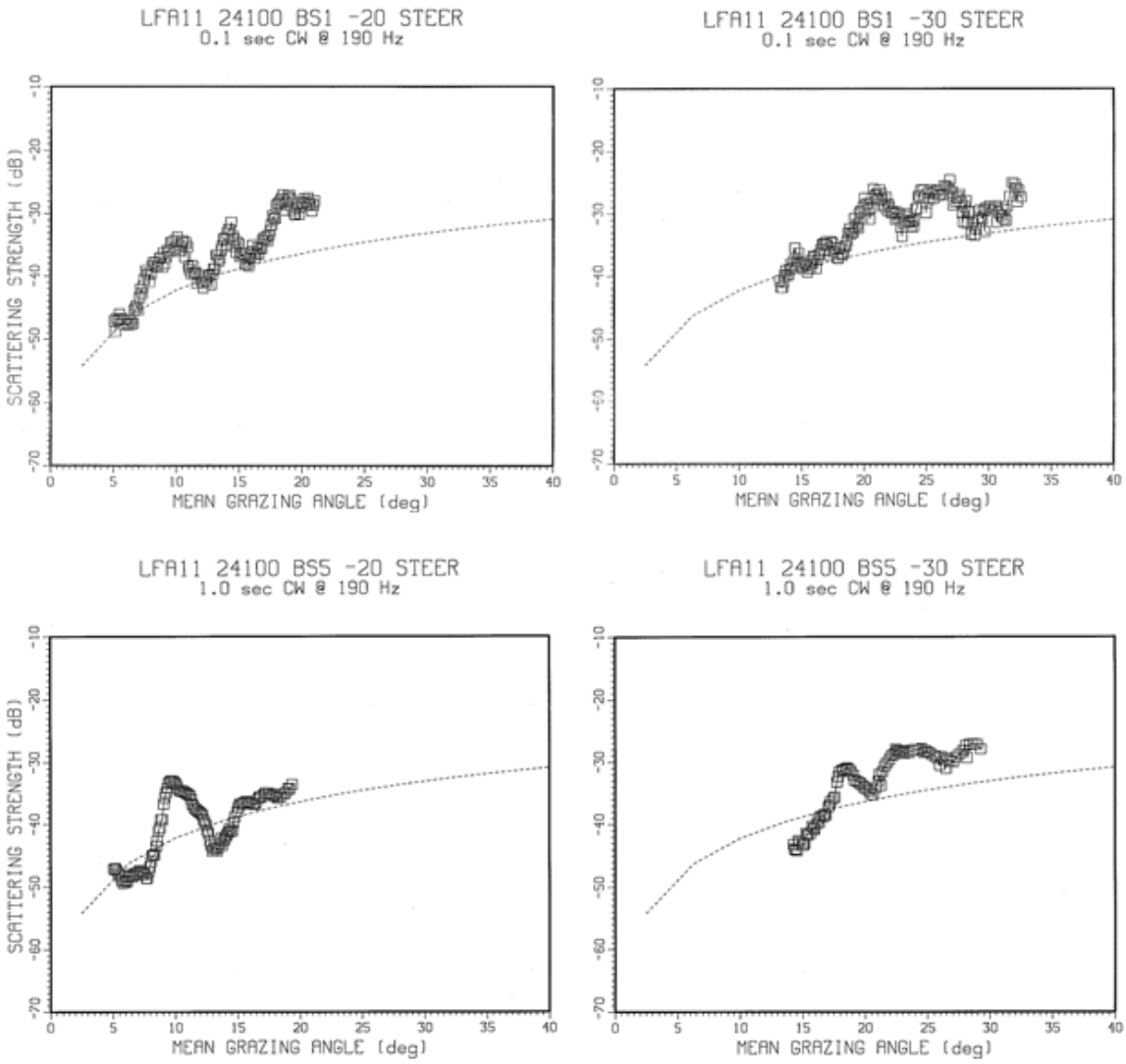

Fig. 8.B-36 – Site 32 LFA-11 BBS vs. grazing angle for 0.1-s (top) and 1-s (bottom) CW signals at 190 Hz and source-steering angles of down 20 (left) and down 30 (right) deg. (Mackenzie curve (dotted) shown as a reference.)

Run 32

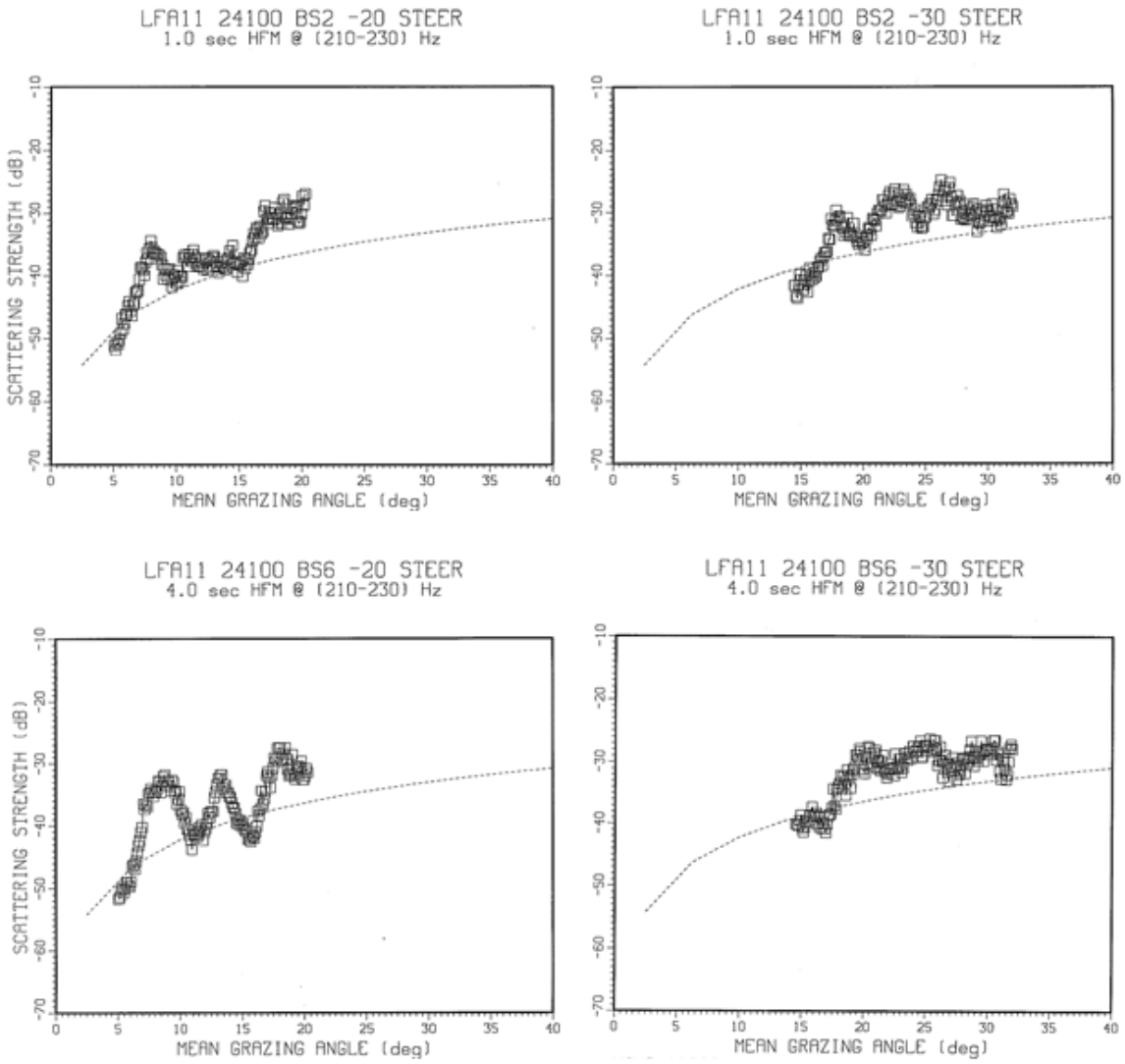

Fig. 8.B-37 – Site 32 LFA-11 BBS vs. grazing angle for 1-s (top) and 4-s (bottom) HFM signals sweeping 210–230 Hz and source-steering angles of down 20 (left) and down 30 (right) deg. (Mackenzie curve (dotted) shown as a reference.)

Run 32

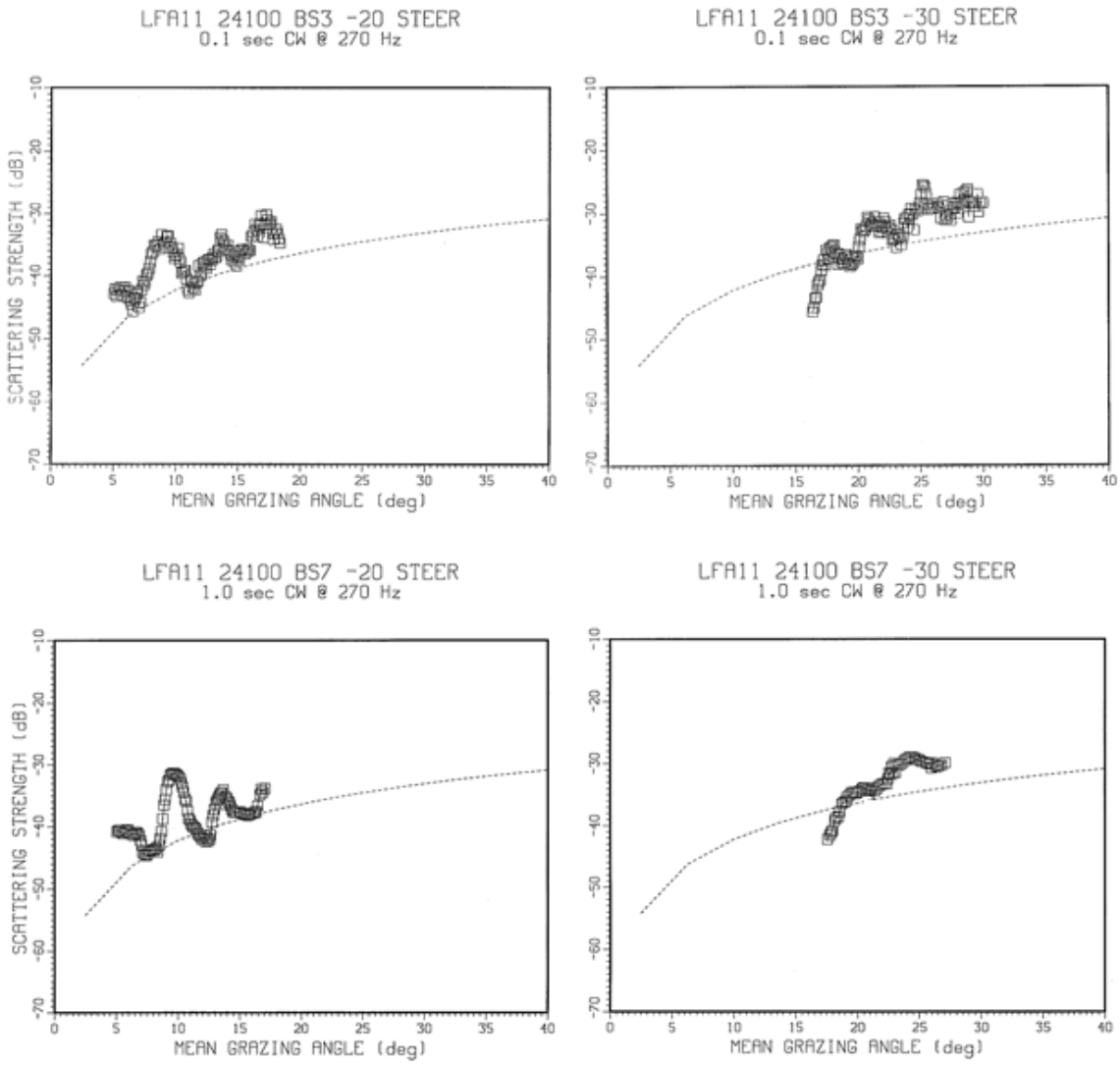

Fig. 8.B-38 – Site 32 LFA-11 BBS vs. grazing angle for 0.1-s (top) and 1-s (bottom) CW signals at 270 Hz and source-steering angles of down 20 (left) and down 30 (right) deg. (Mackenzie curve (dotted) shown as a reference.)

Run 32

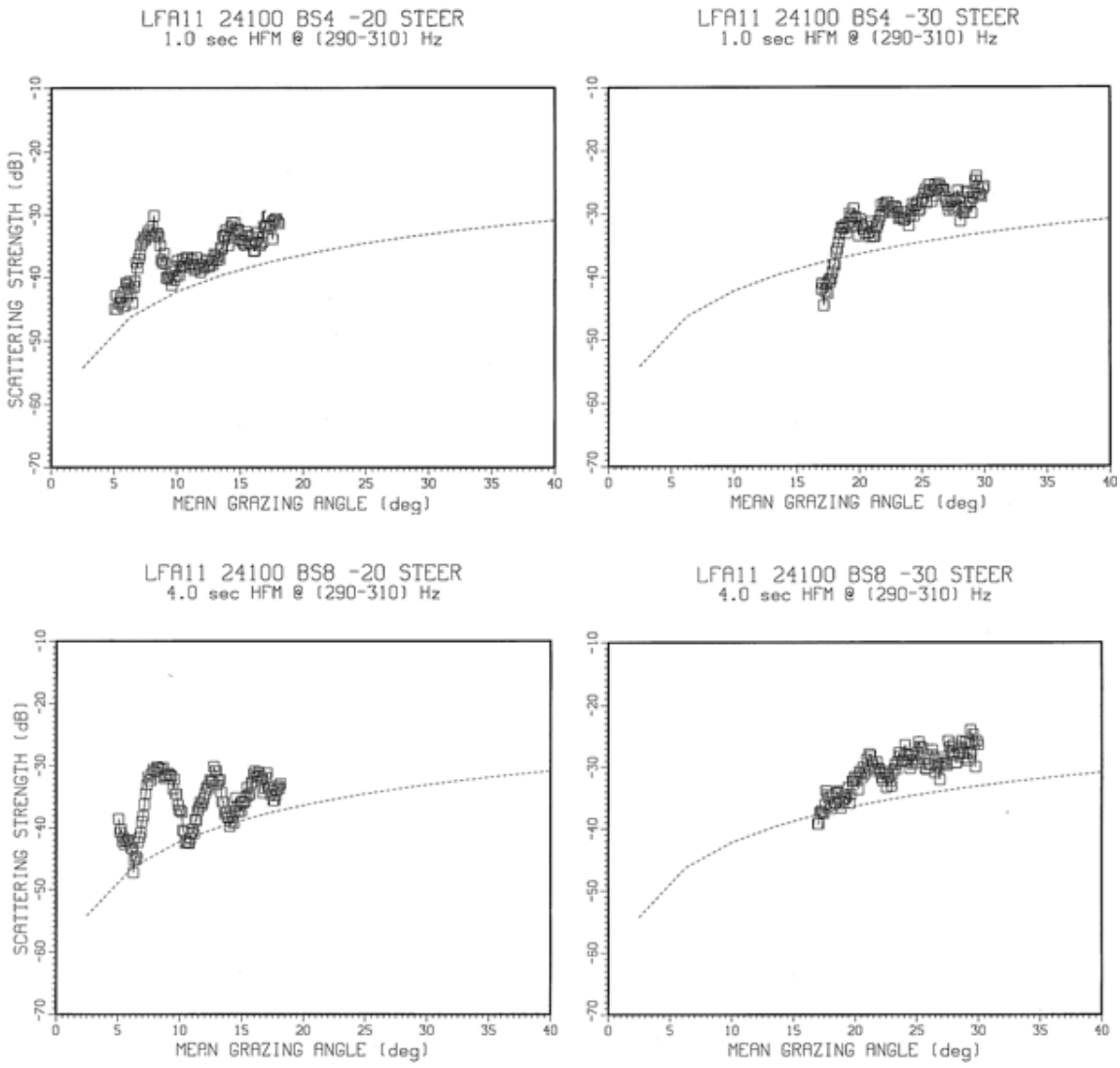

Fig. 8.B-39 – Site 32 LFA-11 BBS vs. grazing angle for 1-s (top) and 4-s (bottom) HFM signals sweeping 290–310 Hz and source-steering angles of down 20 (left) and down 30 (right) deg. (Mackenzie curve (dotted) shown as a reference.)

Run 33

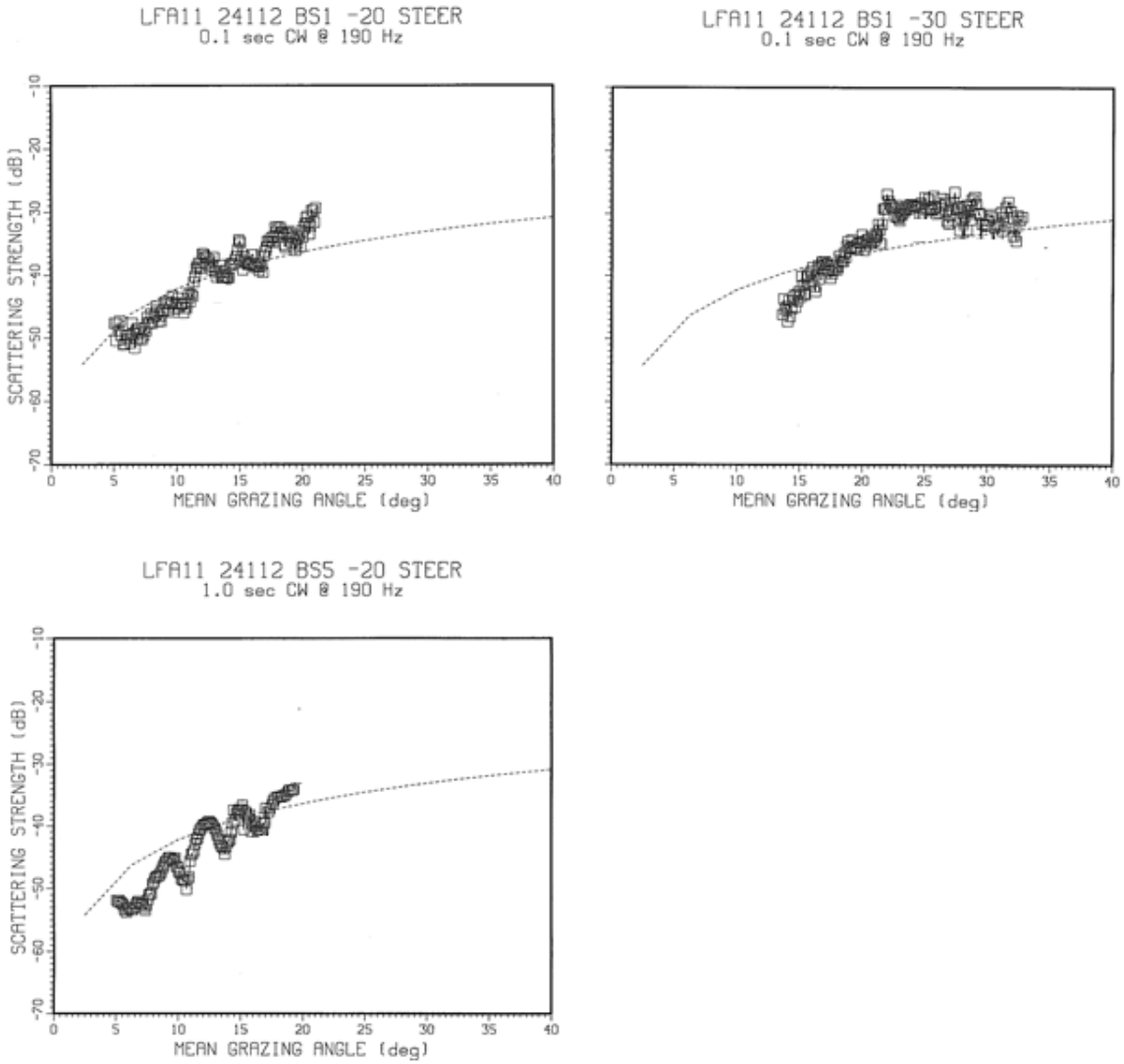

Fig. 8.B-40 – Site 33 LFA-11 BBS vs. grazing angle for 0.1-s (top) and 1-s (bottom) CW signals at 190 Hz and source-steering angles of down 20 (left) and down 30 (right) deg. (Mackenzie curve (dotted) shown as a reference.)

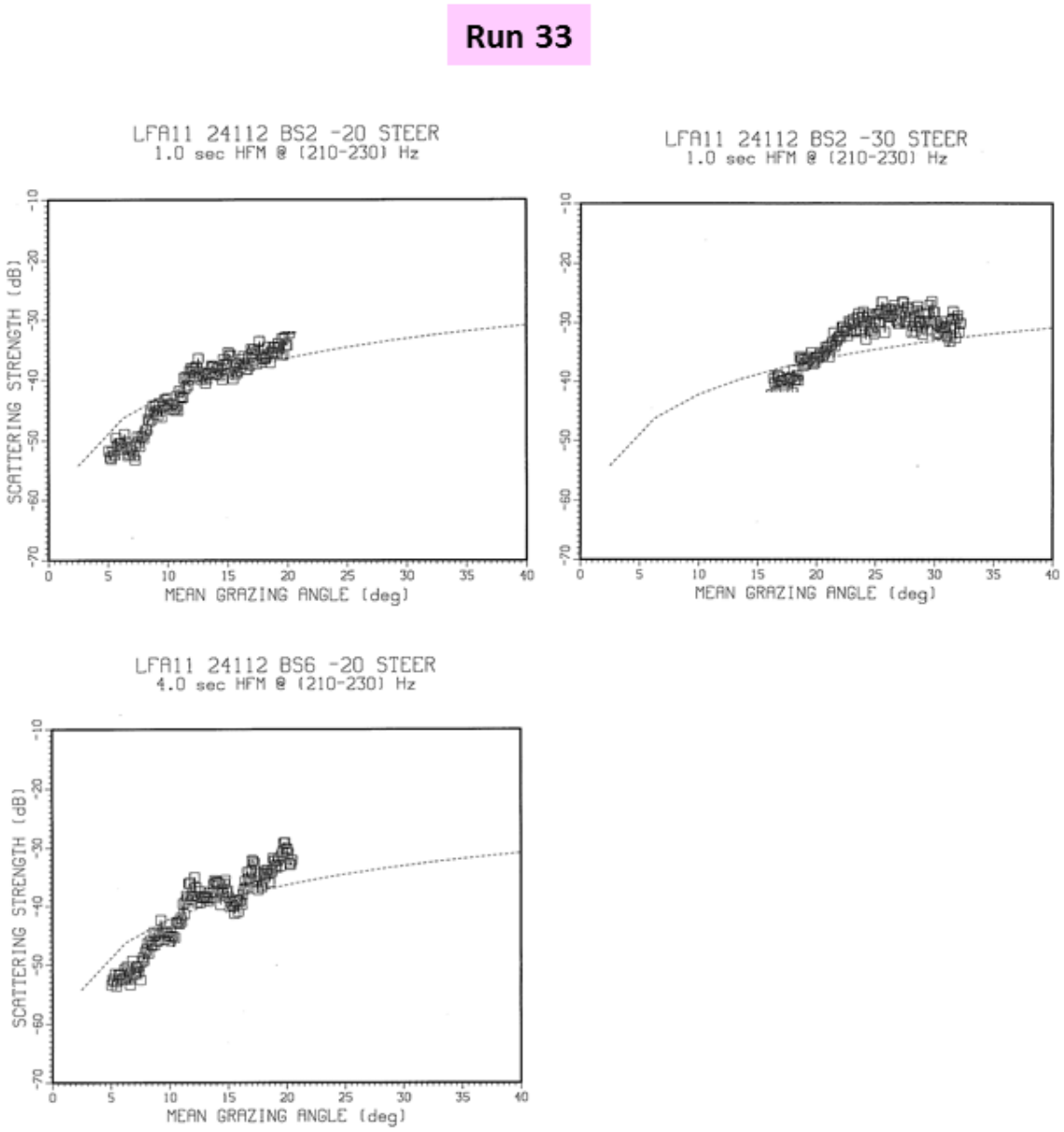

Fig. 8.B-41 – Site 33 LFA-11 BBS vs. grazing angle for 1-s (top) and 4-s (bottom) HFM signals sweeping 210–230 Hz and source-steering angles of down 20 (left) and down 30 (right) deg. (Mackenzie curve (dotted) shown as a reference.)

Run 33

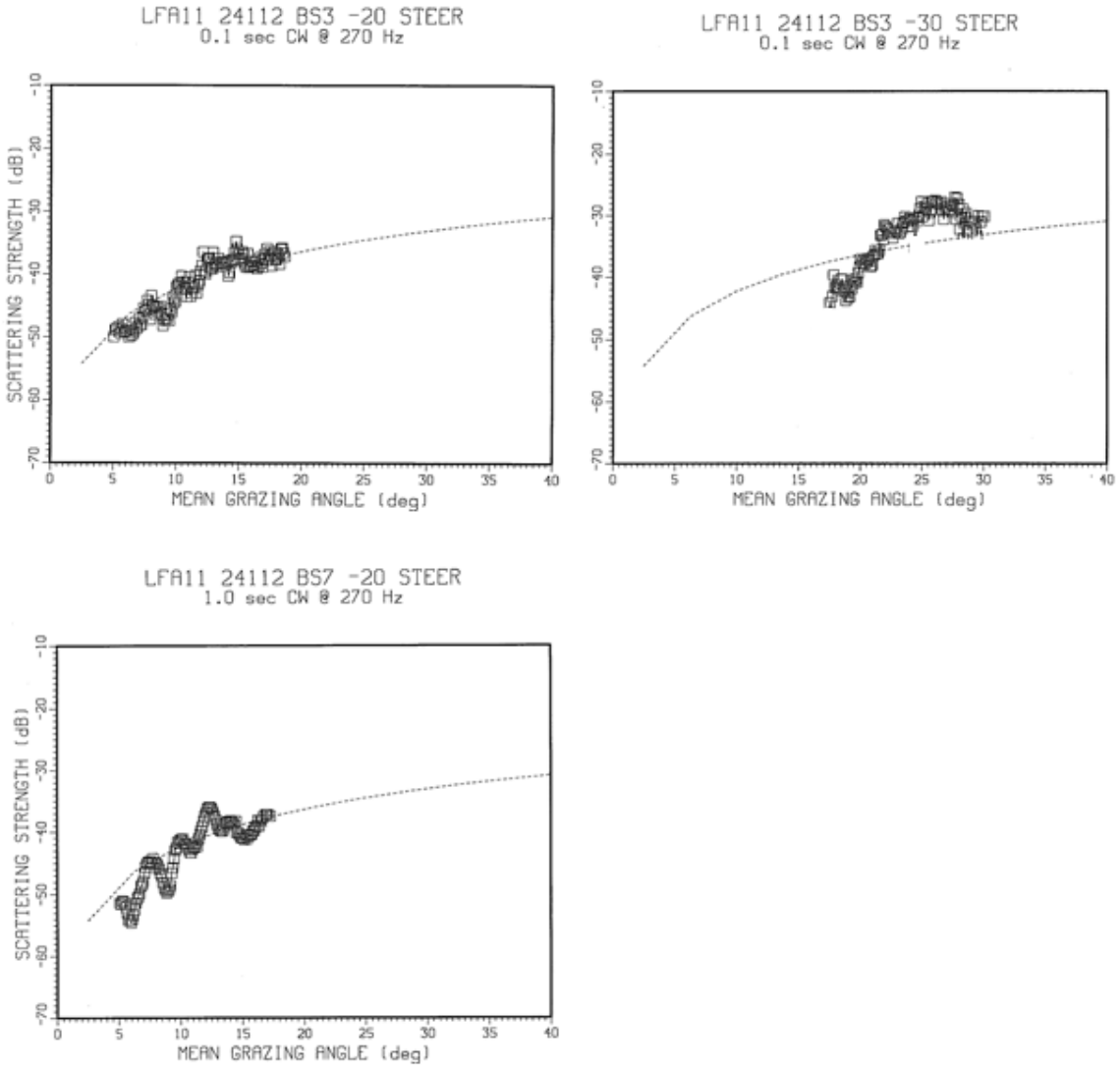

Fig. 8.B-42 – Site 33 LFA-11 BBS vs. grazing angle for 0.1-s (top) and 1-s (bottom) CW signals at 270 Hz and source-steering angles of down 20 (left) and down 30 (right) deg. (Mackenzie curve (dotted) shown as a reference.)

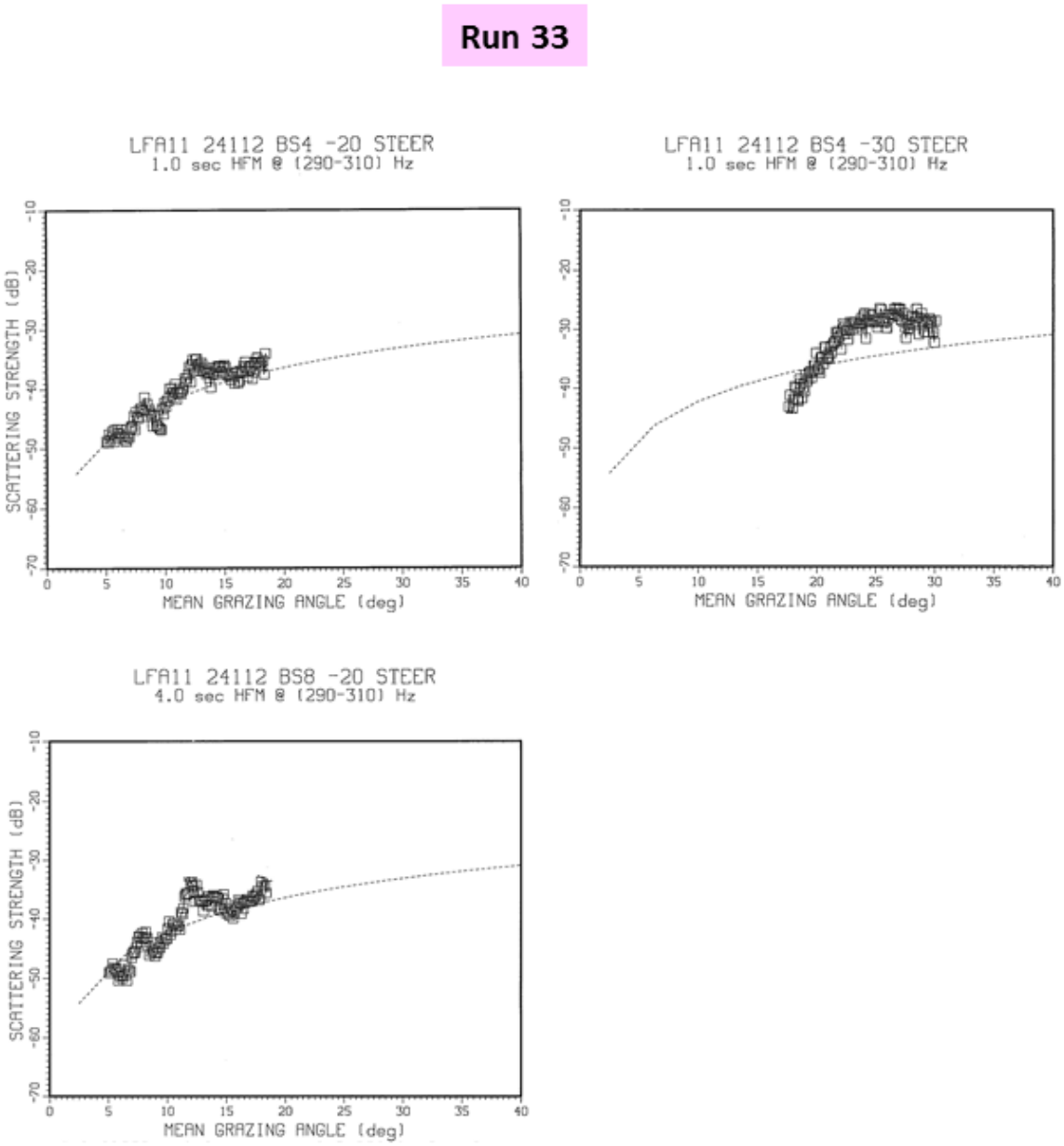

Fig. 8.B-43 – Site 33 LFA-11 BBS vs. grazing angle for 1-s (top) and 4-s (bottom) HFM signals sweeping 290–310 Hz and source-steering angles of down 20 (left) and down 30 (right) deg. (Mackenzie curve (dotted) shown as a reference.)

Run 34

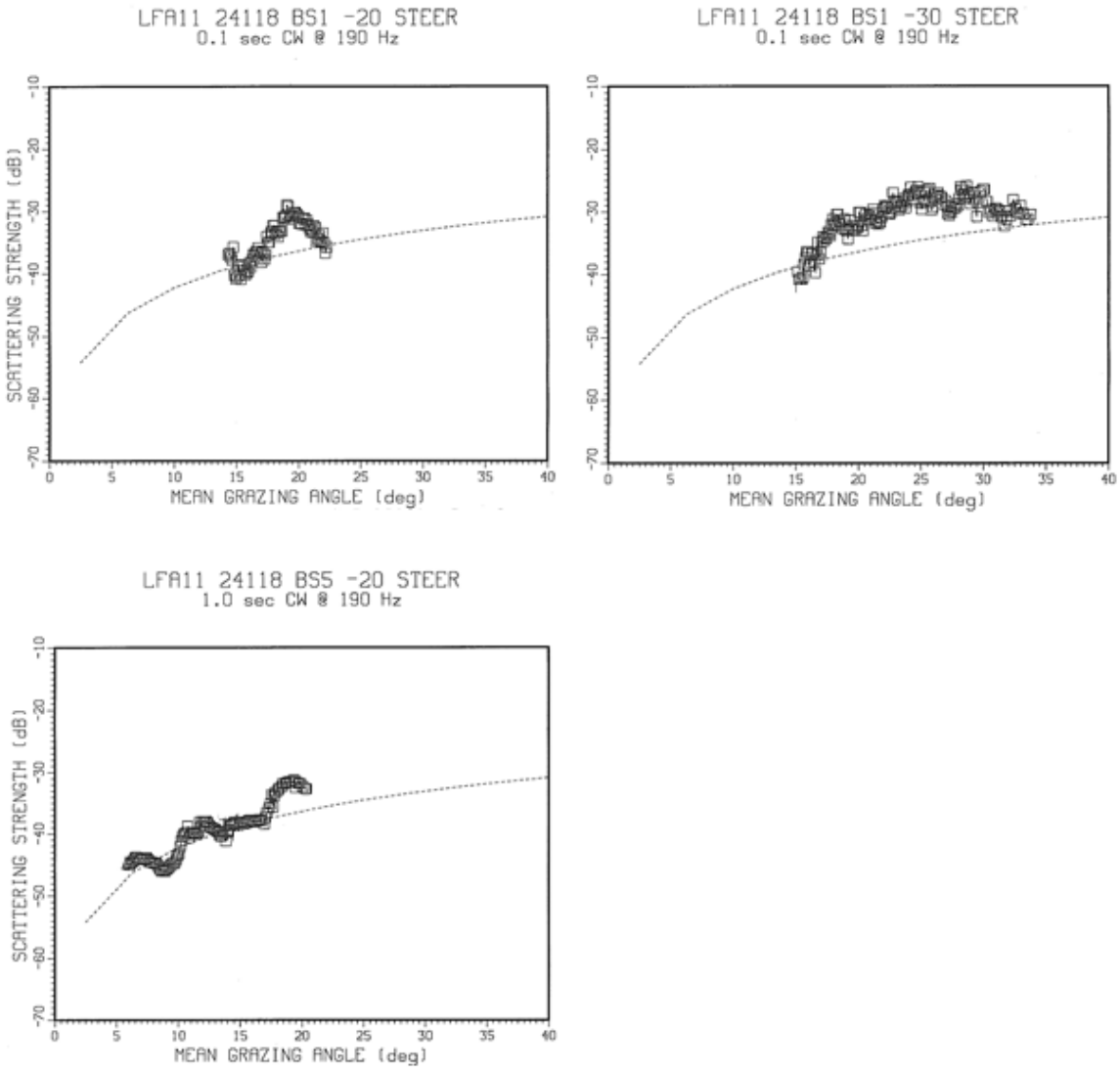

Fig. 8.B-44 – Site 34 LFA-11 BBS vs. grazing angle for 0.1-s (top) and 1-s (bottom) CW signals at 190 Hz and source-steering angles of down 20 (left) and down 30 (right) deg. (Mackenzie curve (dotted) shown as a reference.)

Run 34

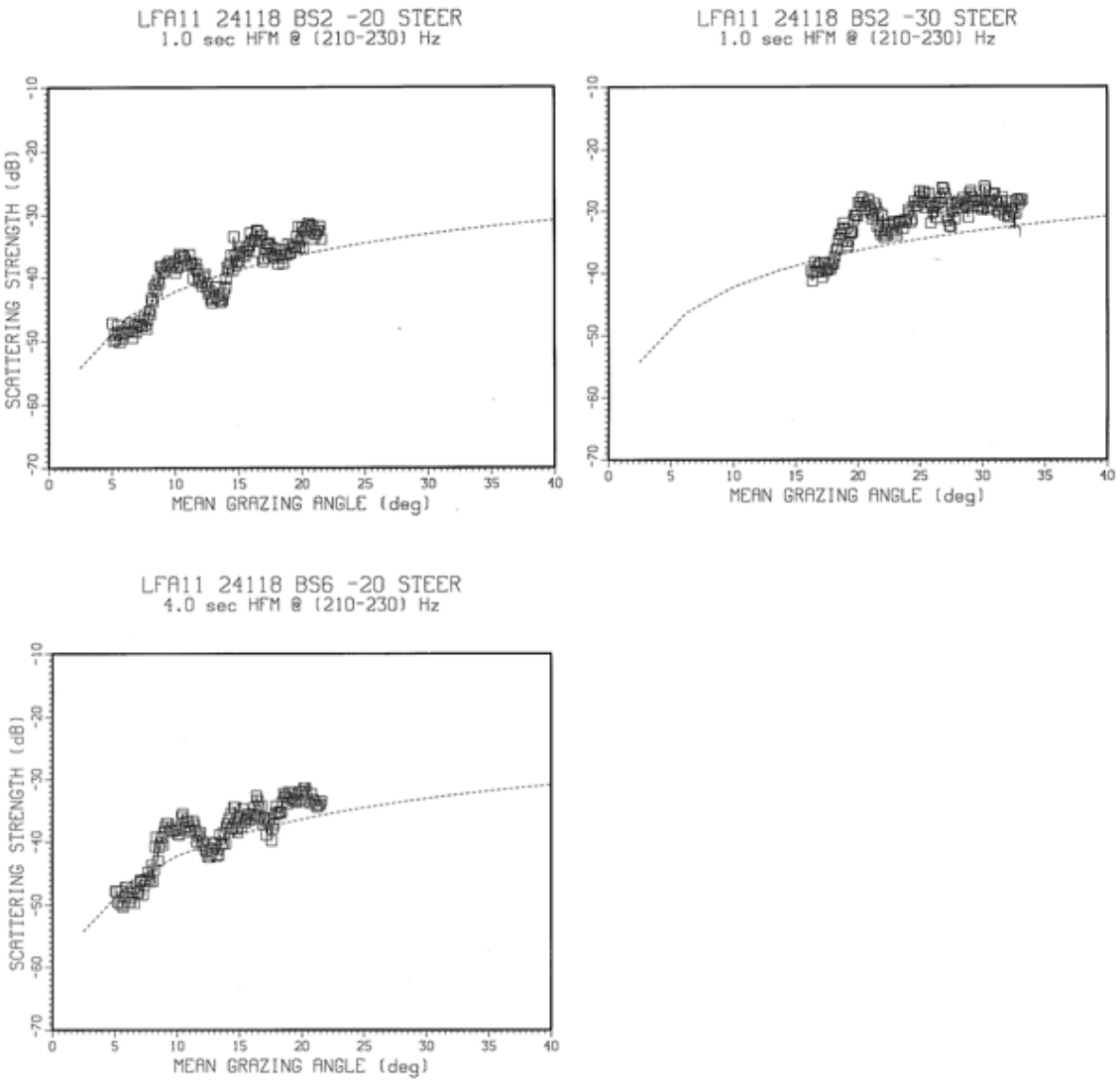

Fig. 8.B-45 – Site 34 LFA-11 BBS vs. grazing angle for 1-s (top) and 4-s (bottom) HFM signals sweeping 210–230 Hz and source-steering angles of down 20 (left) and down 30 (right) deg. (Mackenzie curve (dotted) shown as a reference.)

Run 34

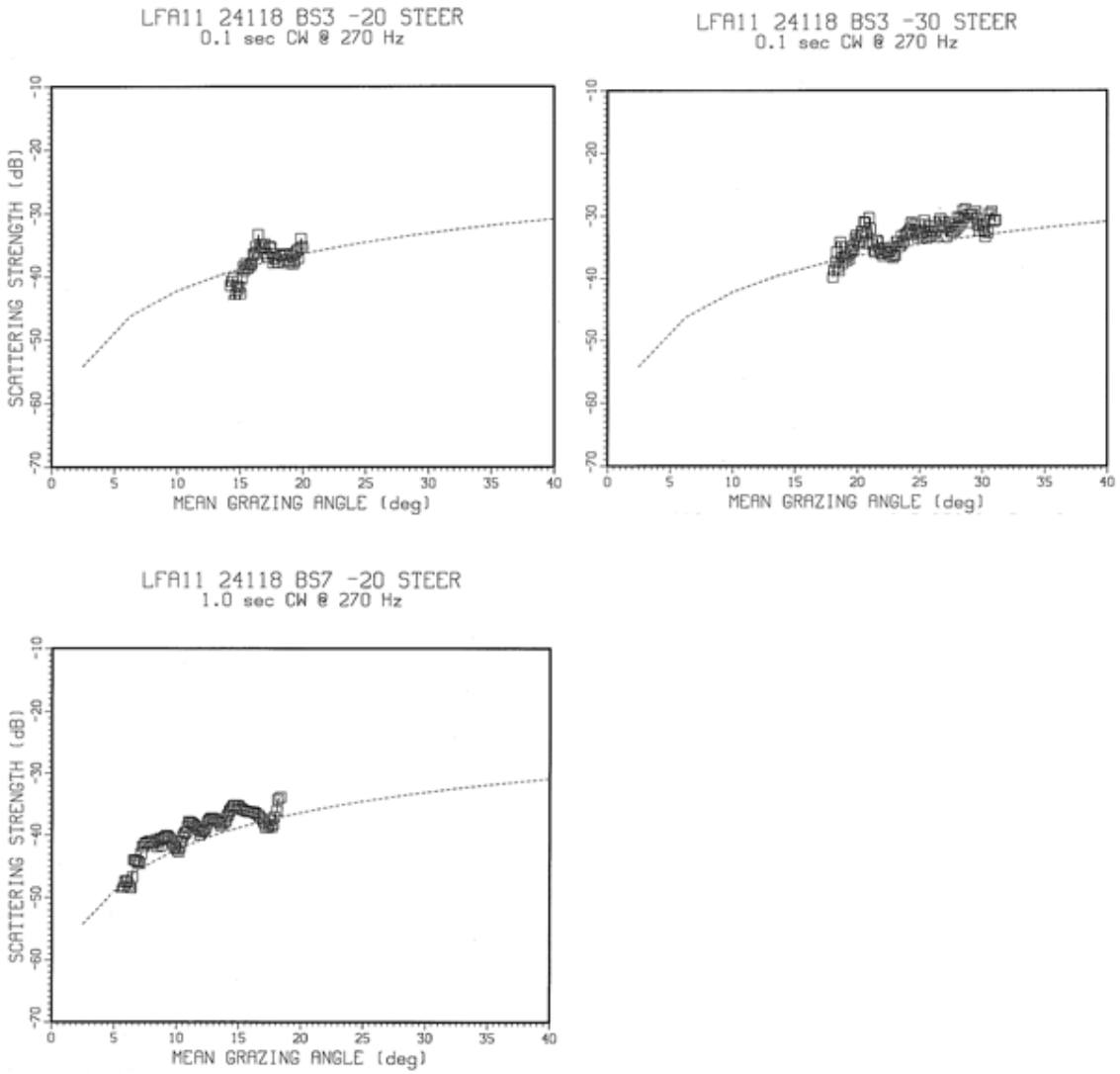

Fig. 8.B-46 – Site 34 LFA-11 BBS vs. grazing angle for 0.1-s (top) and 1-s (bottom) CW signals at 270 Hz and source-steering angles of down 20 (left) and down 30 (right) deg. (Mackenzie curve (dotted) shown as a reference.)

Run 34

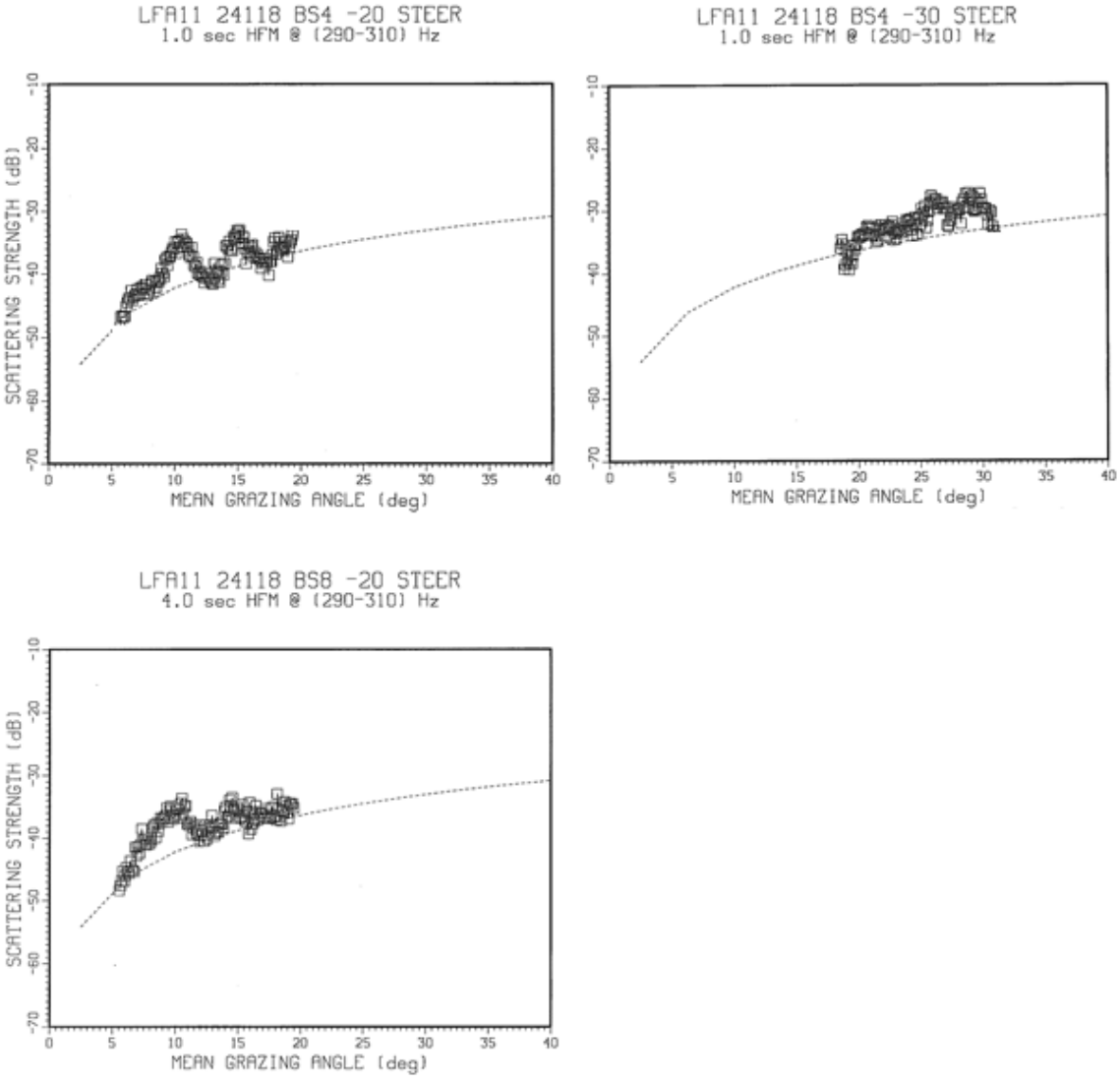

Fig. 8.B-47 – Site 34 LFA-11 BBS vs. grazing angle for 1-s (top) and 4-s (bottom) HFM signals sweeping 290–310 Hz and source-steering angles of down 20 (left) and down 30 (right) deg. (Mackenzie curve (dotted) shown as a reference.)

Run 35

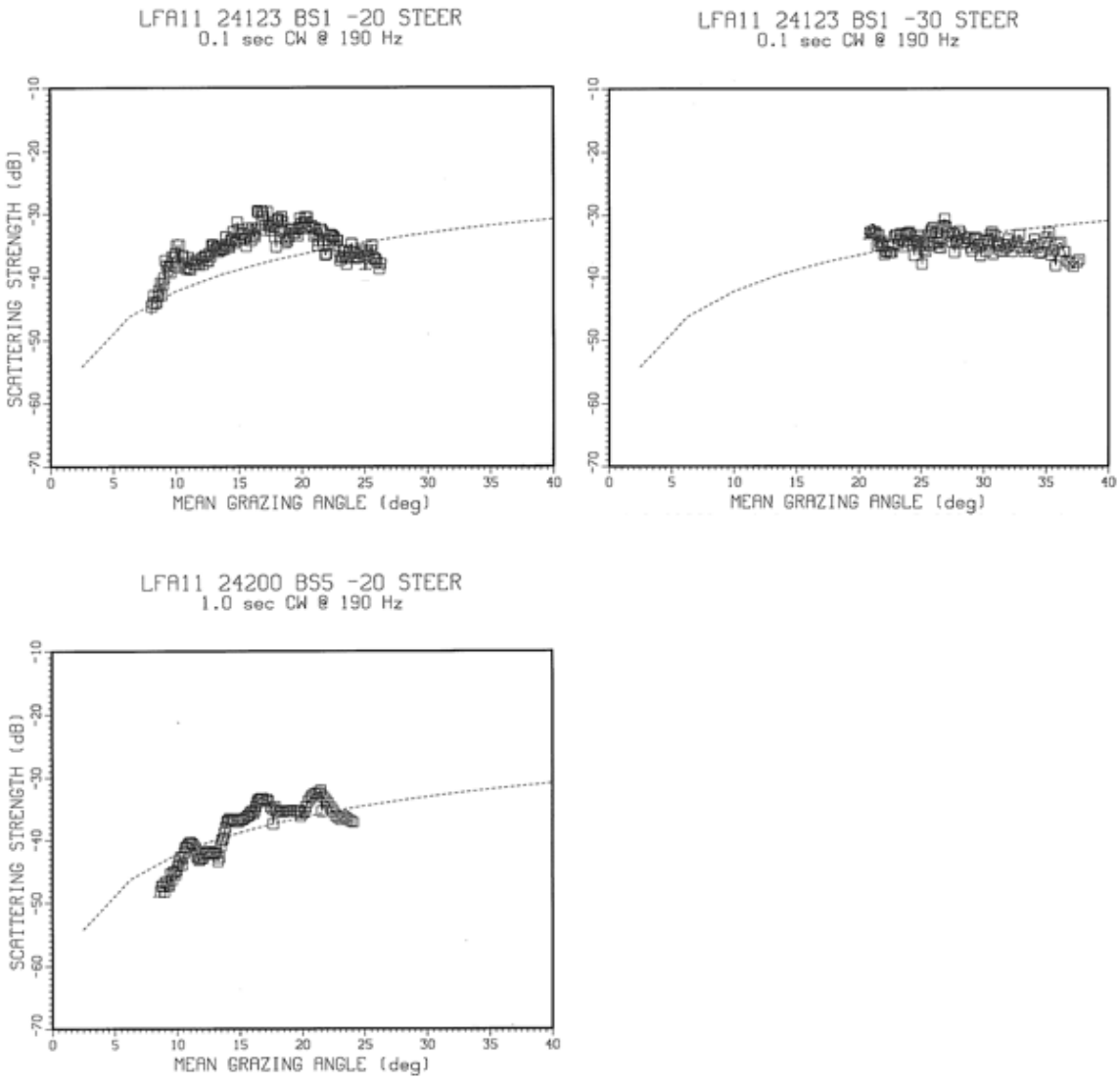

Fig. 8.B-48 – Site 35 LFA-11 BBS vs. grazing angle for 0.1-s (top) and 1-s (bottom) CW signals at 190 Hz and source-steering angles of down 20 (left) and down 30 (right) deg. (Mackenzie curve (dotted) shown as a reference.)

Run 35

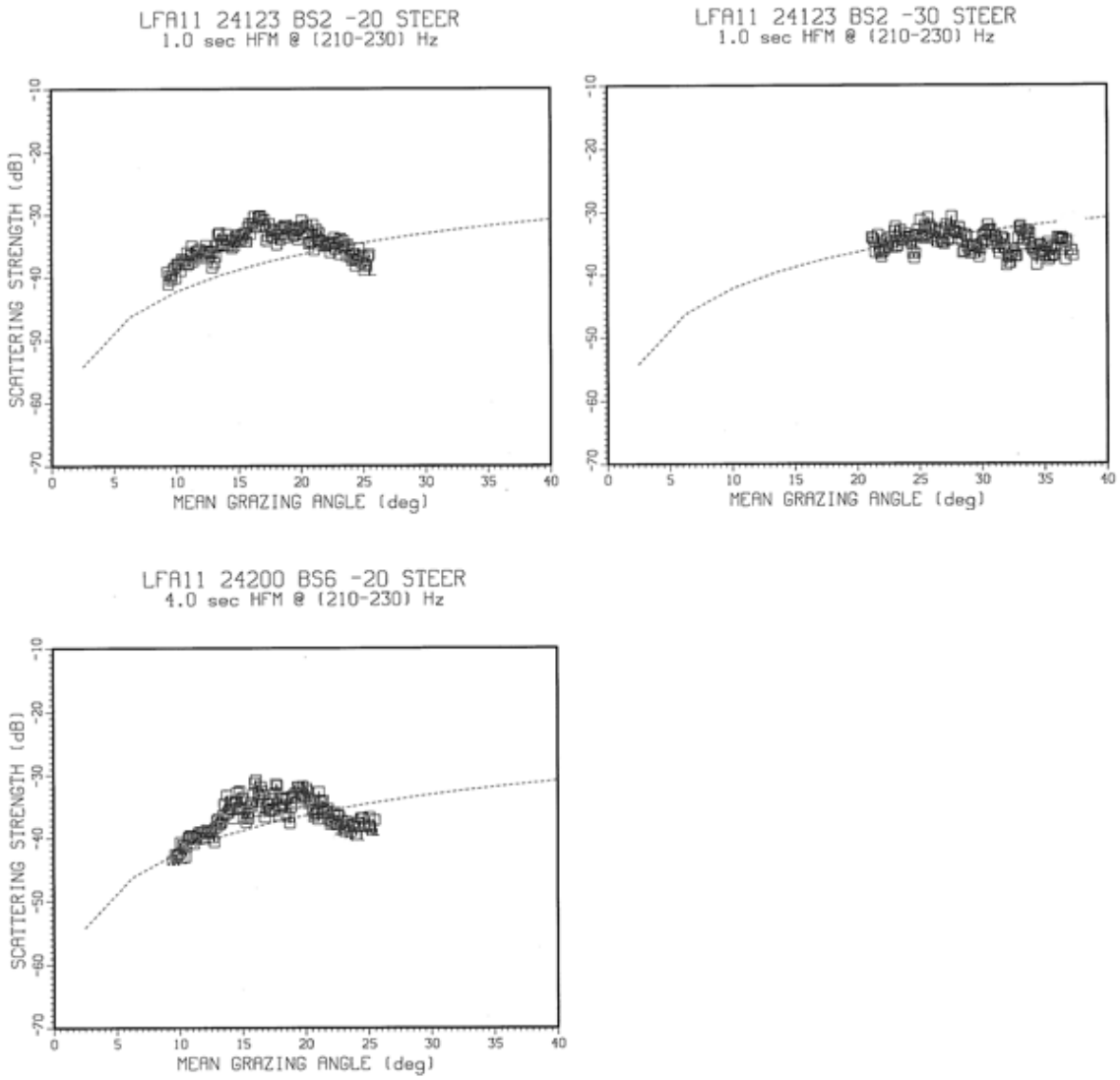

Fig. 8.B-49 – Site 35 LFA-11 BBS vs. grazing angle for 1-s (top) and 4-s (bottom) HFM signals sweeping 210–230 Hz and source-steering angles of down 20 (left) and down 30 (right) deg. (Mackenzie curve (dotted) shown as a reference.)

Run 35

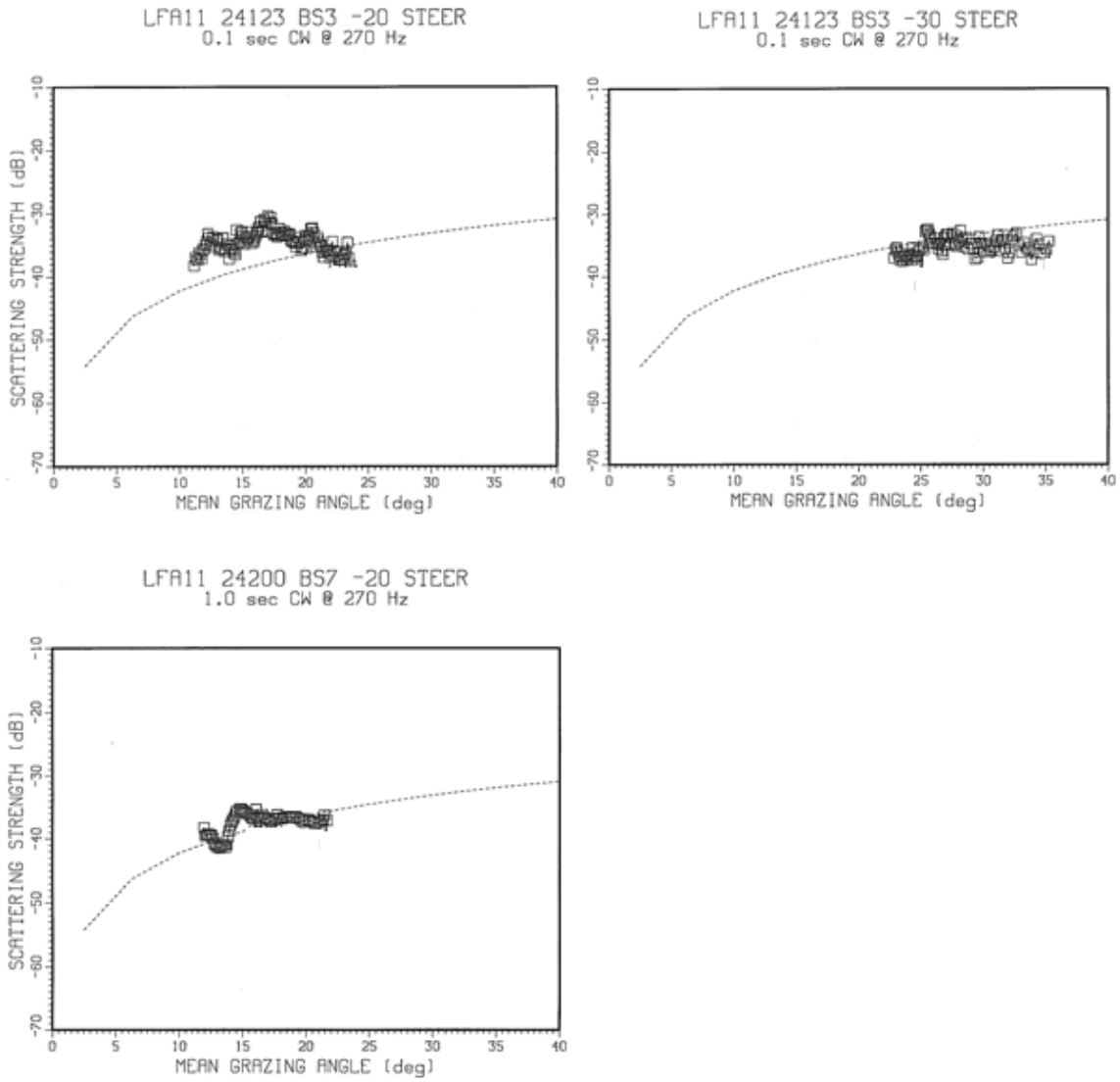

Fig. 8.B-50 – Site 35 LFA-11 BBS vs. grazing angle for 0.1-s (top) and 1-s (bottom) CW signals at 270 Hz and source-steering angles of down 20 (left) and down 30 (right) deg. (Mackenzie curve (dotted) shown as a reference.)

Run 35

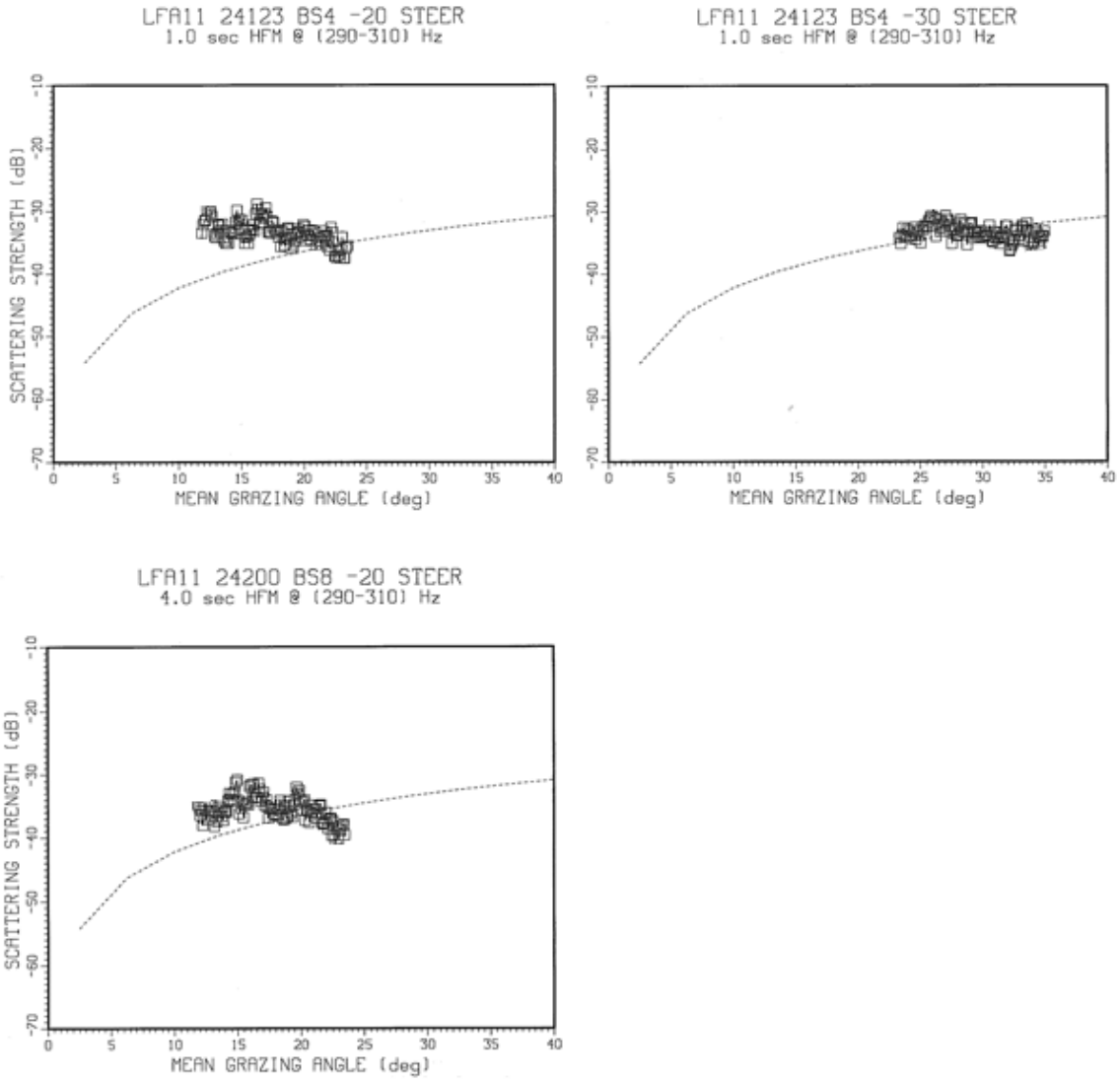

Fig. 8.B-51 – Site 35 LFA-11 BBS vs. grazing angle for 1-s (top) and 4-s (bottom) HFM signals sweeping 290–310 Hz and source-steering angles of down 20 (left) and down 30 (right) deg. (Mackenzie curve (dotted) shown as a reference.)

Run 36

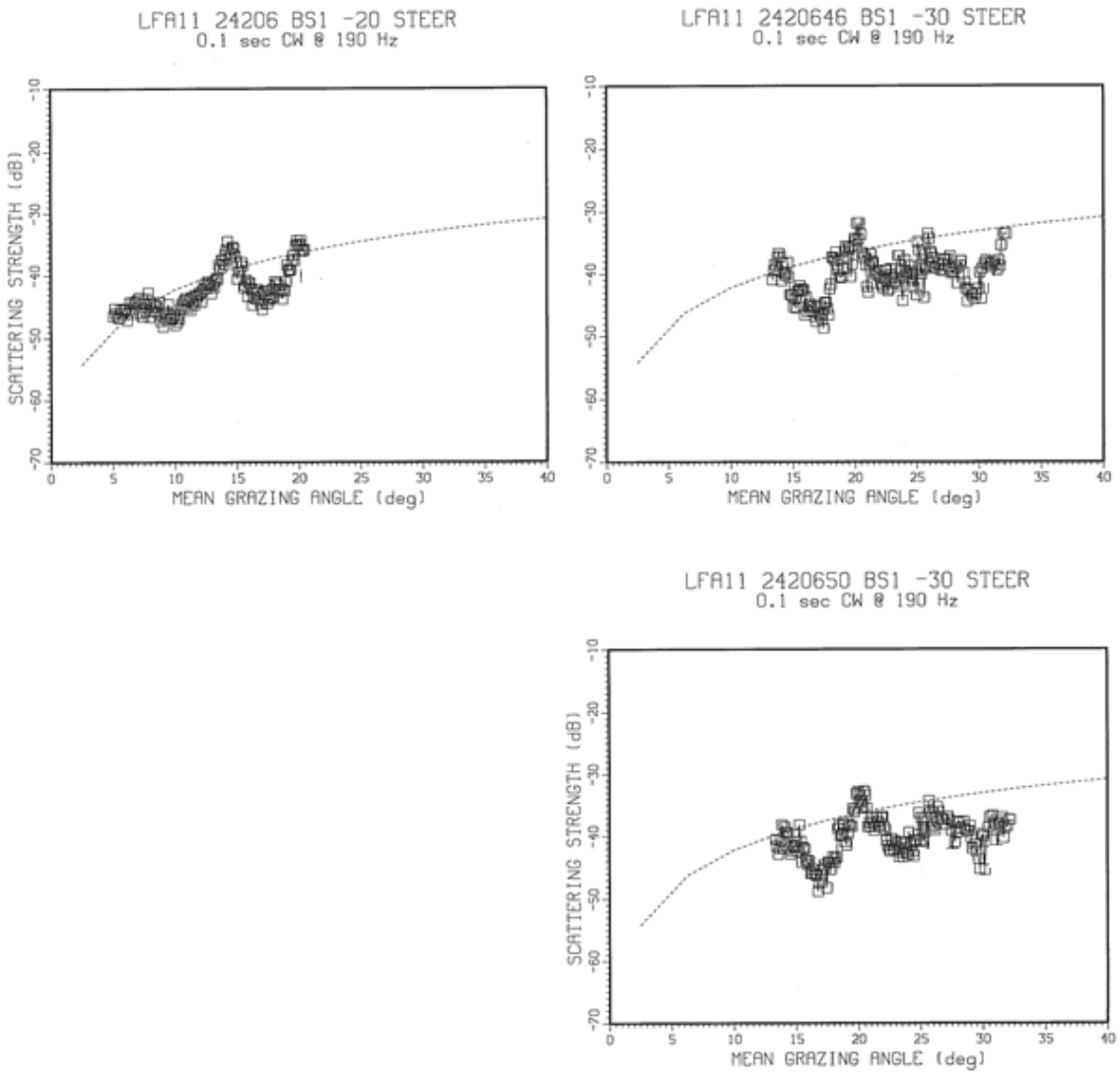

Fig. 8.B-52 – Site 36 LFA-11 BBS vs. grazing angle for 0.1-s 190-Hz CW signals and source-steering angles of down 20 (left) and down 30 (right) deg. (Mackenzie curve (dotted) shown as a reference.)

Run 36

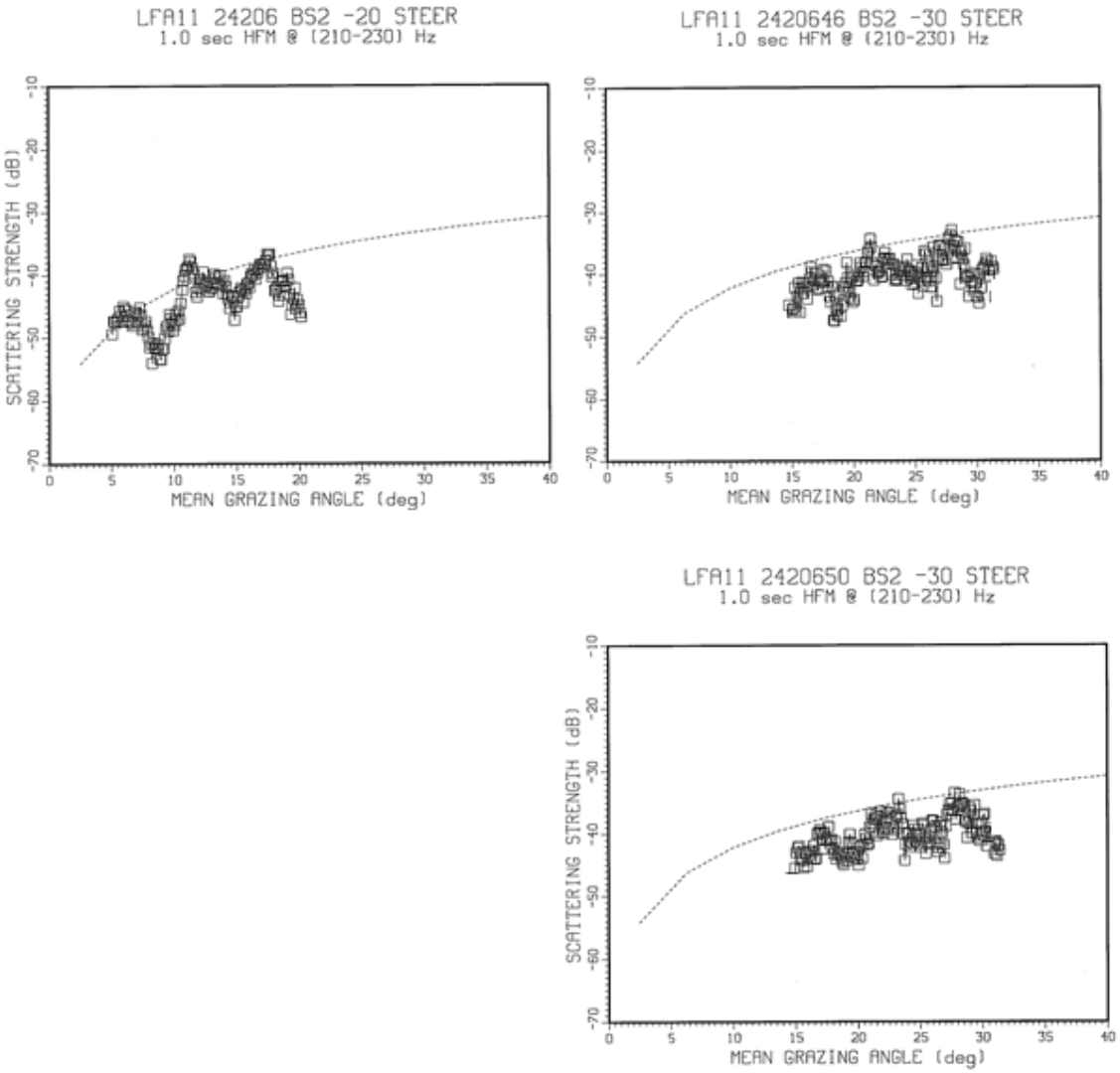

Fig. 8.B-53 – Site 36 LFA-11 BBS vs. grazing angle for 1-s HFM signals sweeping 210–230 Hz and source-steering angles of down 20 (left) and down 30 (right) deg.
(Mackenzie curve (dotted) shown as a reference.)

Run 36

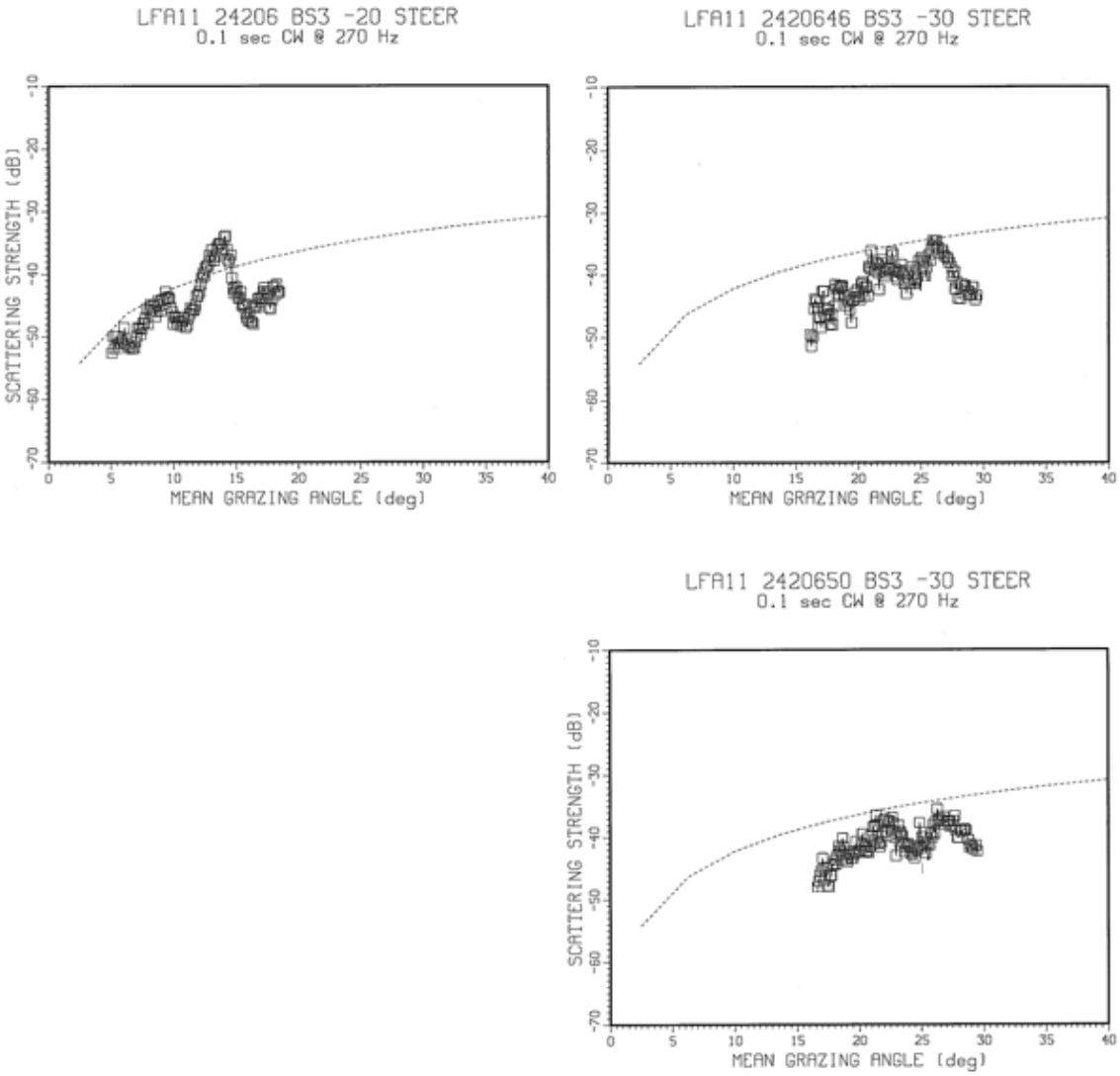

Fig. 8.B-54 – Site 36 LFA-11 BBS vs. grazing angle for 0.1-s 270-Hz CW signals and source-steering angles of down 20 (left) and down 30 (right) deg. (Mackenzie curve (dotted) shown as a reference.)

Run 36

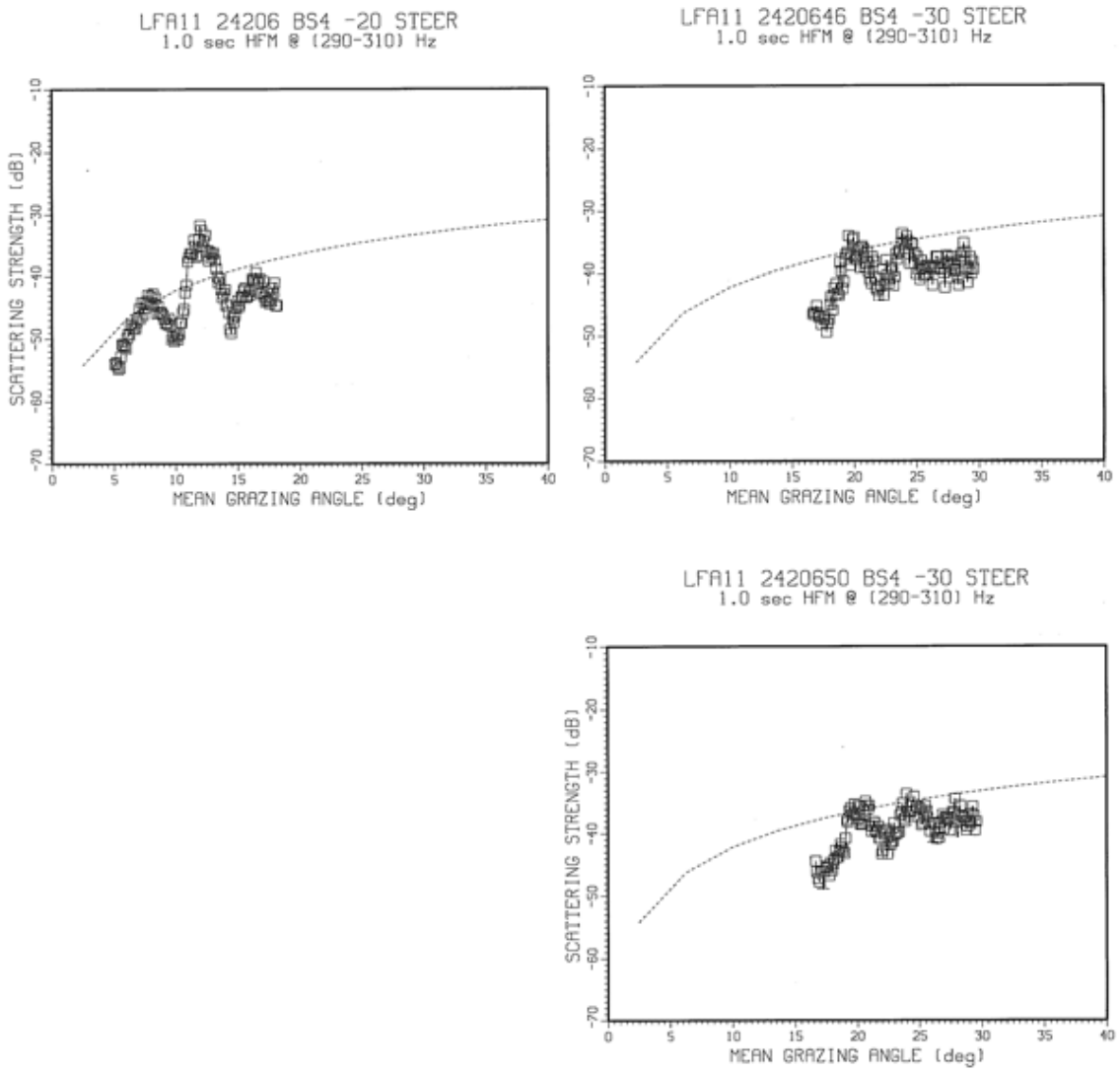

Fig. 8.B-55 – Site 36 LFA-11 BBS vs. grazing angle for 1-s HFM signals sweeping 290–310 Hz and source-steering angles of down 20 (left) and down 30 (right) deg.
(Mackenzie curve (dotted) shown as a reference.)

Run 37

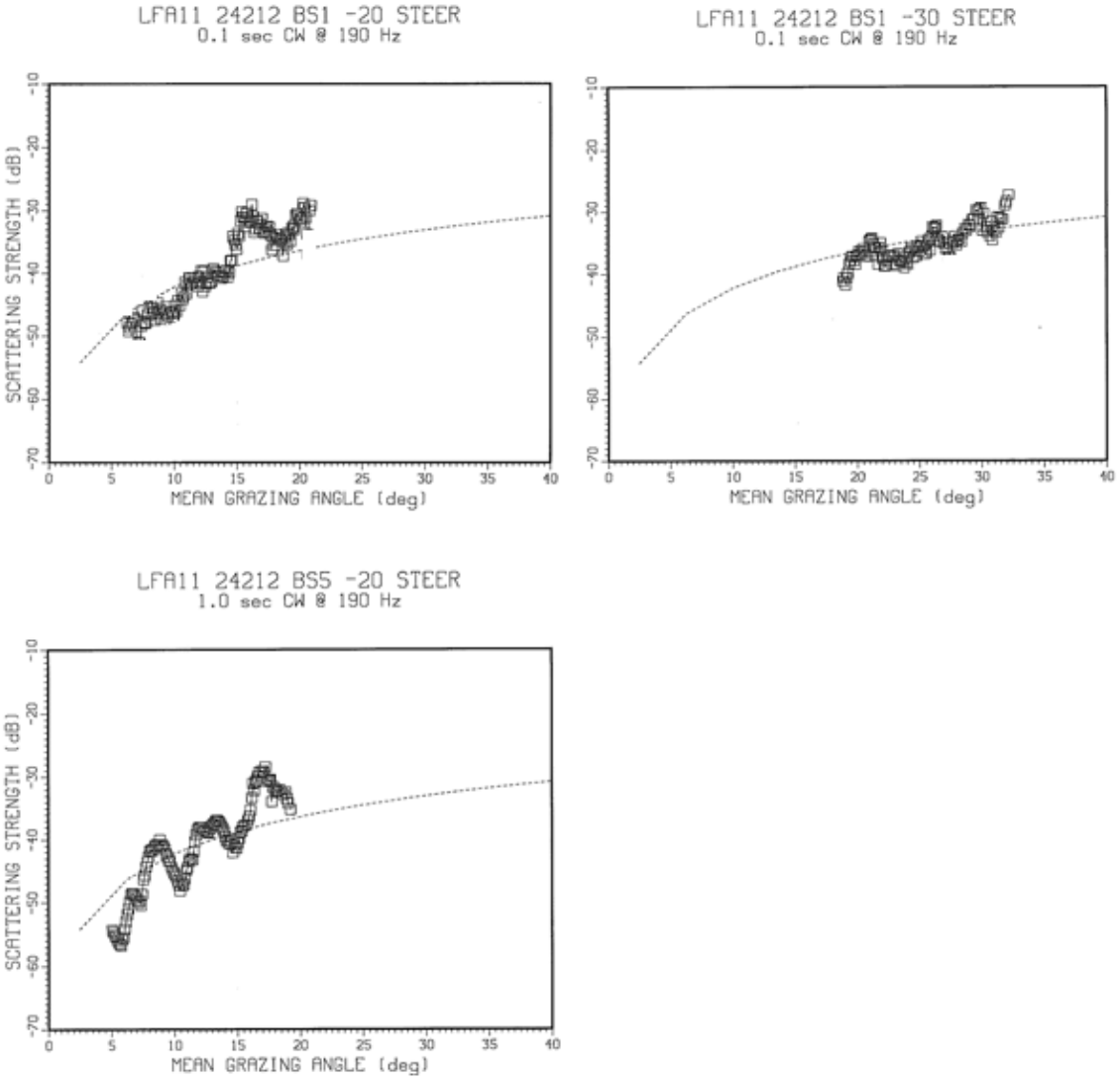

Fig. 8.B-56 – Site 37 LFA-11 BBS vs. grazing angle for 0.1-s (top) and 1-s (bottom) CW signals at 190 Hz and source-steering angles of down 20 (left) and down 30 (right) deg. (Mackenzie curve (dotted) shown as a reference.)

Run 37

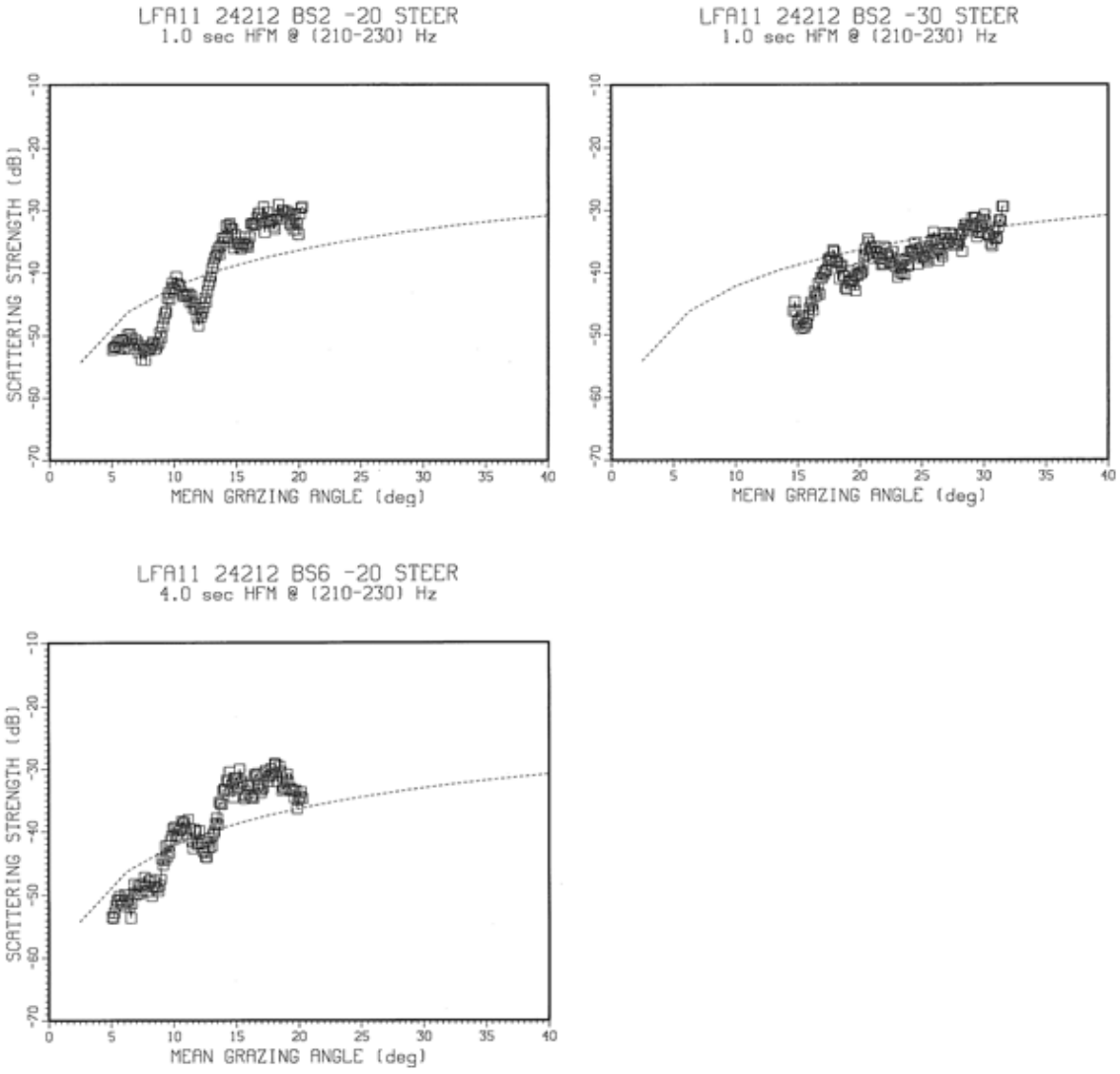

Fig. 8.B-57 – Site 37 LFA-11 BBS vs. grazing angle for 1-s (top) and 4-s (bottom) HFM signals sweeping 210–230 Hz and source-steering angles of down 20 (left) and down 30 (right) deg. (Mackenzie curve (dotted) shown as a reference.)

Run 37

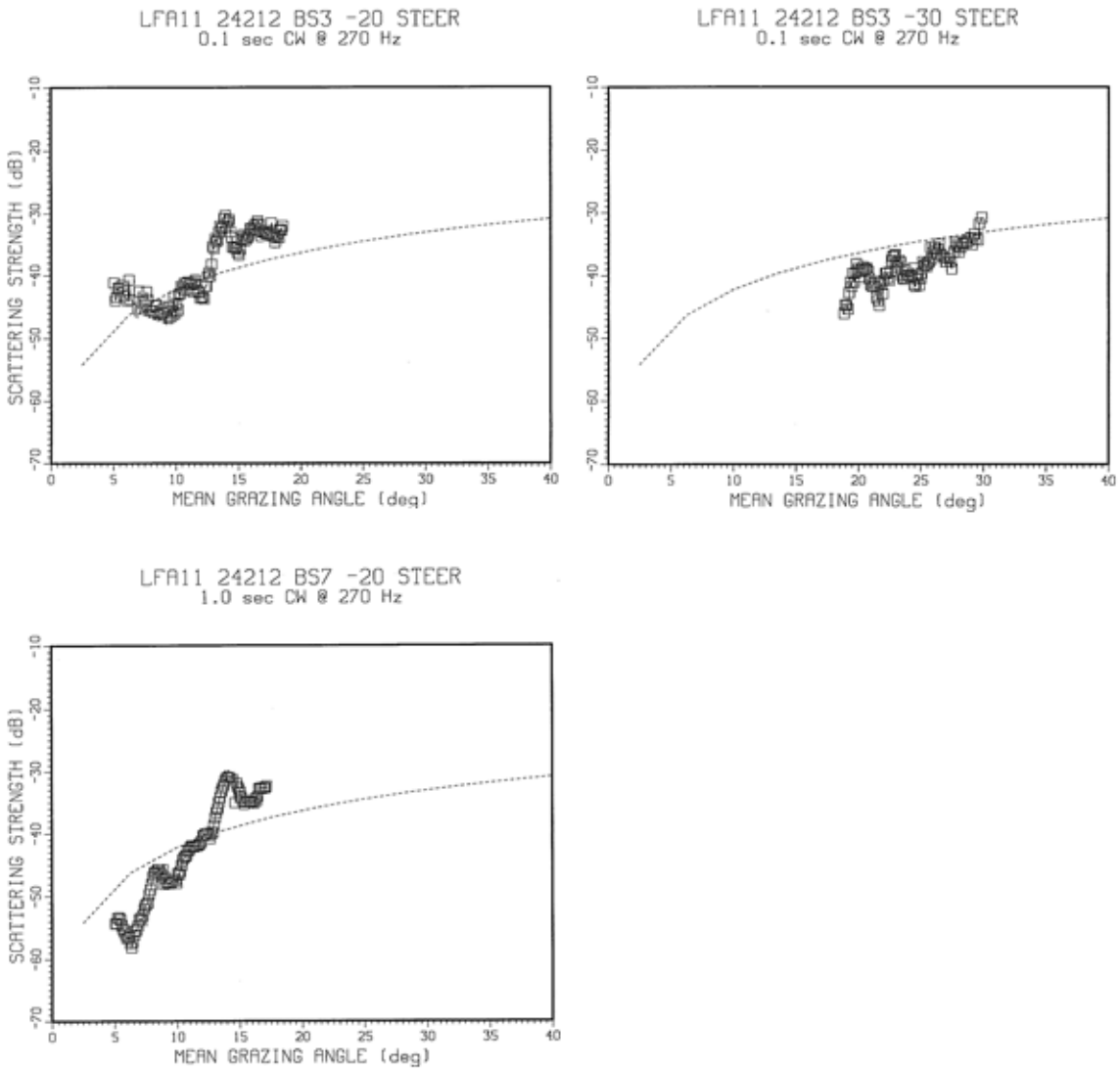

Fig. 8.B-58 – Site 37 LFA-11 BBS vs. grazing angle for 0.1-s (top) and 1-s (bottom) CW signals at 270 Hz and source-steering angles of down 20 (left) and down 30 (right) deg. (Mackenzie curve (dotted) shown as a reference.)

Run 37

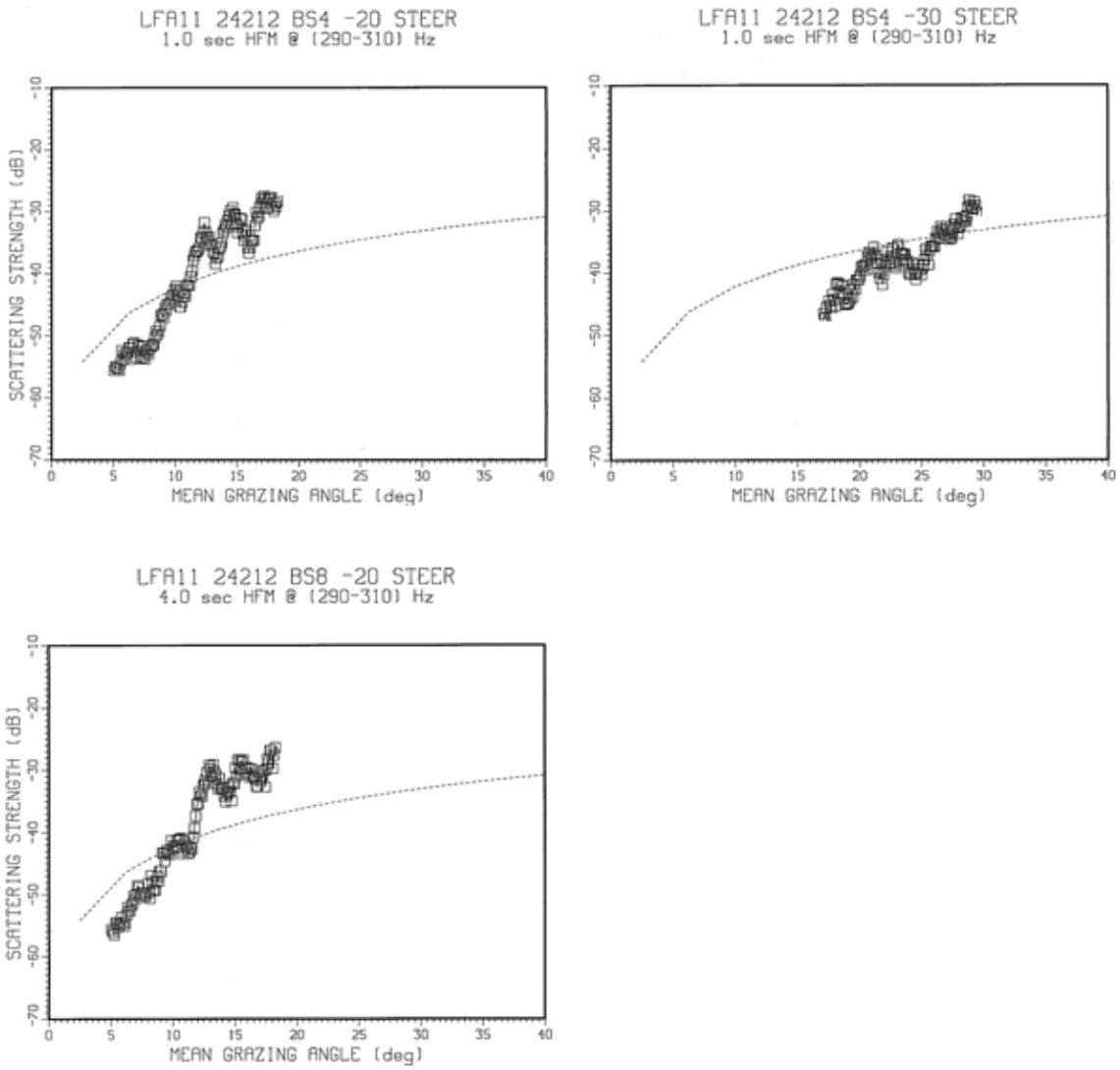

Fig. 8.B-59 – Site 37 LFA-11 BBS vs. grazing angle for 1-s (top) and 4-s (bottom) HFM signals sweeping 290–310 Hz and source-steering angles of down 20 (left) and down 30 (right) deg. (Mackenzie curve (dotted) shown as a reference.)

Run 38

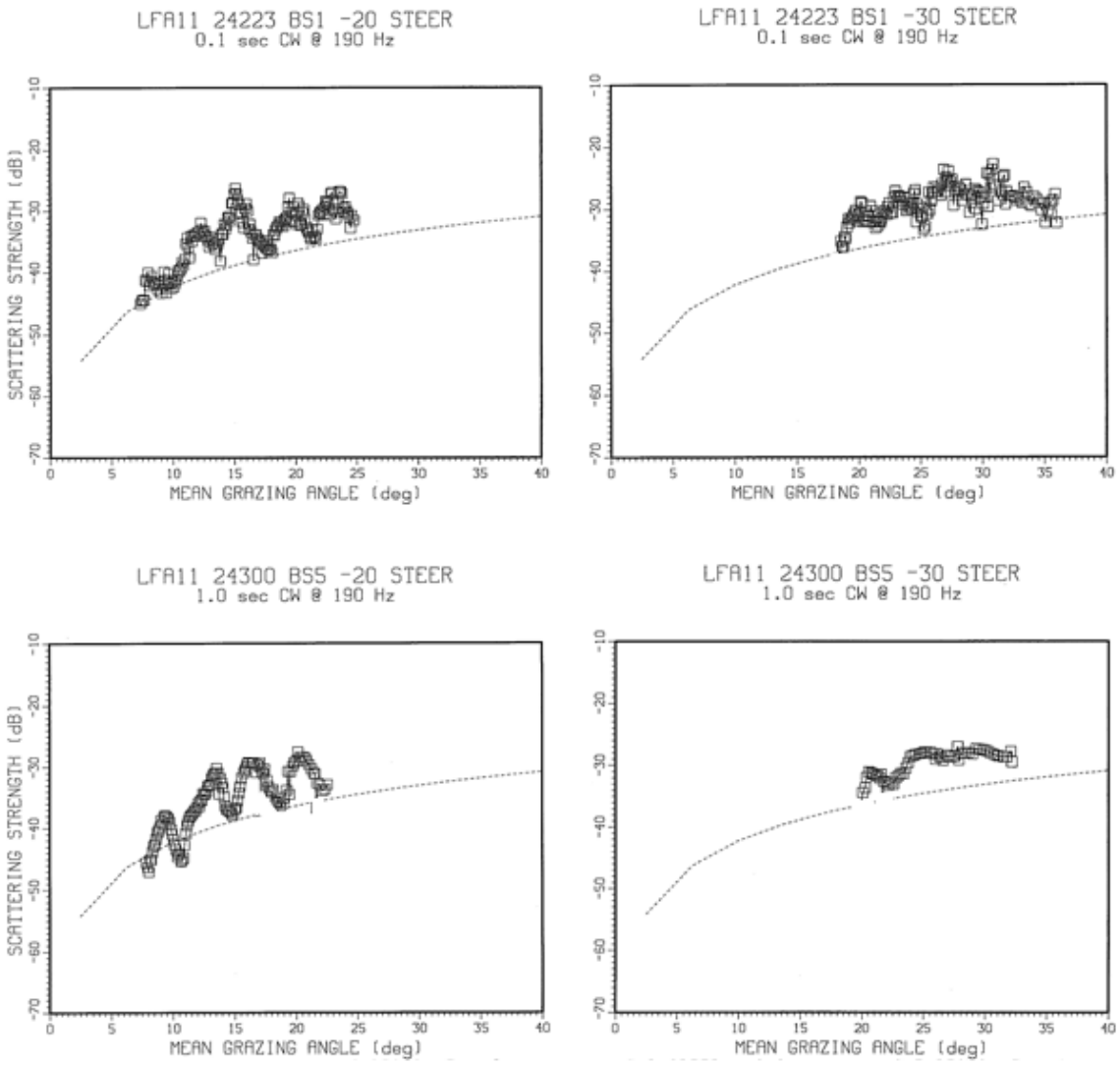

Fig. 8.B-60 – Site 38 LFA-11 BBS vs. grazing angle for 0.1-s (top) and 1-s (bottom) CW signals at 190 Hz and source-steering angles of down 20 (left) and down 30 (right) deg. (Mackenzie curve (dotted) shown as a reference.)

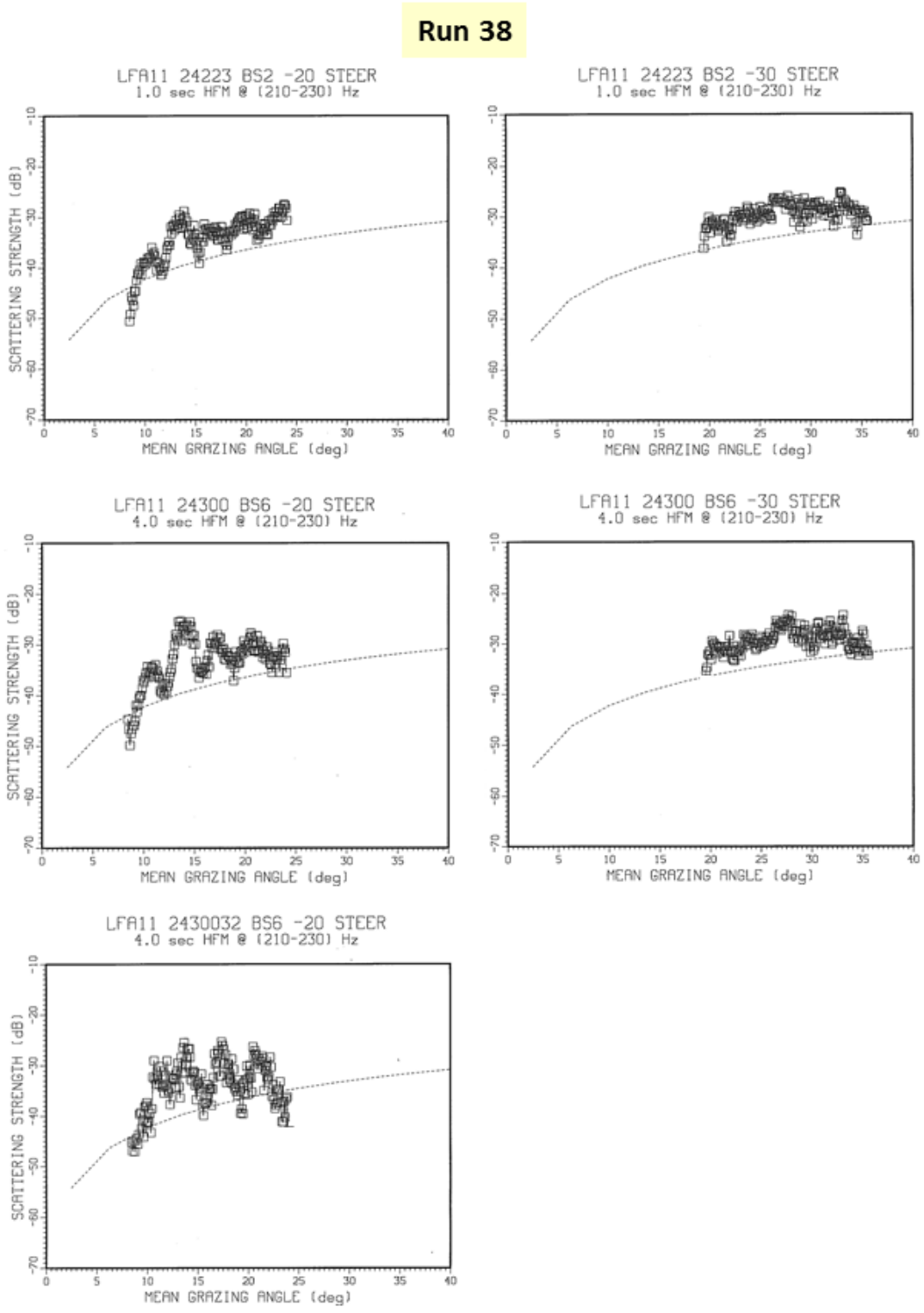

Fig. 8.B-61 – Site 38 LFA-11 BBS vs. grazing angle for 1-s (top) and 4-s (middle; bottom) HFM signals sweeping 210–230 Hz and source-steering angles of down 20 (left) and down 30 (right) deg. (Mackenzie curve (dotted) shown as a reference.)

Run 38

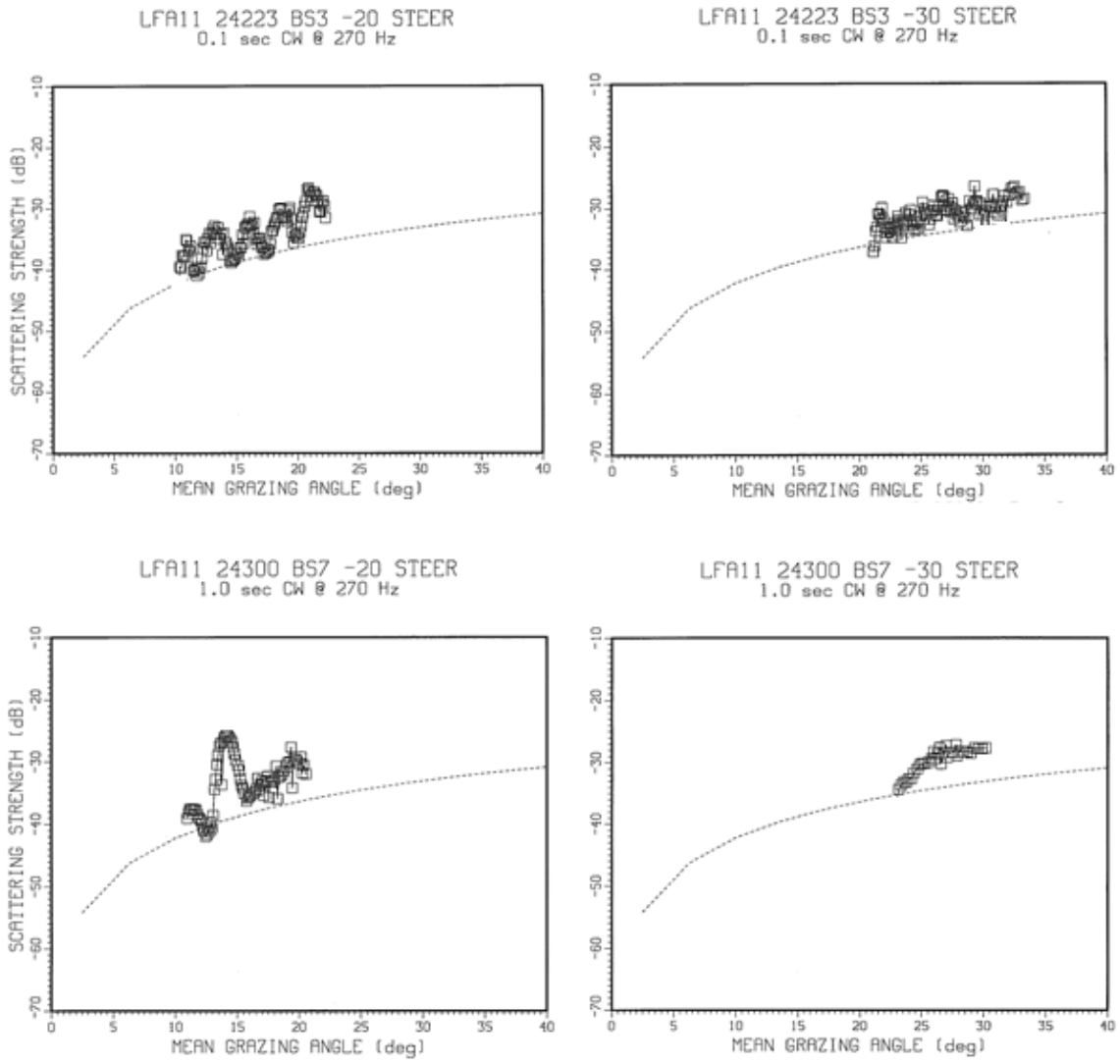

Fig. 8.B-62 – Site 38 LFA-11 BBS vs. grazing angle for 0.1-s (top) and 1-s (bottom) CW signals at 270 Hz and source-steering angles of down 20 (left) and down 30 (right) deg. (Mackenzie curve (dotted) shown as a reference.)

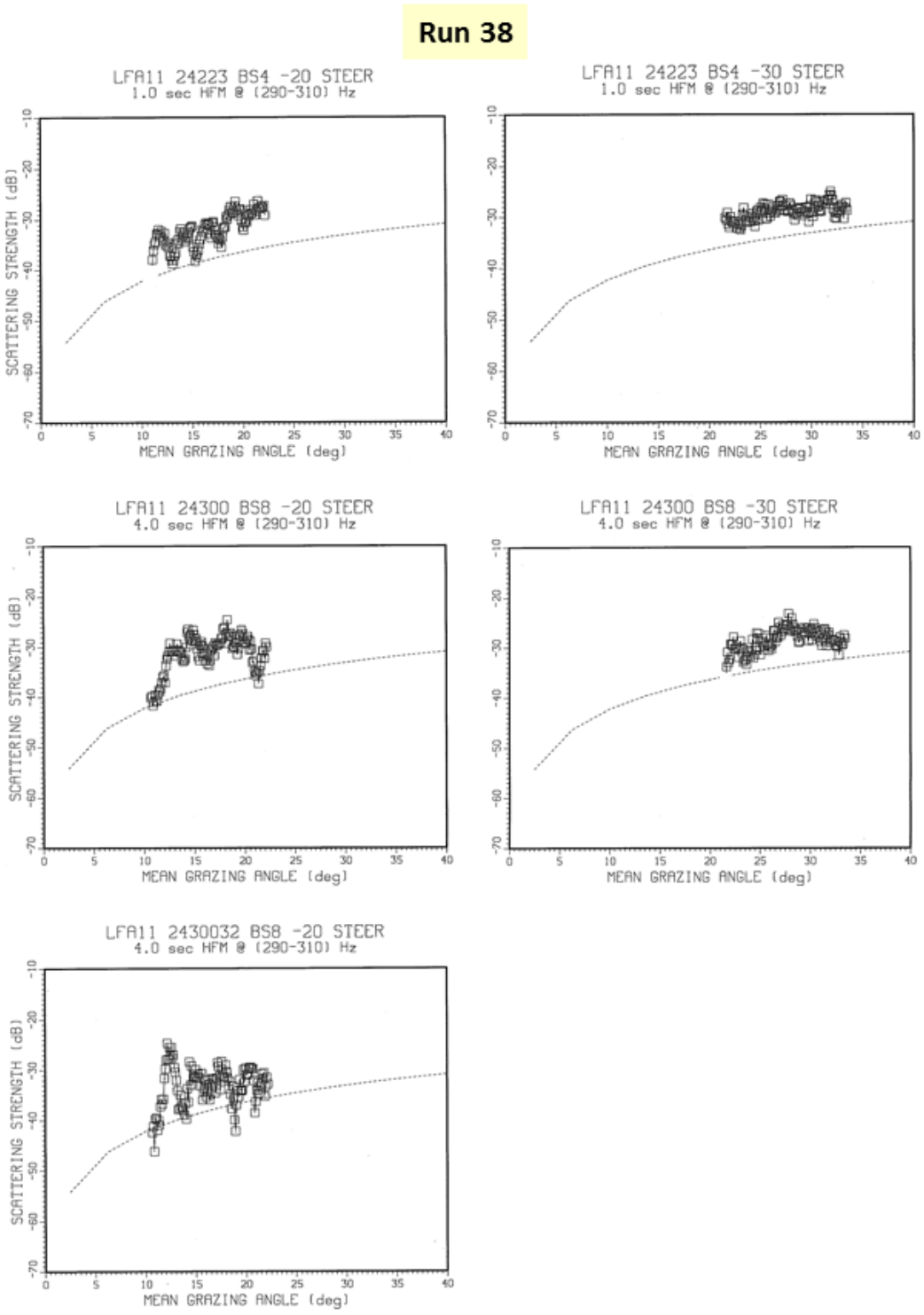

Fig. 8.B-63 – Site 38 LFA-11 BBS vs. grazing angle for 1-s (top) and 4-s (middle; bottom) HFM signals sweeping 290–310 Hz and source-steering angles of down 20 (left) and down 30 (right) deg. (Mackenzie curve (dotted) shown as a reference.)

Run 39

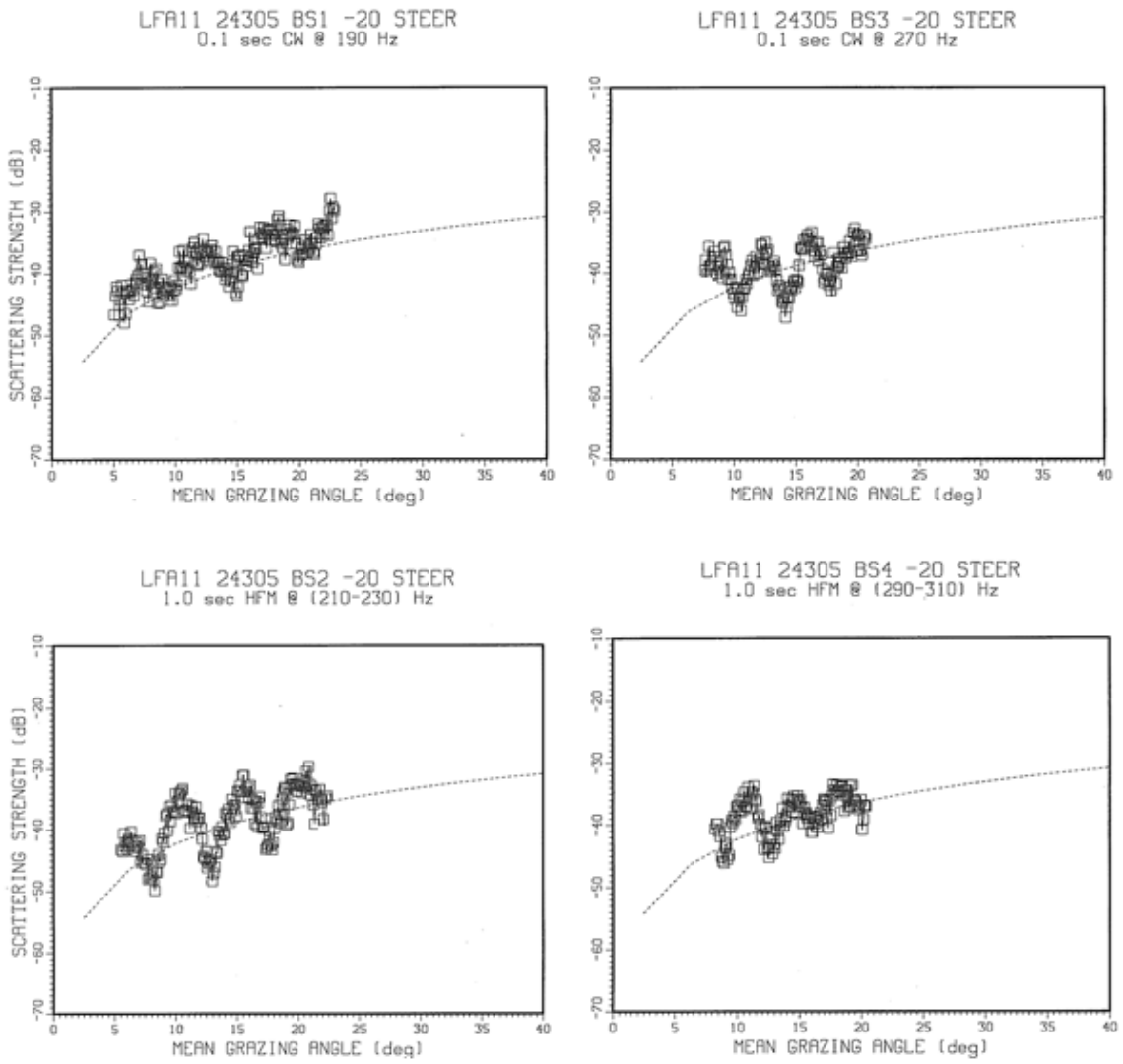

Fig. 8.B-64 – Site 39 LFA-11 BBS vs. grazing angle for 4 signals: 0.1-s CWs (top) at 190 (left) and 270 (right) Hz; and 1-s HFMs (bottom) sweeping 210–230 (left) and 290–310 (right) Hz. The source-steering angle was down 20 deg.
(Mackenzie curve (dotted) shown as a reference.)

C. Comparison to Other Data

Figure 8.C-1 shows BBS vs. grazing angle measured by different source and resolution systems in the vicinity of NRL Site 26 (within 19 km of one another). The non-LFA-11 measurements are by NRL in 1990 (Davis *et al*., 1993) and DREA (Canada) (Robison, 1975).

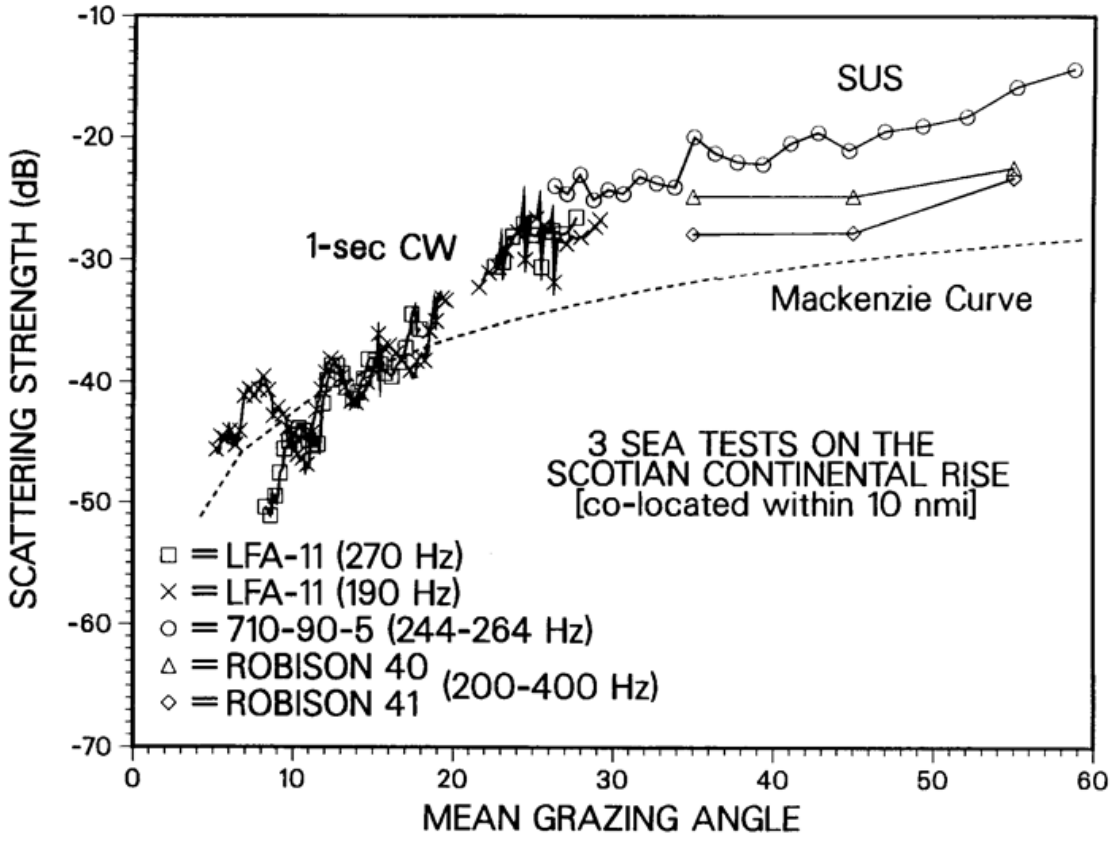

Fig. 8.C-1 – Comparison of NRL LFA-11 Site 26 BBS at 190 and 270 Hz with near-by NRL (710-90-5) and Canadian (Robison) SUS-charge measurements, along with the Mackenzie curve (dashed).

9. OTHER NRL BBS MEASUREMENTS

Other NRL BBS measurements have previously been documented in various reports, in particular those during two research programs: the primarily deep-water Critical Sea Test (CST) program (1988-1996) of SPAWAR (Zittel *et al.*, 2006), and the primarily shallow-water Littoral Warfare Advance Development (LWAD) program of ONR.

A. CST (Deep Water)

The CST BBS data results derive from 68 vertically-bistatic direct-path measurements using SUS explosive charges as sources a horizontal line array (HLA) as a receiver made during 7 experiments conducted by NRL during the CST program. The frequency range is ~50–1500 Hz and the grazing-angle range is ~25–55 degrees (corresponding to reverberation decay times between the first and second fathometer returns).

These data were obtained in mostly thickly-sedimented regions composed primarily of clays, silts, or muds in the: Norwegian Basin (CST-1; foraminiferal clay, marl, or ooze), Icelandic Basin near Hatton Bank (CST-2; mud with high basaltic silt/sand fraction), Bermuda Rise and Hatteras Abyssal Plain (HAP) (CST-3; pelagic clay and turbidite layers, respectively), Aleutian Abyssal Plain (CST-4; pelagic clay overlying turbidites), Messina Rise on the Ionian Abyssal Plain (CST-5; hemipelagic mud), Sila Fracture Zone (CST-7; thinly sedimented), and Herodotus Abyssal Plain up to the Nile Cone (CST-8; thickly sedimented).

The BBS experiments and results are documented in Ogden and Erskine (1993, 1997). However, since those publications**, an extensive CST SUS reprocessing effort revealed recalibration adjustments were needed for the reported CST SUS scattering-strength values (especially in the lowest frequency bands), generally as in Fig. 9.A-1.** (For run-specific #s, contact J. Fialkowski, NRL.)

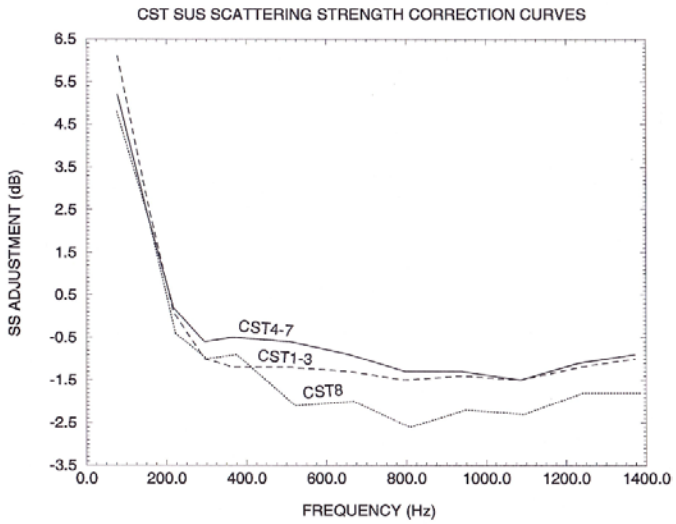

Fig. 9.A-1 – CST SUS scattering strength (SS) recalibration-adjustment values.
(The adjustment values are to be *added* to previously-reported CST SUS SS values.)

Examples of reprocessed cross-CST-experiment results are shown (along with some physics-based model comparisons) in Figs. 9.A-2 and 9.A-3 (Gauss *et al*., 2008).

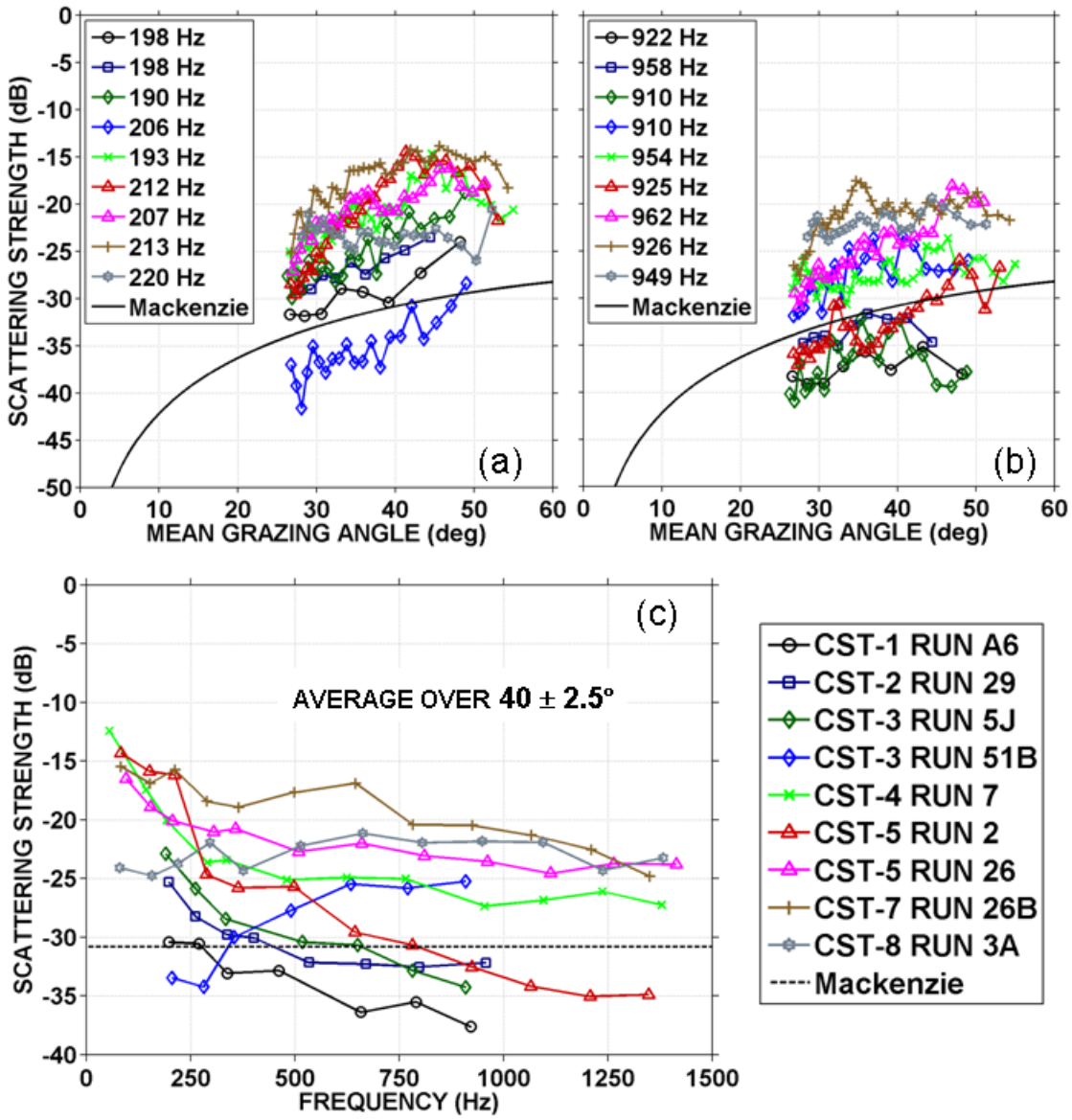

Fig. 9.A-2 – Deep-water BSS from aft-looking beams for representative CST data sets.

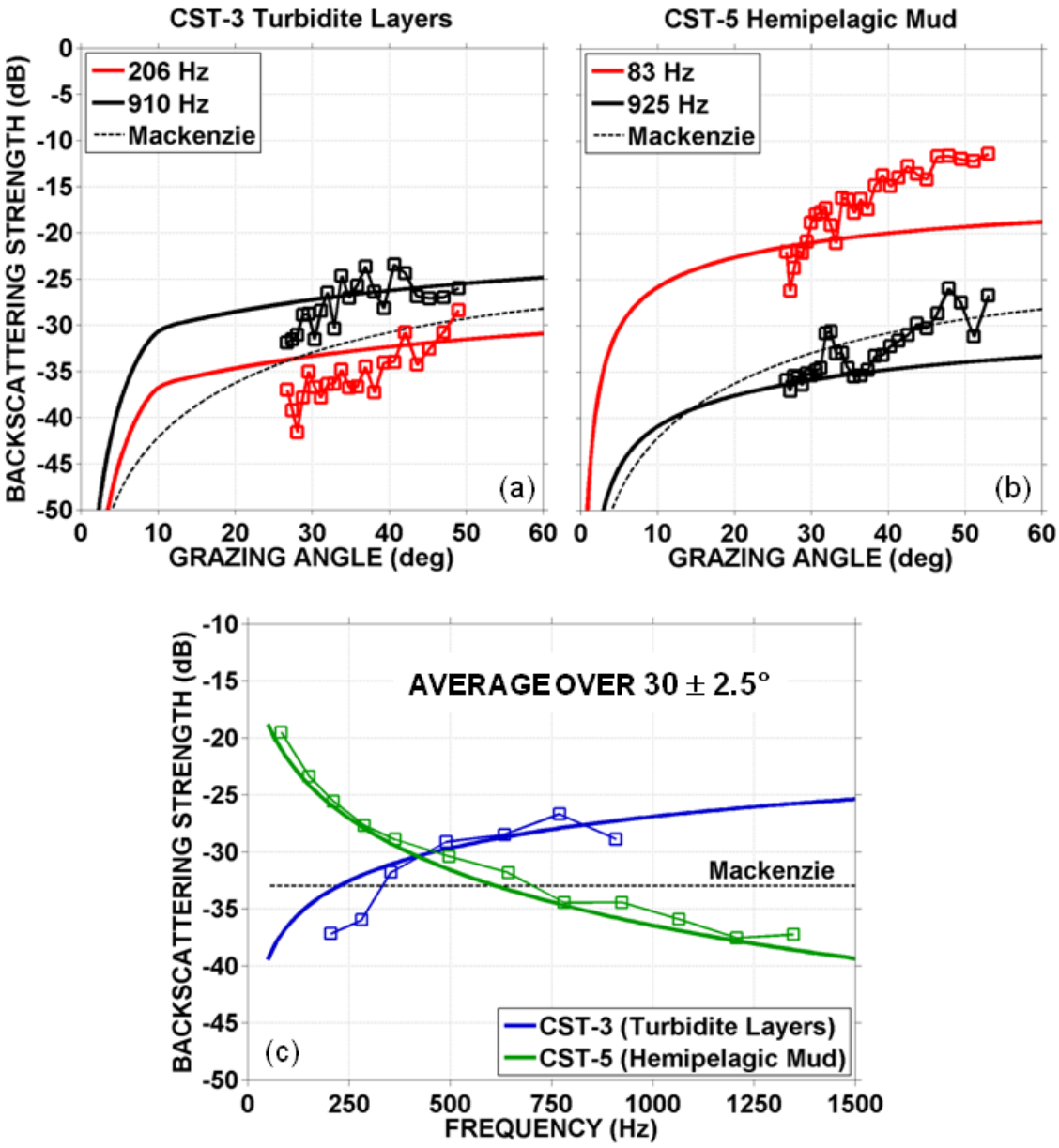

Fig. 9.A-3 – Deep-water data-model comparisons for 2 CST sites. Data (symbolled curves) are from aft-looking beams. Inset table gives key assumed sediment-volume parameter values.

B. LWAD (Shallow Water)

The LWAD BBS measurements were conducted by NRL during 8 experiments (1996 to 2000) using basically the same experimental set up (Fig. 2-1) as the BBS experiments that form the basis of the shallow-water portion of this report[1]. Their dates and locations are:

- LWAD FTE 96-2 Long Bay (Carolina Coast) 1996 7 sites
- LWAD FTE 97-2 Southwest of Key West 1997 1 site
- LWAD SCV 97 Long Bay (Carolina Coast) 1997 7 sites
- LWAD 98-2 Southwest Coast of Florida 1998 2 sites
- LWAD 98-4 Long Bay (Carolina Coast) 1998 4 sites
- LWAD 99-1 Southwest Coast of Florida 1999 4 sites
- LWAD 99-3 Coast of Oregon 1999 2 sites
- LWAD 00-3 Adriatic Sea 2000 2 sites

These LWAD experiments and results are respectively documented in a series of NRL reports: Soukup and Ogden (1997), Soukup and Edsall (1997), Soukup (1998), Kunz (1998), Kunz (Feb 1999), Kunz (Jul 1999), Kunz and Gauss (2000), and Kunz (2001). See Soukup and Gragg (2003) for further analysis/modeling of the LWAD SCV-97 data.

10. DISCUSSION AND CONCLUSIONS

Scattering from the seabed can be a complex mix of surface roughness and volume heterogeneity contributions. This report documents the results from analyzing a series of bottom backscattering strength data collected by NRL at a number of shallow-water locations (New Jersey Shelf, Stanton Banks, Malta Plateau, Heceta Bank) at MF, and on the Scotian Continental Rise at LF. Empirical-power-law fits to the MF results were also presented, as well as a brief examination of the relationships between the T-MAST-02 BBS results and local bottom parameters (surficial grain size and bottom type).

The MF results demonstrate the inadequacies of using Lambert's Law to model bottom backscattering strengths in shallow water, and that, if physics-based BBS predictions are not possible, more general empirical power laws, where not only the strength but the angular exponent can vary, are needed to match the data at a given frequency.

[1] Note as the NRL VLA receiver was recently recalibrated in 2011, the published Kunz and Kunz and Gauss LWAD BBS values need adjustment—those in the Soukup *et a*l. papers are unaffected as they used a different VLA). (See the authors for details.)

ACKNOWLEGDMENTS

This work was supported by the Office of Naval Research. The Malta-Plateau work was also made possible in part by the "Statistical Characterization of Ocean-Acoustic Boundary Interactions" and "Environmental Adaptation for Multistatic Sonars" Joint Research Projects, collaborations between the Applied Research Laboratory, the Pennsylvania State University (ARL-PSU), the Defence Research & Development, Canada-Atlantic (DRDC-A), NRL, and the NATO Undersea Research Centre (NURC)[2]. The LFA-11 data collection was under the aegis of the Space and Naval Warfare Systems Command (SPAWAR) PMW-182.

REFERENCES

1. British Geological Survey, "PEACH" (Sheet 56N 10W) and "TIREE" (Sheet 56N 08W) Sea Bed Sediment maps (1: 250 000 Series), National Environmental Resource Council (NERC), 1990 and 1988 (resp.). © NERC.

2. Davis, N.R., Jeffery, J., and Erskine, F.T., "Measurements of Ocean Surface and Bottom Backscattering Strengths in the Northwestern Atlantic Ocean," NRL Formal Report 7142--93-9570, Naval Research Laboratory, Washington DC, October 8, 1993.

3. Gauss, R.C., Holland C.W., Fialkowski J.M., and Neumann P., "Measurements and modeling of low-frequency bottom scattering strengths from the Scotian Continental Rise," *J. Acoust. Soc. Am.* **100**, 2797 (A) (1996).

4. Harrison, C.H., "Closed-form expressions for ocean reverberation and signal excess with mode stripping and Lambert's law", *J. Acoust. Soc. Am*. **114**, 2744-2756 (2003).

5. Healy, S.G. (QinetiQ Unit, Southampton Oceanography Centre, Southampton, UK), "T-MAST 02 Environment," presentation at T-MAST 02 Planning Meeting, Dec. 12, 2001

6. Holland, C.W., and Neumann, P., "Sub-bottom scattering: A modeling approach", *J. Acoust. Soc. Am*. **104**, 1363-1373 (1998).

7. Holland, C.W, Gauss, R.C, Hines, P.C., Nielsen, P., Preston, J.R., Harrison, C.H., Ellis, D.D., LePage, K.D., Osler, J., Nero, R.W., Hutt, D., and Turgut, A., "Boundary Characterization Experiment Series Overview," IEEE J. Ocean. Engr. **30**, 784-806 (2005).

8. Jackson, D.R., and Richardson, M.D., *High-Frequency Seafloor Acoustics* (Springer, New York, 2007).

[2] The NURC (La Spezia, Italy) was formerly the NATO SACLANT Undersea Research Centre (SACLANTCEN), and is now the Centre for Maritime Research and Experimentation (CMRE).

9. Kunz, E.L., “Bottom Backscattering Measured Off the Southwest Coast of Florida During the Littoral Warfare Advanced Development 98-2 Experiment,” NRL Memorandum Report 7140--98-8196, Naval Research Laboratory, Washington, DC, September 4, 1998.

10. Kunz, E.L., “Bottom Backscattering Measured Off the Carolina Coast During Littoral Warfare Advanced Development 98-4 Experiment,” NRL Memorandum Report 7140--98-8339, Naval Research Laboratory, Washington, DC, February 26, 1999.

11. Kunz, E.L., “Bottom Backscattering Measured Off the Southwest Coast of Florida During the Littoral Warfare Advanced Development 99-1 Experiment,” NRL Memorandum Report 7140--99-8389, Naval Research Laboratory, Washington, DC, July 30, 1999.

12. Kunz, E.L., “Bottom Backscattering Measured in the Adriatic Sea During the Littoral Warfare Advanced Development 00-3 Experiment,” NRL Memorandum Report 7140--01-8523, Naval Research Laboratory, Washington, DC, January 30, 2001.

13. Kunz, E.L., and Gauss, R.C., “Bottom Backscattering Measured Off the Coast of Oregon During the Littoral Warfare Advanced Development 99-3 Experiment,” NRL Memorandum Report 7140--00-8453, Naval Research Laboratory, Washington, DC, June 12, 2000.

14. Kunz, E.L., and Gauss, R.C., Bottom backscattering strengths measured at 2-5 kHz in shallow water west of Scotland. In *OCEANS ‘05 MTS/IEEE Conference*, 19-23 Sept. 2005, Washington, DC (CD-ROM).

15. Ogden, P.M., and Erskine, F.T., *Bottom scattering strengths measured using explosive sources in the Critical Sea Test Program*. Naval Research Laboratory, Washington, DC, NRL/FR/7140--97-9822, Feb. 5, 1997.

16. Ogden, P.M., and Erskine, F.T., Low-frequency bottom backscattering strengths measured using SUS charges. In *Acoustic Classification and Mapping of the Sea-Bed*, Proceedings of the Institute of Acoustics **15**, Pt.2, ed. By N.G. Pace and D.N. Langhorne, 14-16 April 1993, University of Bath, Bath, UK, pp. 271-278.

17. Robison, A.E., “Bottom Reverberation in the North Atlantic,” DREA Technical Memorandum 75/B, Defence Research Establishment Atlantic, Dartmouth, N.S., Canada (1975).

18. Soukup, R.J., “Bottom Backscattering Measured Off the Carolina Coast During Littoral Warfare Advanced Development System Concept Validation Experiment 97 (LWAD SCV 97),” NRL Formal Report 7140--98-9885, Naval Research Laboratory, Washington DC, June 15, 1998.

19. Soukup, R.J., and Edsall, D.W., "Bottom Backscattering Measured Southwest of Key West During Littoral Warfare Advanced Development Focused Technology Experiment 97-2," NRL Memorandum Report 7140--97-7977, Naval Research Laboratory, Washington, DC, September 30, 1997.

20. Soukup, R.J., and Gragg, R.F., "Backscatter from a limestone elastic seafloor at 2–3.5 kHz: Measurements and modeling," *J. Acoust. Soc. Am.* **113**, 2501-2514 (2003).

21. Soukup, R.J., and Ogden, P.M., "Bottom Backscattering Measured Off the South Carolina Coast During Littoral Warfare Advanced Development Focused Technology Experiment 96-2," NRL Memorandum Report 7140--97-7905, Naval Research Laboratory, Washington DC, April 28, 1997.

22. Stoker, M.S., Hitchen, K., and Graham, C.C., *The geology of the Hebrides and West Shetland shelves, and adjacent deep-water areas,* British Geological Survey. London, UK: HMSO, 1993, ch. 13.

23. Vogt, P.R., and Tucholke, B.E., eds., *The Geology of North America, Volume M, The Western North Atlantic Region*, The Geology Society of North America, 1986, chs. 20, 25–26, and Plates 2, 6–7.

24. Zittel, J.D., Erskine, F.T., Holland, C.W., Eller, A.I., Soukup, R.J., Raff, B.E., and Ellison, W.T., *Critical Sea Test Final Report*, SPAWAR CST/LLFA-WP-USWAC-9, Johns Hopkins University, Applied Physics Laboratory, Laurel, MD, 1996.